UNIVERSIDADE FEDERAL DE MINAS GERAIS

Programa de Pós-Graduação em Engenharia Metalúrgica, Materiais e Minas

Tese de Doutorado

"Design, Síntese e Caracterização de Hidrogéis e Nanocompósitos de Carboximetil Celulose com incorporação de Nanopartículas de Prata e Fármaco Doxorrubicina para Potencial Aplicação na Regeneração Epitelial: Estudos *in vitro* de Atividade Antibacteriana e Antitumoral frente à Linhagem Celular de Melanoma Humano"

Aluna: Nádia Sueli Vieira Capanema
Orientador: Prof. Dr. Herman Sander Mansur
Co-orientadora: Dra. Alexandra Ancelmo Piscitelli Mansur

Junho/2018

UNIVERSIDADE FEDERAL DE MINAS GERAIS

Programa de Pós-Graduação em Engenharia Metalúrgica, Materiais e Minas

Nádia Sueli Vieira Capanema

"Design, Síntese e Caracterização de Hidrogéis e Nanocompósitos de Carboximetil Celulose com incorporação de Nanopartículas de Prata e Fármaco Doxorrubicina para Potencial Aplicação na Regeneração Epitelial: Estudos *in vitro* de Atividade Antibacteriana e Antitumoral frente à Linhagem Celular de Melanoma Humano"

Tese de Doutorado apresentada ao Programa de Pós-Graduação em Engenharia Metalúrgica, Materiais e de Minas da Universidade Federal de Minas Gerais

Área de concentração: Ciência e Engenharia de Materiais

Orientador: Prof. Dr. Herman Sander Mansur

Co-orientadora: Dra. Alexandra Ancelmo Piscitelli Mansur

Belo Horizonte

2018

AGRADECIMENTOS

Sumário

Lista de Abreviaturas

A375   Células de melanoma humano

AgNPs   Nanopartículas de prata

CA   Ácido Cítrico (*Citric Acid*)

AFM   Microscopia de força atômica (*Atomic Force Microscopy*)

CB   Ligação Covalente (*Covalent Bond*)

CLSM   Microscopia Confocal de Varredura a Laser (*Confocal Laser Scanning Microscopy*)

CMC   Carboximetil celulose

CN   Controle Negativo

DLS   Espalhamento Dinâmico da Luz (*Dynamic Light Scattering*)

DMEM   Meio Eagle Modificado por Dulbecco (*Dulbecco's Modified Eagle Medium*)

DOX   Doxorrubicina

DP   Desvio Padrão

DSC   Calorimetria Diferencial Exploratória (*Differential Scanning Calorimetry*)

DTA   Análise térmica diferencial (*Differential Thermal Analysis*)

EDC   *N*-(3-Dimetilaminopropil)-*N′*-etilcarbodiimida

EDS   Espectroscopia de Energia Dispersiva (*Energy-Dispersive X-ray Spectroscopy*)

FTIR	Espectroscopia no Infravermelho por Transformada de Fourier (*Fourier Transformed Infrared Spectroscopy*)
GA	Glutaraldeído
DS	Grau de Substituição (*Degree of Substitution*)
HEC	Hidroxietil celulose
HEK 293T	Células embrionárias de rim humano (*Human embryonic kidney cells*)
^{1}H NMR	Espectroscopia de Ressonância Magnética Nuclear de próton (*Proton Nuclear Magnetic Resonance*)
LE	Eficiência no Carregamento (*Loading Efficieny*)
MB	Azul de Metileno (*Methylene Blue*)
MEC	Matriz extracelular
MES	Ácido 2-*N*-morfolinoetanossulfônico
MFI	Intensidade de Fluorescência Média (*Mean Fluorescence Intensity*)
ML	Microscopia Ótica de Luz
MO	Laranja de Metila (*Methyl Orange*)
MTT	Brometo de 3-(4,5-Dimetiltiazol-2-yl)-2,5-difeniltetrazólio
PBS	Solução Salina de Tampão Fosfato (*Phosphate Buffered Saline*)
PEG	Polietileno glicol
pH	Potencial hidrogeniônico
PL	Fotoluminescência (Photoluminescence Spectroscopy)
ζ , ZP	Potencial Zeta (*Zeta Potencial*)

SAED   Área Selecionada de Difração de Elétrons (*Selected Area Electron Diffraction)*

SAOS   Células derivadas de osteossarcoma humano

SAP   Superabsorvente (*Superabsorbent*)

SBF   Fluído Corporal Simulado (*Simulated Body Fluid)*

SD   Grau de Intumescimento (*Swelling Degree)*

SEM   Microscopia Eletrônica de Varredura (*Scanning Eletronic Microscopy)*

TEM   Microscopia Eletrônica de Transmissão (*Transmission Electron Microscopy)*

TGA   Análise Termogravimétrica (*Thermogravimetric Analysis*)

UV-vis   Espectroscopia de ultravioleta-visível (*Ultraviolet-visible spectroscopy)*

XPS   Espectroscopia de fotoelétrons por raios X (*X-ray photoelectron Spectroscopy)*

Resumo

Neste trabalho foi realizado o design, a síntese e a caracterização de membranas de hidrogéis híbridos à base de derivado de celulose funcionalizado com carboximetil (CMC), com dois graus de substituição (DS = 0,77 e 1,22), reticulados quimicamente pelo ácido cítrico (CA) e modificados, separadamente, com polietilenoglicol (PEG), incorporados com nanopartículas de prata (AgNPs) e bioconjugado com droga anticâncer, doxorrubicina (DOX).

Os resultados demonstraram que os hidrogéis produzidos à base de CMC apresentaram comportamento superabsorvente com propriedades moduladas pelo grau de substituição do polímero, pelo teor de ácido cítrico e pela adição do PEG, das AgNPs e da DOX. A formação da estrutura reticulada ocorreu especialmente pela reação dos grupos hidroxilas da CMC com o ácido cítrico e os hidrogéis de CMC, CMC-PEG e CMC-AgNPs apresentaram comportamento não-citotóxico. A adição de PEG levou à uma maior reticulação da rede polimérica na mesma direção do aumento da concentração do reticulante ácido cítrico (CA) e afetou drasticamente as propriedades nanomecânicas do material. Os híbridos de CMC-AgNPs apresentaram atividade antibacteriana eficaz contra patógenos gram positivos (*Staphylococcus aureus*) e contra as cepas gram-negativas (*Escherichia coli* e *Pseudomonas aeruginosa*). Nos estudos com bioconjugados polímero-droga, utilizando hidrogel de CMC com dois graus de substituição (DS = 0,77 e 1,22) e o fármaco cloridrato de doxorrubicina foi formada ligação covalente amida por interação dos grupos aminos da DOX com grupos carboxílicos da CMC, que foi confirmada com a caracterização por espectroscopia de FTIR. Os hidrogéis de CMC conjugados com doxorrubicina apresentaram a possibilidade de controlar a liberação da droga em função do grau de substituição da CMC e formação da ligação covalente droga-polímero, resultando, inclusive em uma liberação mais lenta para as células normais, permitindo uma redução dos efeitos agudos em células não-tumorais.

Portanto, neste trabalho foram desenvolvimentos hidrogéis com características físico-químicas, mecânicas e biológicas compatíveis para a utilização como biomateriais para potenciais aplicações no tratamento de feridas e regeneração epitelial e ainda com a possibilidade de incorporação de propriedades antibacterianas e antitumorais.

Abstract

This study focused on the design, synthesis and comprehensive characterization of environmentally friendly hydrogel membranes based on carboxymethyl cellulose (CMC) for wound dressing and skin repair substitutes. These new CMC hydrogels were prepared with two degrees of functionalization (DS = 0.77 and 1.22) and chemically crosslinked with citric acid (CA) for tuning their properties. Additionally, CMC-based hybrids were obtained by blending with polyethylene glycol (PEG) and nanocomposites with antibacterial and antitumor properties were synthesized combining CMC and silver nanoparticles (AgNPs) and by conjugation of doxorubicin (DOX) with CMC polymer, respectively. The results demonstrated that superabsorbent hydrogels (SAP) were produced which was significantly dependent on the concentration CA crosslinker, the DS of CMC, the addition of PEG as network modifier, the presence of AgNPs and DOX chemotherapeutic. The spectroscopical characterizations indicated that the mechanism of CA crosslinking was mostly associated with the chemical reaction with CMC hydroxyl groups and the CMC-based hydrogels (CMC, CMC-PEG and CMC-AgNPs) were cytocompatible considering the *in vitro* cell viability responses. In addition, PEG played an important role on the formation of a hybrid polymeric network with very distinct morphological and nanomechanical features. CMC–AgNP nanohybrids demonstrated highly effective antibacterial activity against gram-positive multi-resistant wound/skin pathogens (*Staphylococcus aureus*) and moderate effect towards gram-negative strains (*Escherichia coli* and *Pseudomonas aeruginosa*). The carbohydrate-based prodrug composed of CMC bioconjugated with DOX by covalent amide bonds demonstrated the effect of CMC hydrogel network structure with distinct degree of substitution regarding to the process of bioconjugation and on tailoring the DOX release kinetics in vitro and the cytotoxicity towards melanoma cancer cells in vitro. Therefore, SAP hydrogels were designed and produced with properties that are tunable through the extension of crosslinking and degree of substitution of carboxymethyl groups of the cellulose backbone. To this end, they are envisioned as promising hydrogels with key properties for assisting skin wound healing and regeneration, offering promising perspectives for skin disease applications associated with antibacterial activity and topical chemotherapy of melanoma.

Capítulo 1. Introdução

A pele, o maior órgão do corpo, é um tecido muito complexo e um importante obstáculo contra fatores externos, como agentes microbianos patogênicos e radiação ultravioleta. Além disso, desempenha um papel significativo na prevenção da perda substancial de fluidos corporais, auxiliando na termorregulação e defesa imunológica do corpo (GEOFFREY *et al*., 2008, BLANPLAIN, 2010). Várias lesões na pele causadas por acidentes, queimaduras, traumas, feridas crônicas e doenças podem representar um importante problema de saúde. A cura de feridas é um processo dinâmico que envolve múltiplas interações entre células, matriz extracelular (MEC) e fatores de crescimento que reconstroem o tecido após lesão (GEOFFREY *et al*., 2008). Por exemplo, a incidência de feridas crônicas não cicatrizantes, tais como úlcera diabética, continua a aumentar, e tornou-se um problema sério na clínica porque cerca de 20% de diabéticos desenvolverão feridas de pé crônicas e não cicatrizantes, criando gasto crescente para as organizações mundiais (MARTIN, 1997; NEILL, 2015). Além disso, mais de 300 mil mortes ocorrem anualmente como resultado de queimaduras induzidas pelo fogo, com mortes adicionais atribuídas a outras formas de queimaduras (por exemplo, eletricidade, produtos químicos, radiação) de acordo com a Organização Mundial de Saúde (MADAGHIELE *et al*., 2014). As feridas de queimadura são, de fato, as mais desafiadoras a serem gerenciadas, onde perda substancial de fluidos e danos extensivos nos tecidos, resultantes de feridas profundas, prejudicam múltiplas funções vitais realizadas pela pele (GEOFFREY *et al*., 2008; IZAD, 2005).

Tradicionalmente, o tratamento de feridas envolve o controle da infecção, e isso permite que o corpo cure a ferida naturalmente. No entanto, as feridas mais crônicas, como úlceras nas pernas, úlceras por pressão e úlceras do pé diabético, possuem um processo de doença sistêmica subjacente, que interfere persistentemente nos processos bioquímicos e fisiológicos na área da ferida. Como resultado, o processo de cicatrização é dificultado ou mesmo interrompido na fase inflamatória, levando a complicações graves da doença. Para este fim, há uma demanda crescente de biomateriais apropriados e seguros para tratar lesões cutâneas e feridas tópicas, que podem estar relacionadas a um defeito ou uma ruptura na pele, resultantes de lesões físicas ou térmicas e doenças (GEOFFREY *et al*., 2008; LUTOLF *et al*. 2005; CARVALHO *et al*., 2017).

No entanto, a compreensão adequada das relações entre as propriedades da superfície do material e as respostas celulares é essencial para a concepção de materiais para implantação e engenharia de tecidos. Sabe-se que, durante o processo de cicatrização de feridas, o curativo protege a lesão e contribui para a recuperação de tecidos dérmicos e epidérmicos. Por essa razão, os polímeros naturais, como polissacarídeos e derivados (por exemplo, alginatos, quitosana, heparina, celulose), proteoglicanas e proteínas (por exemplo, colágeno, gelatina, fibrina, queratina) são amplamente utilizados no tratamento de feridas devido à sua biodegradabilidade adequada, biocompatibilidade e semelhança com macromoléculas geralmente reconhecidas pelo corpo humano (CARVALHO *et al*., 2017; MOGOŞANU *et al*., 2014).

Entre as várias alternativas de polímeros naturais, a celulose e seus derivados têm sido amplamente utilizados como ingrediente natural para a produção de hidrogéis e desenvolvida para várias aplicações, incluindo engenharia de tecidos, liberação de medicamentos, curativos, principalmente devido a sua biocompatibilidade, biodegradabilidade, solubilidade em água, abundância, baixo custo e ser ecologicamente correta (CARVALHO *et al*. 2017; MOGOŞANU *et al*. 2014).

A carboximetil celulose (CMC) é um derivado de celulose em que os grupos hidroxila da celulose são parcialmente substituídos por grupos carboximetil (CH_2COOH) e tem sido amplamente utilizada para síntese de hidrogéis principalmente devido às vantagens de não toxicidade, solubilidade em água, baixo custo e ser ambientalmente correta. Assim, a CMC foi desenvolvida para várias aplicações, incluindo engenharia de tecidos, liberação de medicamentos, curativos e crescimento de plantas (ZHANG *et al*., 2017; DANG *et al*., 2017).

 Em particular, na última década, uma nova classe de hidrogéis referidos como hidrogéis superabsorventes (ou SAP) à base de polímeros naturais, como celulose e derivados, foram desenvolvidos para aplicações biomédicas (DANG *et al*., 2015; REZA *et al.,* 2010). Essencialmente, os hidrogéis SAP são polímeros tridimensionais reticulados, lineares ou ramificados, hidrofílicos com a capacidade de absorver grandes quantidades de água, solução salina ou soluções fisiológicas em comparação com materiais absorventes gerais (CARVALHO *et al*., 2017; REZA *et al.,* 2010). Apesar da

estabilidade estrutural favorável e das propriedades de biocompatibilidade, os hidrogéis quimicamente reticulados podem apresentar inconvenientes, incluindo a baixa solubilidade em água de precursores de polímeros (por exemplo, celulose, quitosana) e potencial citotoxicidade de reticulantes químicos comuns (por exemplo, formaldeído, glutaraldeído e epicloridrina), devido ao risco de reagentes não reagidos no sistema (DEMITRI *et al.,* 2008; CARVALHO *et al*., 2017; SANNINO *et al*., 2003).

 Portanto, uma alternativa para superar as desvantagens acima mencionadas é preparar hidrogéis usando derivados de polímeros modificados quimicamente, tais como carboximetil celulose, para promover a sua solubilidade em água e usar reagentes e agentes de reticulação eco-amigáveis tais como ácido cítrico através de todo o processo (DEMITRI *et al.,* 2008; DANG *et al*., 2017; SANNINO *et al*., 2003; CHANG *et al*., 2010). Além disso, polímeros como o polietilenoglicol (PEG), por ser um poliéter anfifílico, solúvel em água e em muitos solventes orgânicos e não tóxico contribui para o seu amplo uso na pesquisa biomédica, liberação de medicamentos, *scaffolds*, engenharia de tecidos, funcionalização de superfície, e assim por diante (LEUNG, 2001; RAUCCI *et al*., 2015).

Outro aspecto fundamental a ser abordado no biomaterial sintético, com perspectiva a substituto de pele, é considerado o fato de que a pele é a última barreira entre o corpo humano e o ambiente externo. Assim, além de proteger o corpo contra fatores químicos e físicos exógenos, a pele é a primeira linha de defesa contra microorganismos patogênicos e auxilia nos processos imunológicos (GEOFFREY *et al*., 2008, BOER *et al*., 2016). Assim, existe uma demanda crescente de um curativo apropriado e seguro para tratar lesões cutâneas e feridas tópicas, que podem estar relacionadas a um defeito ou a uma ruptura na pele, resultantes de lesões físicas ou térmicas e doenças. A cicatrização de feridas é um processo fisiológico crítico que requer ausência de bactérias nos locais danificados, que podem ser classificadas como agudos ou crônicos dependendo da natureza e tempo do processo de cicatrização. Em particular, as feridas crônicas, como as relacionadas a úlceras diabéticas ou queimaduras profundas, são um solo fértil para a proliferação de bactérias. Apesar de uma ampla gama de agentes antimicrobianos e antibióticos estarem comercialmente disponíveis, um combate bem sucedido de infecções bacterianas é particularmente desafiador devido ao aumento da

resistência microbiana causada por abuso de tais drogas (SACCO *et al*., 2015; RAI *et al*., 2012).

Historicamente, os compostos de prata (Ag) têm sido utilizados em vários campos para prevenir o crescimento microbiano. Como muitos metais pesados não essenciais, a Ag é um biocida natural, mas comparado com titânio, zinco e cobre, as nanopartículas de Ag mostram a maior eficácia antimicrobiana contra bactérias, vírus e outros microorganismos eucariotas (GONG *et al.,* 2007; SAMBERG *et al.*, 2010). Portanto, as nanopartículas de prata (AgNPs) são amplamente consideradas como as estratégias mais promissoras para superar a resistência microbiana como agentes terapêuticos para a prevenção e erradicação da colonização de feridas por microorganismos. Elas são comparativamente mais eficientes e potentes contra vários agentes patogênicos resistentes aos fármacos em comparação com os antibióticos convencionais (SACCO *et al*., 2015; KALASHNIKOVA *et al.,* 2010).

Por essa razão, as biomembranas híbridas de hidrogel reticuladas com incorporação de nanopartículas de prata emergiram como uma nova classe de biomateriais multifuncionais para engenharia de tecido (SAMBERG *et al.*, 2010).

Outra alternativa promissora aplicação dos hidrogéis à base de polissacarídeos é a de carreador para liberação de fármacos, pois a maioria dos quimioterápicos, especialmente os anticancerígenos, é consideravelmente tóxica às células normais ou carece de especificidade e seletividade (KAMBA *et al*., 2013). O câncer de pele representa um dos carcinomas de ocorrência mais comum em humanos e está crescendo a uma taxa de um milhão de novos casos relatados anualmente. Portanto, o melanoma continua a ser uma importante ameaça à saúde, com a morte muitas vezes ocorrendo por metástase. O melanoma cutâneo primário pode ser administrado por cirurgia no estágio inicial, mas o melanoma metastático avançado não pode ser tratado corretamente por cirurgia isoladamente. Portanto, o melanoma metastático avançado requer métodos terapêuticos adicionais, como quimioterapia, bioquimioterapia, imunoterapia e terapia celular (BHARADWAJ, DAS, PAUL E MAZUMDER, 2016, VISHNUBHAKTHULA, ELUPULA E DURÁN-LARA, 2017). Existem várias vantagens de usar o polímero como carreador para agentes antineoplásicos, incluindo aumento da solubilidade do fármaco, melhor biodisponibilidade, alta estabilidade, liberação controlada do fármaco,

possibilidade de seletividade de órgãos e tecidos e redução da dose total necessária. Além disso, a associação de polímeros com drogas anticancerígenas tóxicas pode minimizar significativamente os efeitos colaterais adversos (RANJBARI *et al*., 2017, VISHNUBHAKTHULA, ELUPULA E DURÁN-LARA, 2017). Por essa razão, carreadores (nano) poliméricos são as plataformas mais estudadas para o tratamento do câncer.

Assim, hidrogéis poliméricos baseados em polissacarídeos têm sido estudados como portadores de fármacos anticancerígenos que não são solúveis em água e altamente citotóxicos para aplicações quimioterapêuticas. A Doxorrubicina (DOX) é uma droga anfifílica anticancerígena mais utilizada clinicamente por causa de sua alta eficiência e um amplo espectro de atividade contra diversos tipos de câncer (por exemplo, câncer de mama, pulmão, pele e cérebro), mas é pouco solúvel em água e meio fisiológico. Portanto, o desenvolvimento de sistemas carreadores polímero-fármaco, econômicos, solúveis em água e biocompatíveis com o encapsulamento eficiente da DOX ainda é altamente necessário contra o câncer de pele. Curiosamente, apesar da pesquisa intensiva no campo dos conjugados polímero-fármaco, incluindo sistemas CMC (HE *et al*., 2015; MOVAGHARNEZHAD & MOGHADAM, 2016; ROY *et al*., 2014), nenhum estudo publicado foi encontrado na literatura de hidrogéis reticulados de CMC-DOX para o tratamento de câncer de melanoma.

Assim, o propósito desse estudo envolveu o design, a síntese e a caracterização físico-química e biológica *in vitro* de hidrogéis e nanocompósitos à base de CMC reticulados com ácido cítrico com introdução de agentes modificadores de rede (PEG), agentes antibacterianos (AgNPs) e drogas antitumorais (DOX) para potencial aplicação na regeneração epitelial.

Capítulo 2. Objetivos

2.1. Objetivo Geral

Design, síntese e caracterização de hidrogéis e nanocompósitos à base de carboximetil celulose (CMC) com propriedades físico-químicas moduladas pela seleção do grau de substituição (DS = 0,77 e DS = 1,22) da CMC, pela incorporação de polímeros modificadores de rede (PEG) e pelo teor de ácido cítrico utilizado como agente de reticulação (CA = 0%, 10%, 15%, 20% e 25%). Nestes hidrogéis foram incorporadas propriedades antibacterianas e antitumorais pela inclusão de nanopartículas de prata (AgNPs) e pela bioconjugação com droga anticâncer doxorrubicina (DOX), respectivamente, visando potencial aplicação na regeneração epitelial tecidual.

2.1.1. Objetivos Específicos

a) Caracterizar o polímero de carboximetil celulose (CMC) com dois graus de substituição (DS = 0,77 e 1,22), utilizado como matéria prima, através de técnicas morfológicas e de espectroscopia.

b) Sintetizar hidrogéis de carboximetil celulose e com adição de PEG (CMC-PEG) utilizando a reticulação química com ácido cítrico (CA) nas concentrações de 10, 15, 20 e 25% m/m do polímero.

c) Sintetizar nanopartículas de prata utilizando a CMC simultâneamente como redutor da prata e agente de estabilização das nanoparticulas formadas e sintetizar hidrogéis/nanocompósitos de carboximetil celulose com incorporação das nanopartículas de prata (CMC-AgNPs) utilizando ácido cítrico como agente de reticulação.

d) Conjugar covalentemente o fármaco doxorrubicina (DOX) com a CMC e sintetizar hidrogéis/nanocompósitos de carboximetil celulose conjugados com doxorrubicina (CMC-DOX) utilizando ácido cítrico como agente de reticulação.

f) Caracterizar os hidrogéis de CMC e nanocompósitos sintetizados através das técnicas de espectroscopia, morfológicas, análise térmica e análises físico-químicas.

g) Avaliar a citotoxicidade *in vitro* dos hidrogéis/nanocompósitos obtidos utilizando o ensaio colorimétrico de redução do brometo de 3-(4,5-Dimetiltiazol-2-yl)-2,5-difeniltetrazólio (MTT) utilizando a linhagem de células embrionárias de rim humano (HEK 293T) em todos os sistemas e as células de melanoma humano (A375) nos nanocompósitos de CMC-DOX.

g) Realizar ensaio de atividade antibacteriana nos hidrogéis com incorporação de AgNPs (CMC-AgNPs) utilizando o método de disco de difusão de ágar com utilização de bactérias gram positivas (*Staphylococcus aureus*) e gram-negativas (*Escherichia coli* e *Pseudomonas aeruginosa*).

h) Realizar a avaliação de liberação da DOX *in vitro* acelular e *in vitro* celular para os nanocompósitos CMC-DOX.

Capítulo 3. Design, síntese e caracterização de hidrogéis à base de carboximetil celulose (CMC) modificados com polietilenoglicol (PEG) para aplicação em curativos de pele

3.1. Graphical Abstract
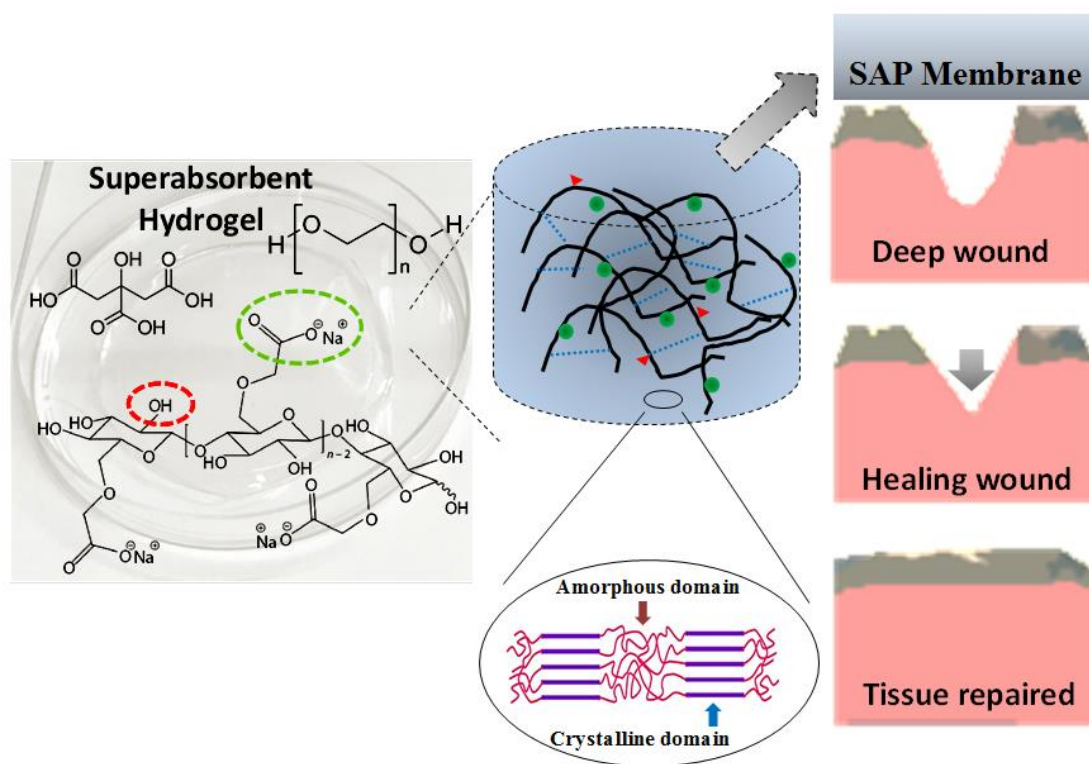
Superabsorbent Crosslinked PEG-Carboxymethyl Cellulose Hydrogels for Potential Treatment of Wounds

3.2. Resumo

Neste estudo foi feita a síntese e caracterização de membranas de hidrogel baseadas em carboximetil celulose (CMC) para aplicações em tratamento de feridas e como materiais para reparação epitelial. Esses novos hidrogéis de CMC foram preparados com dois graus de funcionalização (DS = 0,77 e 1,22) da CMC e reticulados quimicamente com ácido cítrico (CA) nas concentrações de 10, 15, 20 e 25% m/m (CA/CMC) para modulação de suas propriedades. Híbridos à base de CMC foram também preparados pela adição de polietilenoglicol (PEG, 10% e 20% em massa, PEG/(CMC+PEG)) seguida de reticulação com CA. Ensaios de intumescimento e degradação e análises de

espectroscopia de infravermelho, microscopia eletrônica de varredura, microscopia de força atômica, além das análises térmicas (análise termogravimétrica e calorimetria exploratória diferencial), foram utilizadas para avaliação das propriedades físico-químicas e características morfológicas, e também para elucidação dos mecanismos envolvidos na formação dos hidrogéis. Os resultados mostraram que hidrogéis superabsorventes (SAP) foram produzidos com grau de intumescimento variando entre 100% e 5000%, o que foi significativamente dependente do grau de substituição da CMC, da concentração do agente reticulante (CA) e da adição de PEG como modificador de rede. Os resultados mostraram que o mecanismo de reticulação com ácido cítrico está essencialmente associado com a reação química do CA com os grupos hidroxilas da CMC. Além disso, o PEG apresentou um importante papel na formação da rede polimérica. O polietilenoglicol apresentou elevada miscibilidade na CMC e participou da formação dos hidrogéis através de ligações de hidrogênio entre os grupos funcionais de ambos os polímeros (PEG: C-O-C e -OH e CMC: -OH e C=O) sendo observada a formação de uma estrutura híbrida composta de uma fase amorfa especialmente associada às cadeias poliméricas da CMC intercaladas com domínios cristalinos do PEG estabilizados por ligações de hidrogênio. Como consequência, hidrogéis apresentaram características morfológicas muito distintas, dependendo do grau de reticulação e as propriedades nanomecânicas de superfície (por exemplo, módulos elásticos) que foram drasticamente afetadas (de aproximadamente 0,08 GPa para 2,0 GPa) devido à formação de nanoestruturas híbridas de CMC-PEG. Estes hidrogéis baseados em CMC foram citocompatíveis considerando as respostas de viabilidade celular *in vitro* de mais de 95% para células embrionárias de rim humano (HEK 293T) usadas como linhagem celular modelo. Assim, hidrogéis SAP foram projetados e produzidos com propriedades controladas pela extensão de reticulação resultando em uma habilidade de absorver grandes quantidades de água mantendo a baixa degradabilidade das matrizes. Neste sentido, estes materiais apresentam promissora utilização com hidrogéis superabsorventes apresentando propriedades chaves para reparo e regeneração de feridas na pele.

3.3. Artigo

Capanema, Nádia S.V.; Mansur, A.A.P.; de Jesus, A.C.; Carvalho, S.M.; de Oliveira, L.C.; Mansur, H.S. Superabsorbent Crosslinked Carboxymethyl Cellulose-PEG Hydrogels for Potential Wound Dressing Applications. International Journal of Biological Macromolecules, v. 106, p. 1218-1234, 2017. **QUALIS A2 – JCR 3.671**
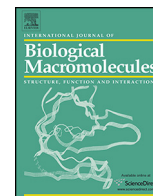
Superabsorbent crosslinked carboxymethyl cellulose-PEG hydrogels for potential wound dressing applications

Nádia S.V. Capanema [a], Alexandra A.P. Mansur [a], Anderson C. de Jesus [a], Sandhra M. Carvalho [a], Luiz C. de Oliveira [b], Herman S. Mansur [a],*

[a] Center of Nanoscience, Nanotechnology and Innovation – CeNano2I, Department of Metallurgical and Materials Engineering, Federal University of Minas Gerais, Brazil
[b] Department of Chemistry, Federal University of Minas Gerais, Brazil

ABSTRACT

This study focused on the synthesis and comprehensive characterization of environmentally friendly hydrogel membranes based on carboxymethyl cellulose (CMC) for wound dressing and skin repair substitutes. These new CMC hydrogels were prepared with two degrees of functionalization (DS = 0.77 and 1.22) and chemically crosslinked with citric acid (CA) for tuning their properties. Additionally, CMC-based hybrids were prepared by blending with polyethylene glycol (PEG, 10 wt.%). The results demonstrated that superabsorbent hydrogels (SAP) were produced with swelling degree typically ranging from 100% to 5000%, which was significantly dependent on the concentration of CA crosslinker and the addition of PEG as network modifier. The spectroscopical characterizations indicated that the mechanism of CA crosslinking was mostly associated with the chemical reaction with CMC hydroxyl groups and that PEG played an important role on the formation of a hybrid polymeric network. These hydrogels presented very distinct morphological features depended on the degree of crosslinking and the surface nanomechanical properties (*e.g.*, elastic moduli) were drastically affected (from approximately 0.08 GPa to 2.0 GPa) due to the formation of CMC-PEG hybrid nanostructures. These CMC-based hydrogels were cytocompatible considering the *in vitro* cell viability responses of over 95% towards human embryonic kidney cells (HEK293T) used as model cell line.

© 2017 Elsevier B.V. All rights reserved.

1. Introduction

The repair of wounds is one of the most complex biological processes that occur during human life. Wound healing is a dynamic process involving multiple interactions between cells, extracellular matrix (ECM) and growth factors that reconstructs tissue following injury [1]. Several injuries to the skin caused by accidents, burns, trauma, chronic wounds and diseases can pose major healthcare problem. For instance, the incidence of chronic nonhealing wounds, such as diabetic ulcers, continues to increase, have become a serious problem in the clinic because approximately 20% of diabetics are likely to develop chronic nonhealing foot wounds [2,3]. Additionally, more than 300,000 deaths occur annually as a result of fire-induced burns, with additional deaths attributed to other forms of burns (*e.g.*, electricity, chemicals, radiation) according to the

World Health Organization. Burn injuries are indeed among the most challenging ones to manage, where substantial fluid loss and extensive tissue damage, resulting from deep wounds, impair multiple vital functions performed by skin [1,4,5]. Traditionally, wound management has involved controlling the underlying causes, such as infection, ischemia, or diabetes, and allowing the body to heal the wound naturally. However, the most chronic wounds such as leg ulcers, pressure ulcers and diabetic foot ulcers have an underlying systemic disease process, which persistently interferes with biochemical and physiological processes in the wound area. As a result, the healing process is delayed or even stopped in the inflammatory phase leading to serious complications of the illness. To this end, there is a growing demand for appropriate and safe biomaterials to treat and repair skin lesions and topical wounds, which can be related to a defect or a break in the skin, resulting from physical or thermal injury and disease conditions [1,6–11].

It is well-known that during the wound-healing process, the dressing protects the injury and contributes to the recovery of dermal and epidermal tissues. For that reason, natural polymers such as polysaccharides and derivatives (*e.g.*, alginates, chitosan, heparin, and cellulose), proteoglycans and proteins (*e.g.*, collagen,
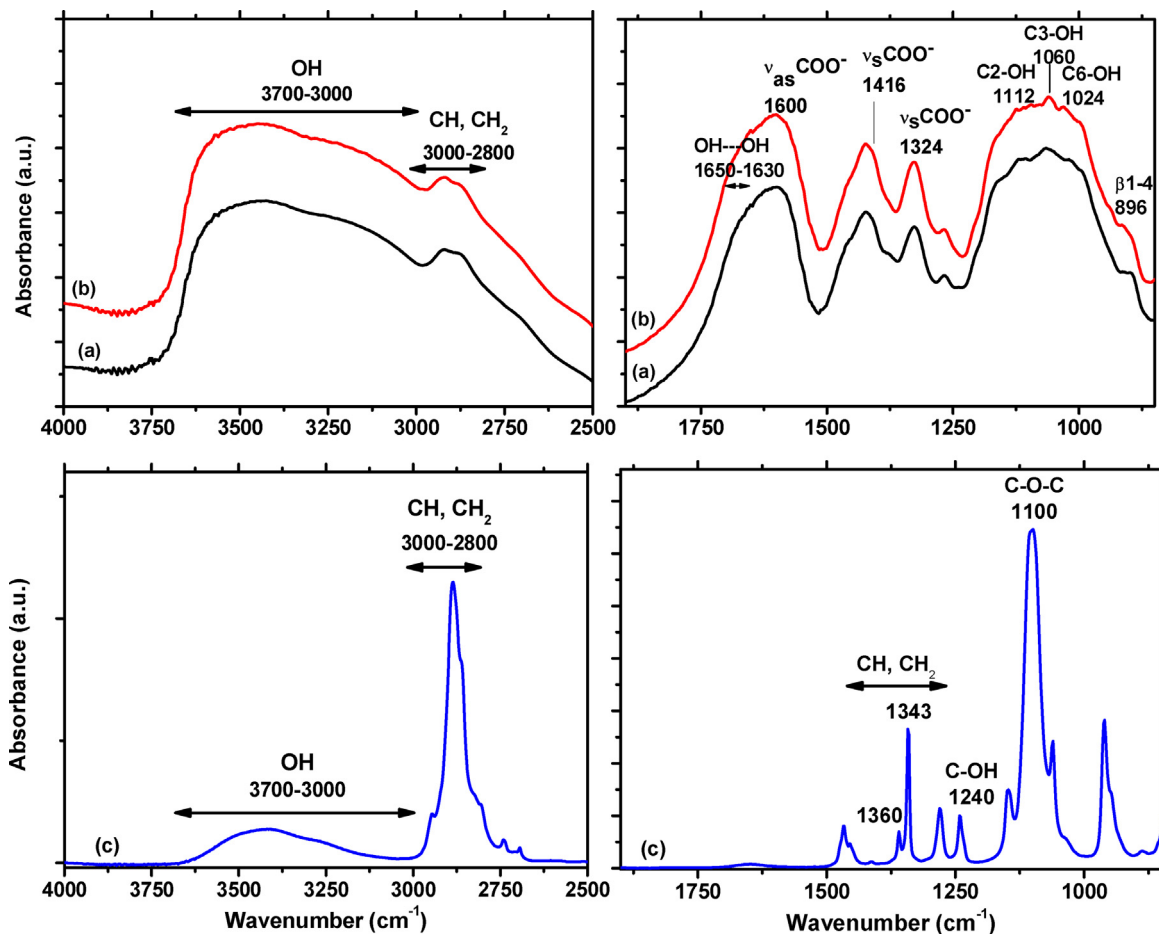
Fig. 1. FTIR spectra of CMC-0.77 (a), CMC-1.22 (b), and PEG (c).

gelatin, fibrin, keratin) are widely used in wounds management and treatment. They present suitable biodegradability, biocompatibility and similarity to macromolecules that are usually recognized by the human body [11–15]. Among several alternatives of natural polymers, cellulose and its derivatives have been broadly used as a natural source for producing of hydrogels and composites in many fields, including wound dressing, drug delivery, and tissue engineering. They usually present the benefits of biocompatibility, biodegradability, water solubility, abundance and low cost, and environmental friendliness [11,12]. Carboxymethyl cellulose (CMC) is a cellulose derivative with a large number of carboxymethyl groups on the cellulose backbone, which has been widely used as a natural ingredient for hydrogels mostly because of these advantages. CMC has been developed for various applications including tissue engineering, drug delivery, wound dressing and plant breeding [16,17]. In particular, in the last decade a novel class of hydrogels referred to as superabsorbent hydrogels (or SAP) based on natural polymers such as cellulose and derivatives have been developed for biomedical applications [18–20]. Essentially, SAP hydrogels are three-dimensional crosslinked hydrophilic, linear or branched polymers with the ability to absorb large quantities of water, saline or physiological solutions compared with general absorbing materials [11,20]. Despite favorable structure stability and biocompatibility properties, chemically crosslinked hydrogels may present drawbacks, including the low water-solubility of polymer precursors (e.g., cellulose, chitosan) and intrinsic cytotoxicity of common chemical crosslinkers (e.g., formaldehyde, glutaraldehyde, epichlorohydrin), due to the risk of unreacted species in the

system [8,11,21]. Therefore, an alternative to overcoming the aforementioned disadvantages is to prepare hydrogels using chemically modified polymer derivatives such as CMC to promote its water-solubility and use biocompatible and eco-friendly crosslinkers (e.g., citric acid) through the entire process [8,17,21–23]. Moreover, polymers such as PEG have been combined with cellulose and CMC systems as an effective network modifier to improve the properties of the hydrogels. PEG Polyethylene glycol (PEG) is a polyether that is amphiphilic and soluble in water as well in many organic solvents. PEG is readily available in a wide range of molecular weights and it has been found to be nontoxic and is approved by the U.S. Food and Drug Administration (FDA). These features contribute to their broad application in biomedical research, drug delivery, tissue engineering scaffolds, surface functionalization, and so forth [24,25].

Thus, in this study, novel CMC hydrogel membranes were developed using distinct degree of carboxymethyl-functionalization, crosslinked with citric acid and modified with PEG. They were produced strictly by a facile one-pot environmentally-friendly aqueous process at room temperature. It was demonstrated that the physicochemical and nanomechanical properties combined with morphological features were tailored by the degree of crosslinking and the effect of PEG as network modifier to mimic the characteristics of natural skin tissue. Therefore, the proposed facile strategy of producing biocompatible superabsorbent hydrogels offers promising perspectives of novel functional platforms of temporary skin substitutes in chronic wound repair and regeneration applications.
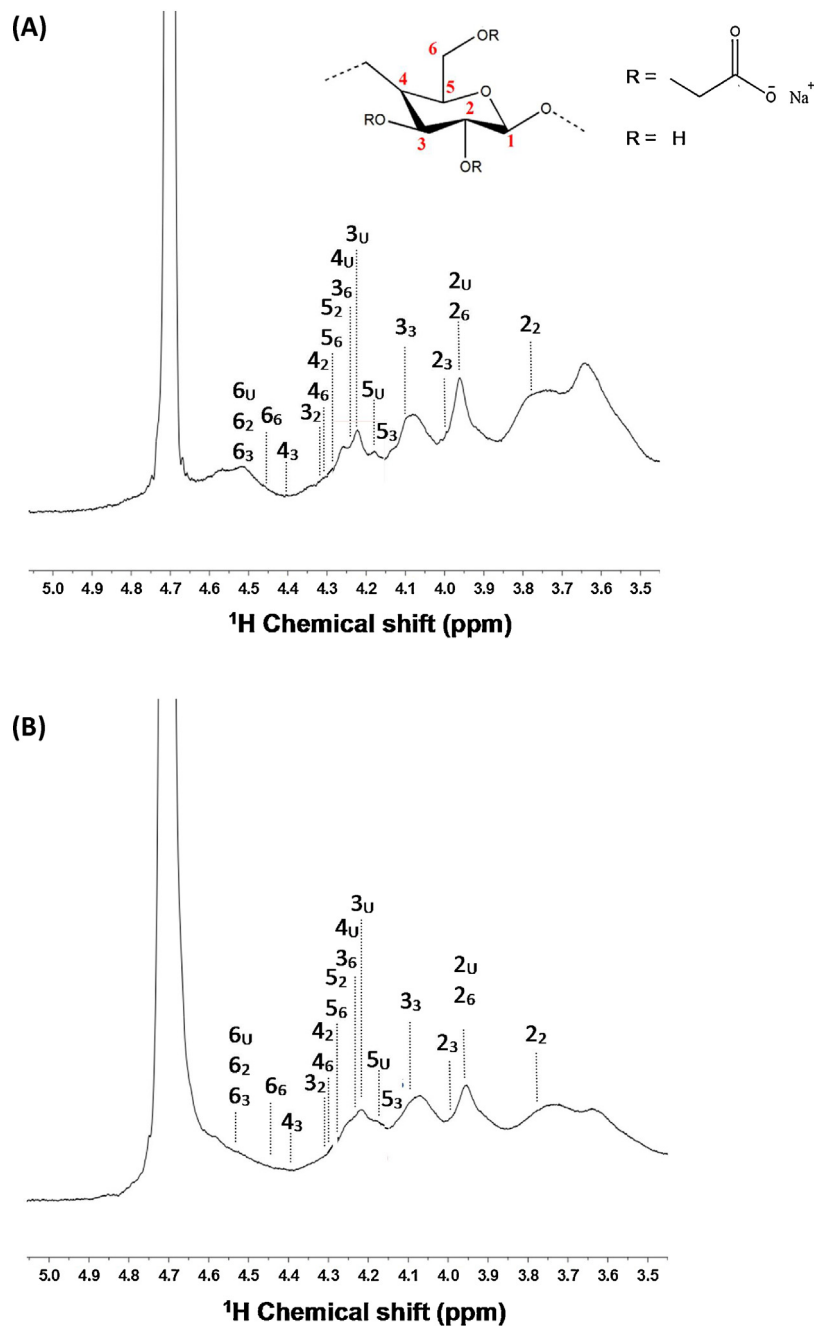
Fig. 2. ^{1}H NMR spectra of CMC-0.77 (A) and CMC-1.22 (B) with the chemical shift assignments of unsubstituted, 2-mono, 3-mono, and 6-mono anhydroglucose units.

## 2. Materials and methods

2.1. Materials

Sodium carboxymethyl cellulose with two degree of substitution DS = 0.77 (CMC-0.77, average molar mass M_w = 250 kDa and, viscosity 735 cps, 2% in H_2O at 25 °C) and DS = 1.22 (CMC-1.22, M_w = 250 kDa, viscosity 660 cps, 2% in H_2O at 25 °C), polyethylene glycol (PEG, M_w = 1521 Da, viscosity 38.2 cps, 50% in H_2O at 20 °C), and citric acid (CA, Sigma-Aldrich, USA, $\geq$ 99.5%, HOC(COOH)(CH$_2$COOH)$_2$) were purchased from Sigma-Aldrich (USA) and used as received. Filter paper from Nalgon (Brazil) with grammage 85 g m^{-2}, ash content 0.00009 g, and pore size of 4 μm was used as reference for cellulose. Unless specified otherwise, deionized water (DI water, Millipore Simplicity^{TM}) with a resistivity

of 18 MΩ cm was used to prepare the solutions and the procedures were performed at room temperature (RT, 23 ± 2 °C).

2.2. Synthesis of crosslinked CMC hydrogel membranes

CMC solution (2% w/v) was prepared by adding sodium carboxymethyl cellulose powder (2.0 g) to 100 mL of DI water and stirring at room temperature until complete solubilization occurred. After dissolution, the crosslinking agent, citric acid (CA), was added under stirring at concentrations of 10% (CMC/CA10), 15% (CMC/CA15), 20% (CMC/CA20), and 25% (CMC/CA25) m/m of CMC polymer and homogenized for 20 min. Then, 10 mL of the solutions were poured into plastic molds (polystyrene petri dish, diameter = 60 mm) and were allowed to dry at 40 ± 2 °C for 24 h to remove water. In the sequence, the samples were kept at 80 ± 2 °C

23
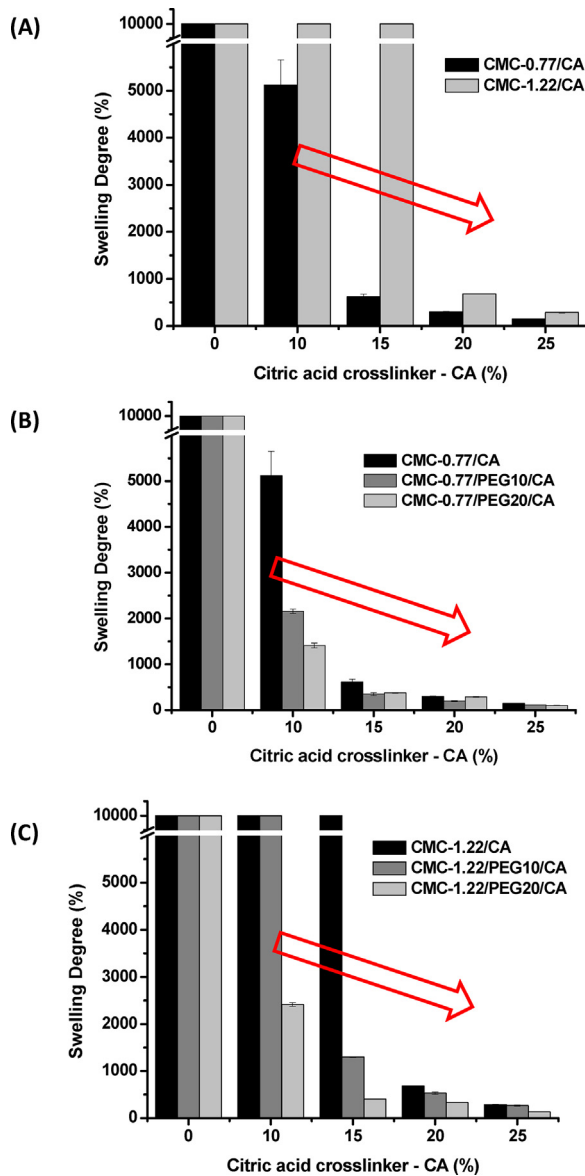
Fig. 3. Histogram of swelling behavior of CMC-based hydrogels with increasing concentration of CA (0%, 10%, 15%, 20%, and 25%). (A) CMC/CA hydrogels; (B) CMC-0.77/PEG/CA and (C) CMC-1.22/PEG/CA hydrogels modified with PEG (10% and 20%).

for 24 h for the crosslinking reaction (slow evaporation method). As a reference, a sample without CA (CMC/CA0) was also prepared and dried following the same thermal treatment.

2.3. Synthesis of crosslinked CMC-PEG hydrogel blends

CMC:PEG solutions were prepared by adding 1.8 g of CMC and 0.2 g PEG (*i.e.*, CMC/PEG10, 10%) or 1.6 g of CMC and 0.4 g of PEG (*i.e.*, CMC/PEG20, 20%) to 100 mL of DI water and stirring at room temperature until complete solubilization occurred. After dissolution, the crosslinking agent CA was added under stirring at concentrations of 10% (CMC/PEG/CA10), 15% (CMC/PEG/CA15), 20% (CMC/PEG/CA20), and 25% (CMC/PEG/CA25) m/m% of CMC + PEG polymer and homogenized for 20 min. Afterwards, the solutions were cast in plastic molds (polystyrene petri dish, diameter = 60 mm) and dried as described in Section 2.2.

2.4. Characterization of CMC and PEG polymers and crosslinked hydrogels

2.4.1. Morphological and spectroscopic analyses

Fourier transform infrared spectroscopy analysis (FTIR) was recorded with a Nicolet 6700 (Thermo Fischer) spectrometer with background subtraction. The CMC powder was mixed with pre-dried KBr (110 ± 5 °C for 2 h) at the mass ratio of 1:100 (sample:KBr), and the mixture was compressed to form a transparent pellet that was analyzed using transmission method (4000–400 cm^{-1}, 16 scans, and a 4 cm^{-1} resolution). The FTIR spectra of the PEG flakes and cast membranes were obtained using attenuated total reflectance (ATR, 4000–675 cm^{-1}, 32 scans, and 4 cm^{-1} resolution).

^{1}H NMR (nuclear magnetic resonance) spectra of CMC were recorded at 30 °C in D$_2$O/HCl using a BRUKER–200 MHz Varian spectrometer (90° pulse and 16 scans).

Thermogravimetric (TG) and differential scanning calorimetry (DSC) analyses were performed using SDT Q-600 instrument (TA Instruments Co.). Samples of approximately 1.5 ± 0.1 mg (hydrogels) and 3.0 ± 0.5 mg (PEG and cellulose) were used for the experiments at a heating rate of 10 °C min^{-1} (ranging from 25 °C to 400 °C for TG of hydrogels and all DSC runs and from 25 °C to 500 °C for TG of cellulose and PEG references). The samples were loaded into an open platinum pan and an empty cup was used as reference and the thermal analyses were performed under the continuous flow of dry nitrogen gas (30 mL min^{-1}).

Atomic force microscopy (AFM) of hydrogel membranes were conducted with a Multimode 8 (Bruker) instrument operated in PeakForce® tapping mode. The scanning rate was 1.0 Hz, and the images were acquired with 512 × 512 pixel resolution. The surface mapping of nanomechanical properties was carried out using SiN probe, at constant K = 0.4 N/m, frequency 70 kHz, temperature at 20–23 °C, calibration based on the absolute method and parameters calculated with software Nanoscope analysis 8.5 (Bruker).

2.4.2. In vitro *swelling and degradation tests*

For fluid uptake measurement and degradation assessments, the hydrogels were cut into 10 × 10 mm^2 samples, dried at 40 ± 2 °C for stabilization of mass, and weighted (W$_0$, initial mass). Then, the hydrogels (triplicates, n = 3) were placed in 70 mL sample pots with 10.0 mL DI water at RT. After 60 min, the hydrogel was removed from solution, gently wiped with filter paper to remove excess of liquid on the sample surface and weighted (W$_s$, swollen mass). In the sequence, samples were dried at 40 ± 2 °C until mass stabilization and the final weight was recorded (W$_f$, final mass).

Weight measurements obtained in each step of the process were used to calculate the swelling degree (SD) and degree of degradation (DD) of the hydrogels using Eqs. (1) and (2), respectively, as reported in the literature [26–29].

$$SD(\%) = ((W_s - W_0)/W_0) \times 100\% \qquad (1)$$

$$DD(\%) = ((W_0 - W_f)/W_0) \times 100\% \qquad (2)$$

2.4.3. Cytotoxicity evaluation

Human embryonic kidney cells (HEK293T) used as model cell line were gently provided by Prof. A. Goes of the Department of Immunology and Biochemistry, UFMG. The HEK293T cells were cultured in DMEM (Dulbecco's modified eagle medium) with 10% fetal bovine serum (FBS), streptomycin sulfate (10 mg mL^{-1}), penicillin G sodium (10 units mL^{-1}), and amphotericin-b (0.025 mg mL^{-1}), all of them were supplied by Gibco BRL (USA), using a humidified atmosphere of 5% CO$_2$ at 37 °C. All of the biological tests were conducted according to ISO 10993-5:2009/(R)2014 (Biological evaluation of medical devices: Tests for *in vitro* cytotoxicity). Before experiments, the samples were sterilized by UV radiation for 60 min.

24
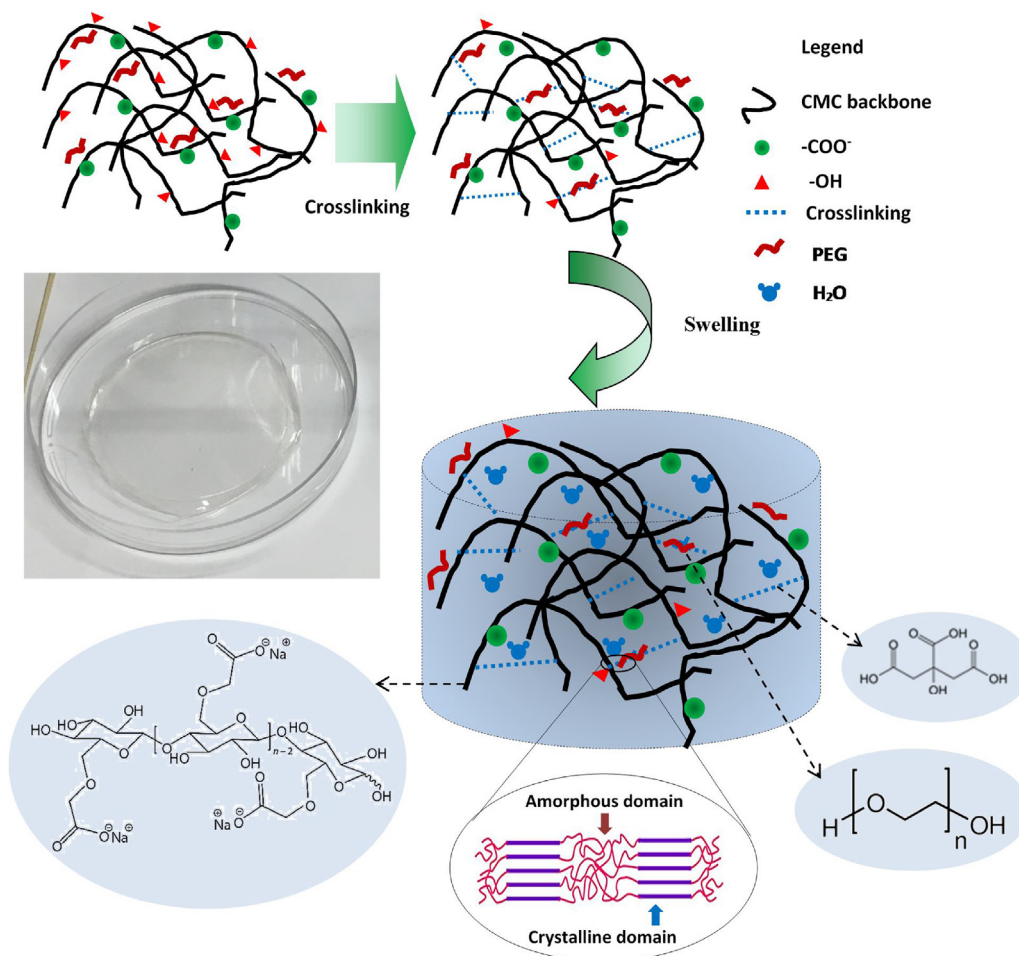
Fig. 4. Representation of the crosslinked hydrogel network. Swollen structure after immersion in water (not to scale).

The cytotoxicity of the samples was evaluated using a standard 3-(4,5-dimethyl-2-thiazolyl)-2,5-diphenyltetrazolium bromide (MTT) assay. Briefly, HEK293T cells on passage 34 were synchronized in serum-free medium for 24 h. After this period, cells were trypsinized and seeded (3×10^5 cells/well) on square samples of hydrogel membranes (4.0×4.0 mm^2 and average thickness $58 \pm 6\,\mu$m) and placed in a 96-well plate. Controls were used with the cells and DMEM with 10% FBS, the positive control with Triton x-100 (1% v/v in PBS, Gibco BRL, USA) and, as a negative control, chips of sterile polypropylene *Eppendorf* tubes (1 mg mL^{-1}, Eppendorf, Germany). After 24 h, all media were aspirated and replaced with 60 μL of culture media containing serum to each well. MTT (5 mg mL^{-1}, Sigma–Aldrich, USA) was added to each well and incubated for 4 h in an oven at 37 °C and 5% CO$_2$. Next, 40 μL SDS (Sigma–Aldrich, USA) solution/4% HCl was placed in each well and incubated for 16 h in an oven at 37 °C and 5% CO$_2$. Then, 100 μL were removed from each well and transferred to a 96-well plate. The absorbance (Abs) was measured at 595 nm on iMark^{TM} Microplate Absorbance Reader (Bio-Rad). Percentage cell viability was calculated according to Eq. (3). The values of the controls (wells with cells, and no samples) were set to 100% cell viability.

(3) Cell viability (%) = (Absorbance of sample and cells/Absorbance of control) × 100%

3. Results and discussion

3.1. Spectroscopic analysis by FTIR and ^{1}H NMR of CMC and PEG

FTIR spectroscopy was used to characterize the CMC and PEG polymers. FTIR spectra of CMC powders with DS = 0.77 and DS = 1.22 are presented in Fig. 1a and b, respectively. FTIR spectrum of PEG is displayed in Fig. 1c. As a general trend common to both polymers (CMC and PEG) it can be observed the broad band in the 3700–3000 cm^{-1} region assigned to νO—H vibrations and the peaks at 3000–2800 cm^{-1} related to νC—H bands. For CMC, it can be observed the major vibrational bands related to carboxylates (COO$^-$) asymmetric (1600 cm^{-1}) and symmetric (1416 cm^{-1} and 1324 cm^{-1}) stretches, overlapped with the band of adsorbed water (1630–1650 cm^{-1}). The acid form of CMC was not detected in the powder sample due to the absence of the characteristic bands of carboxyl groups (—COOH) usually observed at 1715–1730 cm^{-1} and 1240–1250 cm^{-1}, which are assigned to antisymmetric stretching vibration of C=O and C—O stretching, respectively [30,31]. C—O vibrations from primary and secondary alcohols were observed at 1110 cm^{-1} (C2—OH), 1060 cm^{-1} (C3—OH), and 1024 cm^{-1} and 995 cm^{-1} (C6—OH). β1-4 glycoside bonds between glucose units were detected at 898 cm^{-1} [32–36].

The degree of substitution (DS) by carboxymethylation of cellulose is related to the —CH$_2$COOH group that can be attached to every of the three hydroxyl groups of the cellulose monomer unit. Theoretically, the DS value can reach 3 but usually does not exceed 2 [37]. This is an important parameter to characterize because the functionalization render water-soluble and biocompatible cellulose derivative (CMC) with innumerous applications in biology and medicine. FTIR is not only used for characterizing the carboxymethylation of cellulose but also to further evaluate the relative DS values. The band at 1600 cm^{-1} was predominantly associated with the contribution of carboxymethyl groups inserted in the cellulose polymer chain. By taking the ratio of the absorbance of this band (A$_{1600}$) and the reference band of β1-4 glycoside bond at 898 cm^{-1} (A$_{896}$), A$_{1600}$/A$_{898}$, the calculated values were 1.64 ± 0.01 and 1.93 ± 0.03, for CMC 0.77 and CMC 1.22, respectively. Thus, these results indicated that the band at 1600 cm^{-1} is relatively stronger in the CMC with DS = 1.22 due to the higher degree of substitution [38].

For PEG polymer, the bands associated with C—O (alcohol) and C—O—C were observed in the IR spectrum (Fig. 1c) at 1240 cm^{-1} and 1100 cm^{-1}, respectively [39]. In addition, in the CH$_2$ wagging region of the spectrum (1320–1380 cm^{-1}), PEG showed two bands at 1360 cm^{-1} and 1343 cm^{-1}, that characterized the crystalline phase of this polymer [40].

To further investigate the CMC polymers with two degree of substitution (i.e., DS = 0.77 and 1.22), ^{1}H NMR spectroscopy was used as a powerful technique for characterizing polysaccharides such as cellulose and its derivatives and the results are presented in Fig. 2. Carboxymethyl (CM) groups may substitute hydroxyl groups at 2-, 3-, and 6- positions of CMC resulting in eight anhydroglucose rings: unsubstituted (U), 2-mono, 3-mono, 6-mono, 2,3-di, 2,6-di, 3,6-di, and 2,3,6-trisubstituted [37,41]. The signals in the region from 3.5 ppm to 5.0 ppm arise from the C—H protons associated with the C2 to C6 in an anhydroglucose unit (detail in Fig. 2A) and contain important information regarding the substitution in the cellulose backbone. In addition, the chemical shift assignments of unsubstituted and monosubstituted CM groups predominated in the ^{1}H NMR spectrum (Fig. 2), which are supported by the studies of Kono [24,37] and consistent with the low degree of substitution of CMC (DS = 0.77) used in this research. Analogously, the ^{1}H NMR spectrum for CMC with DS = 1.22 presented the equivalent major signals (Fig. 2B), but with the decrease of signals at unsubstituted H2, H3, H5, and H6 positions, which are in agreement with the higher degree of substitution of this cellulose derivative.

3.2. Characterization of CMC hydrogel membranes

3.2.1. Morphological analysis

As a general trend it was observed that uniform and optically transparent membranes were produced before and after crosslinking with increasing concentrations of CA (Fig. 1S – Supplementary Material). In addition, the incorporation of PEG for blending retained the same aspects of the CMC-based hydrogels, without evidences of phase separation (Fig. 2S – Supplementary Material). It was noted that the average thickness of the membranes was reduced by approximately 20% with increasing the concentration of citric acid (CA 25%), which was attributed to combination of the relative reduction of polymer to CA ratio and the crosslinking of polymer chains reducing the volume of hydrogels (i.e., contraction). On the contrary, the addition of PEG promoted the expansion of the volume of hydrogel maybe due to the "spacer effect" of intercalation of PEG between the CMC chains, which was more prominent with DS = 0.77. Regarding to the functionalization of cellulose derivative (CMC), when DS value was increased from 0.77 to 1.22, it was verified an increase of 10–20% of the thickness of the hydrogel. The effect of addition of PEG on the thickness was less evident in
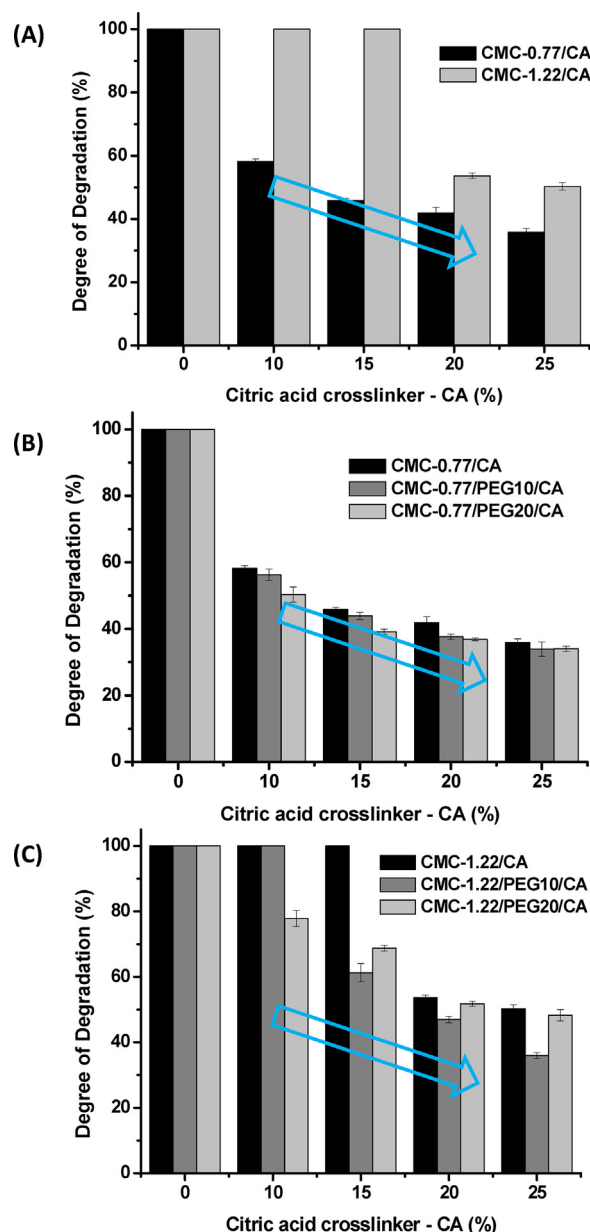

Fig. 5. Histogram of degradation behavior of CMC-based hydrogels with increasing concentration of CA (0%, 10%, 15%, 20%, and 25%). (A) CMC/CA hydrogels; (B) CMC-0.77/PEG/CA and (C) CMC-1.22/PEG/CA hydrogels modified with PEG (10% and 20%).

the crosslinked hydrogel varying from 58 μm to 53 μm for CMC-1.22/CA20 and CMC-1.22/PEG10/CA20, respectively. This trend was mostly attributed to the electrostatic repulsion between negatively charged carboxylate groups balanced by water molecules in the hydrogel network.

3.2.2. In vitro swelling behavior

Swelling measurements are widely used to access the extension of crosslinking of hydrogel networks. Fig. 3A shows the swelling degree (i.e., SD, equilibrium-swelling ratio) of the CMC hydrogels (DS = 0.77 and DS = 1.22) with the gradual increase of the concentration of citric acid crosslinker. It can be observed that, for CMC with DS = 0.77 at lower concentrations of CA (i.e., 10%), superabsorbent hydrogel was produced with SD of over 5000%. However a drastic decrease of SD to approximately 150% was observed at higher concentration of 25% of crosslinker, which evidenced the formation of covalent bonds bridging the functional groups of the polymer
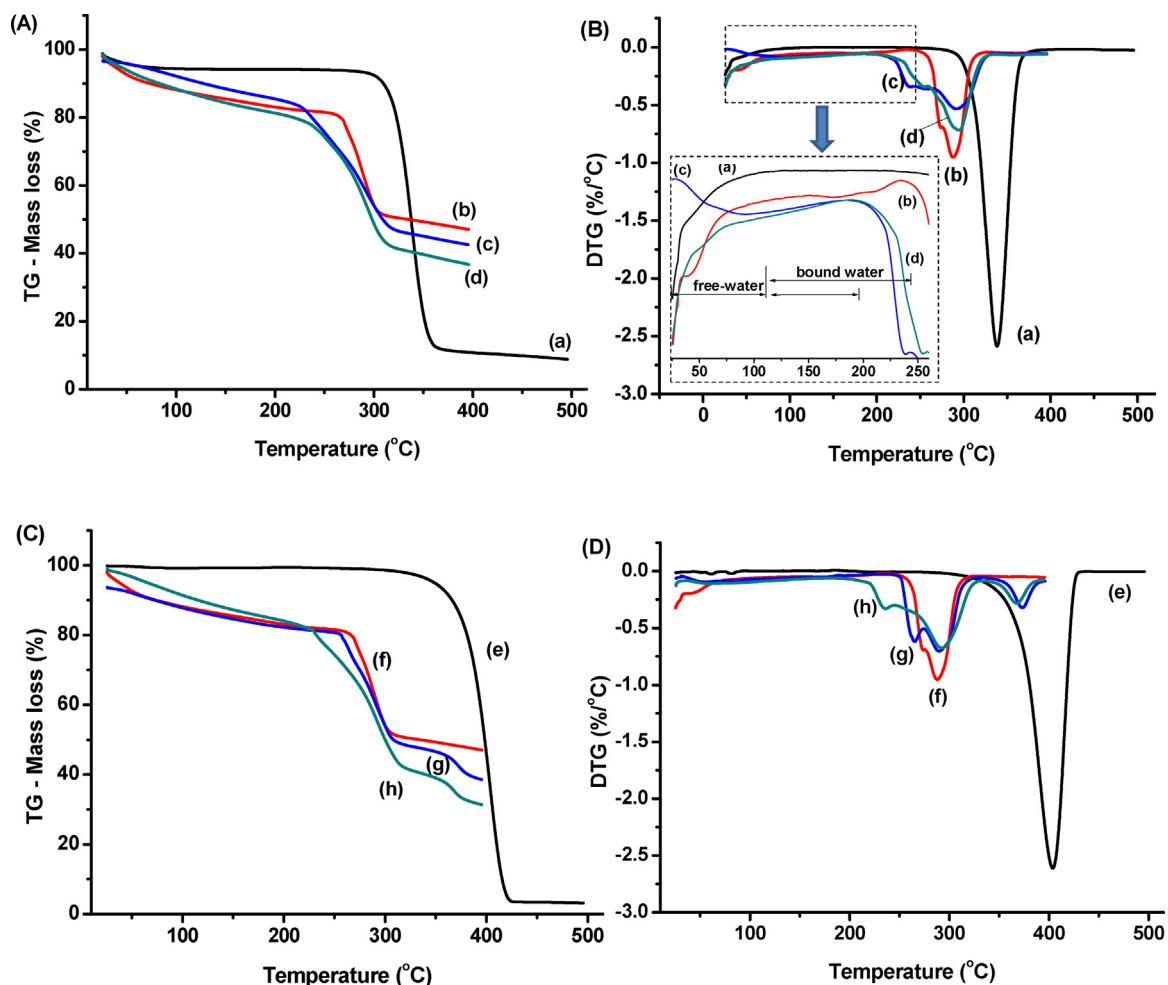
Fig. 6. TG (A,C) and DTG (B,D) curves obtained for pure cellulose (a), CMC-0.77/CA0 (b), CMC-0.77/CA15 (c), CMC-0.77/CA20 (d), pure PEG (e), CMC-0.77/CA0 (f), CMC-0.77/PEG10/CA0 (g), and CMC-0.77PEG10/CA15 (h) samples.

chains and increasing the rigidity of the network. Analogously, for CMC with DS = 1.22 at lower concentrations of CA (10% and 15%) stable hydrogels were not formed and the systems were fully dissolved. At higher concentrations of CA (20% and 25%), superabsorbent hydrogels were formed with the similar trend observed of reduction of the SD as the concentration of crosslinker was increased. So, regarding to the effect of the DS on the swelling behavior, it was verified that the lower concentration of carboxylate groups in the CMC polymer (*i.e.*, DS = 0.77) favored the crosslinking process at low concentration of CA. This behavior was assigned to the fact that the high concentration of carboxylate groups in the CMC (*i.e.*, DS = 1.22) as negatively charged species may have caused the repulsion between adjacent polymer chains, hindering the formation of crosslinking with hydroxyl groups. However, such effect was overcome at higher concentrations of crosslinker (CA), leading to the formation of crosslinked hydrogels comparable to the CMC with DS = 0.77. In Fig. 3B and C, similar patterns were observed when PEG was added to the CMC polymers with DS values of 0.77 and 1.22, respectively. As the concentration of PEG was increased to 10% and 20%, the degree of swelling values were reduced indicating that PEG chains modified the network in the same direction of increasing the concentration of CA crosslinker. Although valid for all concentrations of CA crosslinker, a striking effect was verified on the SD for the CMC hydrogels with 10% PEG. There was a reduction of approximately 3000% of degree of swelling comparing with the CMC samples without addition of PEG with 10% CA (CMC, DS = 0.77) and 15% CA (CMC, DS = 1.22). Thus, the effects of adding CA and PEG

were summed up leading to higher crosslinked networks involving PEG and CMC functional groups producing more rigid hydrogels. These results demonstrated that the CMC hydrogels can have their network structures and physicochemical properties tuned by the concentration of crosslinker and PEG for producing superabsorbent hydrogels (SAP). The schematic representation of CMC-PEG matrix network is depicted in Fig. 4.

Basically, SAP are defined as hydrophilic networks with a high capacity for water uptake, that absorb, swell and retain aqueous solutions up to hundreds of times their own weight (dry sample), which can be tailored for innumerous biomedical applications [42]. The results showed that CMC–based hydrogels produced with a broad range of hydrophilicity (typically from 100 to 5000%) for water incorporation. Hence, they can be potentially suitable for wound dressing and skin tissue substitutes, where the swelling behavior is of paramount importance for promoting a moist microenvironment assisting the wound healing process [9].

3.2.3. In vitro degradation behavior

The degradation of hydrogel plays a crucial role on its performance for potential biomedical applications as the relative degradability will allow the cell diffusion, nutrients flow and the integration with the host tissue. Thus, *in vitro* degradation gravimetric assay was performed using water medium at 25 °C for 24 h as a preliminary evaluation of the chemical stability of the hydrogels and the results are presented in Fig. 5. As expected, the effect of increasing the concentration of CA to CMC hydrogels (DS = 0.77
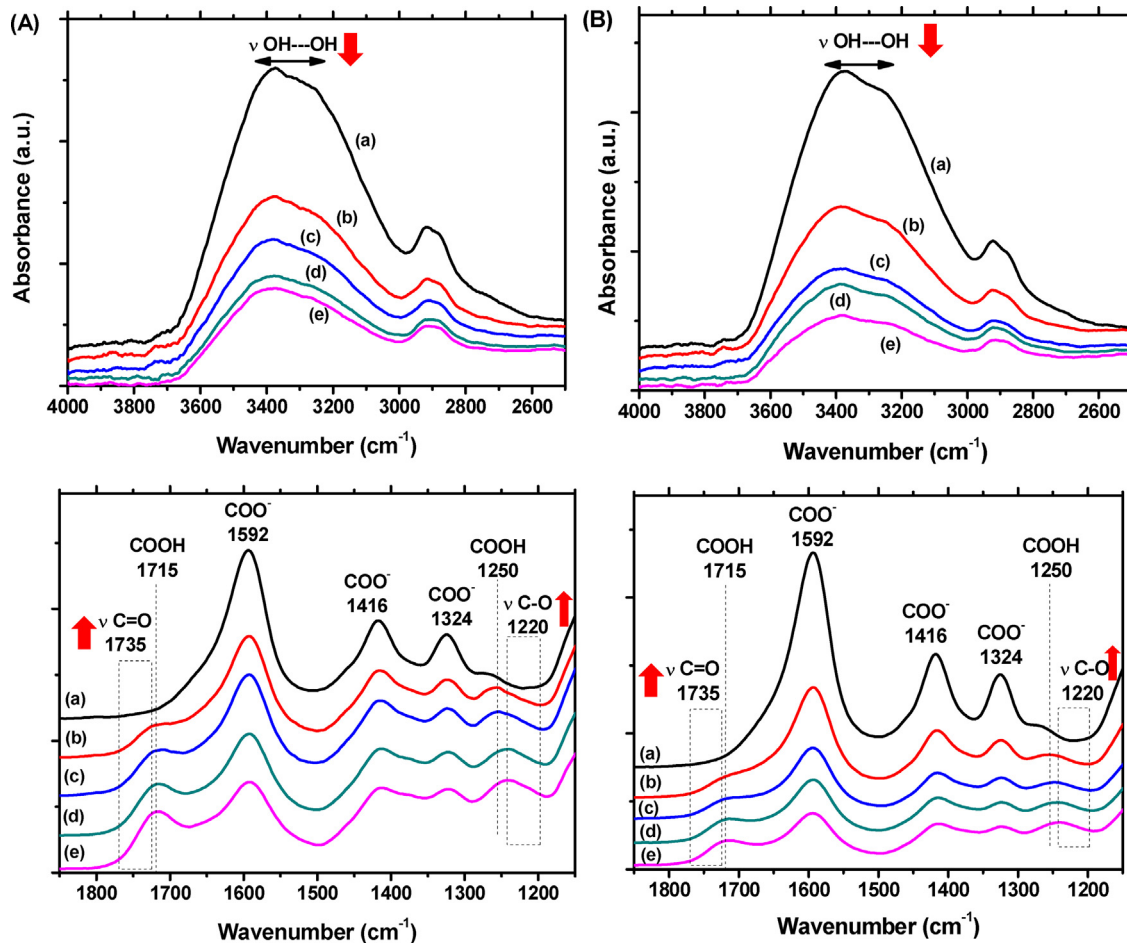
Fig. 7. FTIR spectra of CMC hydrogels (CMC-0.77, left (A) and CMC-1.22, right (B)) not crosslinked (a) and crosslinked with 10% (b), 15% (c), 20% (d), and 25% (e) of CA (m/m, CMC/CA) in the hydroxyl stretching region (4000 cm^{-1}–2500 cm^{-1}) and carbonyl stretching region (1850 cm^{-1}–1150 cm^{-1}).

Table 1
Results of thermogravimetric analysis.

Sample	1st Stage		2nd Stage		3rd Stage		Mass loss at 400 °C [a]
	Temperature range (°C)	Mass loss (%)	Temperature range (°C)	Mass loss (%)	Temperature range (°C)	Mass loss (%)	
Cellulose	25–100 (endo)	5 ± 1	260–390 (exo)	83 ± 2	–	–	88 ± 2
CMC-0.77/CA0	25–230 (endo)	16 ± 1	250–320 (exo)	31 ± 2	–	–	51 ± 2
CMC-0.77/CA15	25–190 (endo)	10 ± 1	200–330 (exo)	39 ± 2	–	–	54 ± 2
CMC-0.77/CA 20	25–190 (endo)	14 ± 1	210–325 (exo)	39 ± 2	–	–	60 ± 2
CMC-0.77/PEG 10/CA0	25–230 (endo)	14 ± 1	240–325 (exo)	34 ± 2	340–395 (endo)	9 ± 1	58 ± 2
CMC-0.77/PEG 10/CA15	25–180 (endo)	14 ± 1	200–325 (exo)	43 ± 2	342–390 (endo)	8 ± 1	68 ± 2
PEG	310–430 (endo)	95 ± 1	–	–	–	–	95 ± 1

[a] 500 °C for cellulose and PEG; (exo: exothermic; endo: endothermic).

and DS = 1.22) on the degradation behavior (Fig. 5A) was opposite to that observed for the degree of swelling, where the higher concentration of crosslinker produced more stable hydrogels (*i.e.*, lower degree of degradation). Consistently to the swelling trend observed in the previous section, a strong reduction of the values of degradation degree were verified at lower concentrations of CA, which dropped from totally soluble without crosslinking (*i.e.*, DD = 100%) to approximately 60% at 10% of CA (CMC-0.77). Further increase of the concentration of CA caused gradual decrease of the degradation degree (DD) but less prominent than at lower concentration (DD = 58% at CA = 10%; DD = 36% at CA = 25%). Similarly, a strong reduction of DD values was verified at lower concentrations of CA with CMC with higher degree of substitution (DS = 1.22), which dropped from practically totally soluble (*i.e.*, DD = 100%) at

10% and 15% of crosslinker to DD = 54% with 20% of CA (Fig. 5A). These results of degradability demonstrated that the degree of substitution (*i.e.*, CM groups) played a key role in the CMC polymer network crosslinked with the tricarboxylic reagent (CA) by affecting the chemical stability of hydrogels. To this end, it can be stated that the CMC hydrogels with DS = 0.77 crosslinked with 10% of CA exhibited the best combination of physicochemical properties regarding to potential skin tissue repair or wound dressing applications. That means, they presented high capacity of absorbing aqueous solutions (*i.e.*, swelling degree ~5000%) combined with moderate degradation of the polymer matrix indicating structural stability. It is important to mention that the degradation observed was predominantly associated with water solvation of the remaining polymer chains, which were not effectively crosslinked forming
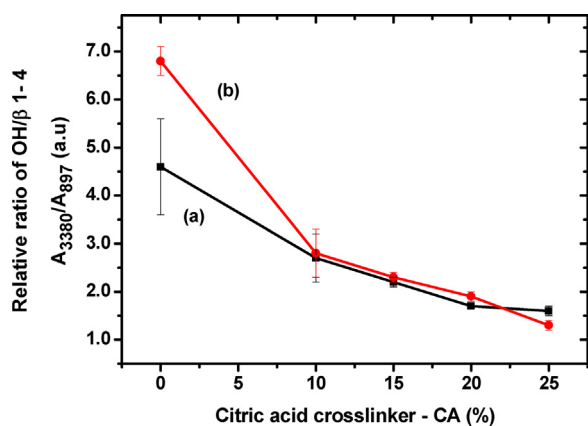
28

Fig. 8. Evolution of hydroxyl vibrational band associated with the crosslinking reaction of CMC by citric acid for CMC-0.77 (a) and CMC-1.22 (b).

the CMC hydrogel network. No polymer degradation related to chain scission is expected to occur under the light experimental conditions used in this study [11].

Regarding to the addition of polyethylene glycol (PEG) to produce hydrogel blends (CMC-PEG), it was observed that PEG improved the chemical stability of the hydrogels as the degradability was reduced, although the effect was less prominent than increasing the CA concentration (Fig. 5B and C). This trend was similar to that observed in the swelling measurements, where PEG acted as bridging agent between CMC polymer chains, which has caused an enhancement of the crosslinking effect. Therefore, the addition of PEG to CMC in the presence of the citric acid crosslinker agent caused the formation of hybrid polymer hydrogels. These hybrids can offer several promising soft materials for wound repair and skin substitutes considering their tunable physicochemical and biological properties, as PEG is known to affect essential biological functionalities including protein adsorption, cell adhesion, immunological response, and others [43].

3.2.4. Thermal analysis

Thermal analysis was used for further accessing the modification of polymeric network by the degree of crosslinking and blend with PEG. Fig. 6A and B exhibit primary thermograms (TG) and derivative thermograms (DTG) for pure cellulose (a), pure CMC (DS = 0.77, b), and CMC crosslinked with CA 15% (c) and 20% (d). For cellulose, two major thermal events were observed. Below 110 °C, a minor mass loss (∼2%) is attributed to desorption of free water from polysaccharide. The second event started at approximately 290 °C and it is completed at approximately 380 °C with mass loss of 85% and corresponds to the decomposition, vaporization and elimination of volatile products.

For pure CMC and crosslinked hydrogel structures, two stages were also observed (Table 1). The first stage is related to water loss and it can be separated in two steps: removal of free water (below 110 °C) and vaporization of bound water tightly attached to polymer matrix (below 240 °C) as showed in the detail in Fig. 6B. The introduction of sodium carboxymethyl groups (Na$^+$/CM$^-$) increased the water absorption of the derivative in comparison to cellulose due to the formation of hydrogen bonds between these hydrophilic polar groups with water molecules [44–46]. For the crosslinked hydrogels in comparison to non-crosslinked, it was observed the reduction of the mass loss associated with water removal and a narrow range of temperature associated with this event. According to the literature [22], CMC crosslinking with CA occurred with consumption of hydroxyl groups resulting in a smaller number of hydrophilic groups available to interact with the water molecules. The second stage is the exothermic degra-
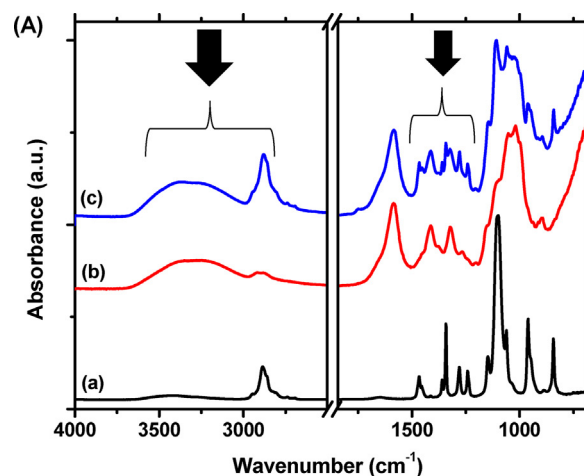

Fig. 9. FTIR spectra of pure PEG (a), pure CMC (b) and non-crosslinked CMC-PEG blends (c) for CMC-0.77 (A) and CMC-1.22 (B).

dation of the polymeric chains (Fig. 3S – Supplementary Material). CMC and crosslinked hydrogels presented a lower thermal stability than neat cellulose clearly observed by the shift of the temperature range of degradation as a result of different interactions between polymeric chains. Cellulose presents a parallel association of chains leading to a supramolecular organization in microfibrils based on intra- and intermolecular hydrogen bonds between hydroxyl groups. Carboxymethylation disrupts the higher order of cellulose polymeric packing by both steric hindrance and electrostatic repulsion lowering the thermal stability. Moreover, the esterification reaction associated with crosslinking can reduce the number of remaining hydrogen bonds of CMC leading to an even lower degradation temperature of crosslinked hydrogels [44–47]. However, as an increase of ester reactions is expected with higher amounts of CA, it was observed a relative increase of the thermal stability for CMC-0.77/CA20 compared to CMC-0.77/CA15. Based on Table 1, it can be also observed that cellulose, despite being more resistant to heat, rapidly decomposed leaving a small amount of residue (approximately 12%). On the contrary, the remaining mass for CMC membranes was about 40–50% attributed to the formation of sodium containing species (Na$_2$CO$_3$ and Na$_2$O) [47]. DSC curves (Fig. 3S – Supplementary Material) were in agreement with the thermal events detected by thermogravimetric analysis.

Thermogravimetric study of pure PEG (Fig. 6C and D, curves (e)) indicated the occurrence of only one major thermal event with mass loss at the temperature ranging from 310 to 430 °C leading to the total degradation of the polymer, as previously reported

29
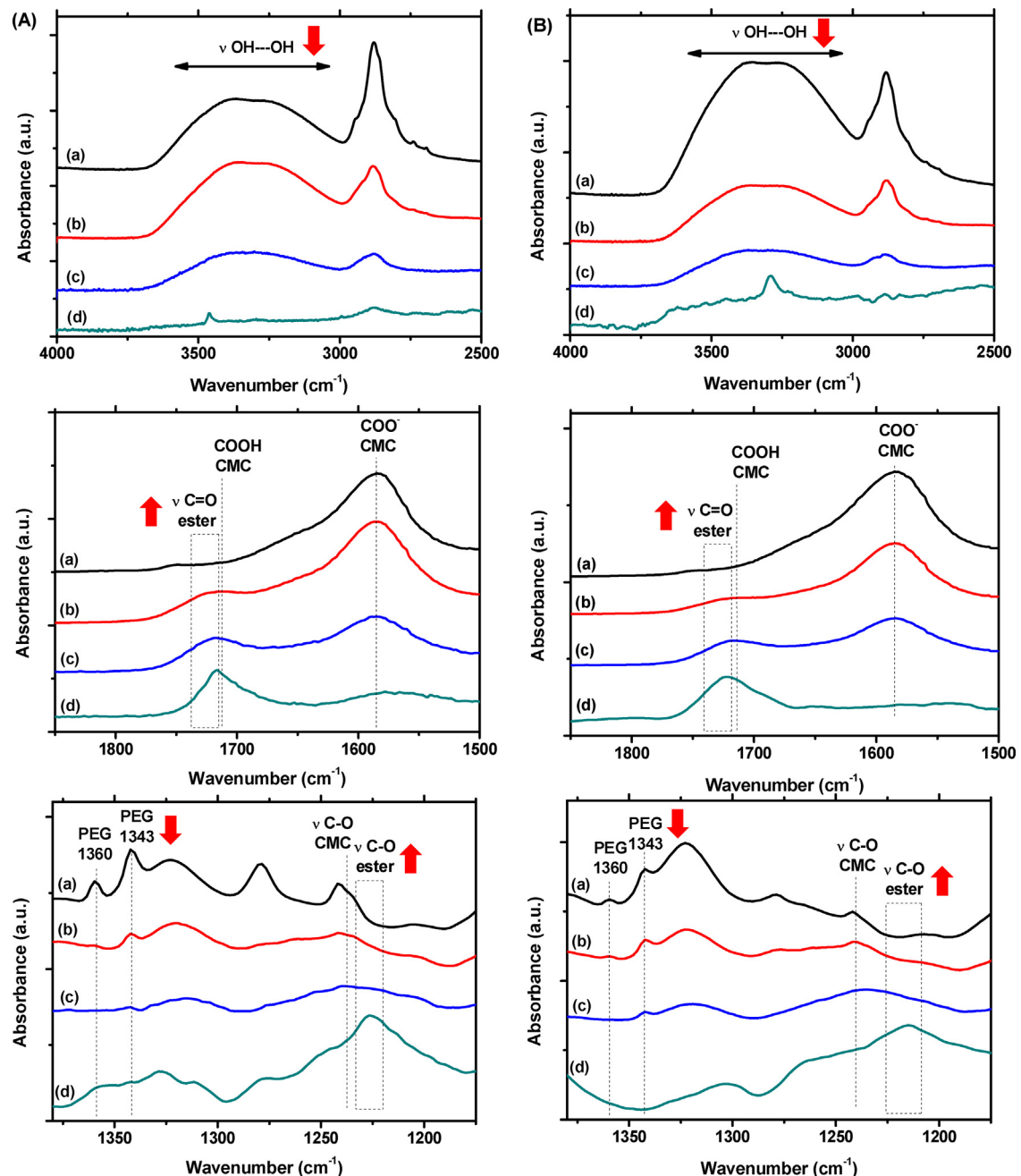
Fig. 10. FTIR spectra of CMC-PEG blends (CMC-0.77, left (A) and CMC-1.22, right (B)) not crosslinked (a) and crosslinked with 10% (b), 20% (c), and 25% (d) of CA (m/m, CMC/CA) in the range of 4000 cm^{-1}–2500 cm^{-1}, 1850 cm^{-1}–1500 cm^{-1}, and 1380 cm^{-1}–1175 cm^{-1}.

in literature [44]. Based on DSC curves (Fig. 4S – Supplementary Material), for CMC-PEG systems (Fig. 4S(c) and (d) – Supplementary Material), the absence of the endothermic peak associated with the melting of PEG at approximately 50 °C (Fig. 4S(a) – Supplementary Material) evidenced the miscibility of PEG (M_w = 1,500 g mol^{-1}) and CMC polymer chains at the molecular level [48], which was attributed to the strong interactions of several functional groups of both molecules.

The TG and DTG curves of CMC-PEG hydrogels (Fig. 6C and D, curves (g) and (h)) were similar to those observed for CMC membranes (with or without crosslinking) with a mass loss essentially associated with water removal from room temperature up to 180–230 °C followed by polymer degradation. However, for PEG modified hydrogels, the decomposition process occurred in two main steps, one exothermic, in the range of CMC degradation, and

other endothermic, near to pure PEG (Fig. 4S – Supplementary Material). These peaks are shifted in comparison with pure CMC and PEG components, as a result of interactions between these two polymers. The incorporation of PEG also reduced the thermal stability of the CMC polymer, as a result of the overall balance of the physical and chemical interactions between these polymer chains. In addition to all the possibilities discussed for CMC and CA, the incorporation of PEG increased the total amount of −OH groups available for esterification reaction, besides the interactions between terminal hydroxyls and C−O−C of PEG with −OH of CMC.

3.2.5. FTIR spectroscopy analysis

FTIR spectroscopy was used to monitor the crosslinking of CMC by CA with the results presented in Fig. 7A (DS = 0.77) and Fig. 7B (DS = 1.22). The FTIR spectra of CMC crosslinked hydro-

30
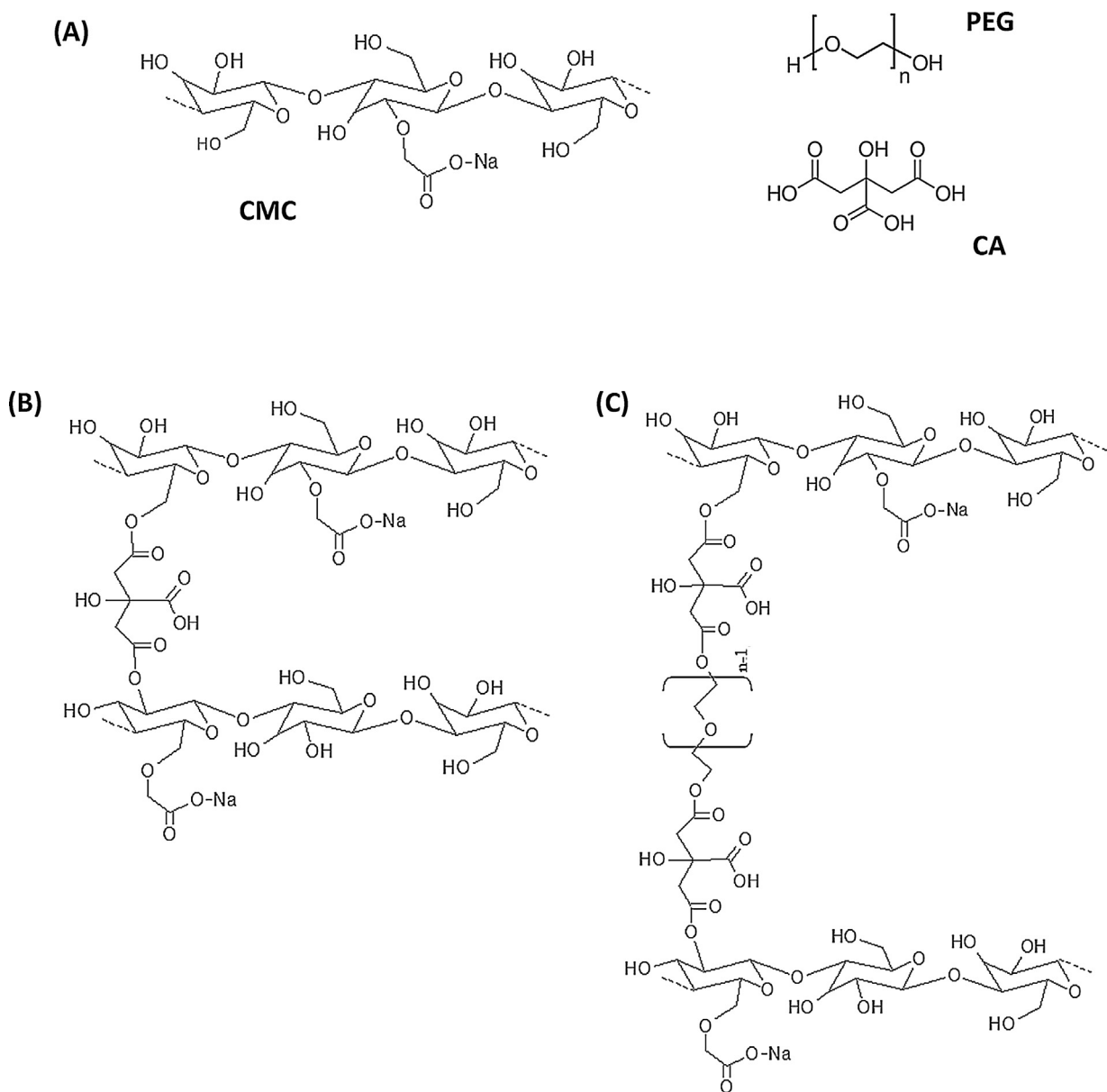
Fig. 11. Schematic representation of: (A) polymers (CMC, PEG) and citric acid crosslinker; crosslinked structures of (B) CMC and (C) CMC-PEG.

gels demonstrated that carboxylates (—COO⁻ bands at 1592 cm⁻¹, 1416 cm⁻¹ and 1324 cm⁻¹) and carboxylic acid (—COOH bands at 1730 cm⁻¹ and 1243 cm⁻¹) co-existed in the CMC hydrogel due to the substitution of Na⁺ by H⁺ in the CMC polymer chains during the acidification promoted by citric acid. Crosslinked cellulose hydrogels showed a relative decrease of intensity of —OH peak at approximately 3400–3200 cm⁻¹, which was verified by the ratio of the of absorbance at 3380 cm⁻¹ (A_{3380}), related to stretching vibration of OH forming hydrogen bonding, and the reference band at 896 cm⁻¹ (A_{896}) of β1-4 glycoside bond. Fig. 8 showed the depletion of hydroxyl groups of CMC during the crosslinking due to the chemical reaction with citric acid forming ester bonds, as reported in the literature [8,22]. Although not quantitative, the relative higher ratio of hydrogen bonded hydroxyl groups of CMC with DS = 1.22 in comparison to DS = 0.77 was associated with the higher concentration of polar ionizable carboxylic moieties (CM) incorporated to the cellulose backbone [41]. In addition, the increased vibration at 1230–1205 cm⁻¹ in the crosslinked hydrogels was ascribed to νC—O of ester bonds formed. Moreover, the relative

increase of the stretching vibration band of νC=O at approximately 1730–1715 cm⁻¹ indicated changes of ester bonds as a result of the crosslinking reaction [49,50]. However, these changes in the FTIR spectra are more difficult to quantify as the reaction progressed due to overlapping with carboxylic bands of CMC.

Analogously, FTIR spectra of hydrogels physically and chemically modified by the incorporation of PEG are showed in Fig. 9 in comparison with the spectra of neat polymers. FTIR spectra of PEG and CMC presented the fingerprint typical of these polymers where major functional groups described in Section 3.1 were detected. The addition of PEG to CMC promoted the formation of hydrogels predominantly stabilized *via* hydrogen bonds between functional groups of both polymers (*i.e.*, PEG: C—O—C and —OH; and CMC: —OH and C=O), which was verified by the significant increase of the vibrational signals of hydroxyl groups from 3000 to 3600 cm⁻¹. Therefore, the FTIR spectra indicated the formation of hydrogels with hybrid structures composed of an amorphous phase mostly assigned to CMC polymer chains and intercalated with semi-crystalline domains of PEG stabilized by hydrogen bond-

31
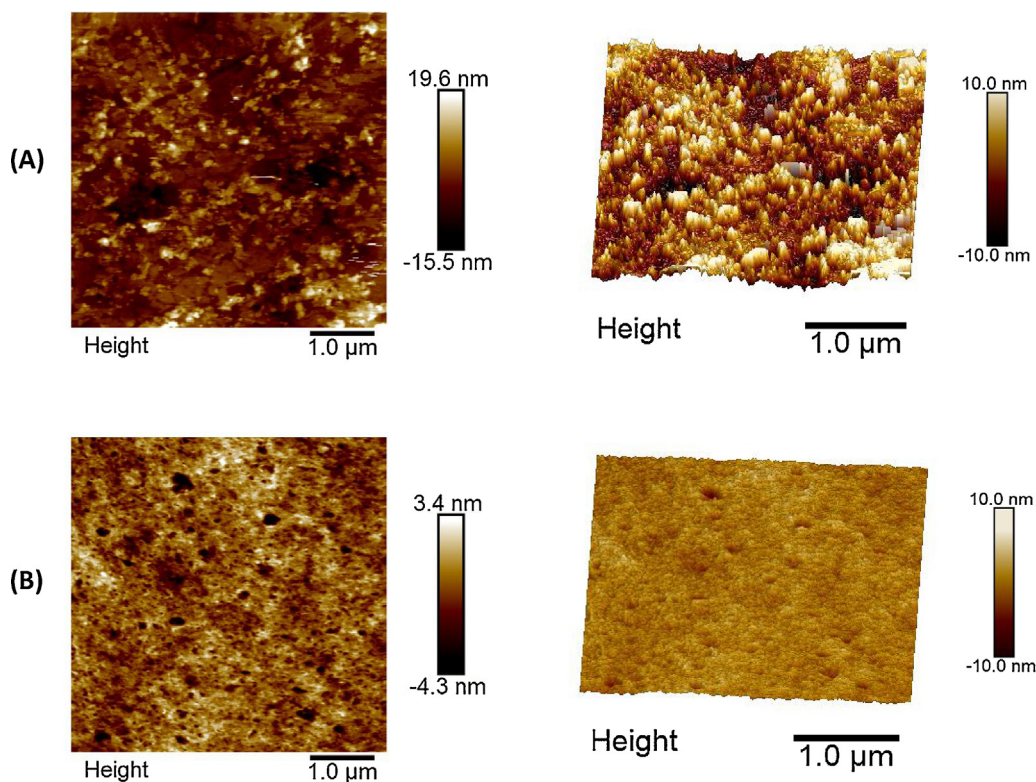
Fig. 12. 2D (left, 5 μm × 5 μm scanning area) and 3D (right, 3 μm × 3 μm scanning area) AFM topographical images of non-crosslinked (A, CMC-0.77/CA0) and crosslinked (B, CMC-0.77/CA20) hydrogels.

ing. This effect was more pronounced by the significant reduction of the peaks as $1360\,cm^{-1}$ and $1343\,cm^{-1}$ associated with PEG crystallinity [40] indicating its higher miscibility in the CMC with DS = 1.22 compared to DS = 0.77.

Considering the esterification reaction between alcohols and carboxylic acids (Eq. (4)), it is expected that the crosslinking reactions between citric acid with CMC-PEG would reduce the hydroxyl groups and increase the ester signal. Therefore, crosslinked CMC-PEG hydrogels (Fig. 10) showed significant decrease of the hydroxyl band at $3200–3600\,cm^{-1}$ with increasing citric acid content. Moreover, the R1—COO—R bands at $1230–1205\,cm^{-1}$ ($\nu C—O$) and $1730–1715\,cm^{-1}$ ($\nu C=O$) increased due to the formation of ester groups, which were very pronounced with CA content of 25%. However, it should be stated that the analysis at this region of the FTIR spectra is very complex because different groups are simultaneously formed and consumed in the reaction. In addition, it is also affected by pH such as the protonation of carboxymethyl groups of CMC by adding citric acid ($RCOO^-/RCOOH$). Therefore, the intensities of these bands are not direct indication of the extension of crosslinking because other interactions can be overlapped in the same region of IR spectrum. It can be observed an increase of miscibility of PEG as the crosslinking reaction progressed: the peaks associated with its crystallinity ($1360\,cm^{-1}$ and $1343\,cm^{-1}$) disappeared for the crosslinked blends and the intensity of the other bands of PEG were also reduced. Hence, compared to CMC, the addition of PEG enhanced the crosslinking most likely due to the presence of its hydroxyl groups stabilizing the polymeric network. Besides, more importantly, the insertion of (nano)crystalline portion of PEG small molecules between CMC chains allowed inter- and intrachain physical crosslinking. These structures made of CMC and CMC-PEG with CA crosslinker are represented in Fig. 11.

$$R - COOH + H - OR' \overset{H^+}{\leftrightarrow} R - COOR'HO \qquad (4)$$

3.2.6. Morphological analysis and nanomechanical properties with AFM

Nanotopographical and nanomechanical analyses were performed as additional characterization techniques to evaluate the CMC hydrogels. AFM images of non-crosslinked (CMC-0.77/CA0) and crosslinked (CMC-0.77/CA20) CMC hydrogels are presented in Fig. 12. The non-crosslinked sample (Fig. 12A) exhibited a coarse morphology with granular features that became significantly refined after crosslinking suggesting a more uniform organization of polymeric chains (Fig. 12B).

The effects of degree of substitution and addition of PEG in the morphology and mechanical properties were also evaluated. In Fig. 13 are displayed representative 2D and 3D topographic AFM micrographs of the CMC and CMC-PEG blend crosslinked samples, with two degree of substitution of CMC. All samples showed an interconnected granular morphology characteristic of crosslinked polysaccharide and CMC-PEG hydrogels due to the formation of the covalent bonded hybrid hydrogel network [51]. As previously discussed in the FTIR analysis, this result is consistent with the formation of alternated amorphous-crystalline domains in the CMC-PEG matrices stabilized by hydrogen bonds. CMC-1.22 hydrogels presented smoother surface (i.e., more amorphous) compared to CMC-0.77 membranes once the formation of aggregates was favored by the lower DS caused by intra- and intermolecular hydrogen bonds occurring between hydroxyl groups. In the case of the crosslinked CMC-PEG hydrogels, these aggregate features were even more evident, probably as the result of the strong influence of the hydrogen bonds between functional groups of PEG and polar groups of CMC polymer (—OH and —COO$^-$).

At this point, it is important to highlight that, beyond the interpretation of these results from a materials chemistry approach, this study focused on developing innovative hydrogels for wound dressings and skin substitutes where some background on this multidisciplinary field is required. Thus, the skin is the largest organ
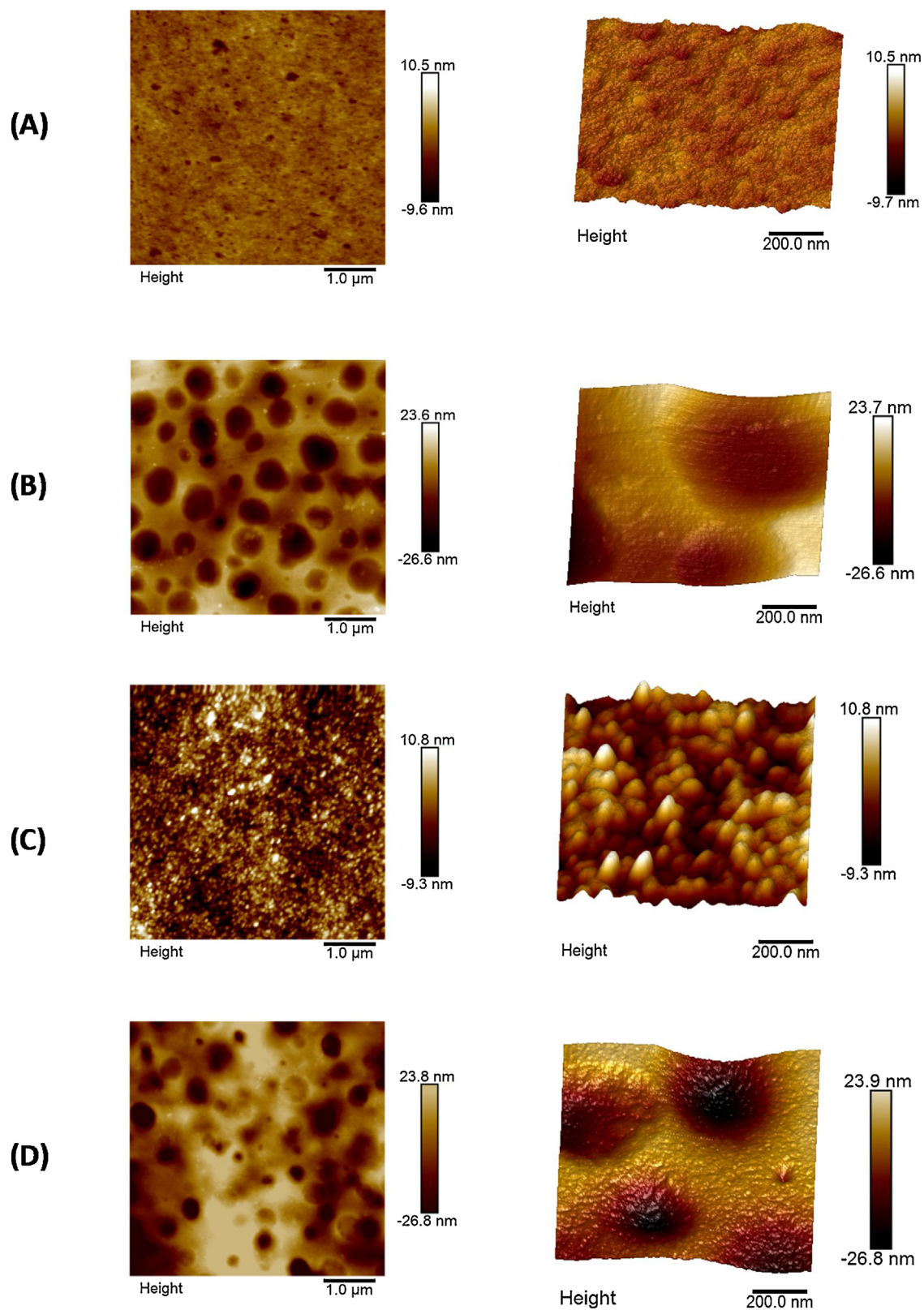
Fig. 13. 2D (left, 5 μm × 5 μm scanning area) and 3D (right, 1 μm × 1 μm scanning area) AFM topographical images of CMC-0.77/CA15 (A), CMC-1.22/CA15 (B), CMC-0.77-PEG10/CA15 (C), and CMC-1.22/PEG10/CA15 (D).

in the body and it fulfils several functions, most importantly as a barrier separating the internal organs of the body and the external environment. Hence, the physical sturdiness of skin is critical to perform this function to resist the many mechanical, chemical and biological harmful organisms from the outside world. However, wound healing can be restricted by diseases and metabolic disorders where the mechanical environment of the wound site is also of fundamental importance for the rate and quality of wound

33
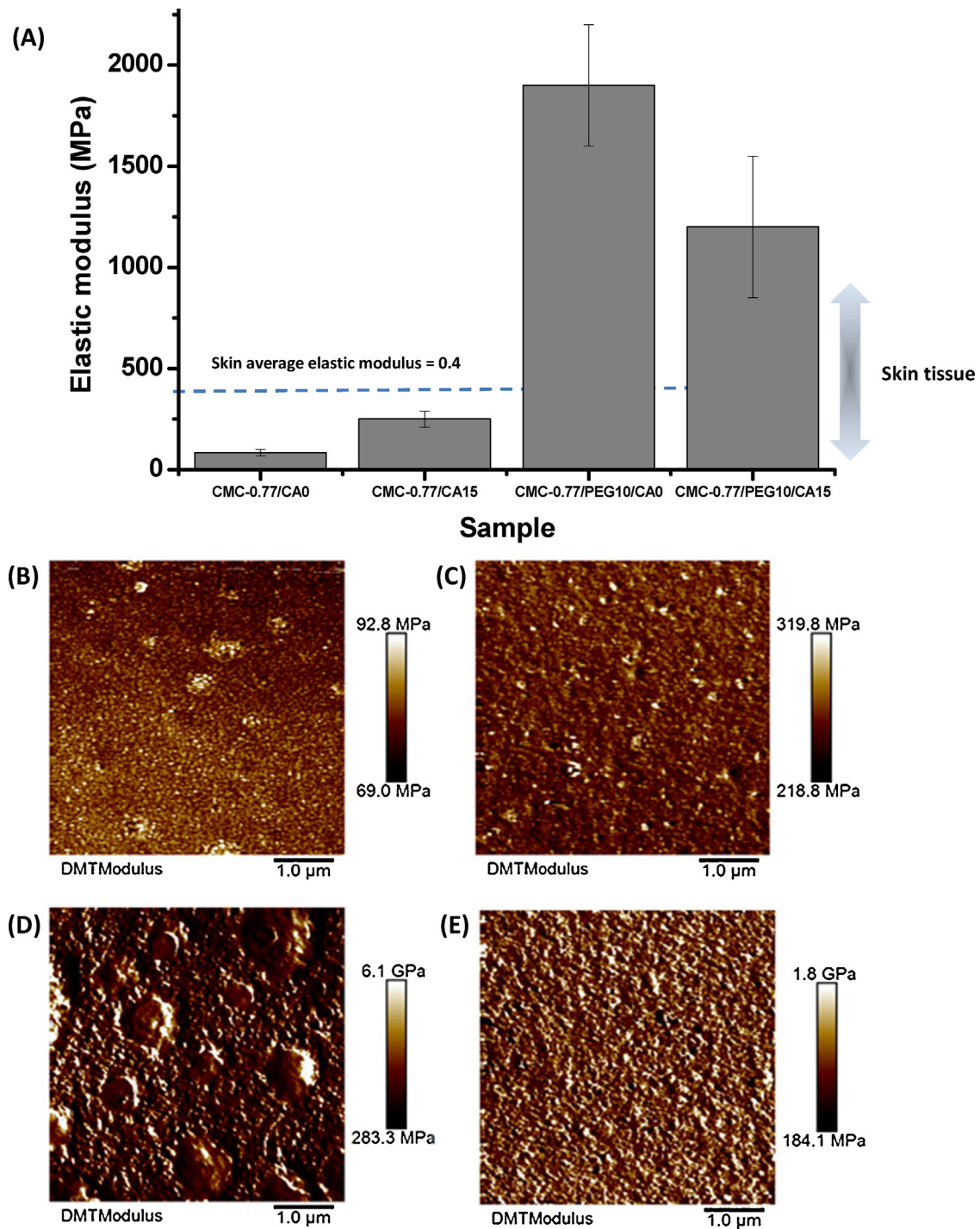
Fig. 14. Histogram of average values of Elastic *Moduli* (A) and maps obtained by Tapping Mode (Peak Force) on the non-crosslinked (CMC-0.77/CA0 (B) and CMC-0.77/PEG10/CA0 (D)) and crosslinked (CMC-0.77/CA15 (C) and CMC-0.77/PEG10/CA15 (E)) hydrogels.

healing. The elastic *moduli* of the skin have been showed to vary in a very broad range from less than 0.001 GPa to approximately 2.0 GPa (*i.e.*, a factor of over 2000). This behavior is assigned to several factors including the method of measurement, temperature, humidity, anatomical location, hydration level, complex anisotropic structure and others [52–54]. Therefore, it is inappropriate to quote a single value for this parameter related to elastic *moduli* of skin. Recently, an average value of 0.4 GPa was reported using AFM by force indentation measurements [55].

In this study, elastic *moduli* (E_M) were evaluated using the characterization method of AFM referred to as "quantita-

tive nanoscale mechanical technology" (QNM maps, PeakForce Tapping®) (Fig. 14), which permitted to compare the effects of crosslinking and PEG-modification of CMC on the stiffness of the hydrogels. The elastic *moduli* of CMC membranes increased by approximately 300%, from 83 ± 15 MPa (CMC-0.77/CA0) to 250 ± 40 MPa (CMC-0.77/CA15), after crosslinking with 15% CA. These findings are supported by the previous results that the chemical crosslinking increased the rigidity of the hydrogel network and reduced the swelling capacity. Analogously, in the case of CMC-PEG hydrogel blends, for the physical hydrogel (uncrosslinked, CMC-0.77/PEG10/CA0) an average stiffness of

34
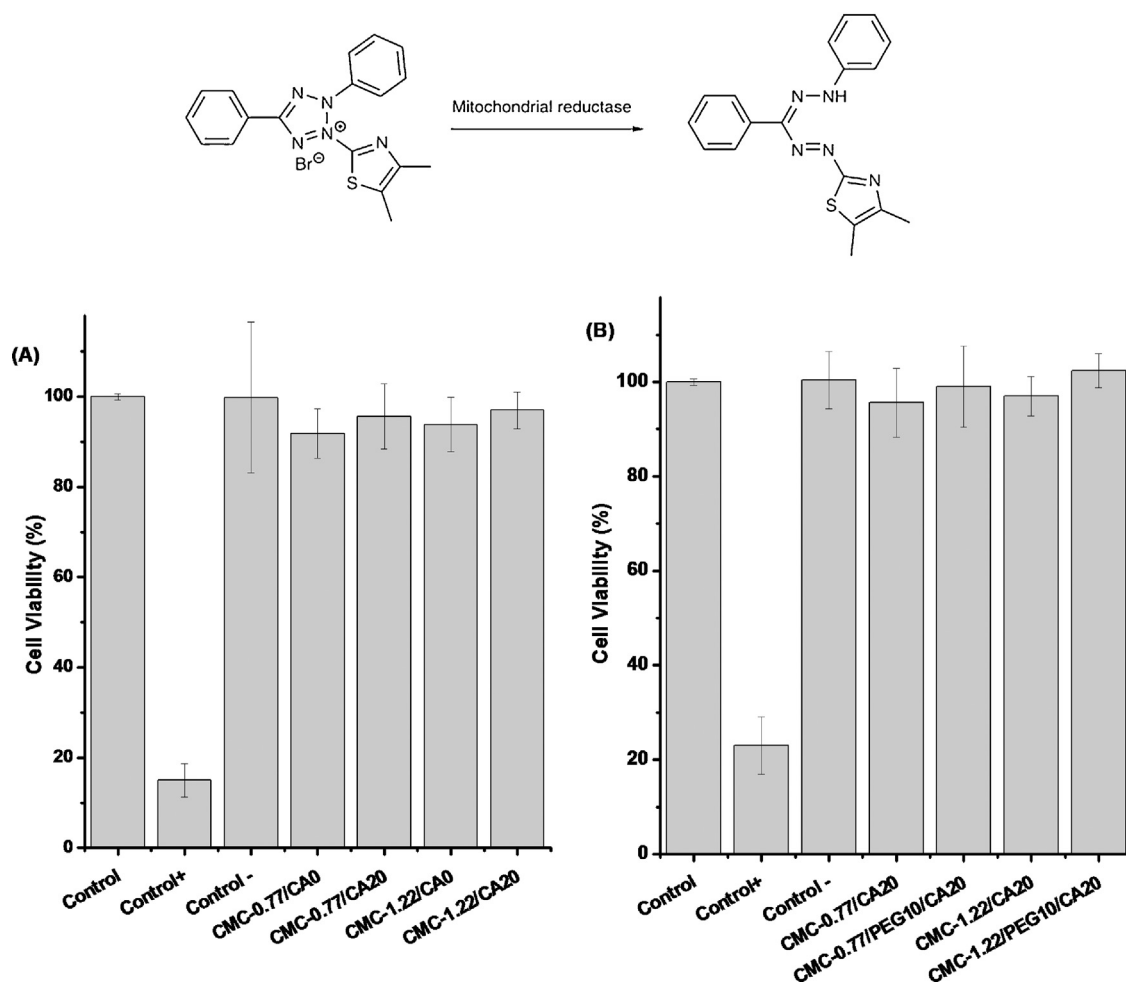
Fig. 15. Cell viability response of HEK293T culture based on MTT assay after 24 h incubation for (A) CMC hydrogels (DS = 0.77 and 1.22) with no crosslinker (CA 0%) and crosslinker (CA 20%) and (B) CMC hydrogels (DS = 0.77 and 1.22) without PEG and with 10% PEG modifier crosslinked with 20% CA.

1900 ± 300 MPa was measured and after the chemical crosslinking (i.e., 15% CA, CMC-0.77/PEG10/CA15) a relevant reduction of stiffness (1200 ± 350 MPa) was observed. As discussed in the previous sections of FTIR spectroscopy and swelling measurements, these results of surface nanomechanical properties demonstrated that there was a drastic effect of the addition of PEG to CMC hydrogels, where the elastic *moduli* increased by over 2 orders of magnitude i.e., from approximately 0.08 GPa (CMC) to 1.9 GPa (CMC-PEG). This effect was accounted to the presence of crystalline and amorphous domains associated with the insertion of PEG chains in the CMC matrix leading to the formation of CMC-PEG hybrid nanostructures. In summary, these results of nanomechanical properties (E_M) associated with the swelling and degradation measurements demonstrated that these innovative CMC and CMC-PEG hydrogels are appropriate for potential applications as wound dressings and skin substitutes.

3.3. Biological characterization of CMC hydrogels

The cytocompatibility of the hydrogel membranes was characterized in vitro through MTT assays, to further validate their potential to be applied in the biomedical field as wound dressings and skin repair materials [56–58]. Human embryonic cells (HEK293T) were used as a model line because they share similarities with epidermal skin cells (e.g., keratinocytes, dermal fibroblasts), which are involved in the wound healing and tissue repairing [56–58]. Therefore, the cytotoxicity of the CMC hydro-

gels, crosslinked with CA and modified with PEG, was evaluated based on the cell viability of HEK293T using direct contact method of MTT assay. This test evaluates the mitochondrial function and cell viability and it is widely accepted as a preliminary assessment of toxicity of biomaterials for potential applications according to the international standard (ISO 10993-5:2009/(R)2014, Biological evaluation of medical devices: Tests for in vitro cytotoxicity). However, it is not recommend to directly extrapolating the response of cell culture in vitro to consider the material health and environmentally safe [58,59].

Fig. 15A shows that hydrogels produced with CMC (DS = 0.77 and 1.22) before and after crosslinking with CA 20% induced no cytotoxic effects, as there were cell viability responses of over 95%, similar to the reference control condition (100%, within statistical variation). Analogously, Fig. 15B shows the cytocompatibility of HEK293T cells towards CMC and CMC-PEG hydrogels. Despite the differences in the morphological features and physicochemical properties of the CMC-based hydrogels characterized in the previous sections, they all demonstrated equivalent cytocompatibility toward HEK293T cells. This fact was attributed to the high biocompatibility of CMC and PEG polymers widely applied in biomedical field favoring the mitochondrial cell activity. Moreover, the choice of using citric acid as the crosslinker for modifying the hydrogel network was based on the fact that it is a natural compound abundantly found in fruits and therefore, eco-friendly and biocompatible. Therefore, based on the aforementioned results and discussion, these CMC-based hydrogels presented physicochemi-

cal properties and *in vitro* cytocompatibility suitable for prospective applications in wound healing and as skin tissue substitutes.

4. Conclusions

In this study, we focused on the synthesis and comprehensive characterization of eco-friendly and biocompatible hydrogel membranes based on carboxymethyl-functionalized cellulose derivative chemically crosslinked by citric acid (CA) and modified with PEG strictly using green aqueous process for wound dressing and skin substitutes. The results demonstrated that superabsorbent hydrogels (SAP) were produced with tailored degree of swelling, ranging from 100% to 5000%, depending on the degree of substitution of CMC, the extension of crosslinking with CA and addition of PEG. The swelling and degradation measurements, FTIR, SEM and AFM analyses evidenced physicochemical properties and morphological features, which were used for understanding the mechanism involved in the crosslinking process forming the hydrogel matrices. These hydrogels presented no cytotoxicity based on over 95% of cell viability responses (HEK297T) using *in vitro* MTT assay. Therefore, SAP hydrogels were designed and produced with properties that are tunable through the extension of crosslinking with the ability to absorb large amounts of water while maintaining the small degradability of the matrices. To this end, they are envisioned as promising superabsorbents hydrogels with key properties for assisting skin wound healing and regeneration, particularly the emerging role of hydrogels as the next generation skin substitutes for the treatment chronic wounds.

Conflicts of interest

The authors declare that they have no competing interests.

Author contributions

The manuscript was written through contributions of all authors. All authors have given approval to the final version of the manuscript

Acknowledgments

Appendix A. Supplementary data

Supplementary data associated with this article can be found, in the online version, at http://dx.doi.org/10.1016/j.ijbiomac.2017.08.124.

References

[1] C.G. Geoffrey, S. Werner, Y. Barrandon, M.T. Longaker, Wound repair and regeneration, Nature 453 (2008) 314–321.

[2] P. Martin, Wound healing – aiming for perfect skin regeneration, Science 276 (1997) 75–81.

[3] J.T. Neill, S.F. Badylak, The use of biologic scaffolds in the treatment of chronic nonhealing wounds, Adv. Wound Care 4 (2015) 490–500.

[4] M. Madaghiele, C. Demitri, A. Sannino, L. Ambrosio, Polymeric hydrogels for burn wound care: advanced skin wound dressings and regenerative templates, Burns Trauma 2 (2014) 153–161.

[5] K. Izadi, P. Ganchi, Chronic wounds, Clin. Plast. Surg. 32 (2005) 209–222.

[6] M.P. Lutolf, J.A. Hubbell, Synthetic biomaterials as instructive extracellular microenvironments for morphogenesis in tissue engineering, Nat. Biotechnol. 23 (2005) 47–55.

[7] C. Yang, L. Xu, Y. Zhou, X. Zhang, X. Huang, M. Wang, Y. Han, M. Zhai, S. Wei, J. Li, A green fabrication approach of gelatin/CM-chitosan hybrid hydrogel for wound healing, Carbohydr. Polym. 82 (2010) 1297–1305.

[8] C. Demitri, R. Del Sole, F. Scalera, A. Sannino, G. Vasapollo, A. Maffezzoli, L. Ambrosio, L. Nicolais, Novel superabsorbent cellulose-based hydrogels crosslinked with citric acid, J. Appl. Polym. Sci. 110 (2008) 2453–2460.

[9] B.K. Sun, B. Siprashvili, P.A. Khavari, Advances in skin grafting and treatment of cutaneous wounds, Science 346 (2014) 941–945.

[10] C. Blanpain, Stem cells: skin regeneration and repair, Nature 464 (2010) 686–687.

[11] I.C. Carvalho, H.S. Mansur, Engineered 3D-scaffolds of photocrosslinked chitosan-gelatin hydrogel hybrids for chronic wound dressings and regeneration, Mater. Sci. Eng. C 78 (2017) 690–705.

[12] G.D. Mogoşanu, M.A. Grymezescu, Natural and synthetic polymers for wounds and burns dressing, Int. J. Pharm. 463 (2014) 127–136.

[13] Y. Zhang, Q. Dang, C. Liu, J. Yan, D. Cha, S. Liang, X. Li, B. Fan, Synthesis characterization, and evaluation of poly(aminoethyl) modified chitosan and its hydrogel used as antibacterial wound dressing, Int. J. Biol. Macromol. 102 (2017) 457–467.

[14] Q. Dang, K. Liu, Z. Zhang, C. Liu, X. Liu, Y. Xin, X. Cheng, T. Xu, D. Cha, B. Fan, Fabrication and evaluation of thermosensitive chitosan/collagen/α, β-glycerophosphate hydrogels for tissue regeneration, Carbohydr. Polym. 167 (2017) 145–157.

[15] Q.F. Dang, H. Liu, J.Q. Yan, C.S. Liu, Y. Liu, J. Li, J.J. Li, Characterizations of collagen from haddock skin and wound healing properties of its hydrolysates, Biomed. Mater. 10 (2015) 015022.

[16] W.J. Zheng, J. Gao, Z. Wei, J. Zhou, Y.M. Chen, Facile fabrication of self-healing carboxymethyl cellulose hydrogels, Eur. Polym. J. 72 (2015) 514–522.

[17] A.T. Reza, S.B. Nicoll, Characterization of novel photocrosslinked carboxymethylcellulose hydrogels for encapsulation of nucleus pulposus cells, Acta Biomater. 6 (2010) 179–186.

[18] A. Sannino, A. Maffezzoli, L. Nicalais, Introduction of molecular spacers between the crosslinks of a cellulose-based superabsorbent hydrogel: effects on the equilibrium sorption properties, J. Appl. Polym. Sci. 90 (2003) 168–174.

[19] G. Marci, G. Mele, L. Palmisano, P. Pulito, A. Sannino, Environmentally sustainable production of cellulose-based superabsorbent hydrogels, Green Chem. 8 (2006) 439–444.

[20] C. Chang, B. Duan, J. Cai, L. Zhang, Superabsorbent hydrogels based on cellulose for smart swelling and controllable delivery, Eur. Polym. J. 46 (2010) 92–100.

[21] H.W. Leung, Ecotoxicology of glutaraldehyde: review of environmental fate and effects studies, Ecotox. Environ. Safe 49 (2001) 26–39.

[22] M.G. Raucci, M.A. Alvarez-Perez, C. Demitri, D. Giugliano, V. De Benedictis, A. Sannino, L. Ambrosio, Effect of citric acid crosslinking cellulose-based hydrogels on osteogenic differentiation, J. Biomed. Mater. Res. Part A 103A (2015) 2045–2056.

[23] S. Lee, Y.H. Park, C.S. Ki, Fabrication of PEG-carboxymethylcellulose hydrogel by thiol-norbornene photo-click chemistry, Int. J. Biol. Macromol. 83 (2016) 1–8.

[24] H. Kono, Characterization and properties of carboxymethyl cellulose hydrogels crosslinked by polyethylene glycol, Carbohydr. Polym. 106 (2014) 84–93.

[25] P. de Cuadro, T. Belt, K.S. Kontturi, M. Reza, E. Kontturi, T. Vuorinen, M. Hughes, Cross-linking of cellulose and poly(ethylene glycol) with citric acid, React. Funct. Polym. 90 (2015) 21–24.

[26] V.C. Dumont, A.A. Mansur, S.M. Carvalho, F.G.L.M. Borsagli, M.M. Pereira, H.S. Mansur, Chitosan and carboxymethyl-chitosan capping ligands: effects on the nucleation and growth of hydroxyapatite nanoparticles for producing biocomposite membranes, Mater. Sci. Eng. C 59 (2016) 265–277.

[27] E.S. Costa-Júnior, E.F. Barbosa-Stancioli, A.A. Mansur, W.L. Vasconcelos, H.S. Mansur, Preparation and characterization of chitosan/poly(vinyl alcohol) chemically crosslinked blends for biomedical applications, Carbohydr. Polym. 76 (2009) 472–481.

[28] H.S. Mansur, H.S. Costa, A.A.P. Mansur, M. Pereira, 3D-macroporous hybrid scaffolds for tissue engineering: network design and mathematical modeling of the degradation kinetics, Mater. Sci. Eng. C 32 (2012) 404–415.

[29] L. Ma, C. Gao, Z. Mao, J. Zhou, J. Shen, X. Hu, C. Han, Collagen/chitosan porous scaffolds with improved biostability for skin tissue engineering, Biomaterials 24 (2003) 4833–4841.

[30] B. Stuart, Infrared Spectroscopy: Fundamentals and Applications, John Wiley & Sons, New York, 2004.

[31] D. Lin-Vien, N.B. Colthup, W.G. Fateley, J.G. Grasselli, The Handbook of Infrared and Raman Characteristic Frequencies of Organic Molecules, first ed., Academic Press, Amsterdam, 1991.

[32] M.S. Cintrón, D.J. Hinchliffe, FT-IR examination of the development of secondary cell wall in cotton fibers, Fibers 3 (2015) 30–40.

[33] H.G. Higgins, C.M. Stewart, K.J. Harrington, Infrared spectra of cellulose and related polysaccharides, J. Polym. Sci. 51 (1961) 59–84.

[34] J.F. Luna-Martínez, D.B. Hernández-Uresti, M.E. Reyes-Melo, C.A. Guerrero-Salazar, V.A. González-González, S. Sepúlveda-Guzmán, Synthesis and optical characterization of ZnS–sodium carboxymethyl cellulose nanocomposite films, Carbohydr. Polym. 84 (2011) 566–570.

[35] A.A.P. Mansur, F.G. de Carvalho, R.L. Mansur, S.M. Carvalho, L.C. de Oliveira, H.S. Mansur, Carboxymethylcellulose/ZnCdS fluorescent quantum dot nanoconjugates for cancer cell bioimaging, Int. J. Biol. Macromol. 96 (2017) 675–686.

[36] V. Zeleňák, Z. Vargová, K. Györyová, Correlation of infrared spectra of zinc (II) carboxylates with their structures, Spectrochim. Acta Part A 66 (2007) 262–272.

[37] H. Kono, NMR characterization of sodium carboxymethyl cellulose: substituent distribution and mole fraction of monomers in the polymer chains, Carbohydr. Polym. 146 (2016) 1–9.

[38] R.K. Singh, O.P. Khatri, A scanning electron microscope based new method for determining degree of substitution of sodium carboxymethyl cellulose, J. Microsc. 246 (2012) 43–52.

[39] E. Khairuddin, S.B. Pramono, V. Utomo, A. Wulandari, W. Zahrotul, F. Clegg, FTIR studies on the effect of concentration of polyethylene glycol on polymerization of Shellac, J. Phys.: Conf, Ser. 776 (2016) 012053.

[40] S.-W. Kuo, C.-L. Lin, F.-C. Chang, Phase behavior and hydrogen bonding in ternary polymer blends of phenolic resin/poly(ethylene oxide)/poly(ε-caprolactone), Macromolecules 35 (2002) 278–285.

[41] F.F.-L. Ho, D.W. Klosiewicz, Proton nuclear magnetic resonance spectrometry for determination of substituents and their distribution in carboxymethylcellulose, Anal. Chem. 52 (1980) 913–916.

[42] J. Ma, X. Li, Y. Bao, Advances in cellulose-based superabsorbent hydrogels, RSC Adv. 5 (2015) 59745–59757.

[43] A.D. Metcalfe, M.W.J. Ferguson, Tissue engineering of replacement skin: the crossroads of biomaterials, wound healing, embryonic development, stem cells and regeneration, J. R. Soc. Interface 4 (2007) 413–437.

[44] C.G.T. Neto, J.A. Giacometti, A.E. Job, F.C. Ferreira, J.L.C. Fonseca, M.R. Pereira, Thermal analysis of chitosan based networks, Carbohydr. Polym. 62 (2005) 97–103.

[45] W. Li, B. Sun, P. Wu, Study on hydrogen bonds of carboxymethyl cellulose sodium film with two-dimensional correlation infrared spectroscopy, Carbohydr. Polym. 78 (2009) 454–461.

[46] T. Hatakeyama, Determination of bound water content in polymers by DTA, DSC and TG, Thermochim. Acta 123 (1988) 153–161.

[47] M.J. Zohuriaan, F. Shokrolahi, Thermal studies on natural and modified gums, Polym. Test. 23 (2004) 575–579.

[48] B. Ghanbarzadeh, H. Almasi, A.A. Entezami, Physical properties of edible modified starch/carboxymethyl cellulose films, Innov. Food Sci. Emerg. Technol. 11 (2010) 697–702.

[49] H.M.C. Azeredo, C. Kontou-Vrettou, G.K. Moates, N. Wellner, K. Cross, P.H.F. Pereira, K.W. Waldron, Wheat straw hemicellulose films as affected by citric acid, Food Hydrocoll. 50 (2015) 1–6.

[50] L. Bagheri, M. Yarmand, A. Madadlou, M.E. Mousavi, Transglutaminase-induced or citric acid-mediated cross-linking of whey proteins to tune the characteristics of subsequently desolvated sub-micron and nano-scaled particles, J. Microencapsul. 31 (2014) 636–643.

[51] S. Amrani, A. Atwal, F. Variola, Modulating the elution of antibiotics from nanospongy titanium surfaces with a pH-sensitive coating, RSC Adv. 5 (2015) 93666–93675.

[52] S. Diridollou, F. Patat, F. Gens, L. Vaillant, D. Black, J.M. Lagarde, Y. Gall, M. Berson, In vivo model of the mechanical properties of the human skin under suction, Skin Res. Technol. 6 (2000) 214–221.

[53] N.D. Evans, R.O. Oreffo, E. Healy, P.J. Thurner, Y.H. Man, Epithelial mechanobiology skin wound healing, and the stem cell niche, J. Mech. Behav. Biomed. Mater. 28 (2013) 397–409.

[54] C. Pailler-Mattei, S. Bec, H. Zahouani, In vivo measurements of the elastic mechanical properties of human skin by indentation tests, Med. Eng. Phys. 30 (2008) 599–606.

[55] R. Álvarez-Asencio, V. Wallqvist, M. Kjellin, M.W. Rutland, A. Camacho, N. Nordgren, G.S. Luengo, Nanomechanical properties of human skin and introduction of a novel hair indenter, J. Mech. Behav. Biomed. Mater. 54 (2016) 185–193.

[56] A.A. Stepanenko, V.V. Dmitrenko, HEK293 in cell biology and cancer research: phenotype, karyotype, tumorigenicity, and stress-induced genome-phenotype evolution, Gene 569 (2015) 182–190.

[57] J.K. Cusick, A. Mustian, K. Goldberg, M.E. Reyland, RELT induces cellular death in HEK 293 epithelial cells, Cell. Immunol. 261 (2010) 1–8.

[58] S.M. Carvalho, A.A.P. Mansur, H.S. Mansur, M.I.M.C. Guedes, Z.I.P. Lobato, M.F. Leite, In vitro and in vivo assessment of nanotoxicity of CdS quantum dot/aminopolysaccharide bionanoconjugates, Mater. Sci. Eng. C 71 (2017) 412–424.

[59] E. Oh, R. Liu, A. Nel, K.B. Gemill, M. Bilal, Y. Cohen, I.L. Medintz, Meta-analysis of cellular toxicity for cadmium-containing quantum dots, Nat. Nanotechnol. 11 (2016) 479–486.

Capítulo 4. Design, síntese e caracterização de nanohíbrido à base de carboximetil celulose (CMC) incorporados com nanopartículas de prata (AgNPs) para aplicação antibacteriana

4.1. Graphical Abstract
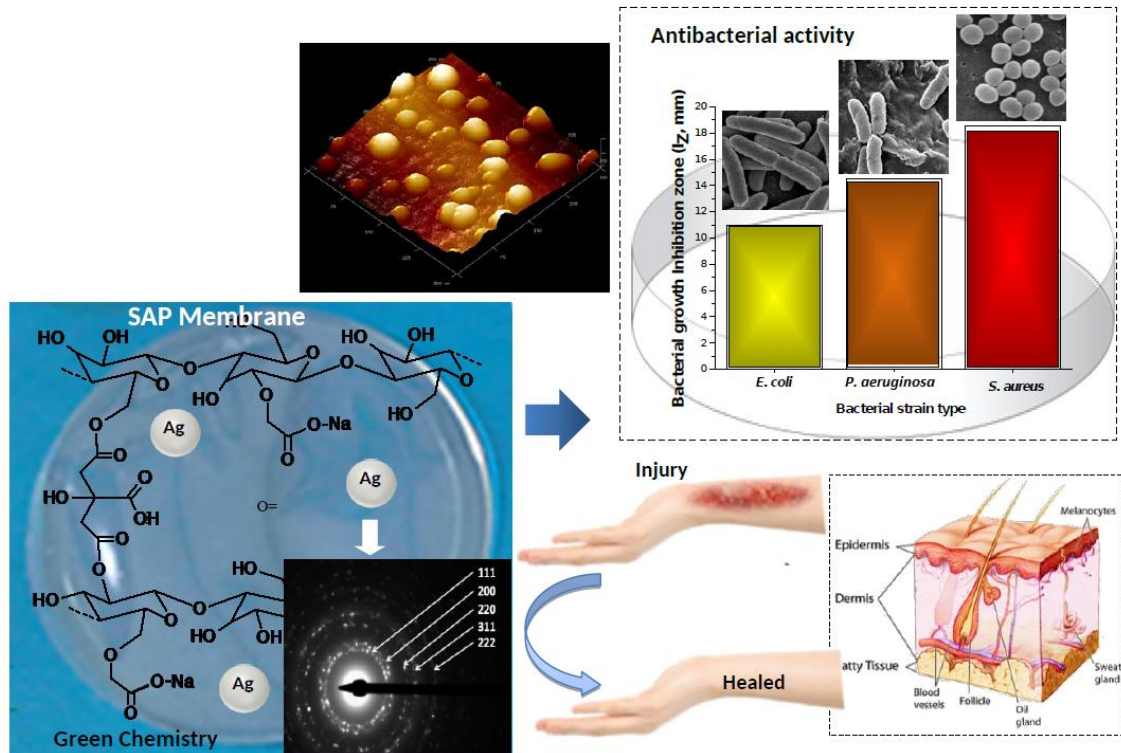
Soft Tissue Engineering Meets Green Nanotechnology: Biocompatible Carboxymethyl Cellulose-Silver Nanoparticle Hybrids with Tunable Antibacterial Activity for Wound Dressing and Epidermal Repair

4.2. Resumo

Lesões na pele podem ser causadas por acidentes, queimaduras, traumas, feridas crônicas e doenças, que são severamente agravadas por infecções bacterianas resistentes a fármacos. Híbridos à base de biopolímeros combinados com nanopartículas de prata (AgNPs) têm potencial aplicação como curativos e no reparo de tecidos cutâneos. Neste sentido, o objetivo deste trabalho foi a síntese verde de nanocompósitos de carboximetil

celulose e nanopartículas de prata (CMC-AgNPs) para produção de membranas de hidrogel, e caracterização das suas propriedades físico-químicas, citocompatibilidade e atividade bacteriana. Esses nanocompósitos foram preparados usando CMC com dois graus de carboximetilação (0,77 e 1,22), diferentes concentrações de ácido cítrico (15% e 20% m/m do polímero) e duas concentrações de AgNPs (0,6% e 1,2% m/m AgNPs/CMC). Inicialmente foram produzidas as nanopartículas de prata por redução química *in situ* utilizando a CMC simultaneamente como agente redutor e agente de estabilização das nanopartículas produzidas. Na sequência foi feita a formação das membranas através de tratamento térmico que permitiu a evaporação do solvente e a ocorrência das reações químicas envolvidas na reticulação pelo ácido cítrico. Os resultados demonstraram que hidrogéis superabsorventes foram produzidos com comportamentos de intumescimento e degradação dependentes da concentração do agente reticulante CA, do grau de carboximetilação da CMC e do teor de AgNPs nas matrizes. Além disso, a análise espectroscópica por infravermelho com transformada de Fourier evidenciou que os principais grupos funcionais da CMC (-COOH e -OH) estavam diretamente envolvidos nas reações químicas para a formação de AgNPs e da reticulação do hidrogel. Estes nanocompósitos foram citocompatíveis utilizando ensaio *in vitro* de viabilidade celular de brometo de 3- (4,5-dimetil-2-tiazolil) -2,5-difeniltetrazólio com células embrionárias renais humanas (HEK 293T) e apresentaram atividade antimicrobiana para cepas bacterianas gram-positivas e gram-negativas. Conclusivamente, os nano-híbridos de CMC-AgNPs apresentaram propriedades potenciais para sua utilização como hidrogéis superabsorventes para aplicação no tratamento e regeneração de feridas epiteliais combinado com atividade antibacteriana altamente eficaz contra patógenos gram-positivos multi-resistentes em ferimentos de pele.

4.3. Artigo

Capanema, Nádia S.V.; Mansur, A.A.P.; Carvalho, S.M.; Ramos, C.P.; Lage, A.P.; Mansur, H.S. Physicochemical properties and antimicrobial activity of biocompatible carboxymethylcellulose-silver nanoparticle hybrids for wound dressing and epidermal repair. Journal of Applied Polymer Science, v. 135, p. 45812, 2018. **QUALIS A2 – JCR 1.86**

Physicochemical properties and antimicrobial activity of biocompatible carboxymethylcellulose-silver nanoparticle hybrids for wound dressing and epidermal repair

Nádia S. V. Capanema,[1] Alexandra A. P. Mansur [iD],[1] Sandhra M. Carvalho,[1] Lorena L. Mansur,[1] Carolina P. Ramos,[2] Andrey P. Lage,[2] Herman S. Mansur [iD][1]

[1]Center of Nanoscience, Nanotechnology and Innovation-CeNano[2]I, Department of Metallurgical and Materials Engineering, Federal University of Minas Gerais/UFMG, Av. Antônio Carlos, 6627-Escola de Engenharia, Bloco 2-Sala 2233, 31.270-901, Belo Horizonte, MG, Brazil

[2]Laboratório de Bacteriologia Aplicada, Departamento de Medicina Veterinária Preventiva, Escola de Veterinária, UFMG, Belo Horizonte, MG, Brazil

Correspondence to: H. S. Mansur (E-mail: hmansur@demet.ufmg.br)

ABSTRACT: Skin loss can be caused by accident, burn, trauma, chronic wounds, and diseases, which is severely aggravated by multidrug-resistant bacterial infections. Soft hybrids based on biopolymers combined with silver nanoparticles (AgNPs) have potential applications as wound dressing supports and skin tissue repair. Thus, our study focused on the design, green synthesis, and comprehensive characterization of carboxymethyl cellulose (CMC–AgNP) nanocomposites for producing hydrogel membranes, with tunable physicochemical properties, cytocompatibility, and biocidal activity for potential application as wound dressing and skin repair. These nanocomposites were prepared using CMC with two degrees of carboxymethylation, distinct concentrations of citric acid (CA) cross-linker, and AgNPs by *in situ* chemical reduction, forming hybrid membranes by the solvent casting method. The results demonstrated that superabsorbent hydrogels were produced with swelling and degradation behaviors dependent on the concentration of CA cross-linker, degree of carboxymethylation of CMC, and content of AgNP in the matrices. Moreover, the Fourier transform infrared spectroscopy analysis evidenced that the CMC functional groups (e.g., —COOH and —OH) were directly involved in the chemical reactions for the formation of AgNPs and hydrogel crosslinking pathway. These nanocomposites were cytocompatible using *in vitro* 3-(4,5-dimethyl-2-thiazolyl)-2,5-diphenyltetrazolium bromide cell viability assay with of human embryonic kidney cells. Conclusively, the CMC–AgNP nanohybrids demonstrated to be simultaneously non-toxic combined with highly effective antibacterial activity against gram-positive multi-resistant wound/skin pathogens (*Staphylococcus aureus*) and moderate effect towards gram-negative strains (*Escherichia coli* and *Pseudomonas aeruginosa*). © 2017 Wiley Periodicals, Inc. J. Appl. Polym. Sci. **2017**, *134*, 45812.

INTRODUCTION

Skin, as the largest organ of body, is a very complex tissue and an important obstacle against external factors, such as pathogenic microbial agents and ultraviolet radiation. In addition, it plays a significant role preventing the substantial loss of body fluids, assisting the thermoregulation and immune defense of the body. However, full-thickness skin defects in large scale cannot repair itself spontaneously.[1,2] Despite some advances in regenerative medicine and tissue engineering, skin repair and restoration is yet a challenge when skin loss or damage occurs

caused by accident, burn, trauma, chronic wounds, and diseases, which have become one of the most serious problems in clinic. Although a variety of artificial skins have been commercially available for clinical use, to date, there are no models of artificial skin that completely replicate normal skin and restore all functionalities of the lost tissue, protecting the wound from bacterial infection and providing a moist and healing environment.[1,3–6]

Natural biopolymers such as cellulose, collagen, chitosan, alginate, fibrin, and derivatives have been investigated as potential

---

Additional Supporting Information may be found in the online version of this article.

sources of synthetic biomaterials to which cells can attach and provide repair by new tissue growth. The first generation of degradable polymers used as biomaterials for tissue engineering were basically adapted materials from other clinical uses, which presented disadvantages mostly related to their mechanical and degradation properties.[1–8] More recently, innovative biomaterials based on soft hybrid hydrogels composed of natural biopolymers such as cellulose and derivatives have been developed to mimic the characteristics of natural tissue facilitating the regeneration and repair the lost or damaged tissue. Cellulose is one of the most abundant natural polymers on earth, which consists of a linear chain of several hundred to over ten thousand linked D-glucose units usually extracted from cell wall of green plants.[7,8] However, cellulose is insoluble in water or organic solvents, which greatly limits its applications. Therefore, functionalization of cellulose is performed predominantly through their hydroxyl groups, rendering water-soluble derivatives like cellulose ethers and salts [e.g., methyl cellulose, ethyl cellulose, hydroxyethyl cellulose, carboxymethyl cellulose (CMC)] with attractive properties for biomedical applications. The properties of CMC depend on the degree of substitution (DS), which usually ranges from 0.5 to 1.0 for slightly substituted and from 2.2 to 3.0 for highly substituted cellulose ether and ester derivatives.[9–11]

Conversely, total solubility of the polymer in water is usually not desired for biomaterial applications such as wound dressing or skin tissue repair where physiochemical and mechanical stabilities are required. In that sense, polymer-based soft materials like hydrogels have been widely explored in biomedical and engineering fields, such as tissue engineering, drug delivery, soft actuator, and soft machines.[6,11,12] Superabsorbent hydrogels (SAP) are capable of absorbing very large amounts of water or aqueous solutions (e.g., 10–1000 times the original volume) in the insoluble crosslinked hydrophilic polymer network through the swelling process in a relatively short time.[6,12]

Hence, due to the merits of non-toxicity, water solubility, low-cost, and environmental friendliness, CMC has been widely used for producing hydrogels, and has been developed in many fields, including tissue engineering, drug delivery, and wound dressing.[12–15] Some bifunctional molecules are employed as the crosslinker for cellulose and its derivatives to covalently bind the polymer molecules in a three-dimensional (3D) hydrophilic network for producing hydrogels. The properties of these hydrogels can be designed and tailored by physically and chemically crosslinking the polymer network. However, the great majority of crosslinkers used for modifying polymer networks are not biocompatible and environmentally safe (e.g., formaldehyde, glutaraldehyde, epichlorohydrin, carbodiimide, etc.), which has raised concerns regarding their toxicity for applications as biomaterials.[6,12–14] Hence, new solutions have emerged based on non-toxic crosslinkers from natural sources such as citric acid (CA) for developing environmentally and biologically friendly hydrogel biomaterials.[5,6,8,13]

Another key aspect to be addressed of perspective synthetic biomaterial candidate for skin substitute is regarded to the fact that it is the last barrier between the human body and the external environment. So, besides protecting the body from exogenous chemical and physical factors, skin is the first line of defense against pathogenic microorganisms, and it assists in immunological processes.[1,16] Thus, there is a growing demand for an appropriate and safe antimicrobial dressing to treat skin lesions and topical wounds resulting from physical or thermal injury and disease conditions. Despite a broad range of antimicrobial agents as well as antibiotics is commercially available, a successful tackling of bacterial infections is particularly challenging due to an increase of microbial resistance caused by an abuse of such drugs.[17–19]

Historically, silver (Ag) compounds have been used in numerous fields to prevent microbial growth. Like many nonessential heavy metals, Ag is a natural biocide, but compared with titanium, zinc, and copper, Ag nanoparticles (AgNPs) present the highest antimicrobial efficacy against bacteria, viruses, and other eukaryotic microorganisms.[20,21] Therefore, AgNPs are widely considered as the most promising strategies to overcome microbial resistance as therapeutic agents for the prevention and eradication of wound colonization by microorganisms. They are comparably more efficient and potent against several drug-resistant pathogens compared to the conventional antibiotics.[17,22] For that reason, hydrogel films, biomembranes, and scaffolds combining polymer crosslinked networks with AgNPs have emerged as a new class of multifunctional biomaterials for skin tissue engineering.[16–21] However, no report was found in the consulted literature investigating nanocomposites made of CMC with distinct degrees of functionalization, crosslinked with CA and incorporated with AgNPs, with antibacterial activity and cytocompatibility for potential skin tissue engineering applications.

Thus, in this study it was designed and produced CMC-based hybrid nanocomposites with AgNPs (CMC/AgNPs) embedded combining physicochemical properties and morphological features with *in vitro* cytocompatibility and effective antibacterial activity against resistant pathogens for potential applications as wound dressing supports and skin repair substitutes.

EXPERIMENTAL

Materials

Sodium CMC with two DS = 0.77 (CMC-0.77, average molar mass M_w = 250 kDa, and viscosity 735 cps, 2% in H_2O at 25 °C) and DS = 1.22 (CMC-1.22, M_w = 250 kDa, viscosity 660 cps, 2% in H_2O at 25 °C), and CA [[Sigma-Aldrich, St. Louis, MO, USA), ≥99.5%, $HOC(COOH)(CH_2COOH)_2$] were purchased from Sigma-Aldrich and used as received. Silver nitrate (≥99.9%) was supplied by Synth (Synth, São Paulo, SP, Brazil). Unless specified otherwise, deionized water (DI water, Millipore Simplicity) with a resistivity of 18 MΩ cm was used to prepare the solutions and the procedures were performed at room temperature (RT, 23 ± 2 °C).

Synthesis of Colloidal AgNPs by *in Situ* Reduction

CMC solution (2% w/v) was prepared by adding sodium CMC powder (2.0 g) to 100 mL of DI water and stirring at RT until complete solubilization occurred (pH 7.5 ± 0.5). After dissolution, silver nitrate solution (10 mL) was added dropwise under

stirring at concentrations of 0.6 (CMC_Ag0.6) and 1.2% (CMC_Ag1.2) m/m of CMC polymer followed by raising the temperature of the reaction medium to boiling (95 ± 5 °C). The reaction mixture was kept under continuous stirring for 15 min after boiling. After that, the suspension of silver nanoparticles (CMC–AgNPs) was let to cool down at RT and stored at 6 ± 2 °C for further use.

Synthesis of Crosslinked CMC–AgNPs Nanocomposite Membranes

The crosslinking agent, CA, was added to CMC–AgNPs colloidal dispersion under stirring at concentrations of 15 (CMC_Ag_CA15) and 20% (CMC_Ag_CA20) m/m of CMC polymer and homogenized for 20 min. Then, 10 mL of the solutions were poured into plastic molds (polystyrene petri dish, diameter = 60 mm) and were allowed to dry at 40 ± 2 °C for 24 h to remove water. In the sequence, the samples were kept at 80 ± 2 °C for 24 h for the crosslinking reaction (slow solvent evaporation method). As reference, samples without CA (CMC_Ag_CA0) were prepared and dried following the same thermal treatment. These concentrations of CA (15 and 20%) were selected based on the initial experimental assessment of the swelling and degradation behaviors of the chemically crosslinked hydrogels, which would be suitable for the biological assays focusing on wound dressing and skin repair applications.

Characterization of CMC–AgNPs Colloidal Dispersions

Ultraviolet–visible (UV–vis) spectroscopy measurements were performed using Perkin-Elmer equipment (Lambda EZ-210) in transmission mode with colloidal samples in a quartz cuvette over a wavelength range between 700 and 190 nm.

Nanostructural characterization of the AgNPs was based on the images and selected-area electron diffraction (SAED) patterns using a Tecnai G2–20-FEI (FEI Company) transmission electron microscope (TEM) at an accelerating voltage of 200 kV. Energy-dispersive X-ray spectra (EDX) were collected for chemical analysis. In all of the TEM analyses, the samples were prepared by placing a drop of dilute CMC–AgNPs suspension onto holey carbon-coated copper grids (Electron Microscopy Sciences) and allowing them to dry at RT overnight. The NP size and size-distribution data were obtained based on the TEM images by measuring at least 100 randomly selected NPs using image processing program (ImageJ, version 1.50, public domain, National Institutes of Health). In addition, the crystallinity of AgNPs was investigated by high-resolution TEM (HRTEM) and SAED.

Dynamic light scattering (DLS) and zeta potential (ZP, ζ-potential) analyses were performed using a ZetaPlus instrument (Brookhaven Instruments Corporation) with a laser light wavelength of 660 nm (35-mW red diode laser) and using a minimum of 10 replicates. The ZP measurements were performed at 25.0 ± 2 °C under the Smoluchowski approximation. CMC–AgNPs suspensions were diluted 1:10 (v/v) before experiments.

X-ray photoelectron spectroscopy (XPS) analysis of AgNPs (CMC-0.77_Ag1.2) was performed using Mg-Kα as the excitation source (Amicus spectrometer, Shimadzu). The samples were prepared from drying CMC–AgNPs colloidal dispersion

poured into a plastic mold at 40 ± 2 °C for 24 h. All peaks positions were corrected based on C 1 s binding energy (284.8 eV).

Characterization of CMC–AgNPs Nanocomposite Hydrogels

Physicochemical Characterization of CMC–AgNPs Nanocomposite Hydrogels. For fluid uptake measurement and degradation assessments, the hybrid hydrogels were cut into 10×10 mm^2 samples, dried at 40 ± 2 °C for stabilization of mass, and weighted (W_0, initial mass). Then, the hydrogels (triplicates, $n = 3$) were placed in 70 mL sample pots with 10.0 mL DI water at RT. After 60 min, the hydrogel was removed from solution, gently wiped with filter paper to remove the excess of liquid on the sample surface, and weighted (W_s, swollen mass). In the sequence, samples were dried at 40 ± 2 °C until mass stabilization and the final weight was recorded (W_f, final mass).

The weights obtained in each step of the process were used to calculate the swelling degree (SD) and degree of degradation (DD) of the hydrogels using eqs. (1) and (2), respectively, as reported in the literature.[23–25]

$$SD(\%) = ((W_s - W_0)/W_0) \times 100\% \qquad (1)$$

$$DD(\%) = ((W_0 - W_f)/W_0) \times 100\% \qquad (2)$$

Morphological and Spectroscopic Analyses of CMC–AgNPs Hybrid Membranes. UV–vis spectroscopy measurements were performed using Perkin-Elmer equipment (Lambda EZ-210) in transmission mode from hybrid membranes over a wavelength range between 600 and 190 nm.

Fourier transform infrared spectroscopy (FTIR) analysis was recorded with a Nicolet 6700 (Thermo Fischer) spectrometer with background subtraction. The FTIR spectra of the hybrid hydrogel membranes were obtained using attenuated total reflectance (ATR, 4000–675 cm^{-1}, 32 scans, and 4 cm^{-1} resolution). In addition, Fourier transform infrared microspectroscopy (FTIR-MIR) analysis of the membranes was performed using Nicolet-iN10 infrared microscope (Thermo Electron Corp., with OMNIC Picta software, Thermo Scientific). ATR image mappings were acquired between 4000 and 675 cm^{-1} with a spectral resolution of 8 cm^{-1}. For each sample, an area of 400×400 µm was randomly selected for imaging and analysis constituting 100 points of spectral data acquisition per region analyzed.

Atomic force microscopy (AFM) of hydrogel membranes were conducted with a Multimode 8 (Bruker) instrument operating in Peak Force tapping mode. The scanning rate was 1.0 Hz, and the images were acquired with a 512×512 pixel resolution. The surface mapping of nanomechanical properties was carried out using SiN probe, at constant $K = 0.4$ N/m, frequency 70 kHz, temperature at 20–23 °C, calibration based on the absolute method and parameters calculated with software Nanoscope analysis 8.5.

Biological Characterization of CMC–AgNPs Hybrid Membranes

Cytotoxicity Evaluation. Human embryonic kidney cells (HEK293T) used as model cell line were gently provided by Prof. A. Goes of the Department of Immunology and Biochemistry, UFMG. The HEK293T cells were cultured in Dulbecco's modified eagle medium (DMEM) with 10% fetal bovine serum

(FBS), streptomycin sulfate (10 mg mL^{-1}), penicillin G sodium (10 units mL^{-1}), and amphotericin-b (0.025 mg mL^{-1}), all of them were supplied by Gibco BRL, using a humidified atmosphere of 5% CO_2 at 37 °C. All of the biological tests were conducted according to ISO 10993-5:2009/(R)2014 (Biological evaluation of medical devices: Tests for *in vitro* cytotoxicity). Before experiments, the samples were sterilized by UV radiation for 60 min.

The cytotoxicity of the samples was evaluated using a standard 3-(4,5-dimethyl-2-thiazolyl)-2,5-diphenyltetrazolium bromide (MTT) assay. Briefly, HEK293T cells on passage 34 were synchronized in serum-free medium for 24 h. After this period, cells were trypsinized and seeded (3 × 10^5 cells/well) on square samples of hydrogel membranes (4.0 × 4.0 mm and average thickness 58 ± 6 μm) and placed in a 96-well plate. Controls were used with the cells and DMEM with 10% FBS, the positive control with Triton x-100 (1% v/v in PBS, Gibco BRL) and, as a negative control, chips of sterile polypropylene *Eppendorf* tubes (1 mg mL^{-1}, Eppendorf, Germany). After 24 h, all media were aspirated and replaced with 60 μL of culture media containing serum to each well. MTT (5 mg mL^{-1}, Sigma-Aldrich) was added to each well and incubated for 4 h in an oven at 37 °C and 5% CO_2. Next, 40 μL SDS (Sigma-Aldrich) solution/ 4% HCl was placed in each well and incubated for 16 h in an oven at 37 °C and 5% CO_2. Then, 100 μL were removed from each well and transferred to a 96-well plate. The absorbance was measured at $\lambda = 595$ nm using iMark Microplate Absorbance Reader (Bio-Rad). Percentage cell viability was calculated according to eq. (3). The values of the controls (wells with cells, and no samples) were set to 100% cell viability.

$$\text{Cell viability}(\%) = (\text{Absorbance of sample and cells} \\ /\text{Absorbance of control}) \times 100\% \quad (3)$$

Antibacterial Studies. *Bacterial culture.* Both Gram-positive (*Staphylococcus aureus,* ATCC 25923) and Gram-negative human bacterial pathogens (*Escherichia coli,* ATCC 25922 and *Pseudomonas aeruginosa,* ATCC 27853) were obtained from the American Type Culture Collection (ATCC). The inoculums of the test organism were incubated at 37 °C in Muller–Hinton medium until reaching the logarithmic phase. The optical density of bacterial suspensions was measured at $\lambda = 620$ nm using a microplate reader (Spectra II Microplate Reader, Tecan) at absorbance mode. All of the materials were sterilized in the autoclave at 120 °C under 1 kgf cm^{-2} for 15 min.

Antibacterial assay. The antibacterial activity of CMC–AgNPs crosslinked hydrogels was evaluated using agar-well diffusion method according to Clinical Laboratory Standards Institute M2-A8 (2003) method. The microbial suspension was adjusted to 1–2 × 10^8 CFU mL^{-1}, comparable to 0.5 turbidity on the McFarland scale, and seeded onto petri dishes with Mueller–Hinton agar. Then, sterile disks of CMC crosslinked hydrogels with (CMC-77_Ag0.6_CA15, CMC-0.77_Ag1.2_CA15, CMC-1.22_Ag0.6_CA15, and CMC-1.22_Ag1.2_CA15) and without (CMC-0.77_CA15 and CMC-1.22_CA15) AgNPs were aseptically placed at plates. The plates were incubated at 37 °C for 18 h (*E. coli* and *P. aeruginosa*) or 24 h (*S. aureus)* and thereafter the zones of inhibition around the disks were photographed

and measured. Ceftiofur (30 μg/disk), Enrofloxacin (5 μg/disk), and Gentamicin (10 μg/disk) antibiotic disks were used as a positive control and the inhibition zones, which were validated according to the ATCC quality control ranges of antimicrobial disk susceptibility test zone diameters for reference strains on Mueller–Hinton Agar assay.[26]

RESULTS AND DISCUSSION

Synthesis and Characterization of CMC–AgNPs Colloidal Dispersions

Characterization of Colloidal Suspension. Typically, cellulose/ metal nanocomposites can be prepared by *in situ* reduction of metallic ions in aqueous suspensions, which commonly involves the use of the water-soluble metal salt precursor (e.g., Ag$^+$, Au^{3+}), the reducing agent and the stabilizer to avoid agglomeration. However, several processes use toxic solvents and reductants (e.g., borohydride, hydrazine) in alkaline medium (e.g., NaOH, KOH) for catalysis and kinetics purposes, which should be avoided because of carcinogenicity and environmental hazards.[27,28] For that reason, it has been reported that metal NPs can be synthesized using polysaccharides (i.e., cellulose, starch, chitosan, and its derivatives) by *in situ* method without requiring the addition of an external reducing agent. The adsorption of metal ions by the polymer functional groups may be subsequently reduced to metallic NPs by the presence of hydroxyl, carboxylic, aldehyde, and ether groups in the polymer molecular structure, acting as a "nanoreactor".[29–31] Despite extensively accepted that hydroxyl groups play a crucial role in the reduction of AgNPS, a more in-depth investigation of the mechanism for the formation of AgNPs using CMC is beyond the scope of this research.

Therefore, in this study, AgNPs were prepared using water as an environmentally benign solvent and CMC serving as both polymer reductant (i.e., Ag$^+$//Ag^0) and stabilizing capping ligand of the colloidal dispersion, conducted in a moderately heated system. The production of CMC–AgNP biohybrids started with the nucleation of AgNPs in water medium using CMC (with DS 0.77 and 1.22) with two concentrations of Ag$^+$ (0.6 and 1.2%, m/m %), combining contrasting properties, cytocompatibility towards HEK293T cells and effective antibacterial activity for skin tissue applications. The chemical reduction of silver ions to metallic particles (Ag$^+ \rightarrow$ Ag^0) was qualitatively monitored by the visual change from colorless to light yellowish-orange color solution, with the gradual increase to dark orange as the reaction evolved (Figure 1).

In addition, the formation and stabilization *in situ* of AgNPs using Ag (0.6%) in CMC with DS 0.77 and 1.22 in water dispersions (CMC–AgNPs) were assessed by UV–vis spectroscopy as presented in Figure 2. I can be clearly observed the peaks with maxima absorbance at approximately $\lambda = 415–430$ nm, with similar spectra for CMC–AgNPs samples with DS = 0.77 [Figure 2(a)] and DS = 1.22 [Figure 2(b)], in comparison to CMC without NPs [Figure 2(c,d)]. These results were assigned to the surface plasmon resonance (SPR) associated with the formation of Ag particles at nanoscale dimension (i.e., AgNPs). Based on the literature, the SPR phenomenon is essentially generated when the incident electromagnetic wave interacts with
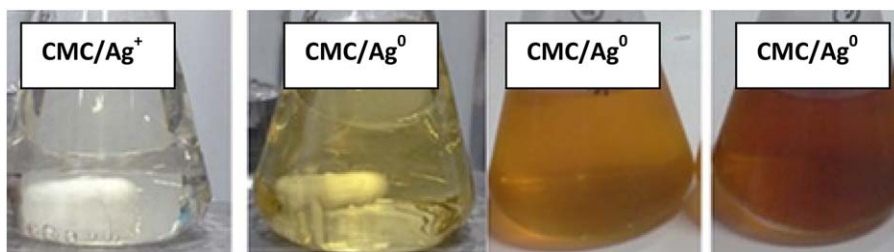
Figure 1. Synthesis of AgNPs performed in water medium using CMC simultaneously as the reducing agent and capping ligand: (a) before and after heating for the formation of AgNPs, (b) 8 min, (c) 12 min, and (d) 15 min. [Color figure can be viewed at wileyonlinelibrary.com]

metal NPs, localized surface plasmon resonance (LSPR or SPR) is excited. As a consequence, SPR leads to absorption and scattering of the incident electromagnetic wave, which is showed by the emergence of an intense band in the UV–vis spectrum.[32,33] Equivalent UV–vis results were observed for higher concentration of Ag^+ in solution (i.e., 1.2%).

The ZP (ζ) is an important indicator of the stability of colloidal dispersions, where the magnitude of the ZP indicates the degree of electrostatic repulsion between adjacent and similarly charged particles in dispersions. Thus, the ZP measurements indicated the formation of negatively charged colloidal AgNPs stabilized by CMC, with average values of $\zeta = -49.2 \pm 4.9$ mV and -56.9 ± 3.4 mV for CMC-0.77_Ag0.6 and CMC-1.22_Ag0.6, respectively. Based on the literature, these results of high ZP (i.e., negative or positive, $\zeta > |30|$ mV) demonstrated that AgNPs were formed and predominantly stabilized by carboxylate groups of CMC by electrostatic repulsion.[34,35] Moreover, the higher value of ζ for CMC with DS = 1.22 supported this statement because it has more carboxylate groups (i.e., anionic species) grafted to the CMC chain compared to CMC with DS = 0.77.

To further characterize the AgNPs in colloidal water system, DLS (also known as photon correlation spectroscopy or quasi-elastic light scattering) was used, which essentially consists of a technique that can be used to determine the size distribution profile of small particles in suspensions or polymers in solution. Thus, the hydrodynamic diameter (or Stokes diameter, H_d) of AgNPs stabilized by CMC in water media typically ranged from 45 to 125 nm, indicating a broad polydispersity of the distribution ($\approx$0.5) due to the interactions among CMC polymer chains at high concentration in solution. These results of colloidal sizes estimated by DLS were expected as the H_d measurements take into account not only the dimension of "core" made of AgNPs but also including the CMC polymer "shell" ligand and the solvation layer.[36,37]

Characterization of AgNPs. It has widely reported in the literature that the interactions of NPs with cells at the biointerfaces are drastically affected by a variability of factors, such as charge, hydrophobicity, size, mechanical properties, composition, and functional groups.[36,37] In that sense, the morphological and compositional features of AgNPs must be properly characterized as they play a critical role on the overall response regarding to either biocompatibility or nanotoxicity. TEM images, histograms of AgNPs size distributions, EDX spectra and SAED diffraction patterns are presented in Figures 3 (CMC-0.77_Ag1.2)

and 4 (CMC-1.22_Ag1.2) and Figure 1S (CMC-0.77_Ag0.6) and Figure 2S (CMC-1.22_Ag0.6) (Supporting Information). As a general trend, it can be observed that both CMC polymers (DS 0.77 and 1.22) produced similar AgNPs with spherical morphology, uniformly distributed, with the average size typically ranging from 10 to 15 nm. Therefore, no relevant tendency was observed regarding to the difference of the DS (i.e., 0.77 and 1.22) or the concentration of Ag (i.e., 0.6 and 1.2%) in solution on the final average size of AgNPs, within the statistical variation. This fact was credited to the high concentration of CMC relative to Ag^+ in the aqueous medium and the absence of catalysts (or strong reductants) in the synthesis, leading to the formation of AgNPs with wider size distributions due to slower nucleation and growth rates.[38]

In addition, the crystallinity and composition of AgNPs were further investigated by HRTEM imaging associated with SAED and EDX analysis. Figures 3(c) and 4(c) show the HRTEM images of the CMC–AgNPs, where the presence of interference fringes confirmed the high crystallinity of the NPs with a multi-faceted pattern associated with crystallographic planes. Figure 3(c) shows the HRTEM image of the CMC–AgNPs with DS = 0.77, with the average distance between the interference fringes determined as $d = 2.32$ Å, which was associated with the interatomic distance of (111) plane of metallic silver. Similarly, Figure 4(c) shows the HRTEM image of the CMC–AgNPs with DS = 1.22, with the average distance $d = 2.33$ Å consistent with
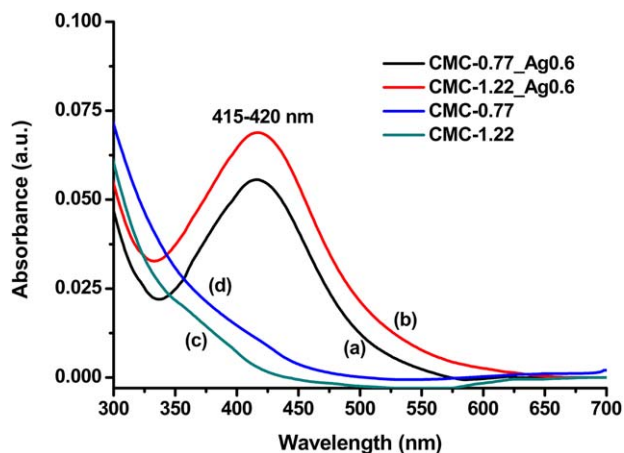
Figure 2. UV–vis spectra of CMC–AgNPs dispersions [(a) CMC-0.77_Ag0.6 and (b) CMC-1.22_Ag0.6] in comparison to CMC pure solutions [(c) CMC-0.77 and (d) CMC-1.22]. [Color figure can be viewed at wileyonlinelibrary.com]
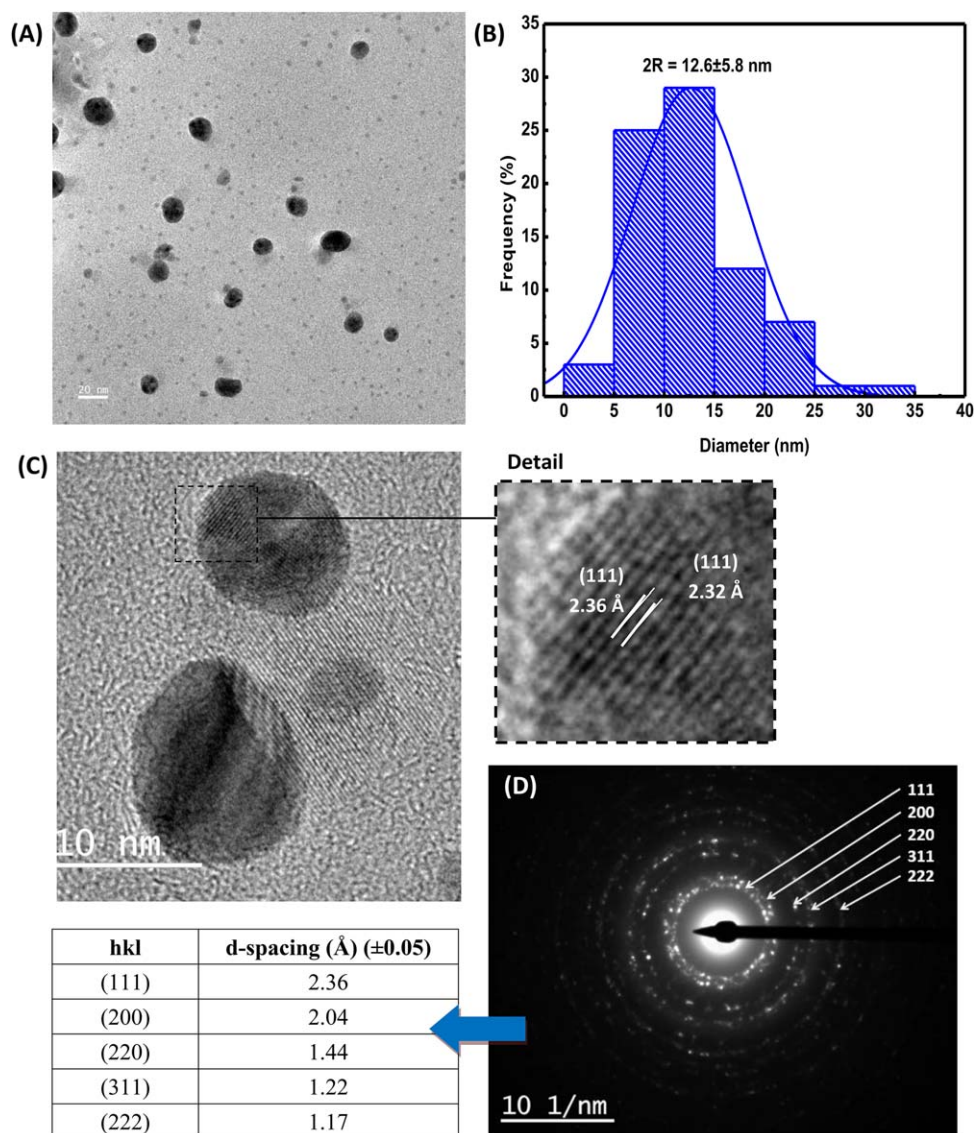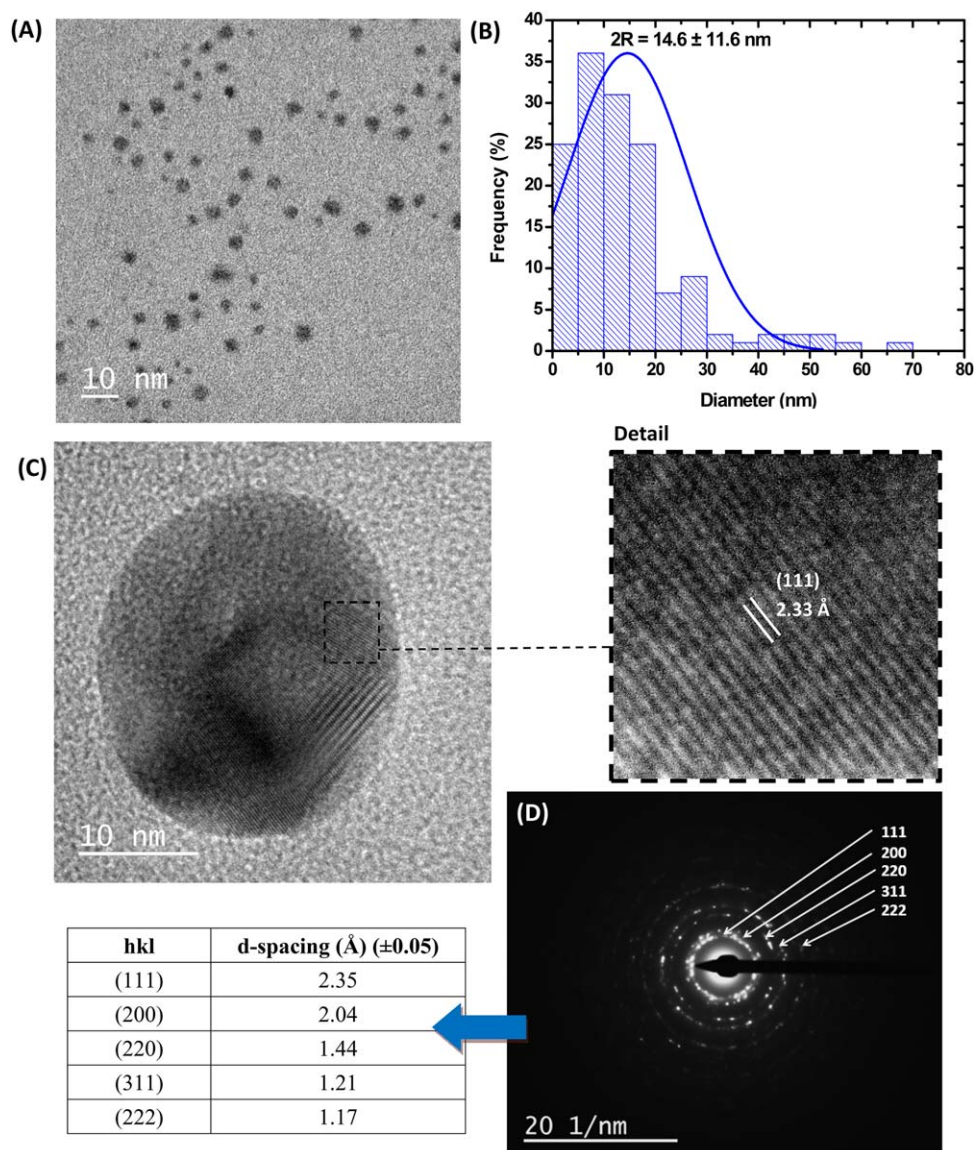
Figure 3. (a) TEM image; (b) Histogram of size distribution; (c) HRTEM image with interplanar distance between lattice fringes (detail); and (d) SAED pattern with d-spacings measured for each observed plane for sample CMC-0.77_Ag1.2. [Color figure can be viewed at wileyonlinelibrary.com]

(111) plane the metallic silver. Figures 3(d) and 4(d) show the typical SAED patterns taken from the synthesized AgNPs in CMC (DS 0.77 and 1.22) colloidal media. The patterns consisted of concentric diffraction rings characteristic of polycrystalline metal NPs. Based on the diffraction rings and the crystallographic theory, they were indexed as (111), (200), (220), (311), and (222) planes of face-centered cubic metallic silver, with respective d-spacings (±0.05) of 2.36, 2.04, 1.44, 1.22, and 1.17 Å for the samples of CMC–AgNPs (DS = 0.77 and 1.22). These results are in agreement with the d-values obtained from HRTEM images. EDX measurements were performed for additional chemical characterization of colloidal AgNPs formed in the CMC water dispersion media. The results are showed in Figures 1S and 2S, where the peaks at 3.0 and 3.2 keV correspond to the binding energies of Ag L_α and Ag L_β transitions, respectively, confirming the formation of AgNPs. The copper peaks in the spectra correspond to the carbon-coated copper grid of TEM. Hence, these results demonstrated

the formation of crystalline metallic AgNPs, which were effectively produced by the *in situ* chemical reduction of Ag^+ in CMC aqueous media (i.e., $Ag^+/CMC \rightarrow Ag^0/CMC$ colloid), supported by the literature.[39,40]

The chemical reduction of Ag^+ forming colloidal Ag metallic NPs (CMC–AgNPs) and their surface features were assessed by XPS spectroscopy. A typical XPS spectrum is presented in Figure 5 (CMC-0.77_Ag1.2). The peaks at 374.2 and 368.2 eV correspond to the Ag $3d_{3/2}$ and Ag $3d_{5/2}$ levels, respectively, and are associated with the Ag (3d) transitions in Ag metal. The spin-orbit components (Ag $3d_{3/2}$ and Ag $3d_{5/2}$) are separated by a binding energy interval of 6.0 eV.[41] Also, loss features are observed to higher binding energy side of each spin-orbit component that is characteristic of the metal.[42] These results corroborated the reduction of silver ions to Ag^0 and indicated no detectable oxidation at the surfaces of AgNPs stabilized by CMC in aqueous media.

Figure 4. (a) TEM image; (b) Histogram of size distribution; (c) HRTEM image with interplanar distance between lattice fringes (detail); and (d) SAED pattern with d-spacings measured for each observed plane for sample CMC-1.22_Ag1.2. [Color figure can be viewed at wileyonlinelibrary.com]

Characterization of CMC–AgNPs Hybrid Membranes

Morphological Characterization CMC–AgNPs Hybrid Membranes. Hybrid nanocomposites were produced based on AgNPs embedded in CMC (DS = 0.77 and 1.22) polymer matrices using two concentrations of AgNPs (0.6 and 1.2%). Typical CMC (DS = 1.22) hydrogel membranes are showed in Figure 6 (digital photos, no magnification) at the concentration of AgNP of 1.2%, without crosslinker (a) and with CA crosslinker (b,c). No relevant visual differences were observed for membranes with lower concentration of Ag (i.e., 0.6%) or CMC with DS = 0.77, with the similar features of semitransparent yellowish color and homogenous composition without noticeable phase segregation.

Physicochemical Characterization of CMC–AgNPs Hybrid Membranes. In vitro *swelling behavior of CMC–AgNPs hybrid membranes.* Swelling measurements is widely used to access the extension of crosslinking of hydrogel networks. Figure 7(a)
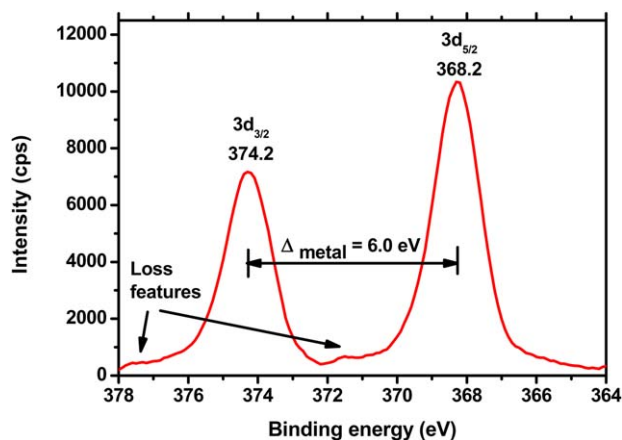
Figure 5. XPS spectrum of Ag 3d region for CMC–AgNPs. [Color figure can be viewed at wileyonlinelibrary.com]
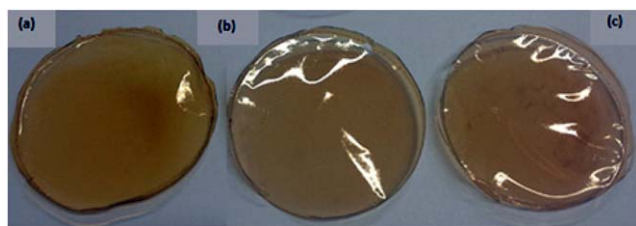
Figure 6. CMC membranes (DS = 1.22) with AgNP (1.2%); (a) not cross-linked and crosslinked with (b) CA 15%, and (c) CA 20%. [Color figure can be viewed at wileyonlinelibrary.com]

shows the SD (equilibrium–swelling ratio) of the CMC–AgNPs hybrid membranes with DS = 0.77 and 1.22 and two concentrations of AgNPs (0.6 and 1.2%) crosslinked with 15% of CA. It is clearly observed the superabsorbent behavior of CMC hydrogels without AgNP with SD of over 500% (CMC DS = 0.77), but with a drastic decrease of swelling behavior when AgNPs were incorporated in the systems at concentrations of 0.6 and 1.2%. This behavior was attributed to the metal–polymer interactions between carboxylate and hydroxyl groups of CMC and AgNP surface.[29,43,44] So, the formation of AgNPs with nanoscale dimensions offers extremely high surface area leading to strong interactions with the CMC polymer network, reducing the SD of the hybrid matrices. This effect was even more pronounced in the CMC hydrogels with higher DS = 1.22, which were initially soluble in water and then stabilized by incorporating AgNPs in the network. Interestingly, the hybrid hydrogel (CMC, DS = 1.22) showed a significant increase in the swelling behavior from approximately 420–1500% at higher concentration of AgNPs (from 0.6 to 1.2%), which may be interpreted as a combination of several aspects. That means, it was associated with the overall contributions of the changes in the CMC hydroxyl groups (i.e., chemical reaction forming AgNPs), the higher concentration of negatively charged species (i.e., lower ζ-potential due to R—COO$^-$ groups) and the conformation of CMC chains after crosslinking, which favored the hydrophilic balance with water molecules as polar solvent in the swollen nanocomposite matrix. Similar behavior was observed when the nanocomposite membranes were crosslinked with 20% of CA (Figure 3S, Supporting Information).

In Figure 7(b) (Ag1.2) and, (Supporting Information, Ag0.6), the effect of CA concentration (0, 15, and 20%) in the nanocomposites with AgNPs (CMC–AgNPs) was evaluated. In the absence of CA crosslinker, after 60 min of immersion, the hybrid membranes were fully dissolved. It was also observed a reduction of the SD as the concentration of crosslinker was increased for both DS (i.e., 0.7 and 1.22), which is a strong evidence of the formation of more covalent bonds bridging the functional groups of the polymer chains (mostly hydroxyls) decreasing the level of freedom of the hybrid hydrogel network.

These results showed that CMC-based hydrogels produced with a broad range of hydrophilicity (typically from 100 to 1500%) for water incorporation. Hence, they can be potentially suitable for wound dressing and skin tissue substitutes, where the swelling behavior is of paramount importance for promoting a moist microenvironment assisting the wound healing process.[45,46]

In vitro *degradation behavior of CMC–AgNPs hybrid membranes.* The degradation of hydrogel plays a key role on the overall performance in biomedical applications as the relative degradability of hydrogel will allow the cell diffusion, nutrients flow, and the integration with the host tissue.[6,45,46] Thus, *in vitro* degradation gravimetric assay was performed using water medium at 25 °C for 24 h as a preliminary evaluation of the chemical stability of the hydrogels and the results are presented in Figure 8 (Figures 5S and 6S, Supporting Information). As expected, based on the swelling behavior evaluated in the previous section, the addition of AgNPs to the CMC polymer hydrogels caused a reduction on the degradation for both DS = 0.77 and 1.22 systems, where no significant differences at concentrations of 0.6 and 1.2% of Ag were observed [Figure 8(a) and Figure 5S]. Again, this effect was more pronounced in CMC with DS = 1.2, which was fully dissolved (i.e., DD = 100%) without AgNPs and stable with AgNPs incorporated in the hybrid matrices (~50%). In addition, regarding to the DS, the CMC samples with DS = 0.77 were more stable to
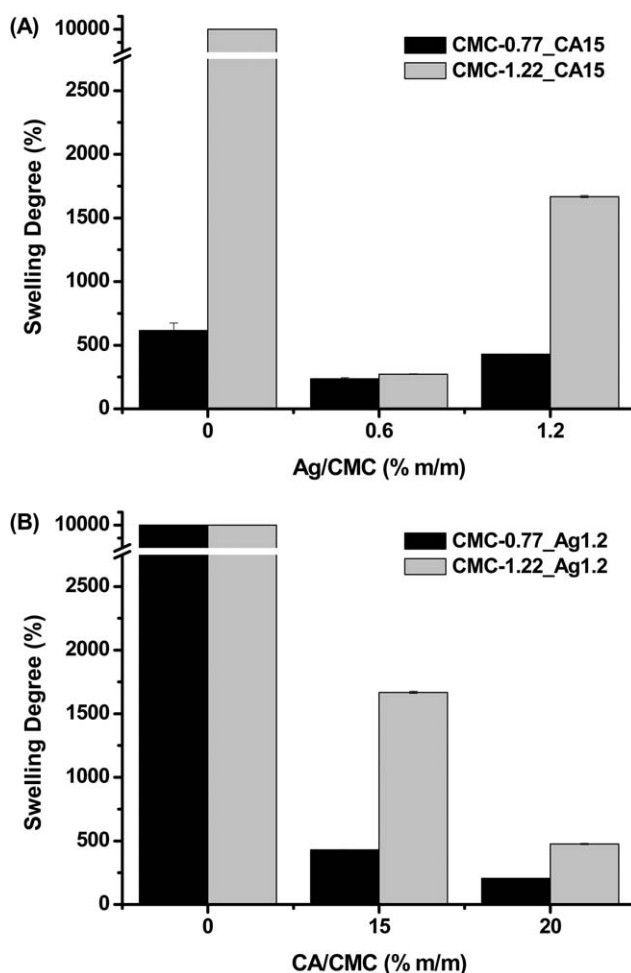
Figure 7. (a) Histogram of swelling behavior of crosslinked (CA 15%) CMC hydrogels with two DS (0.77 and 1.22) and without Ag (0%) and with two concentrations of silver nanoparticles (0.6 and 1.2%). (b) Histogram of swelling behavior of CMC hydrogels with two DS (0.77 and 1.22), with silver nanoparticles (1.2%) without crosslinker (CA 0%) and crosslinked with 15 and 20% of CA.
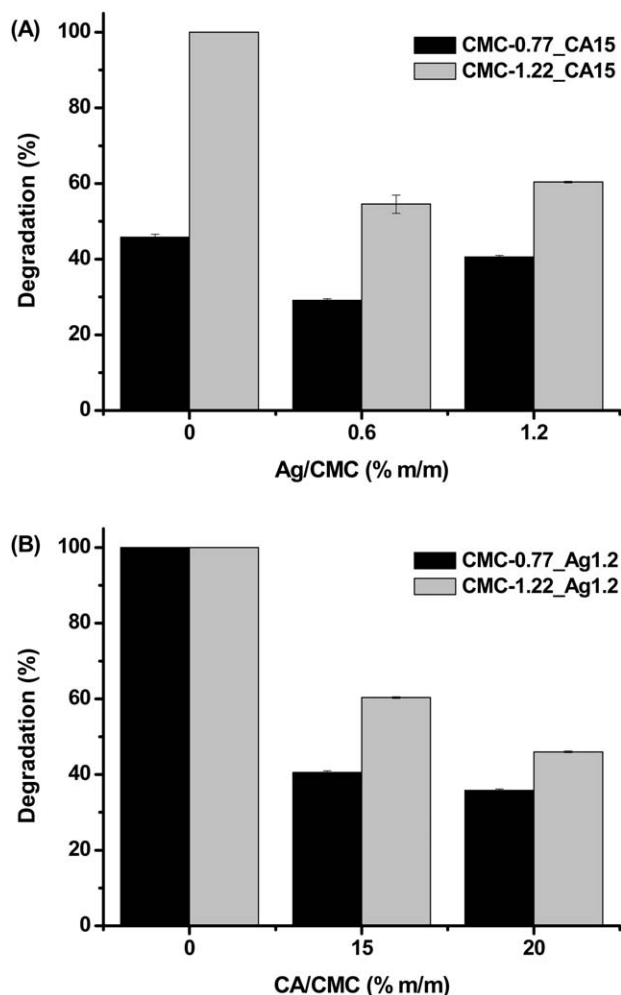
Figure 8. Histogram of degradation behavior of crosslinked (CA 15%) CMC hydrogels with two DS (0.77 and 1.22) and without Ag (0%) and with two concentrations of silver nanoparticles (0.6 and 1.2%). (b) Histogram of degradation of CMC hydrogels with two DS (0.77 and 1.22), with silver nanoparticles (1.2%) without crosslinker (CA 0%) and crosslinked with 15 and 20% of CA.

the degradation in water than CMC DS = 1.22, which was ascribed to the higher concentration of carboxylates facilitating solvation in water media. Consistently to the swelling trend observed in the previous section, a reduction of the values of degradation was verified increasing the concentration of CA [Figure 8(b) and Figure 6S, Supporting Information] with the highest degradation verified for the CMC with higher DS = 1.22.

These results demonstrated undeniably that the DS related to the attached carboxymethyl groups and the concentration of crosslinker played a key role in the formation of CMC polymer network affecting the chemical stability of hydrogels measured by *in vitro* degradation tests. That means, they present high capacity of absorbing water solution or fluids and simultaneously retaining structural stability for potential use as wound dressing and skin substitutes. It is worth mentioning that the degradation evaluated in this study is predominantly related to water solvation of the non-crosslinked polymer chains forming
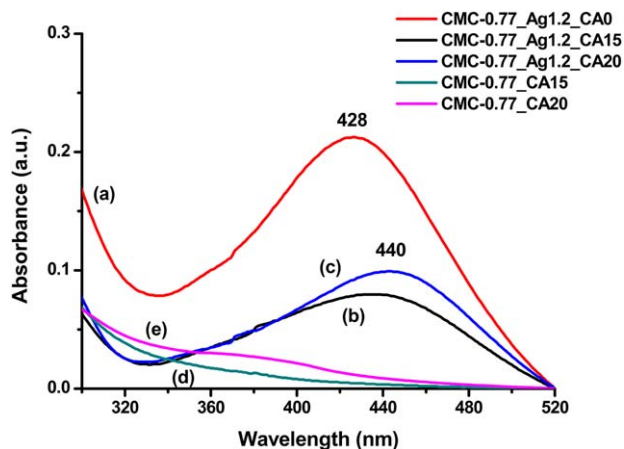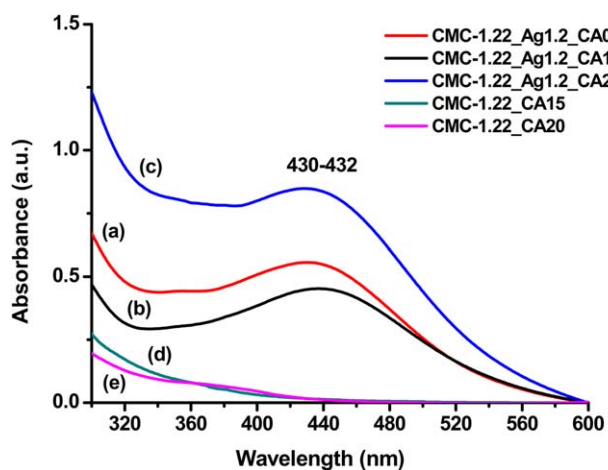

Figure 9. UV–vis spectra of CMC-0.77_Ag1.2 membranes before [(a) CA 0% and after crosslinking (b) CA 15%, and (c) CA 20%] in comparison to hydrogel membranes without silver nanoparticles [(d) CMC-0.77_CA15 and (e) CMC-0.77_CA20]. [Color figure can be viewed at wileyonlinelibrary.com]

the hydrogel network. So, no significant polymer chain degradation (i.e., no chain scission) is expected to occur under light experimental conditions.[6]

Morphological and Spectroscopic Analyses of CMC–AgNPs Hybrid Membranes

UV–Vis Spectroscopy Characterization of AgNPs Embedded in CMC Hybrid Membranes. As discussed in the Characterization of Colloidal Suspension section, the formation of colloidal AgNPs in CMC was monitored by UV–vis spectroscopy and followed after cast the hybrid membranes. The UV–vis results (Figures 9 and 10) indicated the presence of surface plasmon peaks (SPR), a collective excitation of conduction electrons, which are characteristic of nanosized silver particles in the polymer matrices according to the literature.[44,47] In brief, at the concentration of Ag = 1.2%, it was observed an effect of the

Figure 10. UV–vis spectra of CMC-1.22_Ag1.2 membranes before [(a) CA 0% and after crosslinking (b) CA 15%, and (c) CA 20%] in comparison to hydrogel membranes without silver nanoparticles [(d) CMC-1.22_CA15 and (e) CMC-1.22_CA20]. [Color figure can be viewed at wileyonlinelibrary.com]
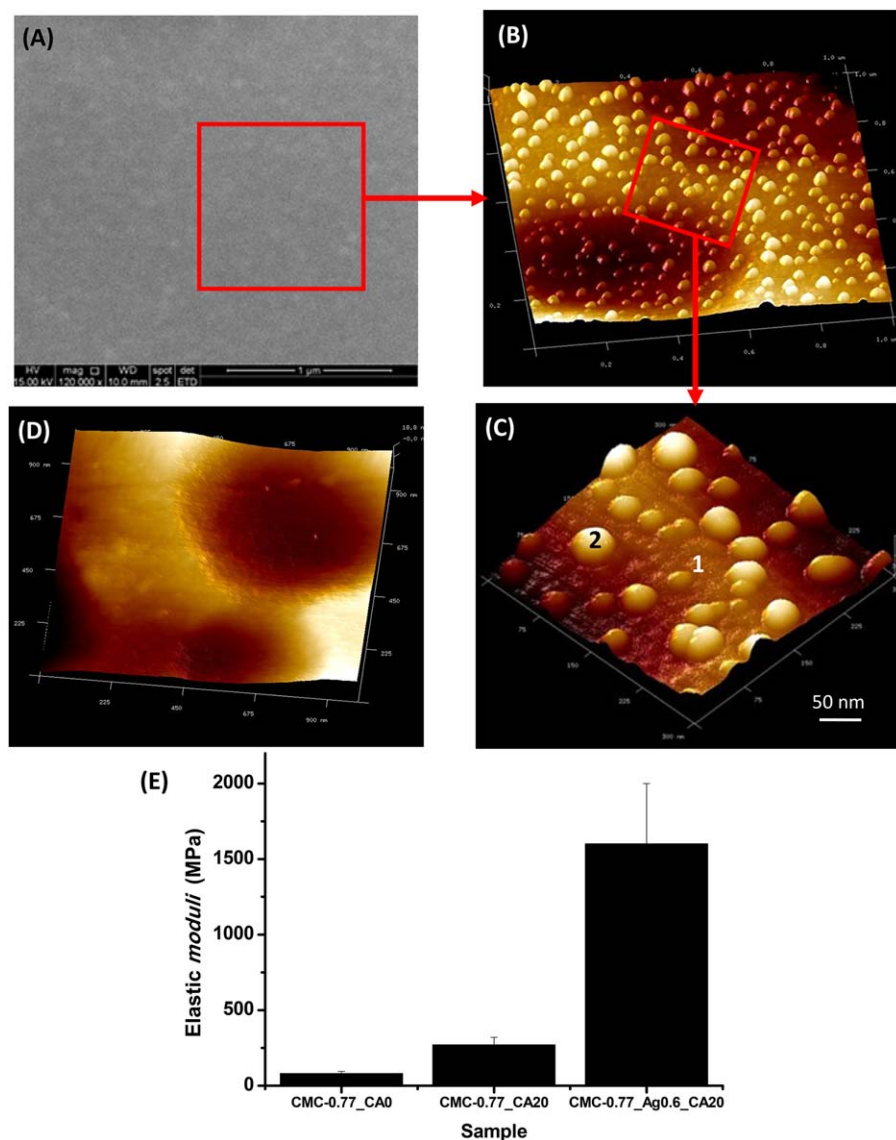
Figure 11. SEM image at magnification 120,000× (a); 3D AFM topographical images of 1 × 1 μm (b), and 300 × 300 nm (c) scanning area of cross-linked hydrogel with 1.2% of AgNPs (CMC-1.22_Ag1.2_CA20). Region (1) associated with polymer network and (2) AgNPs. Reference 3D AFM image of 1 × 1 μm scanning area (d) of crosslinked hydrogel without AgNPs (CMC-1.22_CA20). (e) Histogram of average values of elastic *Moduli*. [Color figure can be viewed at wileyonlinelibrary.com]

presence of CA as crosslinker during the synthesis on the average size of AgNPs formed (CMC, DS = 0.77, Figure 9), with a red-shift of the maxima peak from 428 to 440 nm (or SPR). As the surface plasmon band shifts to lower energy with increasing AgNPs core size, the gradual increase of the concentration of CA crosslinker may have caused further growth of AgNPs, possibility by consuming functional groups (i.e., hydroxyls) of CMC polymer chains or behaving as a reaction catalyst. However, this is just a simplified approach, where other aspects may have also interfered in the SPR shifts (e.g., surface charges and polar groups, 3D conformation of polymer chains, interactions of functional groups, water solvation, etc.).

Conversely, no effect was detected on the CMC system with DS 1.22 (Figure 10), with maxima peak at 430–432 nm for 0–20% of CA. That was attributed to the effect of the higher

concentration of carboxylates in the CMC with DS = 1.22, favoring the stabilization of smaller AgNPs in the colloidal media, independent of the CA concentration, compared to CMC with DS = 0.77. Similar results (Figure 7S, Supporting Information) were observed for lower concentration of silver ions (i.e., 0.6%) in the precursors solutions for CMC with DS = 0.77 and 1.22.

Nanomechanical and Morphological Analyses of CMC–AgNP Hydrogels. Figure 11 shows scanning electron microscopy (SEM, A) and AFM (B and C) images of CMC hybrid membranes crosslinked with CA 20% and with AgNP incorporated by *in situ* chemical reaction during the synthesis. Qualitatively, as a general trend, it can be observed that the hydrogel membranes presented the surface morphology with uniform structural features essentially composed by two highly integrated

regions. The first region (1) presenting mostly flat and "smooth" aspects, characteristic of polymer-based macromolecular network, and the second region (2) with scattered spherical-like components, which were associated with the AgNPs, forming the homogenous nanostructured hybrid matrices. The average size of AgNPs were estimated to range from 20 to 50 nm, which is consistent with the AFM characterization method, where the AgNPs embedded in the CMC polymer matrix are usually overestimated compared to direct techniques (e.g., TEM). These AFM results were fairly similar to all systems based on CMC and AgNP components, where no relevant morphological differences were observed considering the DS parameter (i.e., 0.77 or 1.22), crosslinker concentration (i.e., 15 or 20%), and concentration of Ag^+ (i.e., 0.6 or 1.2%) (Figure 8S, Supporting Information). As a reference, an AFM image of CMC-1.22_CA20 (no AgNPs) is presented in Figure 11(d). In both materials (CMC and CMC–AgNPs), circular valleys smaller than 500 nm of diameter were formed during drying due to water-solvent evaporation.[48]

AFM was also used for the characterization of the structural features at nanoscale dimension and for preliminary assessment of nanomechanical properties of the CMC-based hydrogel membranes with AgNP incorporated into the matrix. For this purpose, a recently developed technique derived from AFM (referred to as "PeakForce Quantitative Nanomechanical Property Mapping") was used for simultaneous quantitative nanomechanical investigation with imaging at high resolution and high speed of the hydrogel membrane. Thus, AFM measurements were performed for evaluating the nanomechanical properties of the CMC hydrogel membranes before and after crosslinking, and the nanocomposite membranes with the incorporation of AgNPs. The results indicated important changes on the surface mechanical properties of CMC hydrogels before and after crosslinking with 20% CA, where the elastic *moduli* (E_M) increased by ~300%, from 80 ± 15 to 270 ± 50 MPa, respectively [Figure 11(e)]. These findings are consistent with the previous results demonstrating that the chemical crosslinking promoted the increase of the rigidity of the polymer hydrogel network causing the reduction of the swelling capacity. In addition, the hybrid membranes composed by CMC crosslinked with 20% CA and with 0.6% of AgNPs showed an even more pronounced increase of the E_M ranging from 1 to 2 GPa (i.e., 5–10 times stiffer than without AgNPs), which is attributed to the extremely high surface area of the AgNPs acting as reinforcement components of the CMC nanocomposite matrix. Hence, these AFM measurements demonstrated the prospective capability of characterizing the surface mechanical properties at nanoscale of CMC–AgNPs nanocomposite membranes dependent of their structural features.

FTIR Characterization of CMC–AgNP Hybrid Membranes. FTIR spectroscopy was used to characterize the CMC, CMC–AgNPs nanocomposites, and crosslinked with CA (Figure 12 and Figure 9S, Supporting Information). In general, CMC-based materials presented a broad band in the 3700–3000 cm^{-1} region assigned to νO─H vibrations including hydrogen bonds formed between OH groups, between water molecules and CH$_2$COONa and OH groups, besides inter- and intrachains hydrogen bonds between

CMC functional groups. In addition, it can be observed the major vibrational bands related to carboxylates (COO$^-$) asymmetric (1592 cm^{-1}) and symmetric (1416 and 1325 cm^{-1}) stretches, adsorbed water (1630–1650 cm^{-1}), and C─O vibrations from primary and secondary alcohols (1110 cm^{-1}, C2─OH; 1060 cm^{-1}, C3─OH; and 1024 cm^{-1} and 995 cm^{-1}, C6─OH). Moreover, the vibrational band associated with β1–4 glycoside bonds between glucose units was detected at 898 cm^{-1}.[49–53]

Regarding to AgNPs formation, the comparison of FTIR spectra of CMC neat hydrogel [Figure 12(a), no AgNPs] and CMC–AgNPs hybrid [Figure 12(b)] indicated that the vibrational bands associated with hydroxyl (OH) functional groups (ca. 3270 and 3385 cm^{-1}) of CMC were relatively reduced by the incorporation of AgNPs in the hybrid matrix. A higher decrease of intensity of the OH band at 3270 cm^{-1} was assigned to O2─H2─O6 intrachain hydrogen bond.[54] This qualitative analysis was confirmed by calculating the ratio of the absorbance of the band of hydroxyls at 3385 cm^{-1} (A_{3385}) and 3270 cm^{-1} (A_{3270}), and the reference band of β1–4 glycoside bond at 898 cm^{-1} (A_{898}), as presented in Figure 13. These findings are consistent with suggested mechanisms of *in situ* chemical reduction of Ag^+ to metallic AgNPs by predominantly through hydroxyl groups of cellulose and derivatives such as CMC.[29–31,38,44] It is considered that the possible mechanism of the formation of AgNPs involves the CMC polymer functional groups not only adsorbing the silver ions in aqueous solution via ion–dipole interactions (1st step), but also playing a key role as reducing chemical species (2nd step), and for stabilizing the colloidal AgNPs (3rd step) via surface interactions.[29–31,38,44]

FTIR spectroscopy was also used to monitor the crosslinking of CMC by CA. The FTIR spectra of CMC-1.22_Ag1.2_CA15 [Figure 12(c)] and CMC-1.22_Ag1.2_CA20 [Figure 12(d)] hydrogels demonstrated that carboxylate bands (1592, 1416, and 1325 cm^{-1}) and carboxylic acid vibrations (─COOH bands at 1730 and 1243 cm^{-1}) co-existed in the CMC crosslinked hydrogel due to the substitution of Na$^+$ to H$^+$ in the CMC chains as a result of the acidification promoted by CA. Crosslinked hydrogels showed a significant decreasing of OH intensity peak at about 3400–3200 cm^{-1} due to chemical reaction of OH groups from CMC with CA-forming ester bonds, as previously reported in literature.[5,55] The calculated values of A_{3385}/A_{898} were 6.9 ± 0.3, 2.7 ± 0.3, and 2.1 ± 0.4 for CMC-1.22_Ag1.2_CA0, CMC-1.22_Ag1.2_CA15, and CMC-1.22_Ag1.2_CA20, respectively. These results indicated the higher depletion of OH band due to the crosslinking reaction with increasing the CA content, in agreement with the swelling and degradation measurements. In addition, the crosslinking reaction was detected by the increase of the intensity in the region associated with ester bonds (R1─COO─R) at 1230–1205 (νC─O) and 1730–1715 cm^{-1} (νC═O). However, it should be stated that the analysis in this region of the spectra is more complex because distinct functional groups are simultaneously formed and consumed in the reaction.

FTIR-MIR Analysis of CMC–AgNP Hybrid Membranes. FTIR-MIR uses infrared radiation to detect and quantify the
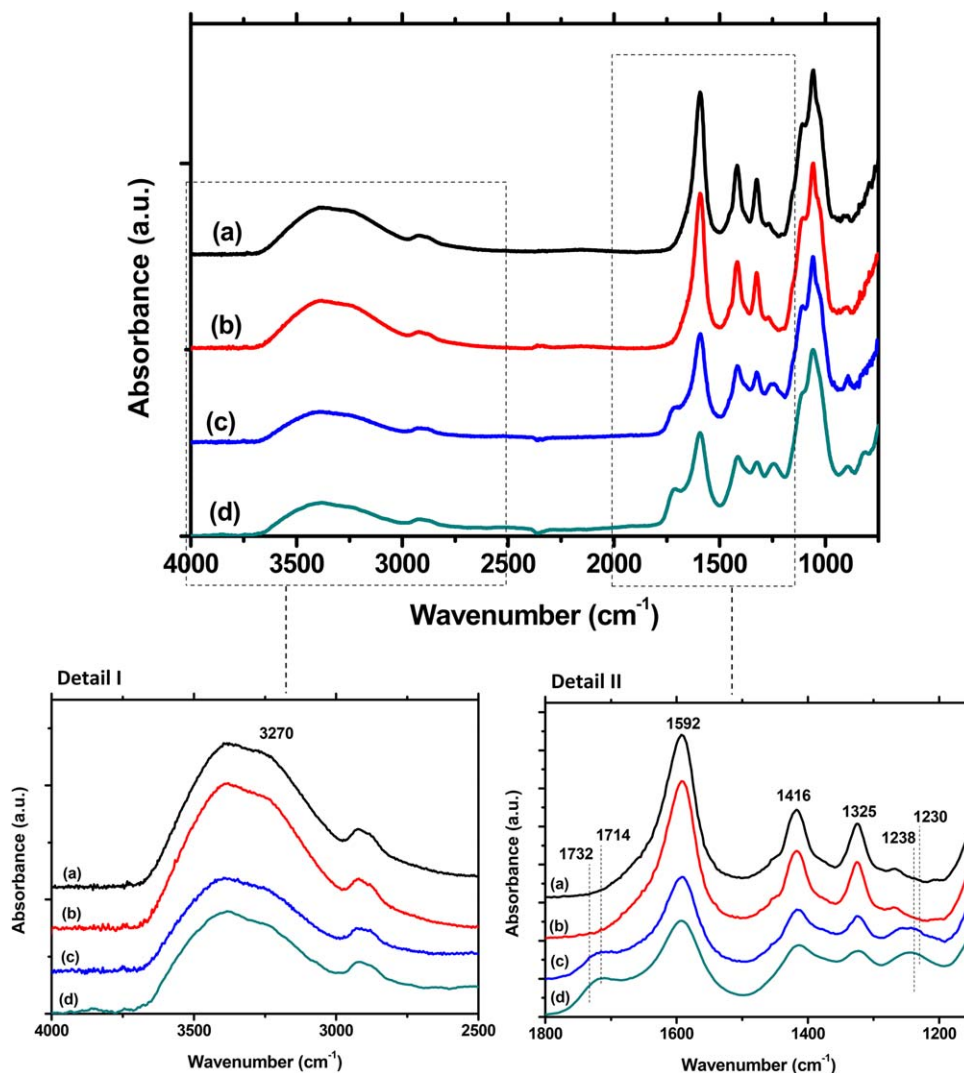
Figure 12. FTIR spectra of (a) CMC polymer (CMC-1.22), (b) CMC–AgNPs (CMC-1.2_Ag1.2_CA0), and CMC–AgNPs crosslinked hydrogels: (c) CMC-1.22_Ag1.2_CA15 and (d) CMC-1.22_Ag1.2_CA20. Detail I: FTIR spectra region from 4000 to 2500 cm^{-1}. Detail II: FTIR spectra region from 1800 to 1150 cm^{-1}. [Color figure can be viewed at wileyonlinelibrary.com]

molecular chemistry of microscopic samples. By combining spectroscopy with microscopy, molecular information can be obtained with spatial resolution at the microscopic level. Samples can be analyzed directly, in air, at RT and pressure, wet or dry, without destroying the sample.[56] In this study, FTIR-MIR was used as a complementary technique to assess the uniformity of the hybrid nanocomposite made of CMC with embedded AgNPs. FTIR-MIR image mapping results displayed in Figure 14 indicated that AgNPs were evenly dispersed in the CMC polymeric matrices, where no agglomeration and segregation based on the signal of hydroxyl functional groups were observed.

Biological Characterization of CMC–AgNPs Hybrid Membranes

Cytotoxicity Characterization by MTT Assay of CMC–AgNPs Hybrid Membranes. The cytocompatibility of the hydrogel membranes was characterized through MTT *in vitro* assays, to

validate the potential of these hydrogels to be applied in the biomedical field as wound dressings and in skin repair.[57–59] The embryonic cell line (HEK293T) was used as a model, since they share similarities with epidermal skin cells (e.g., keratinocytes, dermal fibroblasts), which are involved in the production of essential components of extracellular matrix for tissue repairing.[57–59] In this study, the preliminary assessment of cytocompatibility of the CMC-based crosslinked hydrogels before and after the incorporation of AgNPs was based on analysis of the cell viability of HEK293T using the *in vitro* MTT assay (direct contact method). This test was specifically used to evaluate the mitochondrial function and cell viability and it has been the most widely accepted bioassay for the initial evaluation of *in vitro* toxicity of (nano)materials for potential biomedical applications[21,60] based on the international standard (ISO 10993-5:2009/(R)2014, Biological evaluation of medical devices: Tests for *in vitro* cytotoxicity). However, it should be highlighted that the foremost challenge to design and produce biocompatible
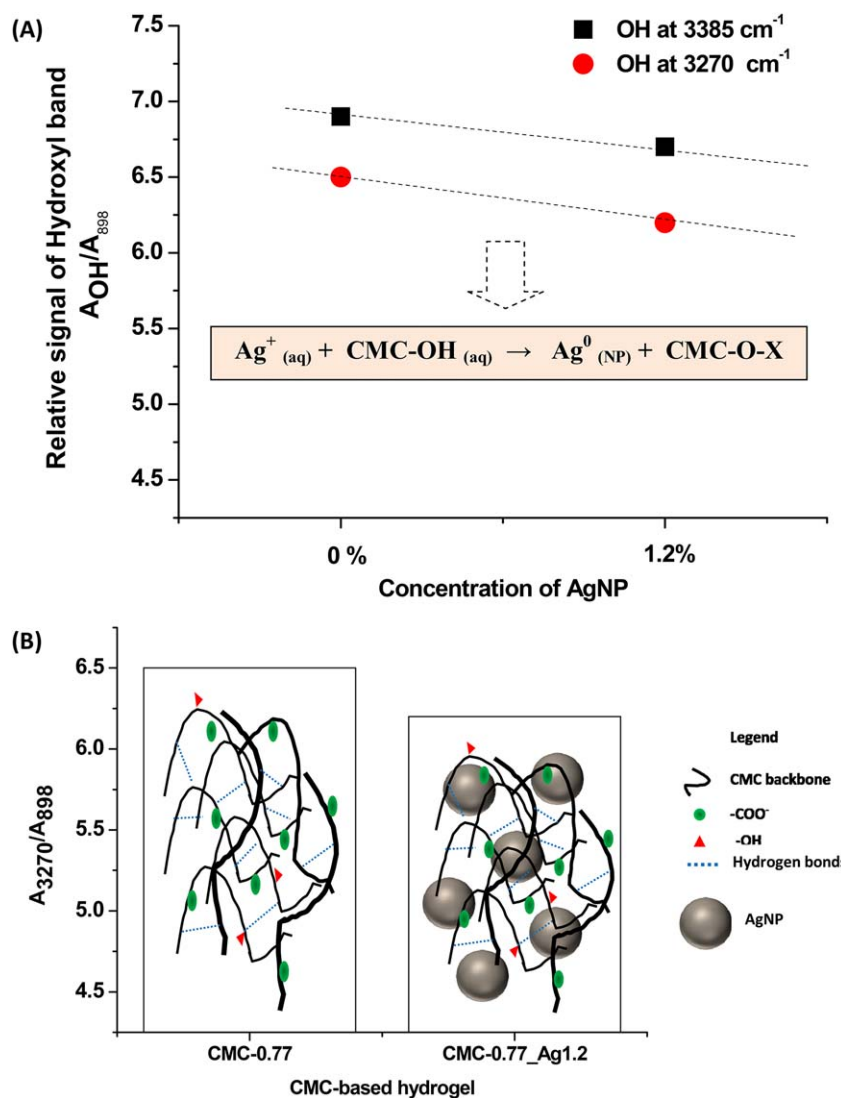
Figure 13. (a) Relative signal of hydroxyl bands for CMC before and after AgNPs synthesis. (b) Absorbance ratio of OH at 3270 cm^{-1} with a schematic representation of CMC membranes (not to scale). [Color figure can be viewed at wileyonlinelibrary.com]
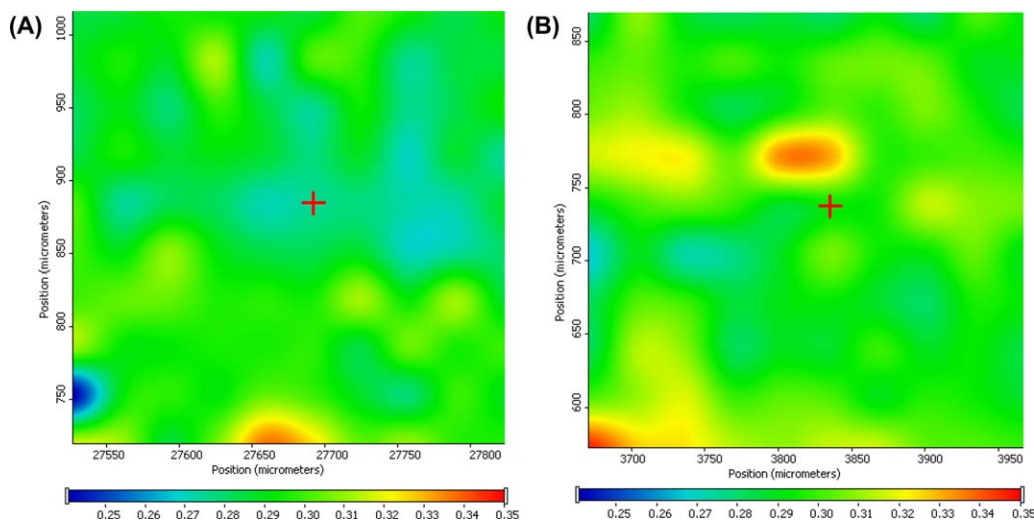
Figure 14. FTIR-microspectroscopy image mapping of OH band at 3270 cm^{-1} for (a) CMC-0.77 and (b) CMC-0.77_Ag0.6. [Color figure can be viewed at wileyonlinelibrary.com]
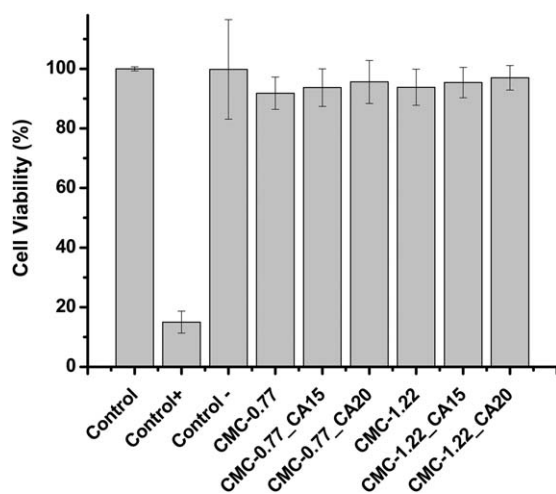
Figure 15. Cell viability response of HEK293T culture based on MTT assay after 24 h incubation with two degree of carboxymethyl substitution (DS 0.77 and 1.22) without crosslinker (CA 0%) and 15 (CA 15%) and 20% crosslinker (CA 20%).

skin substitutes with antibacterial activity is associated with the intrinsic toxicity of metal NPs (nanotoxicity), which could adversely affect the cell viability of the tissue damaged site under repair. To this end, the "smart" biomaterial must combine simultaneously both properties showing appropriate cytocompatibility and antibacterial activity to be suitable as wound dressing and skin repair scaffold. Though, it is not suggested to straight extrapolating the response of cell culture *in vitro* to consider the material tested health and environmentally safe[59,60] for clinical use. For this reason, the CMC-based hydrogel membranes without incorporation of AgNPs were primarily evaluated for cytocompatibility and considered as the reference materials for posterior comparison with the hybrid systems. Figure 15 shows that hydrogel membranes produced with CMC with DS = 0.77 and 1.22 before and after crosslinking with CA (15 or 2 0%) induced no cytotoxic effects, as there were cell viability responses typically over 95%, similar to the control condition (100%, within statistical variation). Despite some minor differences in the architectural and morphological features and physicochemical properties of the CMC-based hydrogels characterized in previous sections, they demonstrated equivalent cytocompatibility towards HEK293T cells, which was attributed to the high biocompatibility of CMC polymers favoring cell metabolic mitochondria activity. Moreover, the choice of using CA as the crosslinker for modifying the hydrogel network was based on the fact that it is a natural compound abundantly found in fruits and therefore, eco-friendly and biocompatible. Therefore, based on the aforementioned results and discussion, CMC hydrogels presented physicochemical properties and cytocompatibility suitable for potential applications in skin tissue replacements.

Figure 16 shows the MTT assay results of cell viability responses towards the hybrid membranes produced with CMC with DS 0.77 and 1.22, crosslinked with CA and with AgNPs embedded in the polymer matrices at two concentrations 0.6 and 1.2%. The effect of AgNPs incorporated in the hydrogel matrices on

the cell viability was demonstrated by a significant reduction compared to CMC hydrogels without AgNPs (Figure 15). However, when the concentration of AgNPs in the nanohybrids was reduced from 1.2 to 0.6% the cell viability was largely increased from approximately 40– 50% to above 70% (Figure 16), which can be considered an acceptable cell viability response for AgNP 0.6% based on the literature[21,60] and according to the biomaterials international standards (ISO 10993-5:2009/(R)2014, Biological evaluation of medical devices: Tests for *in vitro* cytotoxicity). However, it should be highlighted that these results are based on MTT *in vitro* assay and *in vivo* evaluation assays must be performed before any clinical application of these nanocomposites, which is beyond the scope of the current work and should be addressed in future studies.

Antibacterial Activity by Agar Diffusion Method of CMC–AgNPs Hybrid Membranes. In this study, the CMC–AgNP hybrid membranes were tested by antibacterial assay to assess the effectiveness of these systems to potentially inhibit bacterial growth, which is frequently observed in wound infections and injured skin. Essentially, the agar diffusion test (Kirby–Bauer antibiotic testing, KB testing, or disc diffusion antibiotic sensitivity testing) is a test of the antibiotic sensitivity of bacteria. In this test, disks containing antibiotics are placed on an agar plate where bacteria have been placed, and the plate is left to incubate. If an antibiotic stops the bacteria from growing or kills the bacteria, there will be an area around the wafer where the bacteria have not grown enough to be visible, which is called the zone of inhibition (I_Z). So, the size of this zone depends on the effectiveness of the antibiotic for stopping the growth of the bacteria strain, where the higher I_Z value, the stronger is the antibiotic.[26]

Therefore, the antibacterial activity effect of AgNPs with concentrations of 0.6 and 1.2% incorporated in CMC hybrid nanocomposite membranes was tested against both gram-positive (Gram$^+$, *S. aureus)* and gram-negative (i.e., Gram$^-$, *E. coli and*
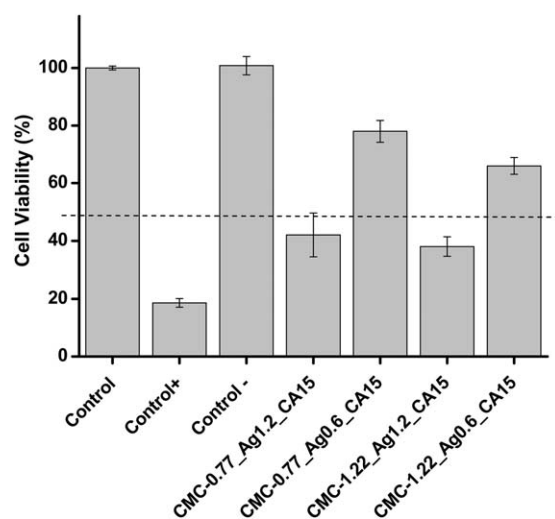

Figure 16. Cell viability response of HEK293T culture based on MTT assay after 24 h incubation with different degree of carboxymethyl substitution (DS 0.77 and 1.22) without crosslinker (CA 0%) and 15% crosslinker (CA 15%) at two concentrations of AgNP (0.6 and 1.22%).

Table I. Results of the Antibacterial Growth Inhibition Zone (I_Z)

Bacteria strain	CMC DS = 0.77		CMC DS = 1.22	
	[AgNP] = 0.6%	[AgNP] = 1.2%	[AgNP] = 0.6%	[AgNP] = 1.2%
E. coli (G⁻)	10.0 ± 0.7	12.0 ± 3.5	11.0 ± 4.2	11.5 ± 0.7
P. aeruginosa (G⁻)	11.0 ± 1.4	13.0 ± 1.4	14.5 ± 3.5	14.0 ± 1.4
S. aureus (G⁺)	13.5 ± 2.1	18.5 ± 3.5	18.5 ± 0.7	16.5 ± 0.7

P. aeruginosa) human bacterial pathogens. The results of the antibacterial growth inhibition zone (I_Z) are summarized in Table I. As a general trend, it was observed that the CMC–

AgNP hybrids with DS = 0.77 with both AgNPs concentrations (0.6 and 1.2%) presented less sensitivity (i.e., lower I_Z values) compared to CMC with DS = 1.22 for all three bacterial strains
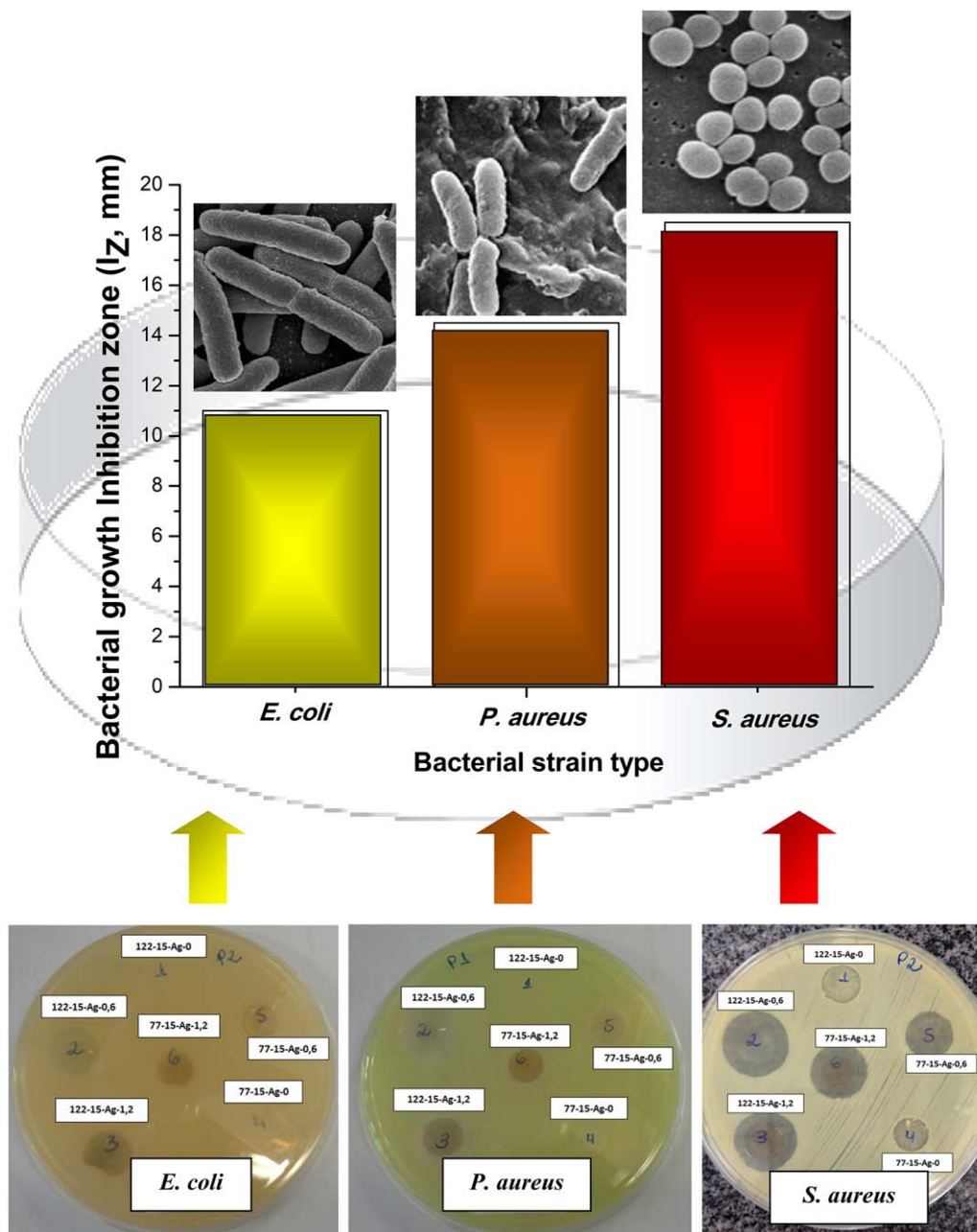
Figure 17. Evaluation of sensitivity of bacteria type towards silver nanoparticles (CMC-0.77_Ag0.6_CA15). Samples identification in petri dishes: 1, CMC-1.22_CA15; 2, CMC-1.22_Ag0.6_ CA15; 3, CMC-1.22_Ag1.2_CA15; 4, CMC-0.77_CA15; 5, CMC-0.77_Ag0.6_CA15; and 6, CMC-0.77_Ag1.2_CA15. Illustrative images of each bacteria strain (top images). [Color figure can be viewed at wileyonlinelibrary.com]

tested. These findings were attributed to the relatively higher kinetics of degradation observed for CMC samples with DS = 1.22, which caused faster release of AgNPs at the cell microenvironment and higher bacteria lethality. Moreover, the sensitivity of bacteria towards AgNPs (i.e., 0.6 and 1.2%) was also found to be very dependent on the strains used, where the maximum zone of inhibition $I_Z = 18.5 \pm 0.7$ mm was observed for CMC–AgNPs (DS = 0.77, 0.6% AgNPs) against *S. aureus* (Gram$^+$) and the minimum inhibition zone of $I_Z = 11.0 \pm 4.2$ mm against *E. coli* (Gram$^-$), with intermediary values for *P. aureus* ($I_Z = 14.5 \pm 3.5$ mm, Gram$^-$). These results are depicted in Figure 17 where a clear effect on bacterial sensitivity dependent on the strain type was verified. Based on the published literature,[61,62] these results can be interpreted considering two major probable mechanisms for the inhibitory effect of AgNPs on bacterial pathogens. The first is associated with the electrostatic attraction between the negatively charged cell membrane of the microorganisms and the positively charged silver ions released at the biomaterial–cell biointerface. The second is the potential formation of pits on the cell wall of bacteria related to silver ions concentration. Fundamentally, AgNPs with positive charge (Ag$^+$) have greater affinity towards negatively charged bacterium by electrostatic interaction causing the most relevant effect regarding to the biocidal activity.[61] In addition, beyond the classification of bacteria according to Gram staining features, Gram-positive bacteria distinguish in many aspects from Gram-negative bacteria. For instance, the plasma membrane is a phospholipid (PL) bilayer consisting of an inner and an outer leaflet that varies among the species not only in PL composition but also in composition of their headgroups and fatty acid moieties. Hence, Gram-positive bacteria have larger fraction of negatively charged phosphatidylglycerol (PG) whereas Gram-negative bacteria contain larger proportions on zwitterionic phosphatidylethanolamine in addition to PG.[62] Thus, due to the relatively higher negative charge on the cell surface, interaction between Gram-positive bacteria (e.g., *S. aureus)* and positive charge on NPs were definitely stronger than that of Gram-negative bacteria (e.g., *E. coli*). To this end, the positive charge containing AgNPs are assumed to bind with negative charge containing bacterial cell membranes and disrupt cell walls as well as surface proteins, finally leading to cell death.[61,62] Furthermore, it is well-known that the antibacterial activity of AgNPs is strongly related to their size and distribution. However, AgNPs with small size tend to aggregate to minimize their surface energy in the process of preparation, which led to a remarkable deterioration of their antibacterial properties. To overcome this shortcoming, it is crucial to find a proper matrix to uniformly and homogeneously host the AgNPs for efficient antimicrobial activity. In this work, the CMC proved to be effective as multifunctional polymer by chemically reducing silver ions and stabilizing the uniformly dispersed metallic particles formed with nanoscale dimensions and rendering a cytocompatible and active antibacterial hybrid nanocomposite biomaterial.[40]

At this point, it is crucial to highlight that the main goal of this work traced back to the idea of exploiting the ability of CMC polysaccharides to form antibacterial and non-cytotoxic hydrophilic hydrogel membranes to be potentially used as dressing in the treatment of non-healing wounds and skin substitutes. Ideally, a wound dressing should offer protection from infections and also should eliminate wound exudates (while retaining at the same time a moist environment) while simultaneously demonstrating lack of cytotoxicity towards skin cells in order to promote the tissue regeneration.[17] Therefore, these results are very interesting, as they clearly demonstrated that the innovative CMC–AgNP hybrid nanocomposites combined both characteristics of cytocompatibility and antimicrobial activity including the higher sensitivity towards the Gram$^+$ bacterial strains (e.g., *S. aureus),* which can offer antimicrobial efficiency and specificity in treatments against multi-resistant skin pathogens in wound injuries.

CONCLUSIONS

In this study, we focused on the synthesis and comprehensive characterization of cytocompatible nanocomposite hydrogels based on carboxymethyl-functionalized cellulose derivative chemically crosslinked by CA and incorporated with AgNPs for antibacterial activity. These nanohybrids were produced strictly using green aqueous process for potential applications as wound dressing and skin substitutes. The results demonstrated that SAP were produced with tailored degree of swelling, ranging from 100 to 1500%, depending on the DS of CMC, controlling the chemical crosslinking and content of AgNPs. The swelling and degradation measurements associated with the spectroscopical and morphological characterization results evidenced that the functional groups of CMC (e.g., hydroxyls and carboxylates) played a relevant role in the mechanism of AgNPs formation and in the crosslinking process of the polymer network forming the nanocomposite membranes. Moreover, these hybrid membranes with uniformly AgNPs incorporated demonstrated suitable cytocompatibility (at concentration of AgNPs of 0.6%) towards live HEK297T cells using MTT *in vitro* assay and simultaneously with high antibacterial activity against Gram-positive and Gram-negative bacteria strains. To that end, they are envisioned as promising novel superabsorbent nanocomposites with key properties for skin wound healing and regeneration associated with antibacterial activity against human skin pathogens, which is particularly relevant as the next generation of "smart" skin repair substitutes.

REFERENCES

1. Geoffrey, C. G.; Werner, S.; Barrandon, Y.; Longaker, M. T. *Nature.* **2008**, *453*, 314.

2. Blanpain, C. *Nature.* **2010**, *464*, 686.

3. Lutolf, M. P.; Hubbell, J. A. *Nat. Biotechnol.* **2005**, *23*, 47.

4. Yang, C.; Xu, L.; Zhou, Y.; Zhang, X.; Huang, X.; Wang, M.; Han, Y.; Zhai, M.; Wei, S.; Li, J. *Carbohydr. Polym.* **2010**, *82*, 1297.

5. Demitri, C.; Del Sole, R.; Scalera, F.; Sannino, A.; Vasapollo, G.; Maffezzoli, A.; Ambrosio, L.; Nicolais, L. *J. Appl. Polym. Sci.* **2008**, *110*, 2453.

6. Carvalho, I. C.; Mansur, H. S. *Mater. Sci. Eng. C.* **2017**, *78*, 690.

7. Shah, R.; Vyroubal, R.; Fei, H.; Saha, N.; Kitano, T.; Saha, P. *AIP Conf. Proc.* **2015**, *1662*, 040007.

8. Chang, C.; Zhang, L. *Carbohydr. Polym.* **2011**, *84*, 40.

9. Harsh, D. C.; Gehrke, S. H. *J. Control. Release.* **1991**, *17*, 175.

10. Kalia, S.; Kaith, B. S.; Kaur, I. Cellulose Fibers: Bio- and Nano-Polymer Composites;Springer-Verlag: Berlin Heidelberg, **2011**.

11. Sannino, A.; Demitri, C.; Madaghiele, M. *Materials.* **2009**, *2*, 353.

12. Ma, J.; Li, X.; Bao, Y. *RSC Adv.* **2015**, *5*, 59745.

13. Zheng, W. J.; Gao, J.; Wei, Z.; Zhou, J.; Chen, Y. M. *Eur. Polym. J.* **2015**, *72*, 514.

14. Ogushi, Y.; Sakai, S.; Kawakami, K. *J. Biosci. Bioeng.* **2007**, *104*, 30.

15. Wang, Z.; Ning, A.; Xie, P.; Gao, G.; Xie, L.; Li, X.; Song, A. *Carbohydr. Polym.* **2017**, *157*, 48.

16. Boer, M.; Duchnik, E.; Maleszka, R.; Marchlewicz, M. *Adv. Dermatol. Allergol.* **2016**, *33*, 1, doi: 10.5114/pdia.2015.48037.

17. Sacco, P.; Travan, A.; Borgogna, M.; Paoletti, S.; Marsich, E. *Mater. Sci. Eng. C.* **2015**, *26*, 128.

18. Pelgrift, R. Y.; Friedman, A. J. *Adv. Drug Deliv. Rev.* **2013**, *65*, 1803.

19. Rai, M. K.; Deshmukh, S. D.; Ingle, A. P.; Gade, A. K. *J. Appl. Microbiol.* **2012**, *112*, 841.

20. Gong, P.; Li, H.; He, X.; Wang, K.; Hu, J.; Tan, W.; Zhang, S.; Yang, X. *Nanotechnology.* **2007**, *18*, 285604.

21. Samberg, M. E.; Oldenburg, S. J.; Monteiro-Riviere, N. A. *Environ. Health Perspect.* **2010**, *118*, 407.

22. Kalashnikova, I.; Das, S.; Seal, S. *Nanomedicine.* **2015**, *10*, 2593.

23. Dumont, V. C.; Mansur, A. A. P.; Carvalho, S. M.; Borsagli, F. G. L. M.; Pereira, M. M.; Mansur, H. S. *Mater. Sci. Eng. C.* **2016**, *59*, 265.

24. Mansur, H. S.; Costa, H. S.; Mansur, A. A. P.; Pereira, M. *Mater. Sci. Eng. C.* **2012**, *32*, 404.

25. Ma, L.; Gao, C.; Mao, Z.; Zhou, J.; Shen, J.; Hu, X.; Han, C. *Biomaterials.* **2003**, *24*, 4833.

26. Balouiri, M.; Sadiki, M.; Ibnsouda, S. K. *J. Pharm. Anal.* **2016**, *6*, 71.

27. Gomes, J. F.; Garcia, A. C.; Ferreira, E. B.; Pires, C.; Oliveira, V. L.; Tremiliosi-Filho, G.; Gasparotto, L. H. S. *Phys. Chem. Chem. Phys.* **2015**, *17*, 21683.

28. Raveendran, P.; Fu, J.; Wallen, S. L. *J. Am. Chem. Soc.* **2003**, *125*, 13940.

29. He, J.; Kunitake, T.; Nakao, A. *Chem. Mater.* **2003**, *15*, 4401.

30. Maneerung, T.; Tokura, S.; Rujiravanit, R. *Carbohydr. Polym.* **2008**, *72*, 43.

31. Dallas, P.; Sharma, V. K.; Zboril, R. *Adv. Colloid Interface Sci.* **2011**, *166*, 119.

32. Kelly, K. L.; Coronado, E.; Zhao, L. L.; Schatz, G. C. *J. Phys. Chem. B.* **2003**, *107*, 668.

33. Hutter, E.; Fendler, J. H. *Adv. Mater.* **2004**, *16*, 1685.

34. Hanaor, D. A. H.; Michelazzi, M.; Leonelli, C.; Sorrell, C. C. *J. Eur. Ceram. Soc.* **2012**, *32*, 235.

35. Mansur, A. A. P.; Ramanery, F. P.; Oliveira, L. C.; Mansur, H. S. *Carbohydr. Polym.* **2016**, *146*, 455.

36. Ramanery, F. P.; Mansur, A. A. P.; Mansur, H. S.; Carvalho, S. M.; Fonseca, M. C. *Nanoscale Res. Lett.* **2016**, *11*, 187.

37. Stewart, M. P.; Sharei, A.; Ding, X.; Sahay, G.; Langer, R.; Jensen, K. F. *Nature.* **2016**, *538*, 183.

38. Sharma, V. K.; Yngard, R. A.; Lin, Y. *Adv. Colloid Interface Sci.* **2009**, *145*, 83.

39. Scholl, J. A.; Koh, A. L.; Dionne, J. A. *Nature.* **2012**, *483*, 421.

40. Shao, W.; Liu, X.; Min, H.; Dong, G.; Feng, Q.; Zuo, S. *ACS Appl. Mater. Interfaces.* **2015**, *7*, 6966.

41. Moulder, J. F.; Stickle, W. F.; Sobol, P. E.; Bomben, K. D. Handbook of X-ray Photoelectron Spectroscopy; Perkin-Elmer Corporation: Eden Prairie, **1992**.

42. Pauly, N.; Yubero, F.; Tougaard, S. *Appl. Surf. Sci.* **2016**, *383*, 317.

43. Wu, X.; Lu, C.; Zhou, Z.; Yuan, G.; Xiong, R.; Zhang, X. *Environ. Sci. Nano.* **2014**, *1*, 71.

44. Song, J.; Kang, H.; Lee, C.; Hwang, S. H.; Jang, J. *ACS Appl. Mater. Interfaces.* **2012**, *4*, 460.

45. Metcalfe, A. D.; Ferguson, M. W. J. *J. R. Soc. Interface.* **2007**, *4*, 413.

46. Sun, B. K.; Siprashvili, Z.; Khavari, P. A. *Science.* **2014**, *346*, 941.

47. Huang, T.; Murray, R. W. *J. Phys. Chem. B.* **2003**, *107*, 7434.

48. Kaczmarek, H.; Nowicki, M.; Vuković-Kwiatkowska, I.; Nowakowska, S. *J. Polym. Res.* **2013**, *20*, 91.

49. Cintrón, M. S.; Hinchliffe, D. J. *Fibers.* **2015**, *3*, 30.

50. Higgins, H. G.; Stewart, C. M.; Harrington, K. J. *J. Polym. Sci.* **1961**, *51*, 59.

51. Luna-Martínez, J. F.; Hernández-Uresti, D. B.; Reyes-Melo, M. E.; Guerrero-Salazar, C. A.; González-González, V. A.; Sepúlveda-Guzmán, S. *Carbohydr. Polym.* **2011**, *84*, 566.

52. Mansur, A. A. P.; de Carvalho, F. G.; Mansur, R. L.; Carvalho, S. M.; de Oliveira, L. C.; Mansur, H. S. *Int. J. Biol. Macromol.* **2017**, *96*, 675.

53. Zeleňák, V.; Vargová, Z.; Györyová, K. *Spectrochim. Acta, Part A.* **2007**, *66*, 262.

56

54. Li, W.; Sun, B.; Wu, P. *Carbohydr. Polym.* **2009**, *78*, 454.

55. Raucci, M. G.; Alvarez-Perez, M. A.; Demitri, C.; Giugliano, D.; De Benedictis, V.; Sannino, A.; Ambrosio, L. *J. Biomed. Mater. Res. Part A.* **2016**, *103A*, 2045.

56. Wetzel, D. L.; LeVine, S. M. *Science.* **1999**, *20*, 1224.

57. Stepanenko, A. A.; Dmitrenko, V. V. *Gene.* **2015**, *569*, 182.

58. Cusick, J. K.; Mustian, A.; Goldberg, K.; Reyland, M. E. *Cell Immunol.* **2010**, *261*, 1.

59. Carvalho, S. M.; Mansur, A. A. P.; Mansur, H. S.; Guedes, M. I. M. C.; Lobato, Z. I. P.; Leite, M. F. *Mater. Sci. Eng. C.* **2017**, *71*, 412.

60. Oh, E.; Liu, R.; Nel, A.; Gemill, K. B.; Bilal, M.; Cohen, Y.; Medintz, I. L. *Nat. Nanotechnol.* **2016**, *11*, 479.

61. Prema, P.; Thangapandiyan, S.; Immanuel, G. *Carbohydr. Polym.* **2017**, *158*, 141.

62. Malanovic, N.; Lohner, K. *Biochim. Biophys. Acta. Biomembr.* **2016**, *1858*, 936.

Capítulo 5. Hidrogéis de carboximetil celulose conjugados com fármaco antitumoral para aplicação no tratamento tópico de câncer de pele

5.1. Graphical Abstract
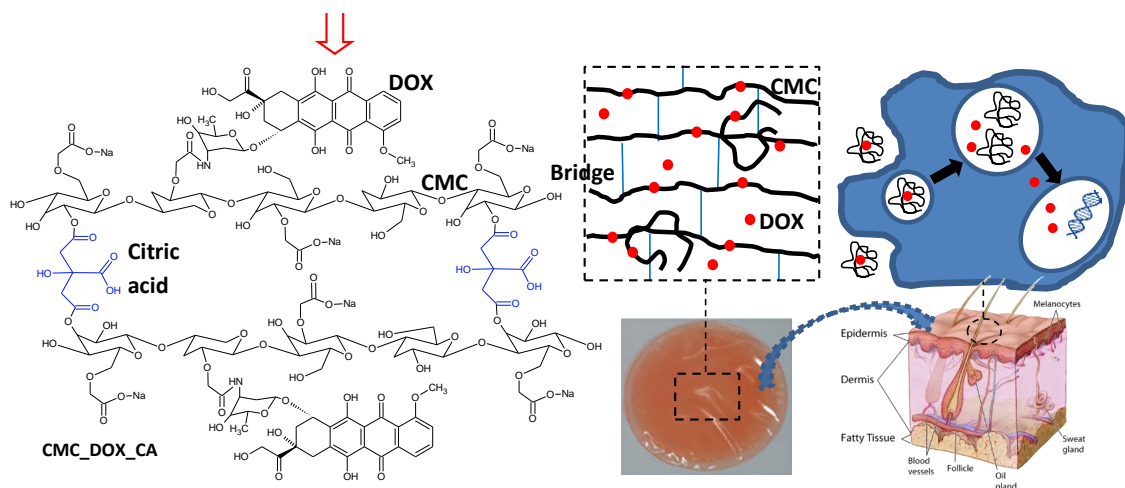
Bioengineered Carboxymethyl Cellulose-Doxorubicin Prodrug Hydrogels for Topical Chemotherapy of Melanoma Skin Cancer

5.2. Resumo

O melanoma é o tipo mais agressivo de câncer de pele com altas taxas de mortalidade. Apesar de grandes avanços nos últimos anos com o desenvolvimento de sistemas de liberação das drogas anticâncer direcionados para o microambiente tumoral, os efeitos colaterais da quimioterapia ainda permanecem como um grande desafio. Neste estudo, projetamos e sintetizamos novos bioconjugados de polímero-droga usando a carboximetil celulose (CMC) com dois graus de substituição (DS = 0,77 e 1,22) e a droga anticâncer, cloridrato de doxorrubicina (DOX), covalentemente ligada na CMC utilizando uma carbodiimida (EDC) como agente de ligação. A formação de uma ligação amida como resultado da reação entre o grupo amina da DOX e o grupo carboxílico da CMC mediada pelo EDC foi comprovada através da espectroscopia de infravermelho (FTIR) e a espectroscopia de ultravioleta-visível (UV-vis) permitiu

avaliar uma eficiência de carregamento superior a 98%. Na seqüência, os bioconjugados CMC-DOX sintetizados foram reticulados com ácido cítrico (CA/CMC 15% m/m) através de uma rota de processamento "verde" para a produção de hidrogéis polímero-droga. Os bioconjugados foram caracterizados por medidas de intumescimento e degradação que foram influenciados pelo grau de substituição do polímero e pela presença da DOX. Os ensaios de liberação *in vitro* acelular mostraram que nas condições de ensaio somente a droga adsorvida ou covalentemente ligada com cadeias de CMC solvatadas foram liberadas, uma vez que a quebra das ligações amida irá ocorrer mediada por enzimas no interior da célula. Além disso, resultados de citotoxicidade dos hidrogéis polímero-droga utilizando células normais (HEK 293T) e células de melanoma (A375) mostraram que o conjugado apresentou modulação da liberação da droga, dependente do DS da CMC e do tipo de célula, que foi mais lenta na droga conjugada em comparação com a DOX livre e mais lenta nas células normais em comparação com a célula cancerígena. Comportamento similar foi observado nos ensaios de internalização da droga que foi avaliada através de microscopia confocal utilizando a luminescência intrínseca do fármaco. Assim, uma plataforma inovadora foi desenvolvida com base em hidrogéis de polissacarídeo-droga que oferecem perspectivas promissoras para aplicação tópica no tratamento do melanoma, com redução dos efeitos agudos nas células normais.

5.3. Artigo

Capanema, Nádia S.V.; Mansur, A.A.P.; Carvalho, S.M.; Carvalho, I.C.; Chagas, P.; de Oliveira, L.C.; Mansur, H.S. Bioengineered Carboxymethyl Cellulose-Doxorubicin Prodrug Hydrogels for Topical Chemotherapy of Melanoma Skin Cancer. Carbohydrate Polymers, v. 195, p. 401-412, 2018. **QUALIS A1 – JCR 4.811**
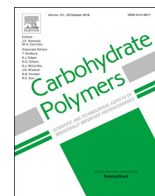
Bioengineered carboxymethyl cellulose-doxorubicin prodrug hydrogels for topical chemotherapy of melanoma skin cancer

Nádia S.V. Capanema[a], Alexandra A.P. Mansur[a], Sandhra M. Carvalho[a], Isadora C. Carvalho[a], Poliane Chagas[b], Luiz Carlos A. de Oliveira[b], Herman S. Mansur[a],*

[a] Center of Nanoscience, Nanotechnology and Innovation—CeNano²I, Department of Metallurgical and Materials Engineering, Federal University of Minas Gerais/UFMG, Brazil
[b] Department of Chemistry—ICEX, Federal University of Minas Gerais/UFMG, Brazil

A B S T R A C T

Melanoma is the most aggressive type of skin cancer with high rates of mortality. Despite encouraging advances demonstrated by anticancer drug carriers in recent years, developing ideal drug delivery systems to target tumor microenvironment by overcoming physiological barriers and chemotherapy side effects still remain intimidating challenges. Herein, we designed and developed a novel carbohydrate-based prodrug composed of carboxymethylcellulose (CMC) polymer bioconjugated with anticancer drug doxorubicin hydrochloride (DOX) by covalent amide bonds and crosslinked with citric acid for producing advanced hydrogels. The results demonstrated the effect of CMC hydrogel network structure with distinct degree of substitution of carboxymethyl groups of the cellulose backbone regarding to the process of bioconjugation and on tailoring the DOX release kinetics *in vitro* and the cytotoxicity towards melanoma cancer cells *in vitro*. To this end, an innovative platform was developed based on polysaccharide-drug hydrogels offering promising perspectives for skin disease applications associated with topical chemotherapy of melanoma.

1. Introduction

Skin cancer represents one of the most commonly occurring carcinoma in human and it is growing at a rate of one million new cases reported annually. Malignant melanoma is the most lethal form of skin cancer and it is associated with poor prognosis causing deaths worldwide. Therefore, melanoma continues to remain an important health threat, with death often occurring by metastasis. Although there are several options for anti-melanoma therapy, it is resistant to some therapies. The primary cutaneous melanoma can be managed by surgery at the early stage, but the advanced metastatic melanoma cannot be properly treated by surgery alone. Therefore, it requires additional therapeutic methods such as chemotherapy, biochemotherapy, immunotherapy, and adoptive cell therapy (Bharadwaj, Das, Paul, & Mazumder, 2016; Vishnubhakthula, Elupula, & Durán-Lara, 2017). To mitigate or avoid side effects commonly caused by oral administration and intravenous injection of drugs (*i.e.,* enteral or parenteral), topical (*i.e.,* local) transdermal drug delivery systems offer a promising alternative strategy as carriers of antineoplastic agents. Thus, the topical administration of chemotherapeutics is considered an encouraging approach for effective therapy of skin cancer (Bharadwaj et al., 2016; Vishnubhakthula et al., 2017). Polymeric-based drug delivery systems are the most interesting vehicles in anti-cancer therapy. There are several advantages of using polymer as carriers for antineoplastic agents, including increased drug solubility, better bioavailability, high stability, controlled drug release, selective organ or tissue distribution, and reduction of the total dose required. Moreover, the association of polymers with toxic anticancer drugs can significantly minimize the adverse side effects (Ranjbari et al., 2017; Vishnubhakthula et al., 2017). For that reason, polymeric (nano)carriers are the most extensively studied platforms for cancer treatment. Polymers are versatile macromolecules that can be engineered to fulfill several properties required for sophisticated biomedical applications in oncology. The research at the interface of polymer chemistry and biomedical sciences has given rise to the polymer-based pharmaceuticals, referred to as 'polymer therapeutics'.

In this regard, polymer therapeutics has emerged as a new promising field of research, which encompasses rationally designed

macromolecular drugs, such as polymer–protein conjugates, polymer-drug conjugates, polyplexes for encapsulating nucleotides (*i.e.,* RNA, DNA), and supramolecular drug-delivery systems (Duncan, 2003, 2013). Numerous polymer–based conjugates with improved chemical and biological stability and pharmacokinetic properties have been developed by coupling low-molecular-weight anticancer drugs to high-molecular-weight polymers through cleavable covalent bonds, including *N*-(2-hydroxypropyl)methacrylamide conjugates of doxorubicin hydrochloride (DOX) and paclitaxel (Duncan, 2003, 2013; Haag & Kratz, 2006). Among different types of biocompatible polymers, carbohydrate-based polymers (or polysaccharides) are the most common natural polymers with chemical structures consisting of long chains of monosaccharide (or disaccharide) units bound by glycosidic linkages. They possess properties such as biocompatibility, biodegradability, non-toxicity, suitable reactivity for facile chemical modification associated with availability and low cost led to their widespread applications in pharmaceutical and biomedical fields including development of nanocarriers for delivery of anticancer therapeutic agents. Generally, polysaccharide-based polymer-drug systems can be used for reducing systemic toxicity, increasing short half-lives and tumor localization of agents for a successful cancer therapy. This approach can overcome the most challenging factor in cancer therapy related to the toxicity of anticancer therapeutic agents for normal cells and therefore, targeted delivery of these drugs to the site of action can be considered as a very promising therapeutic strategy (Duncan, 2003, 2013; Haag & Kratz, 2006; Ranjbari et al., 2017).

One option of rational design of innovative polymer-drug systems for topical drug delivery systems is based on hydrogels. Hydrogels are three-dimensional, hydrophilic polymeric networks that are capable of absorbing large amounts of water, biological fluids, or molecules. These systems possess unique properties to improve the efficacy of the therapeutic agents and minimize undesirable side effects. Hydrogels serve as an *in situ* vehicle for localized delivery of antineoplastic agents by topical application, allowing minimally or noninvasive delivery, avoiding side effects of systemic chemotherapeutics and while reducing infection risk associated with surgical procedures (Vishnubhakthula et al., 2017). Moreover, some properties and important advantages of these hydrogel-based polymer-drugs can be modulated by the chemical crosslinking of the network and the interactions of the hydrogels with the surrounding microenvironment, including drug release dynamics, hydrogel degradation kinetics, drug levels at the cancer site, sustaining duration of therapeutic concentrations, circumventing poor solubility of anticancer drugs, which are critical to chemotherapeutic efficacy and safety (Liu et al., 2016).

Among several alternatives of polysaccharides (*e.g.,* hyaluronic acid, chitosan, and cellulose) for producing polymer-drug conjugates, carboxymethyl cellulose (CMC), as a broadly available derivative of cellulose, finds widespread use in biology, medicine, nutrition and pharmaceutical formulations. It presents excellent characteristics such as biocompatibility and water solubility combined with highly reactive chemical groups including hydroxyl and carboxyl groups, which can allow chemical biofunctionalization and the formation of hydrogels with tailored crosslinked networks. Moreover, CMC is an inexpensive compound with good compatibility to the skin and mucous membranes, which has been approved by the United States Food and Drug Administration (FDA) for parenteral use in drug products (Duncan, 2013; Haag & Kratz, 2006; He et al., 2015; Movagharnezhad & Moghadam, 2016; Ranjbari et al., 2017; Roy et al., 2014). The degree of substitution (or carboxymethylation, DS) of carboxymethyl cellulose plays a pivotal role on all properties, including water solubility, pH-sensitivity, chemical reactivity and stability, rheology and biodegradability, which can be tuned for several applications in biomedical, food, and pharmaceutical fields (Ferro et al., 2017).

To this end, carbohydrate-based polymeric hydrogels have been studied as anticancer drug carriers that are not soluble in water and highly cytotoxic for chemotherapeutic applications. Doxorubicin, an

amphiphilic anticancer drug, is the most clinically used anticancer drug because of its high efficiency and a broad spectrum of activity against diverse cancer types (*e.g.,* breast, lung, skin, and brain cancers) but is poorly soluble in water and physiological medium (solubility of hydrochloride salt < 2%). Therefore, the development of simply synthesized, economical, water-soluble, and biocompatible polymer-drug delivery systems with efficient DOX encapsulation is still highly needed against skin cancers. Interestingly, despite intensive research in the field of polymer-drug conjugates (He et al., 2015; Movagharnezhad & Moghadam, 2016; Roy et al., 2014), no published study was found in the literature of CMC-DOX crosslinked hydrogels for treating melanoma cancer. We hypothesize that it may be possible to perform covalent linkage between carboxymethyl cellulose (*i.e.,* $-COO^-$ groups) with doxorubicin hydrochloride (*i.e.,* $-NH_2$ groups) forming polymer-drug conjugates. In the sequence, they could be chemically crosslinked by citric acid producing hydrogel matrices for active drug delivery against skin cancer cells. Herein, we designed and synthesized CMC-DOX conjugates *via* carbodiimide-mediated reactions for the formation of amide bonds in aqueous medium. These polymer-drug conjugates were used for producing hydrogel networks by chemical crosslinking with eco-friendly citric acid. The results proved that hydrophilic hydrogel membranes based on CMC-DOX conjugates were synthesized with physicochemical characteristics and anticancer drug delivery profiles effective for killing melanoma cells, which offer potential applications as topical transdermal chemotherapy against skin cancer.

2. Material and methods

2.1. Materials and cell cultures

Sodium carboxymethyl cellulose with two degree of substitution DS = 0.77 (CMC-0.77, Product Number: 419311, Batch Number: MKBW1368V, average molar mass $M_w = 250$ kDa and, viscosity 735 cps, 2% in H_2O at 25 °C) and DS = 1.22 (CMC-1.22, Product Number: 419281, Batch Number: MKBV4486V, $M_w = 250$ kDa, viscosity 660 cps, 2% in H_2O at 25 °C), 2-(*N*-Morpholino)ethanesulfonic acid (MES, > 99%, low moisture content), 1-Ethyl-3-[3-dimethylaminopropyl]carbodiimide hydrochloride (EDC, ≥98%), doxorubicin hydrochloride (hydroxydaunorubicin hydrochloride, referred to as DOX, ≥98.0%,), ethalonamine hydrochloride (≥99.0%), and citric acid (CA, ≥99.5%,) were supplied by Sigma-Aldrich (USA).

Aforementioned chemicals were used without further purification, deionized water (DI water, Millipore Simplicity™) with resistivity of 18 MΩ cm was used to prepare the solutions, and the procedures were performed at room temperature (RT, 23 ± 2 °C), unless specified otherwise.

Human embryonic kidney (HEK 293T, American Type Culture Collection – ATCC® CRL-1573™) cells was provided by Federal University of Minas Gerais. Human malignant melanoma (A375, ATCC® CRL-1619™) was purchased from Brazilian Cell Repository (Banco de Células do Rio de Janeiro: BCRJ, Brazil; cell line authentication molecular technique, *Short Tandem Repeat (STR) DNA*; quality assurance based on the international standard NBR ISO/IEC 17025:2005).

2.2. Polymer-drug conjugation

The DOX anticancer drug was conjugated to the CMC polysaccharide backbone with two DS using 1-ethyl-3-[3-dimethylaminopropyl] carbodiimide hydrochloride (EDC) as a "zero-length" coupling agent in MES buffer (0.25 M, pH 5.5 ± 0.1).

Polymer-drug bioconjugation of was performed as follows: 1.0 mL of EDC solution (12.5 wt%) was added to the reaction flask with 10 mL of CMC solution (2.0 wt.% in MES) and magnetically stirred for 15 min at 6 ± 2 °C. Under continuous stirring, 400 µL of DOX solution (0.145 wt.% in MES) was poured into the flask, and the system was incubated at RT for 2 h in the dark. The polymer-drug systems were

61

referred to as "CMC-0.77_DOX" and "CMC-1.22_DOX" depending on the DS of the polymer used for conjugation 0.77 or 1.22, respectively. The molar ratio CMC$_{unit}$:DOX was 1000:1.

All of the samples were kept in the dark at RT overnight and then, ethanolamine hydrochloride was added to the reaction flasks and magnetically stirred for 15 min at final concentration of 1.0 μM to quench the reaction. These synthesized polymer-drug conjugates were dialyzed for 24 h (with water changes after 2 h and 4 h) in the dark against 2 L of distilled water using a Pur-A-Lyzer™ Mega Dialysis Kit (Sigma, cellulose membrane with M$_w$ cut-off of 12 kDa) under moderate stirring at RT. After purification, the polymer-drug solutions were stored at 6 ± 2 °C until further use.

2.3. Synthesis of prodrug hydrogels

Crosslinking agent, citric acid (CA), was added under stirring at concentration of 15% m/m of polymer-drug solutions (CMC-0.77_DOX and CMC-1.22_DOX) and homogenized for 20 min. Then, 10 mL of the solutions were poured into plastic molds (polystyrene petri dish, diameter = 60 mm) and were allowed to dry at 40 ± 2 °C for 24 h to remove water. In the sequence, the samples were kept at 80 ± 2 °C for 24 h for the crosslinking reaction (slow evaporation method). The prodrug hydrogels (Fig. 1) were referred to as "CMC-0.77_DOX_CA" and "CMC-1.22_DOX_CA". The concentration of DOX in both hydrogels was

3.0 mg g^{-1} (5.2 μmol g^{-1}). As references, hydrogels without DOX chemotherapeutic were also synthesized and referred to as "CMC-0.77_CA" and "CMC-1.22_CA".

2.4. Physicochemical characterization of CMC polymer, CMC-DOX polymer-drug conjugates and hydrogels

For CMC polymers, infrared spectroscopy and ^{1}H nuclear resonance spectroscopy (^{1}H NMR) analyses were performed with details described in Supplementary Material. CMC is available as regular commercial product by worldwide reliable supplier and USA FDA approved. Therefore, this study characterized the most relevant aspects by FTIR and ^{1}H NMR spectroscopy techniques.

Fourier-transform infrared spectroscopy (FTIR) spectra were obtained using attenuated total reflectance method (ATR, 4000–675 cm^{-1}, 32 scans, and 4 cm^{-1} resolution, Nicolet 6700, Thermo Fischer) with background subtraction (replicates, n = 3).

Ultraviolet-visible (UV-vis) spectroscopy measurements were performed (Lambda EZ-210, Perkin-Elmer) in transmission mode over the wavelength range between 600 and 350 nm (n = 3).

Photoluminescence spectroscopy (PL) was performed at RT using a violet diode laser at 405 nm excitation wavelength (λ$_{exc}$) (150-mW, Roithner LaserTechnik) coupled to a USB4000 VIS-NIR (visible-near infrared) spectrophotometer (Ocean Optics, Inc.) (n = 3).
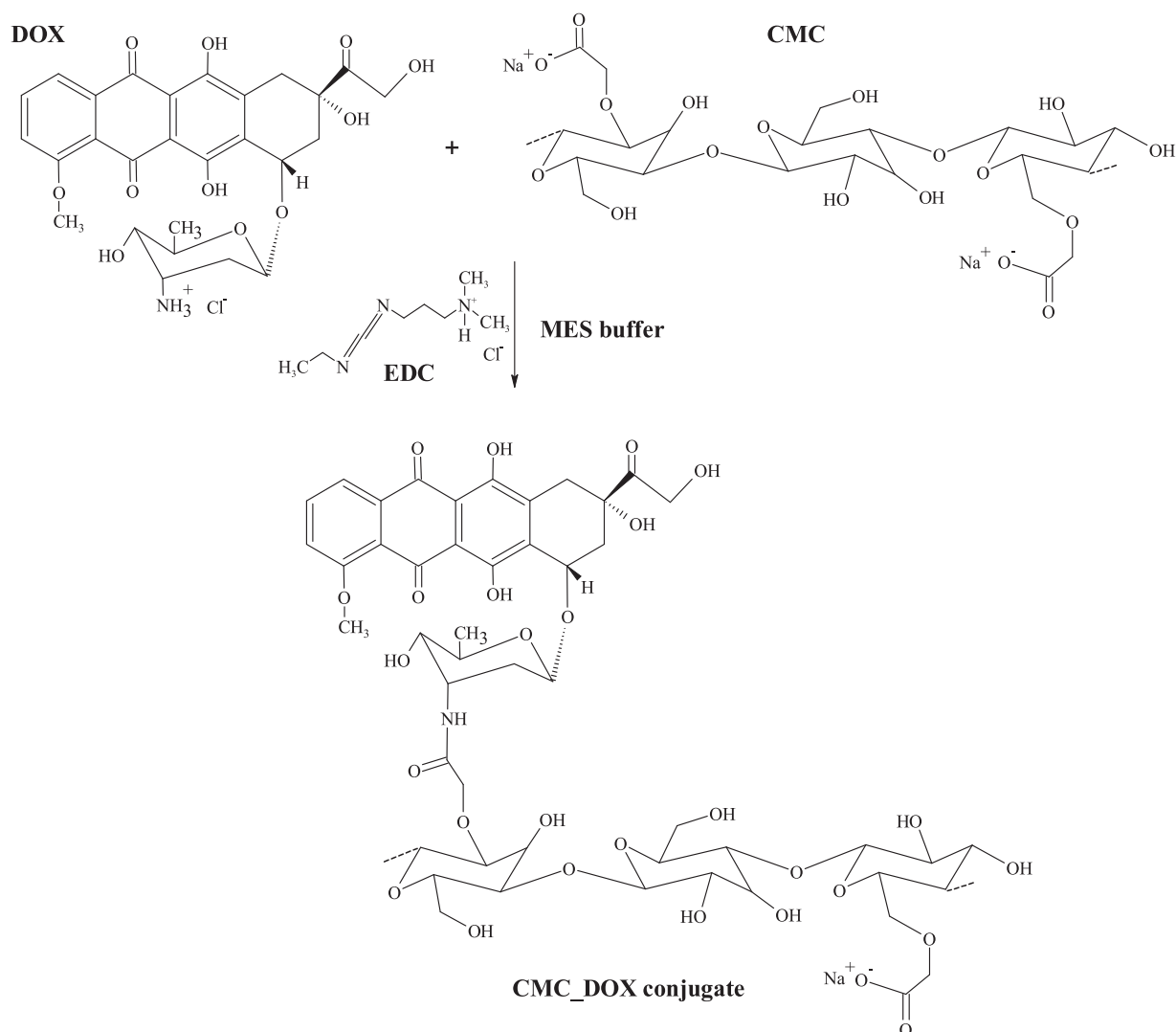

Fig. 1. Schematic representation of the precursors, reaction and CMC_DOX conjugate product.

62

Zeta potential (ZP or ζ-potential) analysis was performed using ZetaPlus instrument (Brookhaven Instruments, 35 mW red diode laser light, wavelength λ = 660 nm) at 25 ± 2 °C under the Smoluchowski approximation method (n ≥ 10).

For evaluating the loading efficiency, the polymer-drug conjugates were centrifuged (15 min at 14,000 rpm and 4 ± 1 °C, Hettich Mikro 200R) using an ultracentrifuge filter with a 50 kDa cut-off cellulose membrane (Amicon filter, Millipore). The filtrate was collected and analyzed by UV–vis spectroscopy (Lambda EZ-210, Perkin Elmer) to determine the DOX concentration based on the Beer–Lambert correlation curve (Fig. 1S). The loading efficiency (LE, %) was calculated using Eq. (1).

$$LE = ((A − B)/A) \times 100 \qquad (1)$$

where A (mg mL^{-1}) is the initial concentration of DOX in solution and B (mg L^{-1}) is the concentration of DOX at filtrate.

For fluid uptake measurement and solvation assessments, the hydrogels were cut into 10×10 mm^2 samples, dried at 40 ± 2 °C for stabilization of mass, and weighted (W$_0$, initial mass). Then, the hydrogel samples (n = 3) were placed in 70 mL sample pots with 10.0 mL PBS (phosphate buffered saline, pH 7.4) at 37 ± 1 °C. After 60 min, the hydrogel was removed from solution, gently wiped with filter paper to remove excess of liquid of the sample surface and weighted (W$_s$, swollen mass). In the sequence, samples were dried at 40 ± 2 °C until mass stabilization and the final weight was recorded (W$_f$, final mass).

The measurements of weight obtained in each step of the process were used to calculate the swelling degree (SD) and gel fraction (GF) of the hydrogels using Eqs. (2) and (3) (Dumont et al., 2016; Fekete, Borsa, Takács, & Wojnárovits, 2017).

$$SD (\%) = ((W_s − W_0)/W_0) \times 100\% \qquad (2)$$

$$GF (\%) = (W_f/W_0) \times 100\% \qquad (3)$$

In vitro drug release from hydrogels was performed in triplicate at 37.0 ± 0.1 °C in PBS buffer (pH 7.4). Prodrug hydrogels (6 cm^2) were placed inside a plastic basket immersed into 15 mL of PBS under magnetic stirring and drug release monitored for 24 h (n = 3). At determined time intervals, 1 mL of PBS medium was collected and analyzed by UV–vis to determine the DOX concentration based on the Beer–Lambert correlation curve (λ = 484 nm).

2.5. Biological characterization of hydrogels

2.5.1. Cell viability in vitro – Mitochondrial activity (MTT) assay
MTT (3-(4,5-dimethylthiazol-2yl) 2,5-diphenyl tetrazolium bromide) experiments were performed to evaluate the toxicity of free DOX and prodrug conjugates at final concentration of 25 μM after incubation with HEK 293T and A375 cells for 6 h, 24 h and 48 h (detailed protocol in Supplementary Material). The percentage of cell viability was calculated after blank corrections, according to Eq. (4), where the values of the control group were set to 100% cell viability.

Cell viability = (Absorbance of sample and cells)/(Absorbance of control) × 100   (4)

2.5.2. Cellular uptake of polymer-drug bioconjugates – confocal laser scanning microscopy (CLSM)
DOX distribution inside the cells was monitored using CLSM after treatment of HEK 293T and A375 cells for 30 min, 1 h, 2 h and 6 h, using the inherent fluorescence imaging capability of DOX and TO-PRO®-3 (Invitrogen™, USA) to selective staining the nuclei of the cells (detailed protocol in Supplementary Material).

3. Results and discussion

3.1. Characterization of CMC polymer

To avoid redundancy, the characterization of carboxymethylcellulose with two degree of substitution (DS) was performed using FTIR (Fig. 2S) and ^{1}H NMR (Fig. 3S) techniques and the results are presented in Supplementary Material. In brief, the FTIR analysis showed the most important chemical functionalities of CMC polymer (*e.g.,* carboxylic, carboxylates and hydroxyls) and CMC with higher DS values (*i.e.,* DS = 1.22 > 0.77) presented more prominent spectroscopy intensities associated with the carboxymethyl groups grafted in the cellulose polymer backbone. In ^{1}H NMR spectra, resonance signals associated with unsubstituted and substituted hydroxyls were detected. The integration of the unsubstituted protons signals for CMC polymers for both DS values indicated the reduction of the relative intensity of hydroxyls for DS = 1.22 due to the higher carboxymethylation content of the polymer (*i.e.,* cellulose-O-H → cellulose-O-CM).

3.2. Physicochemical characterization of polymer-drug conjugates

CMC polymer has no electronic transitions in the visible range (Fig. 2A(d and e)) due to the absence of unsaturated bonds of conjugated π-electrons for this absorption. Conversely, DOX is an anthracycline antibiotic with a chromophore anthraquinone nucleus linked to daunosamine amino sugar through a glycosidic bond, which presents a characteristic resonance peak at 484 nm assigned to π→π* energy state transitions of quinonoid (Fig. 2A(a)) (Mohan & Rapoport, 2010). For that reason, both polymer-drug conjugates made of CMC with DS = 0.77 and 1.22 (Fig. 2A(b and c)) presented the same transition due to activity of DOX as chromophores.
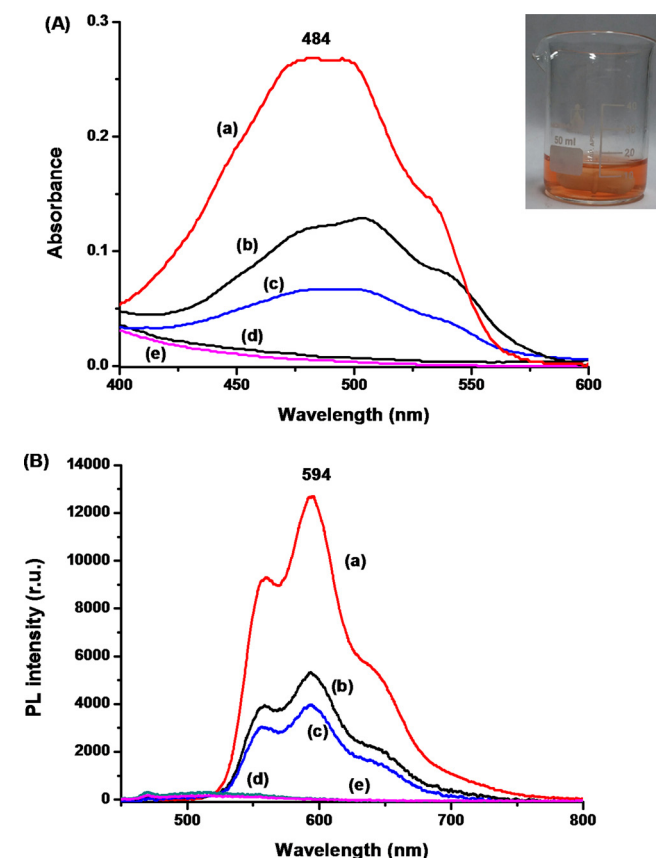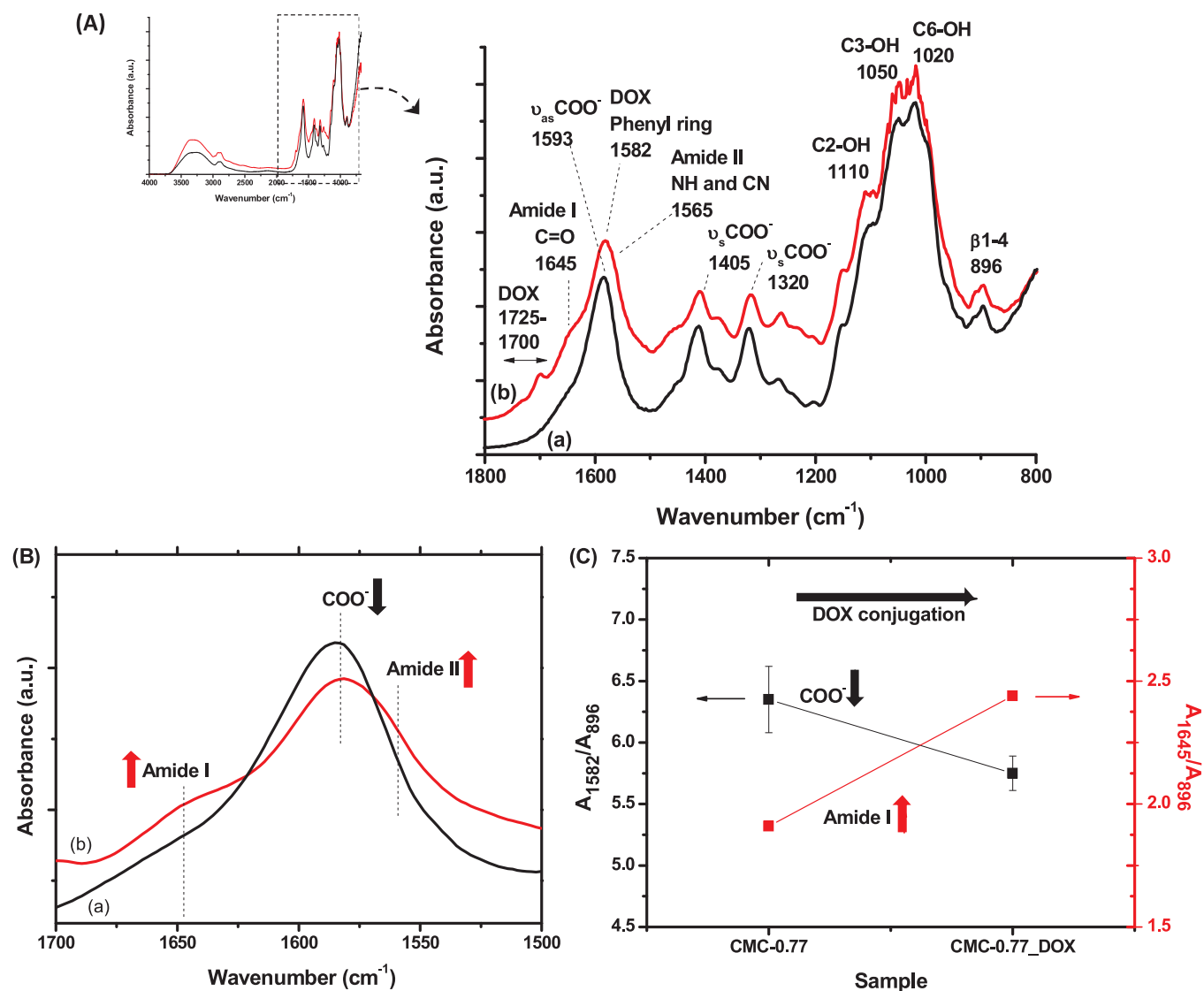

Fig. 2. (A) Absorbance (visible) and (B) Emission (PL) spectra of (a) DOX, (b) CMC-0.77_DOX, (c) CMC-1.22_DOX, (d) CMC-0.77 and (e) CMC-1.22 solutions.

63

Fig. 3. (A) FTIR spectra of CMC-0.77 before (a) and after (b) conjugation with DOX. (B) Detail of FTIR spectra region associated with the range of Amide I, Amide II and $\nu_{as}COO^-$ vibrations. (C) Evolution of Amide I and carboxylate bands due to chemical conjugation reactions.

Fluorescence spectrum of DOX (Fig. 2B(a)) shows an orange emission at λ = 594 nm with a characteristic Stokes shift of 110 nm from the absorption peak at λ = 484 nm (Motlagh, Parvin, Ghasemi, & Atyabi, 2016). This inherent fluorescence can be used as biomarker providing information on drug distribution inside cells and tissues (Mohan & Rapoport, 2010) providing therapeutic and bioimaging capabilities combined in the same molecule. CMC_DOX prodrugs (Fig. 2B(b and c)) presented similar spectra with lower intensity, which was attributed to fluorescence quenching caused by molecular interactions after the conjugation reaction. Therefore, based on the optical absorption and emission spectra it is affirmed that DOX was effectively coupled to CMC polymer and retained its chemical stability as chromophore after the EDC-mediated reaction.

FTIR spectroscopy (Figs. 3A (DS = 0.77) and 4S(A) (DS = 1.22)) was used to monitor changes in the polysaccharide polymer chains caused by chemical conjugation. After the coupling reaction with EDC zero-length linker, two new bands appeared associated with Amide I (C=O) and Amide II (NH and CN) at 1645 cm⁻¹ and 1565 cm⁻¹, respectively (detailed in Figs. 3B and 4S(B)). In addition, the presence of vibration bands related to DOX at 1725 cm⁻¹ (δN−H), 1710 cm⁻¹ (nC=O, C−H₂, O−H) and 1582 cm⁻¹ (phenyl ring) was detected (Das et al., 2010). Fig. 3C shows the relative increase of Amide I

(1645 cm⁻¹) and decrease of $\nu_{as}COO^-$ (1582 cm⁻¹) bands using β1-4 vibration at 896 cm⁻¹ as the internal reference band, caused by the formation of amide bonds between carboxylic groups of CMC and amino groups of DOX in agreement with the literature (Cao et al., 2017; Li et al., 2017; Mansur & Mansur, 2012; Mansur, Mansur, Soriano-Araújo, & Lobato, 2014). Thus, these FTIR results provided additional strong evidence of the effective covalent conjugation of the CMC to anticancer chemotherapeutic drug *via* chemical amide bonds, which validated the hypothesis of this research.

Zeta potential analyzes are crucial for investigating conjugated systems based on polymer-drugs for biomedical and pharmaceutical applications. The presence of local and global surface charges on the systems can drastically affect the responses when in contact with biological microenvironment *in vitro* and *in vivo*. The results of ZP measurements showed the relative reduction of the average negative values of CMC (absolute values, standard deviation, SD = ± 2 mV) before and after conjugation with DOX, from −39.4 mV to −36.9 mV, and from −50.6 mV to −43.1 mV, for CMC-0.77 and CMC-1.22 systems, respectively. These values are coherent with the designed chemical reaction developing amide bonds between negative groups of CMC (−COO⁻) with positive groups of protonated DOX (−NH₃⁺) under mildly acidic or physiological conditions. In addition, it was observed
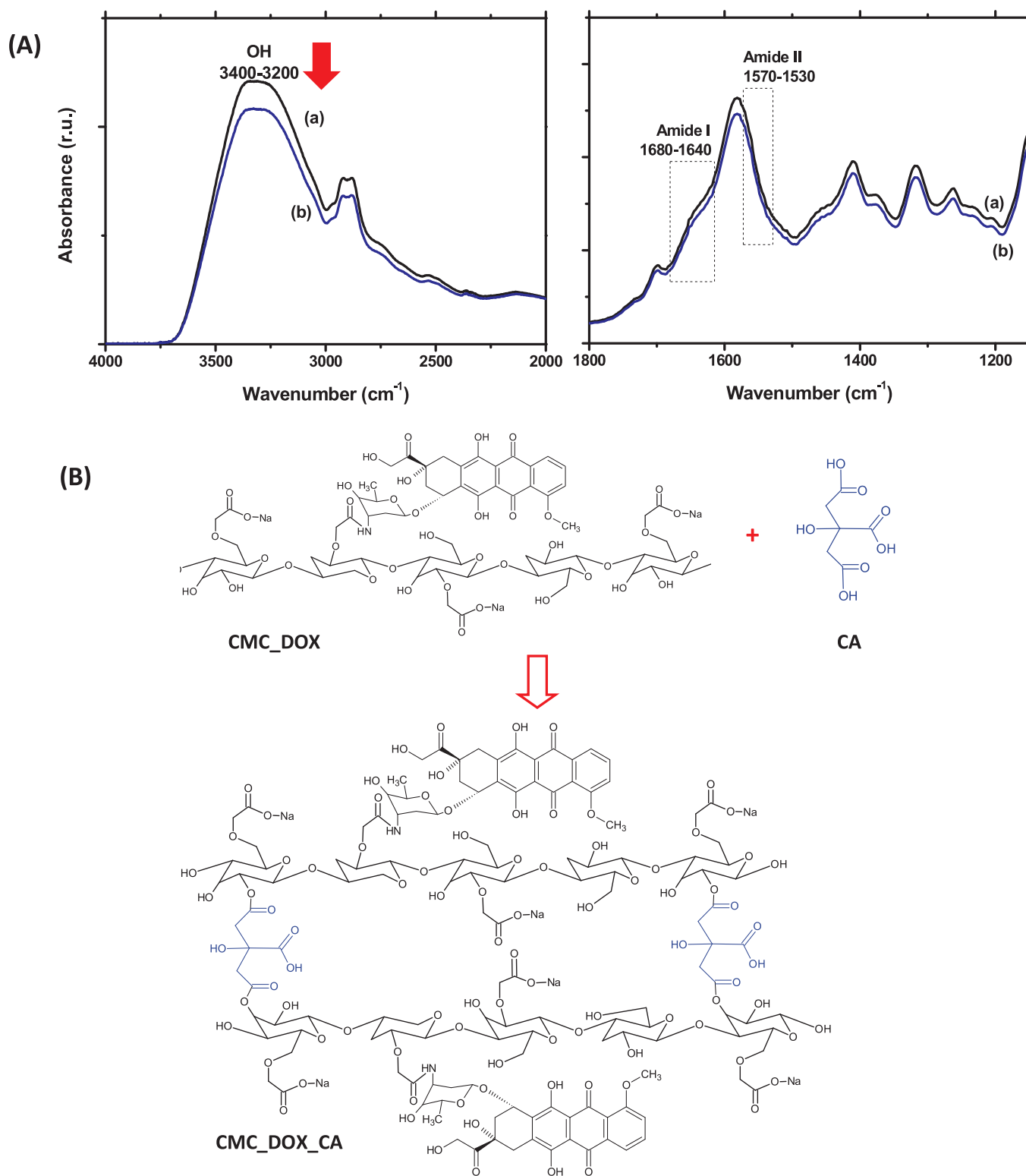
Fig. 4. (A) FTIR spectra of CMC-0.77_DOX polymer not crosslinked (a) and crosslinked with CA. (B) Schematic representation of CMC_DOX_CA crosslinked structure and precursors (CMC_DOX and CA).

higher values of ZP for CMC polymer with superior degree of substitution (CMC DS = 1.22, ZP = −50.6 mV > CMC DS = 0.77, ZP = −39.4 mV), which was assigned to the higher concentration of negatively charged carboxylate groups inserted in the polysaccharide chain. These results endorsed the findings of previous sections and validated the mechanism of covalent coupling of CMC with DOX producing macromolecular structures.

Loading efficiency (LE) measured after synthesis (pH 5.5, MES buffer) was more than 98% for both hydrogels (DS = 0.77 and 1.22). Based on FTIR results, the formation of polymer-drug covalent bonded conjugates by the presence of the amide linkage between the COO⁻ groups of CMC and amino groups (NH₂) of the sugar moiety of DOX anticancer drug was confirmed. However, due to the presence of electrostatic interactions between protonated DOX molecules (*i.e.*,
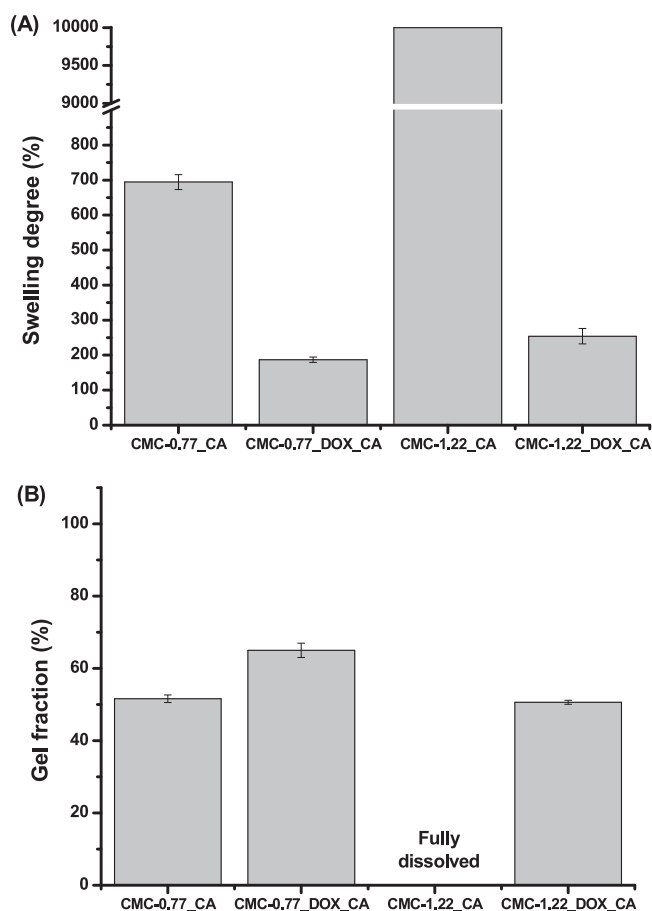
Fig. 5. Histograms of (A) Swelling degree and (B) Gel fraction obtained from hydrogels.

positively charged, pKa = 8.2 (He et al., 2015)) and negatively charged CMC chains forming water soluble complexes cannot be ruled out.

3.3. Physicochemical characterization of prodrug hydrogels

CMC-DOX bioconjugates were crosslinked with eco-friendly citric acid (CA) for producing 2D hydrogel membranes as prodrug carriers against skin cancer cells. These hydrogels were characterized and the UV–vis spectra are presented in Fig. 5S. The characteristic initial absorbance bands of DOX were also observed in the polymer-drug hydrogels indicating the chemical stability of DOX after the crosslinking reaction of CMC-based conjugates with citric acid.

FTIR spectroscopy was used to monitor the crosslinking of CMC_DOX macromolecules by CA. Crosslinked hydrogels (CMC_DOX_CA, Figs. 4A and 6S) showed a significant decrease of OH intensity peak at approximately 3400–3200 cm^{-1} due to the formation of ester bonds by the consumption of hydroxyls from CMC in the reaction with CA, as reported in literature (Capanema et al., 2017). In addition, as expected, amide bonds were not affected by this crosslinking reaction. The schematic representation of the crosslinking chemical reaction is depicted in Fig. 4B.

Fig. 5A shows the swelling degree of the hydrogels with DS 0.77 and 1.22 crosslinked with 15% of CA using CMC and CMC-DOX conjugates. For hydrogels without DOX, the CMC-1.22_CA system was fully dissolved in aqueous medium (*i.e.*, absence of stable crosslinked network) but the swelling value for CMC-0.77_CA indicated the formation of covalent bonds bridging the functional groups of the polymer chains causing an increase of the rigidity of the hydrogel. This behavior may be explained by considering the higher concentration of COO$^-$ groups in the CMC with DS 1.22 that increased its hydrophilicity (*i.e.,* solvation

in water) and also caused repulsion between adjacent negatively charged carboxylate groups, restricting the formation of crosslinking bonds inter-intra cellulose polymer chains. The results for hydrogels made with polymer-drug conjugates (187 ± 7.5% for CMC-0.77_DOX_CA and 254.0 ± 22% for CMC-1.22_DOX_CA) showed important reduction of the swelling behavior indicating that the covalent coupling with DOX reduced the polarity of the system for solvation with water molecules. This trend was assigned to the consumption of carboxylate groups of CMC during the initial formation of amide bonds with DOX combined with intra- and intermolecular interactions between chemical functionalities of CMC and DOX and the presence of hydrophobic regions in the aromatic structure of the drug.

Similarly, the gel fraction results are presented in Fig. 5B. For CMC with higher degree of substitution (DS = 1.22), the hydrogel changed from practically soluble (*i.e.,* GF = 0%) to approximately 50% of gel fraction due to the presence of DOX. For lower DS = 0.77, the observed trend was the same, *i.e.* decrease of GF for drug loaded hydrogel, consistent with the swelling behavior. It is important to mention that the gel fraction measurements are associated with the combination of effects. The fraction from the polymer chains that were effectively crosslinked by CA forming the hydrogel network and remained stable after solvation combined with the release of physically entangled CMC chains. No degradation of polymer chain backbone is expected to occur under these mild experimental conditions. Regarding to the application as polymer-drug therapeutics, this means that part of the loaded DOX drug will be more readily available because it is conjugated to uncrosslinked CMC (*i.e.,* loose chains) or due to the DOX absorbed to CMC by electrostatic interactions (*i.e.,* not covalently bonded). Conversely, the DOX bonded to CMC crosslinked polymer forming the hydrogel structure will be available only after biochemical degradation processes at the site of application, which occurs at much slower kinetics. It should be stressed that, in order to effectively alter the drug release profile, the cleavage of the amide bonds between DOX with CMC polymer chains is expected to occur mostly at lysosomes after cellular uptake (catalyzed by proteases, *etc.*) (Zhang, Li, You, & Zhang, 2017). Therefore, this profile is very appropriate for potential topical transdermal application for polymer-drug chemotherapy of skin cancer as it can promote tuned release of the drug for longer periods of time. Moreover, recent studies revealed that topical transdermal administration is being considered for the systematic drug circulation. Transdermal delivery (*e.g.,* hydrogel, gel cream, ointment and paste) offers several clinical benefits over conventional oral, nasal, intramuscular, and intravenous administration because it requires a lower daily dose, it has direct access to the target site and minimize the pain and prevent systemic side-effects (Alkilani, McCrudden, & Donnelly, 2015; Mandal et al., 2017). Hence, the hydrogels developed in this study based on CMC-DOX conjugates forming crosslinked matrices were designed to be potentially utilized as transdermal "patches" favoring skin penetration due to their physicochemical properties such as hydrophilicity, high swelling degree at physiological conditions, chemical stability, and non-toxicity. They offer prospective capability to continuously release low water-soluble anticancer therapeutic agents across the skin *via* diffusion transport for longer period of time in a more convenient manner than enteral or parenteral administration. As a result, this controlled, sustained, and release profile of DOX from the swollen hydrogel network at the melanoma site would be maintained until the concentration gradient ceases to exist, which could reduce the risk of high-level spikes of therapeutics in the systemic circulation.

In vitro test of drug release performed in aqueous medium aims at preliminary accessing the profiles associated with the changes on the hydrogel bioconjugates, which are a combination of events: (a) DOX adsorbed ("DOX$_{ads}$") entrapped in the hydrogel matrix; (b) DOX covalently conjugated to uncrosslinked CMC chains (solvated in water, "DOX$_{Sol}$"); (c) CMC-DOX conjugates immobilized in the crosslinked hydrogel network ("DOX$_{Cross}$"). The release profile of both CMC-DOX conjugates with DS 0.77 and 1.22 (Fig. 6A) indicated the initial burst in

66
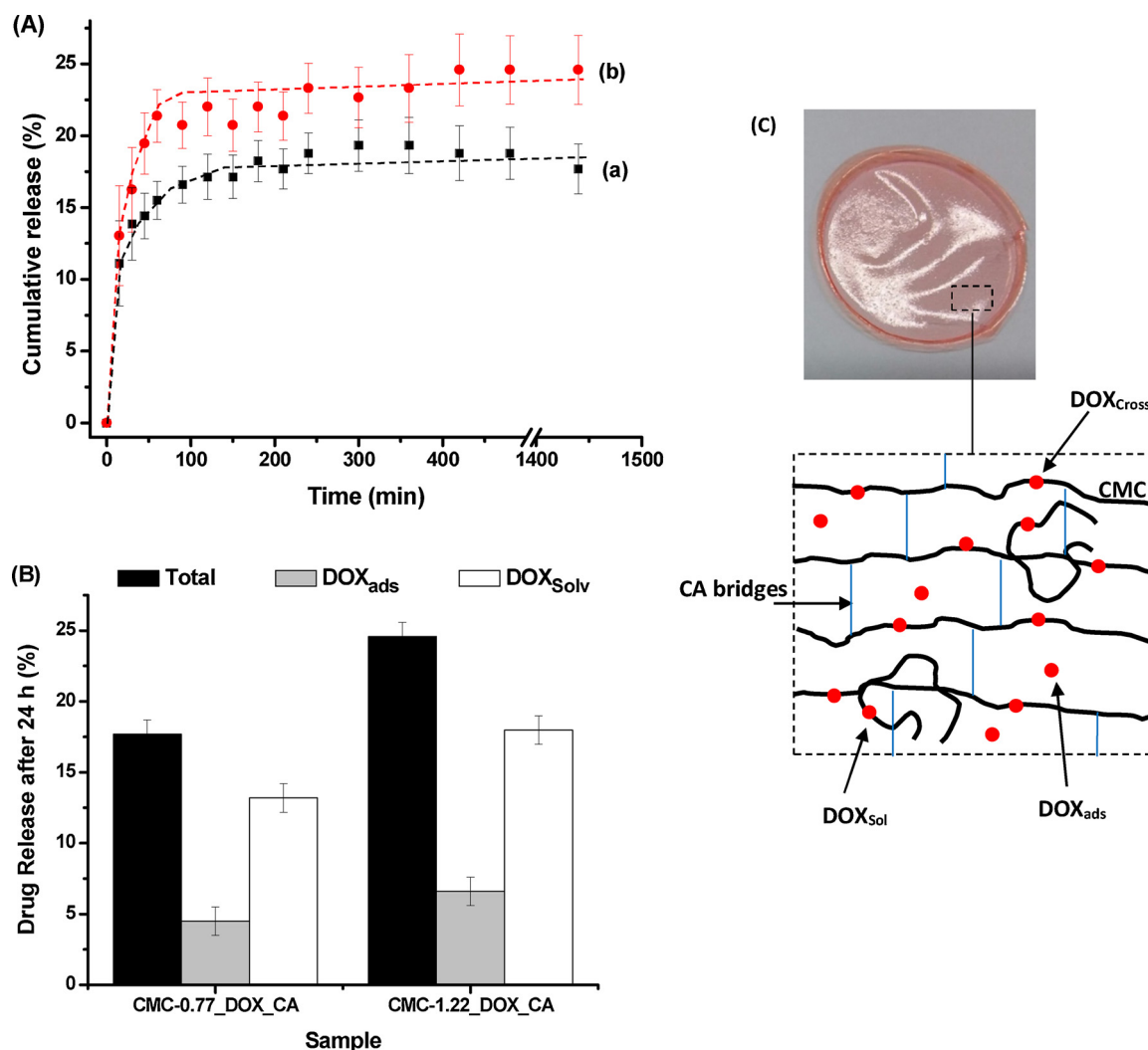
Fig. 6. (A) *In vitro* release of DOX by solvation (a) CMC-0.77_DOX_CA and (b) CMC-1.22_DOX_CA prodrug hydrogels. (B) Contributions of different "types" of DOX (DOX_ads, DOX_sol, DOX_Cross) after 24 h of release. (C) Schematic representation of hydrogel structure.

the first hour and then a sustained release up to 24 h (1440 min). The cumulative release of "DOX" from prodrug hydrogels CMC-0.77_DOX_CA and CMC-1.22_DOX_CA was $18 \pm 2\%$ and $25 \pm 2\%$, respectively. In order to evaluate the amount of DOX_ads and DOX_Sol, aliquots of the media were collected after 24 h and centrifuged (Amicon filter, Millipore, cut-off 50,000 kDa, 15 min at 14,000 rpm and $4 \pm 1\,°C$). The amount of DOX in the filtrate was quantified using Beer-Lambert correlation curve. The results (Fig. 6B) indicated that "DOX_ads" content was $5 \pm 1\%$ (CMC-0.77_DOX_CA) and $7 \pm 1\%$ (CMC-1.22_DOX_CA), indicating the majority of covalent conjugation ($> 90\%$) in the prodrugs. As expected, these results evidenced the effective release of DOX at distinct kinetics rates. Initially driven by the drug readily available DOX_ads (*i.e.,* unbound to CMC and "free" in the hydrogel network), followed by DOX_sol (conjugated to CMC but uncrosslinked, solvated in water medium) at slower rate. However, DOX of conjugates immobilized in the crosslinked hydrogel network ("DOX_Cross") are not expected to be released in this *in vitro* assay as the mild conditions used do not favor the cleavage of the amide bonds of CMC_DOX, but only inside cellular vesicles where enzyme catalyzed reactions occur.

3.4. Biological characterization of hydrogels

3.4.1. Cell viability in vitro – Mitochondrial activity (MTT) assay

Cell viability assays are of pivotal importance for preliminary evaluation of new materials and devices for potential biomedical applications in order to verify possible cytotoxicity of the system. Thus, MTT *in vitro* bioassay was performed with A375 cancer cells and HEK 293T normal cells at concentration of 25 μM of free DOX and CMC_DOX hydrogels and three incubation times (6 h, 24 h and 48 h) as shown in Fig. 7. For free DOX, after 6 h of incubation, cell viability responses indicate a high lethality of the chemotherapeutic drug, with a reduction to approximately 35–40% for both cell types. On contrary, only a small reduction of cell viability (65–75%) was observed for novel CMC-DOX hydrogels, independent of the cell type and degree of substitution of CMC. At 24 h of incubation, free DOX showed even a higher toxicity (cell viability < 20%) for both cell lines, comparable to positive control, but for all of the polymer-drug hydrogels the cell viability remained above 50%. At the higher incubation time (48 h) of anticancer compound, the cytotoxicity was similar for both normal and cancer cells and for free DOX and conjugates. No statistical difference (Bonferroni Multiple Analysis Test, one way analysis of variance, α: 0.05) was verified for cell viability of normal and tumor cells at the same condition of assay. Although the cell viability by MTT assay indicated slightly higher responses for CMC with DS = 0.77 compared to 1.22,
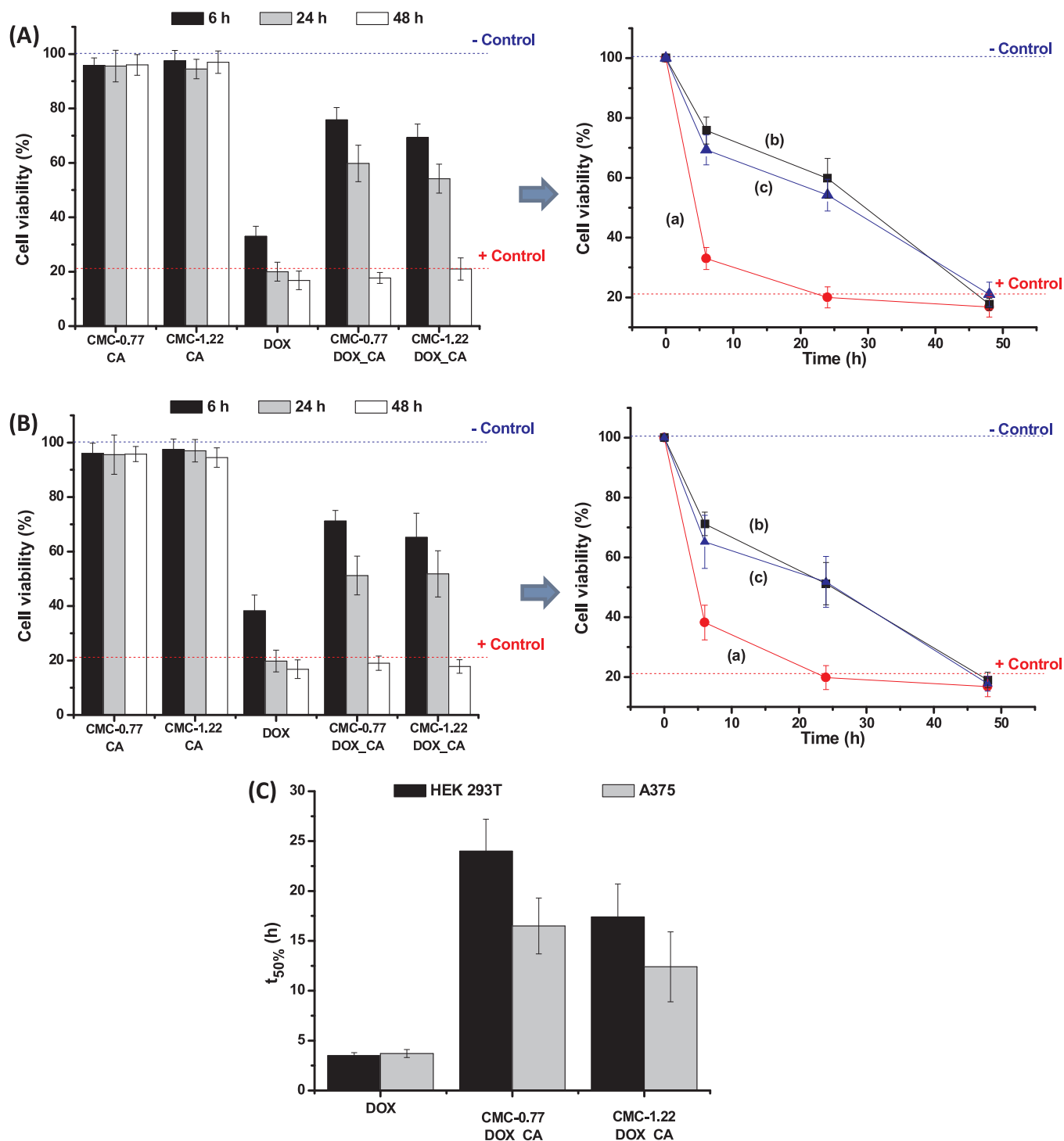
Fig. 7. Evaluation of *in vitro* cytotoxicity of (A) HEK 293T and (B) A375 cell lines after incubation with DOX, DOX-loaded prodrug hydrogels and CMC hydrogels after 6 h, 24 h and 48 h of incubation ((a) DOX, (b) CMC-0.77_DOX_CA and (c) CMC-1.22_DOX_CA). (C) $t_{50\%}$ results.

the results were statistically equivalent. However, more importantly, these MTT results evidenced the modulation of drug cytotoxicity with time by conjugation strategy and its dependence on cell type and carboxylate content of CMC as quantified by the time of 50% ($t_{50\%}$) cell viability response (Fig. 7B). As summarized in Fig. 7C, there is no difference between $t_{50\%}$ for free DOX effect in cancer or normal cells. However, $t_{50\%}$ was 3.3-fold and 4.5-fold delayed for CMC-DOX with DS 1.22 and 0.77, respectively, for A375 melanoma cells, and 5.0-fold (CMC-1.22_DOX_AC) and 6.9-fold delayed (CMC-0.77_DOX_AC) for HEK 293T cells. This important delayed effect of toxicity observed for

CMC-DOX conjugate hydrogels was attributed to the combination of physicochemical features related to the presence of amide bonds between CMC and DOX that requires the cleavage inside the cell for releasing the active drug with the specific biochemical behavior of each cell type (*i.e.,* A375 cancer cells and HEK 293T). The differences on the behaviors of CMC-DOX bioconjugate hydrogels with DS 0.77 and 1.22 are in agreement with the physicochemical properties of swelling, gel fraction and *in vitro* release presented in Section 3.3. Moreover, the dependence on cell type is related to the metabolism of cancer cells, which are much more active than normal cells combined with the more
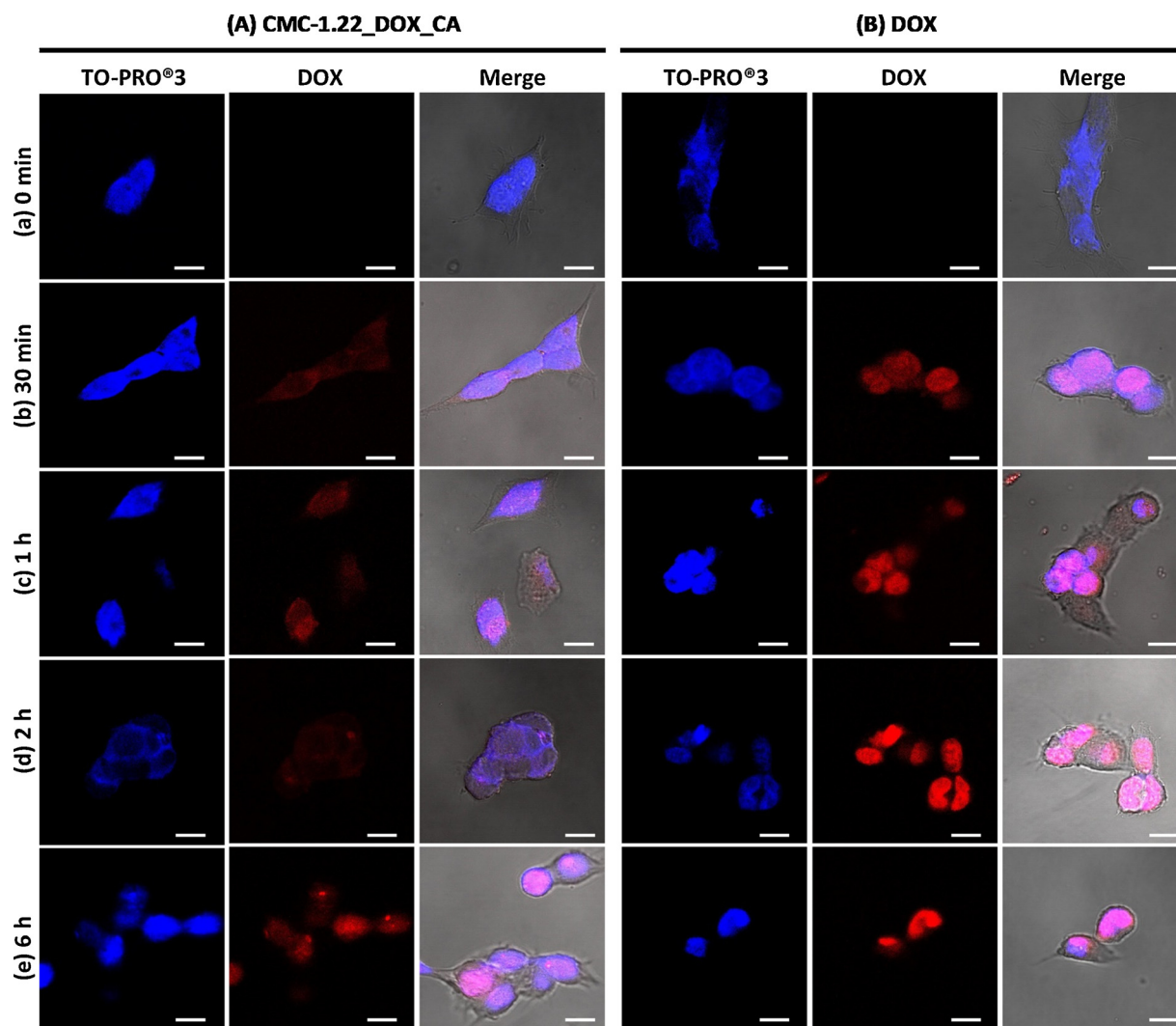
(A) CMC-1.22_DOX_CA   (B) DOX

Fig. 8. CLSM images of cellular uptake of (A) free DOX and (B) CMC-1.22_DOX_CA by HEK 293T cells after incubation for (a) 0 min, (b) 30 min, (c) 60 min, (d) 2 h and (e) 6 h (scale bar = 10 μm).

acidic pH of cytosol favoring the kinetics of DOX release from conjugates (Wang, Bhattacharyya, Mastria, & Chilkoti, 2017). Based on these results, these novel polymer-drug prodrugs made of CMC-DOX hydrogels emerge as new tools for tailoring drug delivery with killing activity against cancer cells and reducing acute effects in normal cells, which validated the hypothesis of this study.

3.4.2. Cellular uptake of polymer-drug bioconjugates – Confocal laser scanning microscopy (CLSM)

According to the literature (Dai et al., 2008), DOX acts in the cancer cells by intercalation into DNA and disruption of topoisomerase-II-mediated DNA repair. To reach the nucleus, DOX in free form or loaded into prodrug hydrogels has to undergo cellular uptake. Free DOX is known to be taken up by cells mostly through passive diffusion. Conversely, endocytosis is the most common mechanism for internalizing macromolecules and nanoparticles across the cellular membrane (Speelmans, Staffhorst, de Kruijff, & de Wolf, 1994) followed by endo-lysosomal trafficking and lysosomal degradation amide bonds that release DOX at cytosol. After reaching the cytosol, DOX migrates to nucleus due to its high affinity for DNA where triggers cell death.

To evaluate DOX distribution pattern inside the cell, the inherent fluorescence of DOX was explored combined with cellular staining with TO-PRO®-3 that has a very strong binding affinity for double strand DNA and therefore, a high selectivity for nuclear over cytoplasmic

staining. Confocal laser scanning microscopy (CLSM) images were obtained after 0 min (control), 30 min, 60 min, 2 h and 6 h of incubation of HEK 293T (Fig. 8) and A375 (Fig. 9) cell lines with free DOX and CMC-1.22_DOX_CA prodrug hydrogel.

For CMC_DOX_CA anticancer hydrogels (Figs. 8A and 9A) and free DOX samples (Figs. 8B and 9B), from 30 min up to 6 h, fluorescence was mostly concentrated at the nucleus and increasing with time for both cell types. To evaluate the kinetics of DOX accumulation in the nucleus, the Mean Fluorescence Intensity – MFI of DOX emission was calculated by image processing software (ImageJ, v.1.5+) for normal and melanoma cells and the results are presented in Fig. 10. These profiles endorsed our previous findings indicating the initial burst, a smaller concentration of DOX localized at the nucleus for prodrug hydrogel in comparison to free DOX in agreement with the delayed toxicity observed by MTT assays. Additionally, this is consistent with the slower process of cleavage of the amide bonds to release DOX from CMC conjugates before reaching the nucleus. When comparing free DOX (uptake mostly by passive diffusion) in normal and cancer cells, a relative faster accumulation rate (or higher slope of the curve) of DOX at nucleus for HEK 293T than for A375 cells and a higher MFI was observed. This behavior is related to the permeability of HEK 293T cell membranes, which usually present higher transfection efficiency (*e.g.*, virus and nucleotides) than other cell lines. In addition, the slower rate and MFI intensity verified for HEK 293T incubated with prodrug
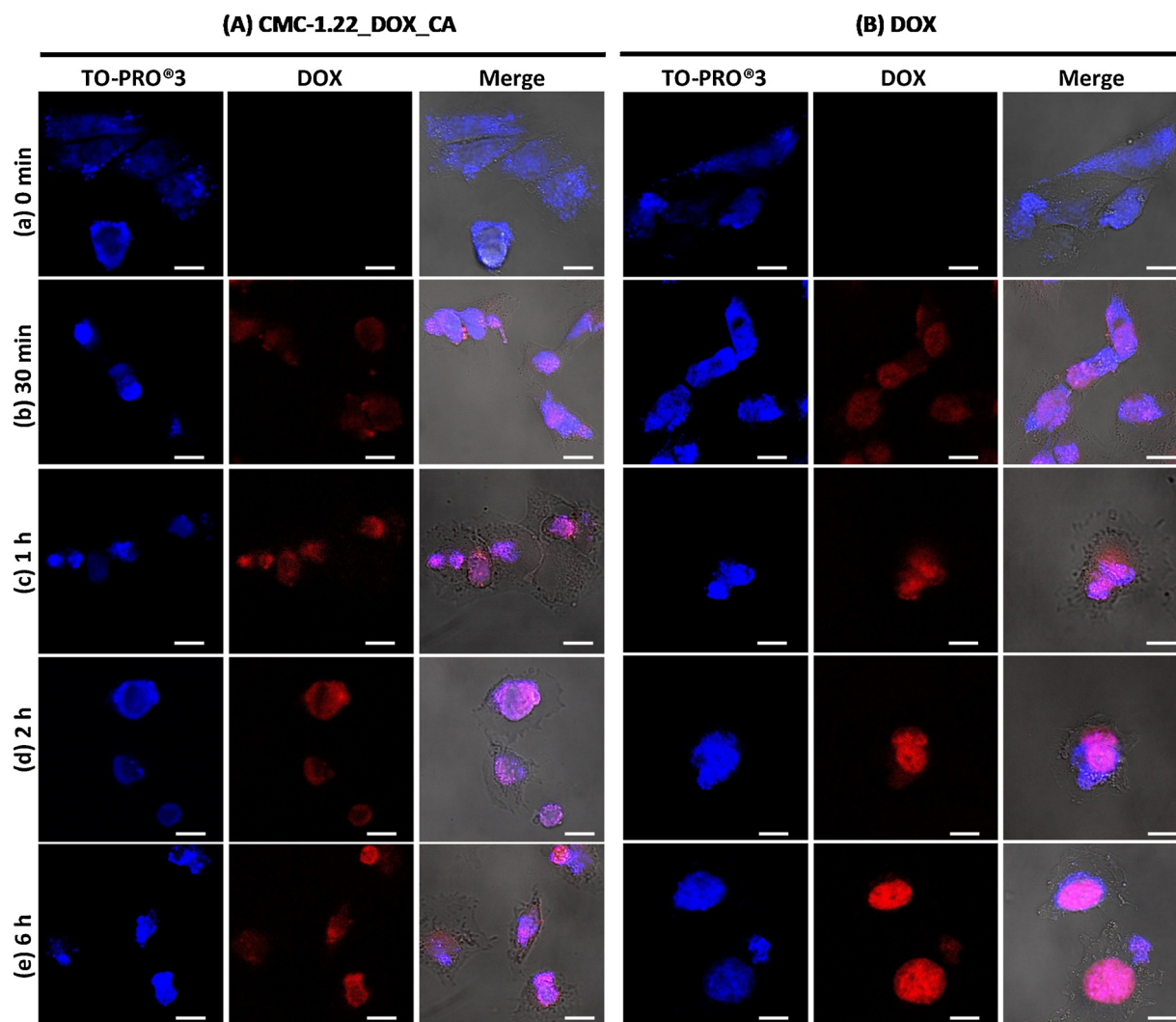
(A) CMC-1.22_DOX_CA

(B) DOX

Fig. 9. CLSM images of cellular uptake of (A) free DOX and (B) CMC-1.22_DOX_CA by A375 cells after incubation for (a) 0 min, (b) 30 min, (c) 60 min, (d) 2 h and (e) 6 h (scale bar = 10 μm).

hydrogel evidenced the lower $t_{50\%}$ previously observed and probably associated with the reduced metabolism of normal cells in comparison to melanoma cancer cells.

4. Conclusions

In this study, we designed and synthesized novel CMC_DOX polymer-drug bioconjugates using carboxymethylcellulose derivative with two degree of substitution DS = 0.77 and 1.22. These systems were characterized by several spectroscopy methods, which proved the hypothesis of effective conjugation of the carboxylic groups of the biopolymer with amino groups of DOX *via* the formation of covalent amide bonds. In the sequence, these bioconjugates were crosslinked with citric acid using a "green" processing route for producing polymer-drug hydrogels with swelling and gel fraction behaviors affected by the degree of carboxymethylation of CMC (DS). Moreover, the results demonstrated the effect of CMC-DOX hydrogel matrices with distinct DS values on tailoring the DOX release kinetics *in vitro* and the cytotoxicity response towards melanoma cancer cells. Hence, new polysaccharide-based polymer-drug hydrogels were developed for prospective applications in topical anticancer chemotherapy against highly lethal skin melanoma cells.

Conflicts of interest

The authors declare that they have no competing interests.

Appendix A. Supplementary data

Supplementary data associated with this article can be found, in the online version, at https://doi.org/10.1016/j.carbpol.2018.04.105.
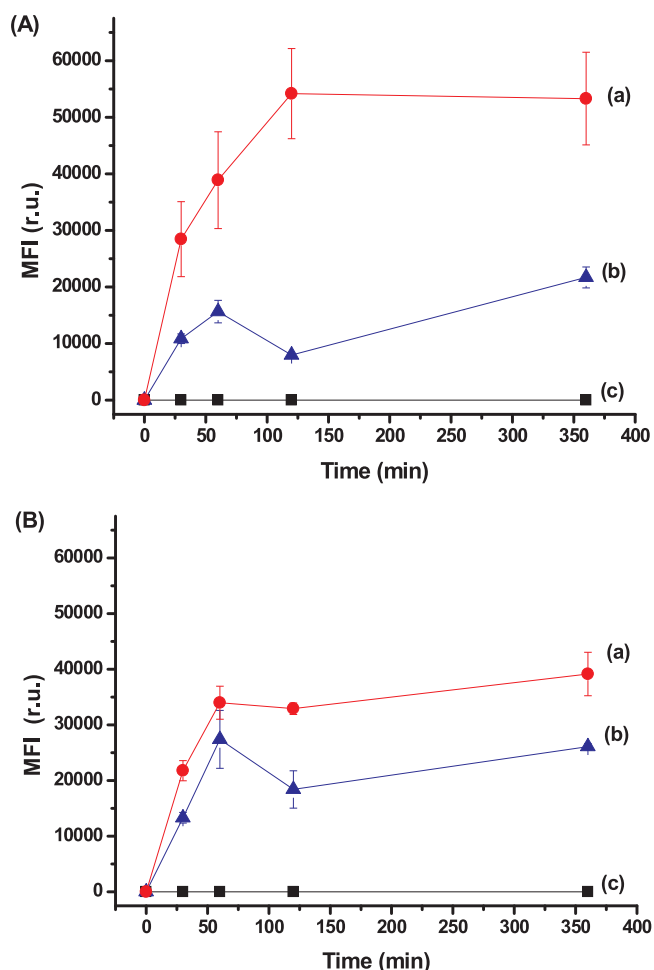
(A)

(B)

Fig. 10. MFI profiles at nucleus: (A) HEK 293T and (B) A375 cells after incubation with (a) DOX and (b) CMC-1.22_DOX_CA and (c) control samples.

References

Alkilani, A. Z., McCrudden, M. T. C., & Donnelly, R. F. (2015). Transdermal drug delivery: Innovative pharmaceutical developments based on disruption of the barrier properties of the stratum corneum. *Pharmaceutics, 7*, 438–470.

Bharadwaj, R., Das, P. J., Paul, P., & Mazumder, B. (2016). Topical delivery of paclitaxel for treatment of skin cancer. *Drug Development and Industrial Pharmacy, 42*, 1482–1494.

Cao, Z., Shen, Z., Luo, X., Zhang, H., Liu, Y., Cai, N., et al. (2017). Citrate-modified maghemite enhanced binding of chitosan coating on cellulose porous membranes for potential application as wound dressing. *Carbohydrate Polymers, 166*, 320–328.

Capanema, N. S. V., Mansur, A. A. P., de Jesus, A. C., Carvalho, S. M., de Oliveira, L. C., & Mansur, H. S. (2017). Superabsorbent crosslinked carboxymethyl cellulose-PEG hydrogels for potential wound dressing applications. *International Journal of Biological Macromolecules, 106*, 1218–1234.

Dai, X., Yue, Z., Eccleston, M. E., Swartling, J., Slater, N. K., & Kaminski, C. F. (2008). Fluorescence intensity and lifetime imaging of free and micellar-encapsulated doxorubicin in living cells. *Nanomedicine, 4*, 49–56.

Das, G., Nicastri, A., Coluccio, M. L., Gentile, F., Candeloro, P., Cojoc, G., et al. (2010). FT-IR, Raman, RRS measurements and DFT calculation for doxorubicin. *Microscopy Reseach and Technique, 73*, 991–995.

Dumont, V. C., Mansur, A. A. P., Carvalho, S. M., Borsagli, F. G. L. M., Pereira, M. M., & Mansur, H. S. (2016). Chitosan and carboxymethyl-chitosan capping ligands: Effects on the nucleation and growth of hydroxyapatite nanoparticles for producing biocomposite membranes. *Materials Science and Engineering C, 59*, 265–277.

Duncan, R. (2003). The dawning era of polymer therapeutics. *Nature Reviews Drug Discovery, 2*.

Duncan, R. (2013). Polymer therapeutics-prospects for 21 st century: The end of the beginning. *Advanced Drug Delivery Reviews, 65*, 60–70.

Fekete, T., Borsa, J., Takács, E., & Wojnárovits, L. (2017). Synthesis of carboxymethylcellulose/starch superabsorbent hydrogels by gamma-irradiation. *Chemistry Central Journal, 11*, 46.

Ferro, M., Castiglione, F., Panzeri, W., Dispenza, R., Santini, L., Karlsson, H. J., et al. (2017). Non-destructive and direct determination of the degree of substitution of carboxymethyl cellulose by HR-MAS ^{13}C NMR spectroscopy. *Carbohydrate Polymers, 169*, 16–22.

Haag, R., & Kratz, F. (2006). Polymer therapeutics: Concepts and applications. *Angewandte Chemie International Edition, 45*, 1198–1215.

He, L., Liang, H., Lin, L., Shah, B. R., Li, Y., Chen, Y., et al. (2015). Green-step assembly of low density lipoprotein/sodiumcarboxymethyl cellulose nanogels for facile loading and pH-dependent release of doxorubicin. *Colloids and Surfaces B: Biointerfaces, 126*, 288–296.

Li, N., Chen, G., Chen, W., Huang, J., Tian, J., Wan, X., et al. (2017). Multivalent cations-triggered rapid shape memory sodium carboxymethyl cellulose/polyacrylamide hydrogels with tunable mechanical strength. *Carbohydrate Polymers, 178*, 159–165.

Liu, J., Qi, C., Tao, K., Zhang, J., Zhang, J., Xu, L., et al. (2016). Sericin/dextran injectable hydrogel as an optically trackable drug delivery system for malignant melanoma treatment. *ACS Applied Materials & Interfaces, 8*, 6411–6422.

Mandal, B., Rameshbabu, A. P., Soni, S. R., Ghosh, A., Dhara, S., & Pal, S. (2017). In situ silver nanowire deposited cross-linked carboxymethyl cellulose: A potential transdermal anticancer drug carrier. *ACS Applied Materials & Interfaces, 9*, 36583–36595.

Mansur, H. S., & Mansur, A. A. P. (2012). Fluorescent nanohybrids: Quantum dots coupled to polymer recombinant protein conjugates for the recognition of biological hazards. *Journal of Materials Chemistry, 22*, 9006–9018.

Mansur, A. A., Mansur, H. S., Soriano-Araújo, A., & Lobato, Z. I. (2014). Fluorescent nanohybrids based on quantum dot-chitosan-antibody as potential cancer biomarkers. *ACS Applied Materials & Interfaces, 6*, 11403–11412.

Mohan, P., & Rapoport, N. (2010). Doxorubicin as a molecular nanotheranostic agent: Effect of doxorubicin encapsulation in micelles or nanoemulsions on the ultrasound-mediated intracellular delivery and nuclear trafficking. *Molecular Pharmaceutics, 7*, 1959–1973.

Motlagh, N. S. H., Parvin, P., Ghasemi, F., & Atyabi, F. (2016). Fluorescence properties of several chemotherapy drugs: Doxorubicin, paclitaxel and bleomycin. *Biomedical Optics Express, 7*, 2400–2406.

Movagharnezhad, N., & Moghadam, P. N. (2016). Folate-decorated carboxymethyl cellulose for controlled doxorubicin delivery. *Colloid and Polymer Science, 294*, 199–206.

Ranjbari, J., Mokhtarzadeh, A., Alibakhshi, A., Tabarzad, M., Hejazi, M., & Ramezani, M. (2017). Anti-cancer drug delivery using carbohydrate-based polymers. *Current Pharmaceutical Design, 23*, 6019–6032.

Roy, A., Murakami, M., Ernsting, M. J., Hoang, B., Undzys, E., & Li, S. D. (2014). Carboxymethylcellulose-based and docetaxel-loaded nanoparticles circumvent p-glycoprotein-mediated multidrug resistance. *Molecular Pharmaceutics, 11*, 2592–2599.

Speelmans, G., Staffhorst, R. W. H. M., de Kruijff, B., & de Wolf, F. A. (1994). Transport studies of doxorubicin in model membranes indicate a difference in passive diffusion across and binding at the outer and inner leaflets of the plasma membrane. *Biochemistry, 33*, 13761–13768.

Vishnubhakthula, S., Elupula, R., & Durán-Lara, E. F. (2017). Recent advances in hydrogel-based drug delivery for melanoma cancer therapy: A mini review. *Journal of Drug Delivery, 2017*, 7275985.

Wang, J., Bhattacharyya, J., Mastria, E., & Chilkoti, A. A. (2017). Quantitative study of the intracellular fate of pH-responsive doxorubicin-polypeptide nanoparticles. *Journal of Controlled Release, 260*, 100–110.

Zhang, X., Li, X., You, Q., & Zhang, X. (2017). Prodrug strategy for cancer cell-specific targeting: A recent overview. *European Journal of Medicinal Chemistry, 139*, 542–563.

71

6. Conclusões Gerais

Neste estudo foi realizado o design, a síntese e a caracterização de novas membranas de hidrogéis eco-amigáveis com base no derivado de celulose funcionalizado com grupos carboximetil (carboximetil celulose, CMC) quimicamente reticuladas por ácido cítrico (CA). Os resultados evidenciaram que os hidrogéis de CMC foram produzidos com sucesso sendo possível modular as propriedades físico-químicas, nanomecânicas e biológicas pelo grau de substituição da CMC, pela concentração do agente de reticulação, pela introdução de polímeros modificadores da rede, pela incorporação de nanopartículas de prata e pela conjugação de agentes antitumorais. Todos os materiais produzidos (exceto os com incorporação do fármaco antitumoral) foram não-citotóxicos.

Os resultados dos hidrogéis de CMC modificados demonstraram que os hidrogéis superabsorventes (SAP) foram produzidos com um grau de intumescimento variando de 100% a 5000%, dependendo do grau de substituição de CMC, da extensão da reticulação com CA, da adição de PEG, da incorporação das AgNPs e da conjugação com DOX.

A introdução de PEG resultou no desenvolvimento de hidrogéis constituídos de uma matriz híbrida amorfa-cristalina que influenciou diretamente as propriedades físico-químicas e nanomecânicas.

Nanopartículas de prata foram sintetizadas utilizando a CMC como agente redutor e de estabilização das nanopartículas e os hidrogéis/nanocompósitos produzidos com CMC-AgNPs incorporaram aos hidrogéis alta atividade antibacteriana contra cepas de bactérias gram-positivas e gram-negativas.

Hidrogéis de CMC conjugados com doxorrubicina apresentaram a possibilidade de controlar a liberação da droga em função do grau de substituição da CMC e formação da ligação covalente droga-polímero, resultando, inclusive em uma liberação mais lenta para as células normais, permitindo uma redução dos efeitos agudos em células não-tumorais.

Capítulo 7. Contribuições para a Literatura

7.1. Artigos completos publicados em periódicos

Capanema, Nádia S.V.; Mansur, A.A.P.; Mansur, H.S.; de Jesus, A.C.; Carvalho, S.M.; Chagas, P.; de Oliveira, L.C. Eco-friendly and biocompatible crosslinked carboxymethyl cellulose hydrogels as adsorbents for the removal of organic dye pollutants for environmental applications. Environmental Technology, v. 13, p. 1-42, 2017. **QUALIS A1 – JCR 1.751**

Capanema, Nádia S.V.; Mansur, A.A.P.; Carvalho, S.M.; Ramos, C.P.; Lage, A.P.; Mansur, H.S. Physicochemical properties and antimicrobial activity of biocompatible carboxymethylcellulose-silver nanoparticle hybrids for wound dressing and epidermal repair. Journal of Applied Polymer Science, v. 135, p. 45812, 2018. **QUALIS A1 – JCR 1.86**

Capanema, Nádia S.V.; Mansur, A.A.P.; de Jesus, A.C.; Carvalho, S.M.; de Oliveira, L.C.; Mansur, H.S. Superabsorbent crosslinked carboxymethyl cellulose-PEG hydrogels for potential wound dressing applications. International Journal of Biological Macromolecules, v. 106, p. 1218-1234, 2017. **QUALIS A2 – JCR 3.671**

Capanema, Nádia S.V.; Mansur, A.A.P.; Carvalho, S.M.; Carvalho, I.C.; Chagas, P.; de Oliveira, L.C.; Mansur, H.S. Bioengineered carboxymethyl cellulose-doxorubicin prodrug hydrogels for topical chemotherapy of melanoma skin cancer. Carbohydrate Polymers, v. 195, p. 401-412, 2018. **QUALIS A1 – JCR 4.811**

Dumont, V.C.; Mansur, H.S.; Mansur, A.A.P.; Carvalho, S.M; **Capanema, Nádia S.V.**; Barrioni, B.R. Glycol chitosan/nanohydroxyapatite biocomposites for potential bone tissue engineering and regenerative medicine. International Journal of Biological Macromolecules, v. 93, p.1465-1478, 2016. **QUALIS A2 – JCR 3.671**

7.2. Trabalhos publicados em anais de eventos (completo)

Capanema, Nádia S.V.; Mansur, A.A.P.; Mansur, H.S. Hidrogéis de carboximetilcelulose reticulados com ácido cítrico para potencial aplicação biomédica In: Anais do 14º Congresso Brasileiro de Polímeros - CBPOL, v. 1. p. 890 – 894, 2017.

Capítulo 8. Sugestões para trabalhos futuros

- Produção de Filmes de Carboximetil Celulose (CMC) de Massa Molar MM = 250.000 g.mol^{-1} com grau de substituição (DS = 0,77 e DS = 1,22) reticulados com ácido cítrico (CA), [CA]/[CMC] = 15% m/m, com a utilização do Nanopartículas de prata (AgNPs) e a incorporação permanente de um fármaco antitumoral, a Doxorrubicina (DOX) para obtenção de melhoria das propriedades antibacterianas no desenvolvimento de curativos epiteliais com liberação controlada de droga antitumoral, principalmente após excisões cirúrgicas de melanomas.

- Sintetizar e caracterizar filmes de hidrogéis de Carboximetil Celulose com diferentes graus de substituição (DS = 0,77 e DS = 0,84) e diferentes MM (MM = 250.000g·mol^{-1} e MM = 700.000g·mol^{-1}), reticulados com ácido cítrico (CA) e com a incorporação de nanocristais de celulose (CNC) em sua estrutura e analisar a melhoria de reforço nas suas propriedades para aplicação biomédica.

Referências Bibliográficas

BLANPAIN, C. Stem cells: Skin regeneration and repair. *Nature*, *464*, 686, 2010.

BHARADWAJ, R.; DAS, P. J., PAUL; MAZUMDER, B. Topical delivery of paclitaxel for treatment of skin cancer. *Drug Development and Industrial Pharmacy*, *42,* 1482-1494, 2016.

BOER, M.; DUCHNIK, E.; MALESZKA, R.; MARCHLEWICZ, M. *Adv. Dermatol. Allergol*, *33*, 1, 2016.

CARVALHO, I. C.; MANSUR, H. S. Engineered 3D-scaffolds of photocrosslinked chitosan-gelatin hydrogel hybrids for chronic wound dressings and regeneration. *Mater. Sci. Eng. C*, 78, 690–705, 2017.

CHANG, C.; DUAN, B.; CAI, J.; ZHANG, L. Superabsorbent hydrogels based on cellulose for smart swelling and controllable delivery. *Eur. Polym. J*., 46, 92–100, 2010.

DANG, Q.F.; LIU,H.; YAN, J.Q. LIU, C.S.; LIU, Y.; LI, J.; LI, J.J. Characterizations of collagen from haddock skin and wound healing properties of its hydrolysates. *Biomed. Mater.,* 10, 015022, 2015.

DEMITRI, C.; R. DEL SOLE, R.; SCALERA, F.; SANNINO, A.; VASAPOLLO, G.; MAFFEZZOLI, A.; AMBROSIO, A.; L.; NICOLAIS, L. Novel superabsorbent cellulose based hydrogels crosslinked with citric acid. *J. Appl. Polym. Sci*., 110, 2453–2460, 2008.

GEOFFREY, C.G., S. WERNER, Y. BARRANDON, M.T. LONGAKER. *Wound repair and regeneration*, *Nature,* 453, 314–321, 2008.

GONG, P.; LI, H.; WANG, K.; HU, J.; TAN, W.; ZHANG, S.; YANG, X. *Nanotechnology*, 18, 285604, 2007.

IZADI, K.; GANCHI, P. Chronic wounds. *Clin. Plastic. Surg*., 32, 209–222, 2005.

KALASHNIKOVA, I.; DAS, S.; SEAL, S. *Nanomedicine*, 10, 2593, 2015.

KAMBA, S.A.; ISMAIL, M.; HUSSEIN-AL-ALI, S.H.; TENGKU, T.A.; IBRAHIM 2 AND ZUKI ABU BAKAR ZAKARIA, Z.A.B. In Vitro Delivery and Controlled Release of Doxorubicin for Targeting Osteosarcoma Bone Cancer. *Molecules*, 18, 10580-10598, 2013.

LEUNG, H.W. Ecotoxicology of glutaraldehyde: review of environmental fate and effects studies, Ecotox. *Environ. Safe,* 49, 26–39, 2001.

LUTOLF, M. P.; HUBBELL, J. A. Synthetic biomaterials as instructive extracellular microenvironments for morphogenesis in tissue engineering. *Nat. Biotechnol*., 23, 47–55, 2005.

MADAGHIELE, M.; DEMITRI, C.; SANNINO, A.; AMBROSIO, L. Polymeric hydrogels for burn wound care: Advanced skin wound dressings and regenerative templates. *Burns Trauma*, 2, 153–161, 2014.

MARTIN, P. Wound healing – aiming for perfect skin regeneration. *Science,* 276, 75–81, 1997.

MOGOŞANU, G. D.; GRYMEZESCU, M. A. Natural and synthetic polymers for wounds and burns dressing. *Int. J. Pharm*., 463, 127–136, 2014.

NEILL, J. T.; BADYLAK, S. F. The use of biologic scaffolds in the treatment of chronic nonhealing wounds. *Adv. Wound Care*, 4, 490–500, 2015.

RAI, M. K.; DESHMUKH, S. D.; INGLE, A. P.; GADE, A. K. J. *Appl. Microbiol*., 112, 841, 2012.

RAUCCI, M. G.; ALVAREZ-PEREZ, M. A.; DEMITRI, C.; GIUGLIANO, D.; DE BENEDICTIS, V.; SANNINO, A.; AMBROSIO, L. Effect of citric acid crosslinking cellulose-based hydrogels on osteogenic differentiation. *J. Biomed. Mater. Re*s., Part A 103A, 2045–2056, 2015.

REZA, A. T.; NICOLL, S. B. Characterization of novel photocrosslinked carboxymethylcellulose hydrogels for encapsulation of nucleus pulposus cells. *Acta Biomater*., 6, 179–186, 2010.

SACCO, P.; TRAVAN, A.; BORGOGNA, M.; PAOLETTI, S.; MARSICH, E. *Mater. Sci. Eng. C*, 26, 128, 2015.

SAMBERG, M.E.; OLDENBURG, S.J.; MONTEIRO-RIVIERE, N. A. *Environ. Health Perspect*, 118, 407, 2010.

SANNINO, A.; MAFFEZZOLI, A.; NICALAIS, L. Introduction of molecular spacers between the crosslinks of a cellulose-based superabsorbent hydrogel: effects on the equilibrium sorption properties. *J. Appl. Polym. Sci.,* 90, 168–174, 2003.

VISHNUBHAKTHULA, S., ELUPULA, R., & DURÁN-LARA, E.F. Recent advances in hydrogel-based drug delivery for melanoma cancer therapy: A mini review. *Journal of Drug Delivery*, 7275985, 2017.

ZHANG, Y.; DANG, Q.; LIU, C.; YAN, J.; CHA, D.; LIANG, S.; LI, X.; FAN, B. Synthesis, characterization, and evaluation of poly(aminoethyl) modified chitosan and its hydrogel used as antibacterial wound dressing. *Int. J. Biol. Macromol.,* 102, 457−467, 2017.

Anexo

Hidrogéis de carboximetil celulose reticulados e biocompatíveis como adsorventes para a remoção de poluentes de corantes orgânicos para aplicações ambientais

Graphical Abstract
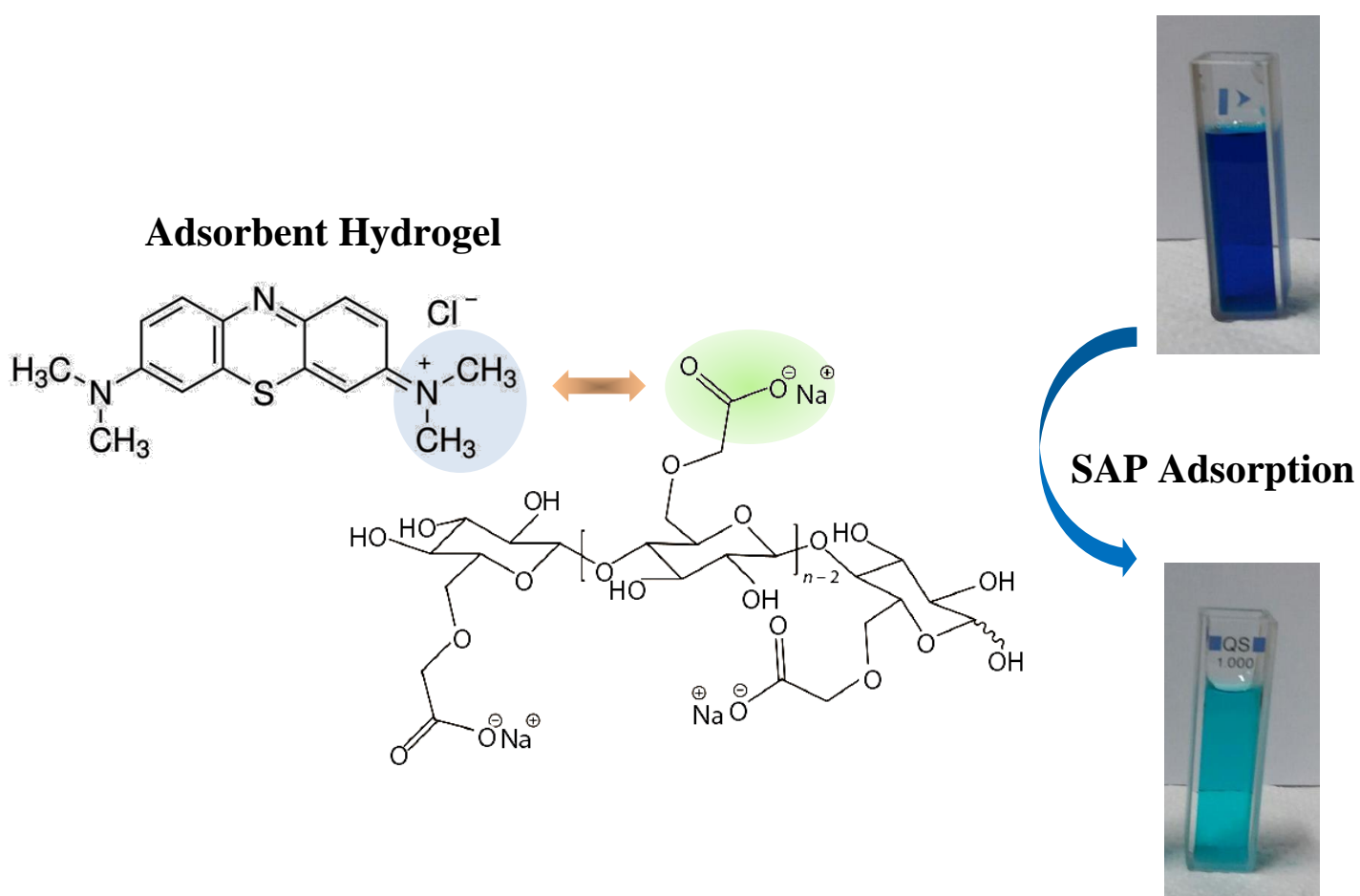
Green Superabsorbent Crosslinked Hydrogels based on Carboxymethyl Cellulose Polyelectrolyte for Removal of Organic Dye Pollutants for Environmental Applications

Resumo

Neste estudo foram sintetizados novos hidrogéis superabsorventes baseados em carboximetil celulose (CMC) grau de substituição (DS) 0,77 quimicamente reticulados

com ácido cítrico (CA) utilizando um processo verde em solução aquosa e aplicada para a adsorção de azul de metileno (MB). Análises espectroscópicas por ^{1}H RMN e por FTIR demonstraram o mecanismo de reticulação através da reação de grupos funcionais hidroxila da CMC com CA. Estes hidrogéis de CMC mostraram características morfológicas muito distintas, dependendo da extensão da reticulação e as suas propriedades nanomecânicas foram drasticamente aumentadas em aproximadamente 300% após reticulação com 20% de CA (por exemplo, módulos elásticos de 80 ± 15 a 270 ± 50 MPa). Além disso, os hidrogéis de CMC com CA foram biocompatíveis usando ensaio *in vitro* de viabilidade celular em contato com células derivadas de osteossarcoma humano (SAOS) por 24 h. Esses hidrogéis à base de CMC exibiram eficiência de adsorção acima de 90% (24 h) e capacidade máxima de remoção de MB de 5 a 25 mg.g^{-1}, dependendo da concentração de corante (de 100 a 500 mg.L^{-1}), que foi utilizado como modelo poluente orgânico catiônico. A adsorção do processo de MB foi bem ajustada ao modelo cinético de pseudo-segunda ordem. A dessorção de MB por imersão em solução de KCl (3 mol.L^{-1}, 24 h) mostrou uma eficiência de recuperação típica de mais de 60% com reutilização concebível desses hidrogéis baseados em CMC. Por outro lado, os hidrogéis de CMC repeliram o corante de laranja de metila (MO) usado como modelo poluente aniônico, comprovando o mecanismo de adsorção pela formação de complexos polieletrólito/corante carregados. Assim, estes hidrogéis de CMC comportaram-se como adsorventes ambientalmente amigáveis para a remoção de corantes MB proporcionando uma nova alternativa potencial para a descontaminação de poluentes da água.

Artigo

Capanema, Nádia S.V.; Mansur, A.A.P.; Mansur, H.S.; de Jesus, A.C.; Carvalho, S.M.; Chagas, P.; de Oliveira, L.C. Eco-friendly and biocompatible crosslinked carboxymethyl cellulose hydrogels as adsorbents for the removal of organic dye pollutants for environmental applications. Environmental Technology, v. 13, p. 1-42, 2017. **QUALIS A1 – JCR 1.751**

Taylor & Francis
Taylor & Francis Group

Check for updates

Eco-friendly and biocompatible cross-linked carboxymethylcellulose hydrogels as adsorbents for the removal of organic dye pollutants for environmental applications

Nádia S. V. Capanema[a], Alexandra A. P. Mansur[a], Herman S. Mansur[a], Anderson C. de Jesus[a], Sandhra M. Carvalho[a], Poliane Chagas[b] and Luiz C. de Oliveira[b]

[a]Center of Nanoscience, Nanotechnology and Innovation – CeNano²I, Department of Metallurgical and Materials Engineering, Federal University of Minas Gerais, Belo Horizonte, Minas Gerais, Brazil; [b]Department of Chemistry, Federal University of Minas Gerais, Belo Horizonte, Minas Gerais, Brazil

ABSTRACT

In this study, new eco-friendly hydrogel adsorbents were synthesized based on carboxymethylcellulose (CMC, degree of substitution [DS] = 0.7) chemically cross-linked with citric acid (CA) using a green process in aqueous solution and applied for the adsorption of methylene blue (MB). Spectroscopic analyses demonstrated the mechanism of cross-linking through the reaction of hydroxyl functional groups from CMC with CA. These CMC hydrogels showed very distinct morphological features dependent on the extension of cross-linking and their nanomechanical properties were drastically increased by approximately 300% after cross-linking with 20% CA (e.g. elastic moduli from 80 ± 15 to 270 ± 50 MPa). Moreover, they were biocompatible using an *in vitro* cell viability assay in contact with human osteosarcoma-derived cells (SAOS) for 24 h. These CMC-based hydrogels exhibited adsorption efficiency above 90% (24 h) and maximum removal capacity of MB from 5 to 25 mg g^{-1} depending on the dye concentration (from 100 to 500 mg L^{-1}), which was used as the model cationic organic pollutant. The adsorption of process of MB was well-fit to the pseudo-second-order kinetics model. The desorption of MB by immersion in KCl solution (3 mol L^{-1}, 24 h) showed a typical recovery efficiency of over 60% with conceivable reuse of these CMC-based hydrogels. Conversely, CMC hydrogels repelled methyl orange dye used as model anionic pollutant, proving the mechanism of adsorption by the formation of charged polyelectrolyte/dye complexes.
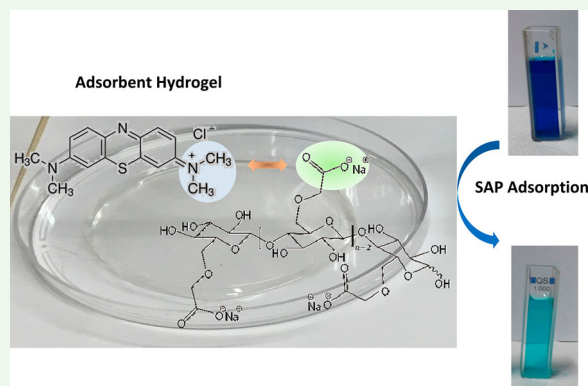
1. Introduction

In modern society, due to the growing world population and intensive industrial processes, increasing amounts of hazardous organic compounds are produced and are often being discharged into the environment. Among these pollutants, dyes, phenolics, and pesticides have recently been of great concern because of their extreme toxicity and persistency in the environment. Although chemical and biological treatments are

available for the removal process of some organic compounds, their byproducts of degradation can be also harmful and nondegradable [1–4].

Dyes are a relatively large group of organic chemicals usually classified based on their molecular structure, which are extensively used in many industries such as textile, paper printing, plastic, cosmetics, rubber, tannery, and paints. Usually dyes are difficult to degrade because of their complex aromatic structures. They can cause several diseases to humans and animals such as allergy, irritation, dermatitis, and even cancer [2,4,5]. For dye removal from wastewater, methods such as adsorption, flocculation, oxidation, and electrolysis are common methods, where the adsorption method can transform dyes from the effluent to a solid phase. Methylene blue (MB) and other aromatic compounds have been widely used as model organic compounds for investigating the adsorption process of dyes by innovative adsorbent systems [6].

Adsorption is most commonly used as an effective and simple technique for the removal of nondegradable dye organic compounds even at low concentrations from drinking water or from industrial wastewater [7,8]. Conventionally, activated carbon has been used for dye adsorption from several effluents but its application is often limited because it is recalcitrant and of high cost. Therefore, in recent years, the interest in searching for new effective substitutes based on natural polymers and derivatives such as starch, cellulose, chitosan, and lignin has significantly increased considering the concept of economical and environmentally friendly materials (referred to as e^2) [3,5,8]. In that sense, among several alternatives, polymer-based adsorbents have been used for water decontamination and wastewater treatments, as they present hydrophilic networks with functional groups for developing chemical interactions with metallic ions and organic compounds [9]. To this end, highly absorbent polymer hydrogels (or superabsorbent polymer, SAP) have been broadly used in a variety of applications such as pharmaceuticals in drug delivery, nutrition, agriculture, and as bioadsorbents for water treatment and remediation [10–13].

Cellulose is the most abundant biodegradable natural polymer on earth, low cost, renewable, and with annual cellulose synthesis by plants of approximately 10^{12} tons, which is being extensively used to construct hydrogels. Although cellulose is insoluble in water and most common organic solvents, cellulose derivatives such as carboxymethylcellulose (CMC) are soluble in a wide range of solvents. Therefore, CMC, generally used as the sodium salt NaCMC (or CMC), is one of the most widely used cellulose derivatives, which is an anionic and water-soluble polyelectrolyte,

with vast applications in the food, pharmaceutical, personal care, cosmetic, paper, and other industries. Cellulose and its derivatives are a broad class of polymers in which molecular mass and chemical functionalization play crucial roles in their properties for a variety of applications [2,14–22].

In recent years, an attractive class of soft materials has been developed based on cross-linked polyelectrolytes forming hydrogel networks that swell in water instead of dissolving in it, which can retain extremely large amounts of aqueous medium relative to their own mass (i.e. SAP polyelectrolyte-based hydrogel). This behavior is caused by chemical interactions, predominantly as the result of the formation of hydrogen bonding between functional groups of the polymer network with water molecules, leading to water absorption from 10 to 100 times its weight (∼10–50 times its volume). The total absorbency and swelling capacity of SAP is controlled by the selection of the polymer, its molecular mass, and functional groups, the choice of cross-linker and the degree of cross-linking for tuning the physicochemical properties of the SAP hydrogel. Importantly, despite the availability of several chemical cross-linkers such as glutaraldehyde, epichlorohydrin, and carbodiimides, most of them are toxic and not biocompatible and eco-friendly, where citric acid (CA) and other natural products are very promising alternatives [2,20,23].

Owing to polyelectrolyte-based hydrogels being biocompatible and environmentally friendly, numerous studies reported their use for biomedical and pharmaceutical applications, although more recently, the development of cellulose and derivatives of SAP hydrogels for environmental purposes is one of the emerging areas of research. Novel SAP hydrogels are developed with designed networks via cross-linking and multiple chemical functionalities focusing on adsorption properties for the removal of hazardous dyes and heavy metal ions for environmental applications [22,24–27].

Thus, this study, reports on the synthesis and extensive characterization of novel highly absorbent CMC hydrogel membranes, originating from renewable and sustainable natural resources, with adsorption properties for MB dye removal. These CMC hydrogels featured tunable physicochemical properties modified by chemical cross-linking with CA via a strictly environmentally friendly process. Moreover, they were biocompatible and behaved as anionic adsorbents with approximately 95% removal efficiency and maximum adsorption capacity of 25 mg g^{-1} of MB used as the model cationic organic dye pollutant in aqueous medium. The adsorption experimental data followed the pseudo-second-order kinetics through the formation of biopolymer–dye complexes.

2. Materials and methods

2.1. Materials

All of the reagents, including sodium carboxymethylcellulose (CMC, Aldrich, USA, average molecular mass, Mw = 250 kDa, degree of substitution [DS] = 0.77, and viscosity 735 cps, 2% in H_2O at 25°C), CA (Sigma-Aldrich, USA, ≥99.5%, $HOC(COOH)(CH_2COOH)_2$), MB (Synth, Brazil, $C_{16}H_{18}N_3SCl\cdot3H_2O$), and methyl orange (MO, Synth, Brazil, $C_{14}H_{14}N_3NaO_3S$), were used as received. Unless specified otherwise, deionized (DI) water (Millipore Simplicity™) with a resistivity of 18 MΩ cm was used to prepare the solutions and the procedures were performed at room temperature (RT, 23 ± 2°C).

2.2. Synthesis of cross-linked hydrogel membranes

CMC solution (2% w/v) was prepared by adding sodium carboxymethylcellulose powder (2.0 g) to 100 mL of DI water and stirring at RT until complete solubilization occurred. After dissolution, the cross-linking agent, CA, was added under stirring at concentrations of 10% (CA 10%), 15% (CA 15%), 20% (CA 20%), and 25% (CA 25%) m/m of CMC polymer and homogenized for 20 min. Then, 10 mL of the solutions were poured into plastic molds (polystyrene petri dish, diameter, $d = 60$ mm) and were allowed to dry at 40 ± 2°C for 24 h to remove water. In the sequence, the samples were kept at 80 ± 2°C for 24 h for the cross-linking reaction. As a reference, a sample without CA was also prepared and dried following the same thermal cycle.

2.3. Characterization of CMC and cross-linked membranes

2.3.1. Morphological and spectroscopic analyses

Atomic force microscopy (AFM) of hydrogel membranes was conducted with a Multimode 8 (Bruker) instrument operating in Peak Force® tapping mode. The scanning rate was 1.0 Hz, and the images were acquired with a 512 × 512 pixel resolution. The surface mapping of nanomechanical properties was performed using a silicon-nitride probe, at constant $K = 0.4$ N/m, frequency 70 kHz, temperature 20–23°C, calibration based on the absolute method, and parameters calculated with software Nanoscope analysis 8.5.

Fourier-transform infrared spectroscopy (FTIR) analysis was recorded with a Nicolet 6700 (Thermo Fischer) spectrometer with background subtraction. The CMC powder was mixed with pre-dried KBr (110 ± 5°C for 2 h) at the mass ratio 1:100, sample:KBr, and the mixture was compressed to form a transparent pellet that was analyzed using the transmission method (4000–400 cm^{-1}, 16 scans, and a 4 cm^{-1} resolution). The FTIR spectra of the cast membranes were obtained using attenuated total reflectance (4000–675 cm^{-1}, 32 scans, and 4 cm^{-1} resolution).

^{1}H NMR (nuclear magnetic resonance) spectra were recorded at 30°C in D_2O/HCl using a BRUKER-200 MHz Varian spectrometer (90 pulse and 16 scans).

2.3.2. Physicochemical characterization

For fluid uptake measurements, the hydrogels were cut into 10 × 10 mm^2 samples, dried at 40 ± 2°C for stabilization of mass, and weighed (W_0, initial mass). Then, the hydrogels (triplicates, $n = 3$) were placed in 70 mL sample pots with 10.0 mL of DI water at RT. After 60 min, the hydrogel was removed from the solution, gently wiped with filter paper to remove the excess liquid on the sample surface and weighed (W_s, swollen mass). In the sequence, samples were dried at 40 ± 2°C until mass stabilization and the final weight was recorded (W_f, final mass). The weight measured in each step of the process was used to calculate the degree of swelling (SD) of the hydrogels using Equation (1), as reported in the literature [28–32].

$$SD(\%) = ((W_s - W_0)/W_0) * 100. \tag{1}$$

2.3.3. Cytotoxicity evaluation

Immortalized human osteosarcoma-derived (SAOS) cells were provided by Prof. A. Goes of the Department of Immunology and Biochemistry, UFMG (Federal University of Minas Gerais). The SAOS cells were cultured in Dulbecco's modified eagle medium (DMEM) with 10% fetal bovine serum (FBS), streptomycin sulfate (10 mg mL^{-1}), penicillin G sodium (10 units mL^{-1}), and amphotericin-b (0.025 mg mL^{-1}), all supplied by Gibco BRL (USA), using a humidified atmosphere of 5% CO_2 at 37°C. All of the biological tests were conducted according to ISO 10993-5:2009/(R)2014 (Biological evaluation of medical devices: Tests for *in vitro* cytotoxicity). Before experiments, the samples were sterilized by UV radiation for 60 min.

The cytotoxicity of the samples was evaluated using a standard 3-(4,5-dimethyl-2-thiazolyl)-2,5-diphenyltetrazolium bromide (MTT) assay. Briefly, SAOS cells on passage 34 were synchronized in serum-free medium for 24 h. After this period, cells were trypsinized and seeded (3 × 10^5 cells/well) on square samples of hydrogel membranes (4.0 × 4.0 mm^2 and average thickness 58 ± 6 μm) and placed in a 96-well plate. Controls were used with the cells and DMEM with 10% FBS, the positive control with Triton X-100 (1% v/v in PBS, Gibco BRL, USA)

and, as a negative control, chips of sterile polypropylene *Eppendorf* tubes (1 mg mL^{-1}, Eppendorf, Germany). After 24 h, all media were aspirated and replaced with 60 μL of culture media containing serum to each well. MTT (5 mg mL^{-1}, Sigma-Aldrich, USA) was added to each well and incubated for 4 h in an oven at 37°C and 5% CO_2. Next, 40 μL sodium dodecyl sulfate (Sigma-Aldrich, USA) solution/4% HCl was placed in each well and incubated for 16 h in an oven at 37°C and 5% CO_2.

Then, 100 μL were removed from each well and transferred to a 96-well plate. The absorbance (Abs) was measured at 595 nm on an iMark™ Microplate Absorbance Reader (Bio-Rad). The percentage cell viability was calculated according to Equation (2). The values of the controls (wells with cells, and no samples) were set to 100% cell viability.

$$\text{Cell viability (\%)} = (\text{Abs of sample and cells/Abs of control}) * 100. \quad (2)$$

2.3.4. Dye adsorption studies
2.3.4.1. Dye adsorption by CMC hydrogels.
The dye removal activity of the hydrogel membrane was evaluated via the adsorption of MB, which was used as the model cationic organic dye pollutant in water medium. MB solutions were prepared from a stock solution of 500 mg L^{-1} in DI water with three concentrations (100, 250, and 500 mg L^{-1}). Adsorption experiments were conducted by adding 0.2 g of CMC membrane (dry mass) into 10 mL of each MB solution. Unless specified otherwise, the experiments were conducted at constant pH = 5.0 ± 0.5 and temperature of 23 ± 2°C in a dark chamber. Adsorption kinetics experiments were performed to determine the time for equilibrium for the MB adsorption (at 100 mg L^{-1}) and at increasing time intervals up to 1440 min. The effect of MB concentration on the adsorption process was evaluated at three concentrations (100, 250, and 500 mg L^{-1}), where the CMC sorbents were weighed and immerged into each MB dye solution for 2 and 24 h to achieve adsorption equilibrium.

In addition, the effect of the pH on the adsorption was studied by changing the initial pH of MB solutions (100 mg L^{-1}) from 5.0 ± 0.5 to 7.5 ± 0.5 (adjusted with NaOH 1.0 mol L^{-1}). Before hydrogel membrane immersion and after increasing time intervals, aliquots of the MB solutions were collected and analyzed by UV–VIS spectroscopy (Lambda EZ-210, Perkin Elmer) to determine the dye concentration based on the Beer–Lambert correlation curve. The correlation of the absorbance with the dye concentration was studied at the characteristic maximum absorption wavelength of MB

(i.e. $\lambda = 664$ nm). Appropriate dilution was processed to ensure that the concentration of the solution was within the range of the standard working curve.

The dye removal efficiency (R, %) by the adsorbent was calculated using Equation (3) [4]

$$R = ((C_0 - C_t)/C_0) * 100 \quad (3)$$

and the adsorption capacity (q, mg g^{-1}) was calculated according to Equation (4) [6]:

$$q = ((C_0 - C_t) * V)/W, \quad (4)$$

where C_0 (mg L^{-1}) is the initial concentration of dye in the solution, C_t (mg L^{-1}) is the concentration of MB in the solution at time t, V (mL) is the volume of the solution, and W (g) is the initial mass of the CMC hydrogel membrane.

Similarly, the adsorption procedure was repeated for the MO dye, used as the model anionic toxic pollutant. The dye concentration was calculated based on the Beer–Lambert correlation curve at the characteristic maximum absorption wavelength of MO at $\lambda = 464$ nm.

2.3.4.2. Dye recovery analysis.
As a preliminary assessment of the potential recovery of MB from CMC hydrogels, desorption experiments were performed using samples submitted to the adsorption process described in the previous section. Basically, after saturated adsorption of MB (at 100, 250, and 500 mg L^{-1} after 24 h), the CMC dye-loaded sorbents were immersed into aqueous KCl solution (3 mol L^{-1}, ionic strength = 1.5) or HCl solution (pH 4.0 ± 0.3) to evaluate desorption due to the ion exchange and pH effects, respectively. After 2 h of ultrasonication, the final MB concentrations in the solution were analyzed based on Beer–Lambert correlation curves and compared to the amount of dye previously adsorbed, where the dye recovery was calculated according to the literature [6].

3. Results and discussion

3.1. Spectroscopic analysis by FTIR and NMR

The FTIR spectrum of CMC powder is presented in Figure 1(a). The broad band in the 3700–3000 cm^{-1} region is associated with vO–H vibrations and the peaks at 3000–2800 cm^{-1} are related to vC–H bands. The asymmetric stretching mode of carboxylate (COO$^-$) at about 1600 cm^{-1} (asymmetric) overlapped with the band of adsorbed water (1630–1650 cm^{-1}) was detected in the range of 1800–1500 cm^{-1}. The bands at 1416 and 1324 cm^{-1} were associated with the symmetric stretching of COO$^-$ groups. The bands at 1425, 1267, and 1237 cm^{-1} are consistent with the bending modes of
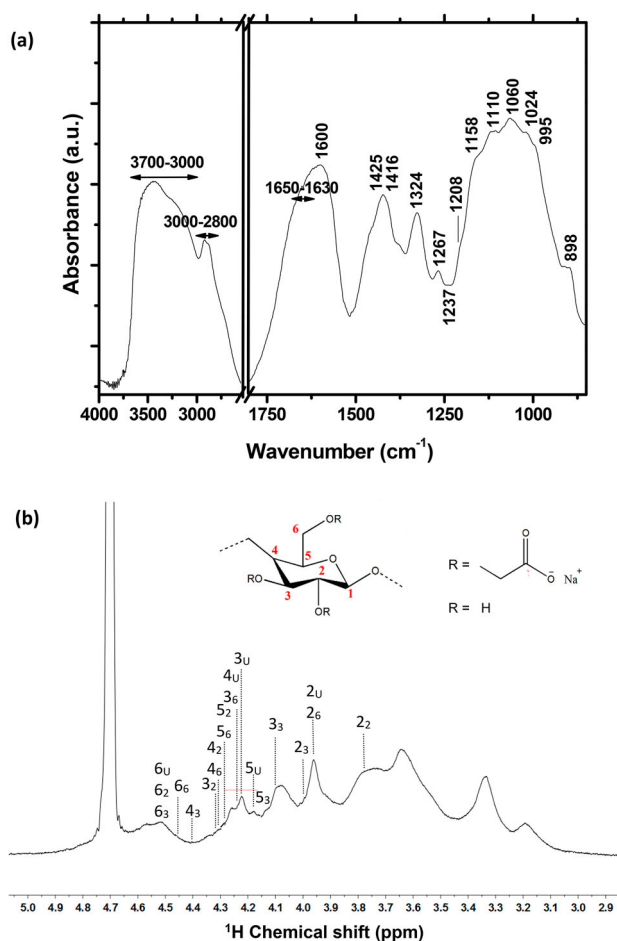
Figure 1. FTIR spectrum (a) and ^{1}H NMR spectrum with the chemical shift assignments of unsubstituted, 2-mono, 3-mono, and 6-mono anhydroglucose units (b) of CMC powder as supplied.

CH$_2$, CH, and OH groups, respectively. Characteristic bands of C–O–C from a pyranose ring were observed at approximately 1208 and 1158 cm^{-1}, which are assigned to the symmetric and asymmetric stretching vibrations, respectively. In addition, C–O vibrations from primary and secondary alcohols were observed at 1110 cm^{-1} (C2-OH), 1060 cm^{-1} (C3-OH) and 1024 and 995 cm^{-1} (C6-OH). The band at 898 cm^{-1} was assigned to the β1-4 glycoside bonds [33–37].

NMR is a powerful technique for characterizing polysaccharides such as cellulose and its derivatives. Carboxymethyl (CM) groups may substitute hydroxyl groups at 2-, 3-, and 6-positions of CMC resulting in eight anhydroglucose rings: unsubstituted (U), 2-mono, 3-mono, 6-mono, 2,3-di, 2,6-di, 3,6-di, and 2,3,6-trisubstituted [38,39]. The signals in the region from 3 to 5 ppm arise from the C–H protons associated with the C2–C6 in an anhydroglucose unit (detail in Figure 1(b)) and contain important information regarding the substitution in the cellulose backbone. In addition, the chemical shifts

assignments of unsubstituted and monosubstituted CM groups predominated in the ^{1}H NMR spectra (Figure 1 (b)), which is consistent with the low degree of substitution of the CMC (DS = 0.77) used in this research according to the literature [39].

3.2. Characterization of hydrogel membranes

### 3.2.1. Effect of cross-linking on the morphology of hydrogels

As a general trend, it was observed that uniform and optically transparent CMC hydrogel membranes were produced before and after cross-linking with increasing concentrations of CA (Figure 2). It was observed that the average thickness of the membranes was significantly reduced by approximately 20%, from 58 ± 1.7 µm not cross-linked to 48 ± 1.7 µm with increasing the concentration of the CA cross-linker to 25%. This fact was credited to the relative reduction of the ratio [CMC/CA] (i.e. CMC polymer/CA cross-linker) and the effective cross-linking of polymer chains reducing the volume of the hydrogel network or contraction of its structure.

3.2.2. Effect of cross-linking on the physicochemical properties of hydrogels

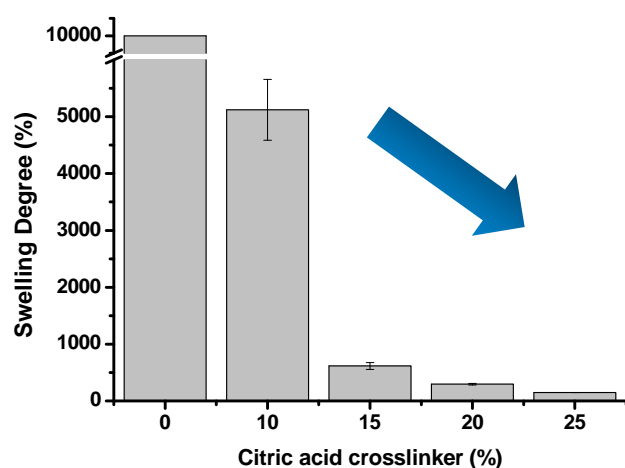#### 3.2.2.1. Swelling behavior of green CMC hydrogels in vitro. Swelling measurements are widely used to access the extension of cross-linking of hydrogel networks. Figure 3 shows the swelling degree (i.e. SD at equilibrium) of the CMC hydrogels with the degree of substitution of CM groups of DS = 0.77, without (i.e. 0%) and with the gradual increase of the concentration of CA as the cross-linker agent. It can be observed that CMC is totally soluble without the addition of the CA cross-linker due to the presence of the ionic carboxylate groups causing the solvation of the polymer chain in water. For CMC at lower concentrations of CA of 10% (CA/CMC, m/m), a highly absorbent hydrogel was produced with SD of over 5000%, and with a drastic decrease of swelling behavior to approximately 150%, at the highest concentration of 25% of the CA cross-linker.

It is important to highlight that these CMC-based hydrogels presented very high absorption of water in the swollen state broadly known as SAP due to its hydrophilic polymer network, which is distinct from the adsorption property toward specific chemical species (e.g. organic dyes) addressed in the next section. Basically, SAP hydrogels are defined as hydrophilic networks with a high capacity for water uptake, which can absorb, swell, and retain aqueous solutions up to hundreds of times their own weight (dry sample). Therefore, these
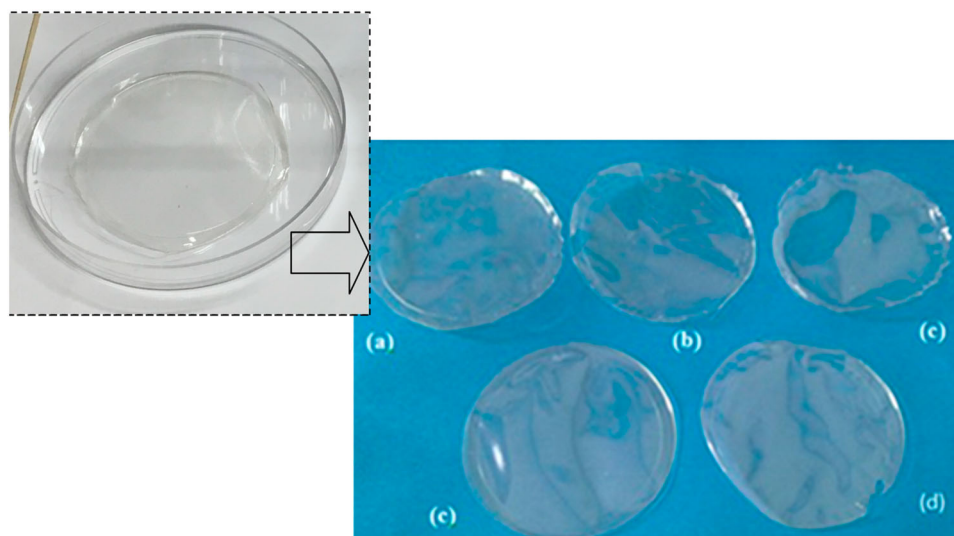
Figure 2. Typical images of CMC hydrogel membranes at increasing concentrations of CA: before cross-linking, 0% CA (a), 10% CA (b), 15% CA (c), 20% CA (d), and 25% CA (e).

findings evidenced the formation of covalent bonds bridging the functional groups of the CMC polymer chains causing the increase of the rigidity of the hydrogel network and the reduction in the amount of water in the swollen state, which are consistent with the variations of thickness (i.e. volume contraction) discussed in the previous section. Moreover, these results demonstrated that the CMC hydrogels can have their network structure tuned by the relative concentration of CA, an eco-friendly cross-linker, for producing highly absorbent hydrogels with a broad range of hydrophilicity (typically varying from 100% to 5000%), which can be used in adsorption processes [40]. Moreover, this swelling behavior revealed that the hydrogel membranes possess structures with

Figure 3. Histogram of swelling behavior of CMC hydrogels in water at 25°C after immersion for 24 h, with increasing concentrations of CA (0%, 10%, 15%, 20%, 25%).

hydrophilic features associated with the ionic nature of the polyelectrolyte network of CMC, which significantly increased the water containing capacity. The major steps of the production process of CMC hydrogels are depicted in Figure 4. Therefore, based on the set of features including the high water absorption properties, these hydrogel matrices are very promising systems for dye removal in environmental applications.

3.2.2.2. FTIR characterization of hybrid hydrogels. FTIR spectroscopy was used to monitor the cross-linking of CMC by CA and the results are presented in Figure 5. The FTIR spectra of the CMC cross-linked hydrogel demonstrated that carboxylates ($-COO^-$ bands at 1592, 1416, and 1324 cm^{-1}) and carboxylic acid ($-COOH$ bands at 1715 and 1246 cm^{-1}) co-exist in the CMC hydrogel due to the substitution of Na^+ by H^+ on the CMC polymer chains during the acidification promoted by the addition of CA.

Cross-linked cellulose hydrogels showed a reduction in the intensity of the band associated with the hydroxyl group at approximately 3400–3200 cm^{-1} (Figure 6(A), which was estimated by the ratio of the absorbance at 3380 cm^{-1} (A_{3380}), related to the hydrogen bonding stretching vibration (OH … OH), and the reference band of β1-4 glycoside bond at 896 cm^{-1} (A_{896}). Figure 6(B) shows the consumption of hydroxyl groups during cross-linking due to the chemical reaction of OH groups from CMC with CA forming ester bonds, as previously reported in the literature [41] and consistent with the SD results. The reaction between CA and CMC depends on the reaction that forms anhydride
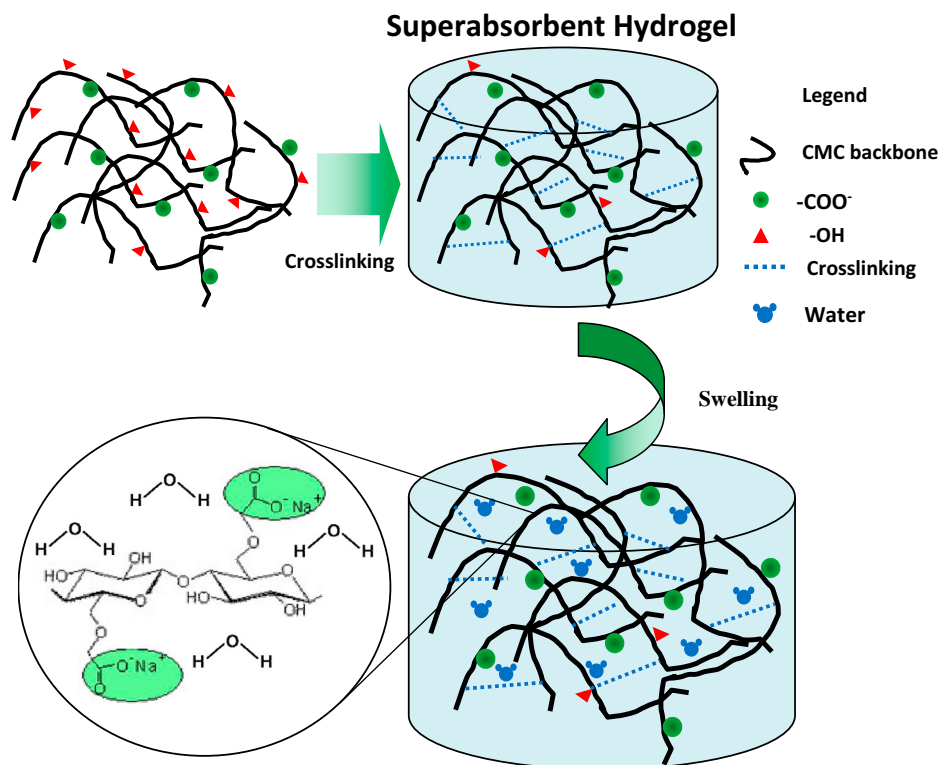
Figure 4. Representation of the cross-linked hydrogel network. Swollen structure after immersion in water (not to scale).

intermediates from CA during the thermal treatment at 80°C with a characteristic band at 1738 cm^{-1}. In the spectra obtained from this region (detail of Figure 5), this peak is absent, indicating that the reactive groups formed during the heating were consumed in the reaction [10]. The chemical reaction of CMC with the CA cross-linker is depicted in Figure 7.

3.2.3. Morphological analysis and mechanical properties of the cross-linking of hydrogels with SEM and AFM

Figure 8 shows SEM (a,b) and AFM (c) images of CMC hydrogel membranes without cross-linking and cross-linked with 20% CA. As it can be observed that the surface morphology of the non-cross-linked sample (I) exhibits a coarse structure with granular features that became smoother and interconnected after the cross-linking reaction (II) probably due to the formation of the macromolecular network characteristic of the covalent bonded hydrogel. Both materials presented some circular valleys, smaller than 500 nm in diameter, formed during water evaporation [42].

To better understand the effect of surface properties of the film on the final pattern formation, AFM was used to characterize the structural and mechanical properties of the cross-linked hydrogel membranes. The AFM technique has proven to be a valuable instrument to characterize qualitatively and quantitatively the

combination of mechanical and morphological properties of soft materials such as hydrogels. For this purpose, a recently developed method, *PeakForce* nanomechanical mapping, has enabled simultaneous quantitative nanomechanical investigation with imaging at high resolution and high speed, by controlling the force and application point at the nanoscale.

Thus, in this study, AFM investigations of the soft hydrogel specimens were performed for the comparison of the nanomechanical properties before and after the chemical cross-linking and the results are summarized in Figure 9. Drastic changes of the surface mechanical properties of CMC hydrogels before (Figure 9 – I) and after cross-linking (Figure 9 – II) with 20% CA for the elastic modulus (Figure 9(b)), adhesion (Figure 9(c)), and dissipation (Figure 9(d)) were observed. For instance, the stiffness of the hydrogel membrane was increased by approximately 300% after cross-linking with 20% CA by assessing the elastic moduli from 80 ± 15 to 270 ± 50 MPa, respectively.

Similarly, the adhesion parameter reduced by approximately 300% after cross-linking, from 21 ± 3 to 8 ± 3 nM. These findings are consistent with the discussion of the previous section that the chemical cross-linking increased the rigidity of the hydrogel network and decreased the swelling capacity. The AFM measurements showed the capability of characterizing the surface mechanical properties at the nanoscale order of soft
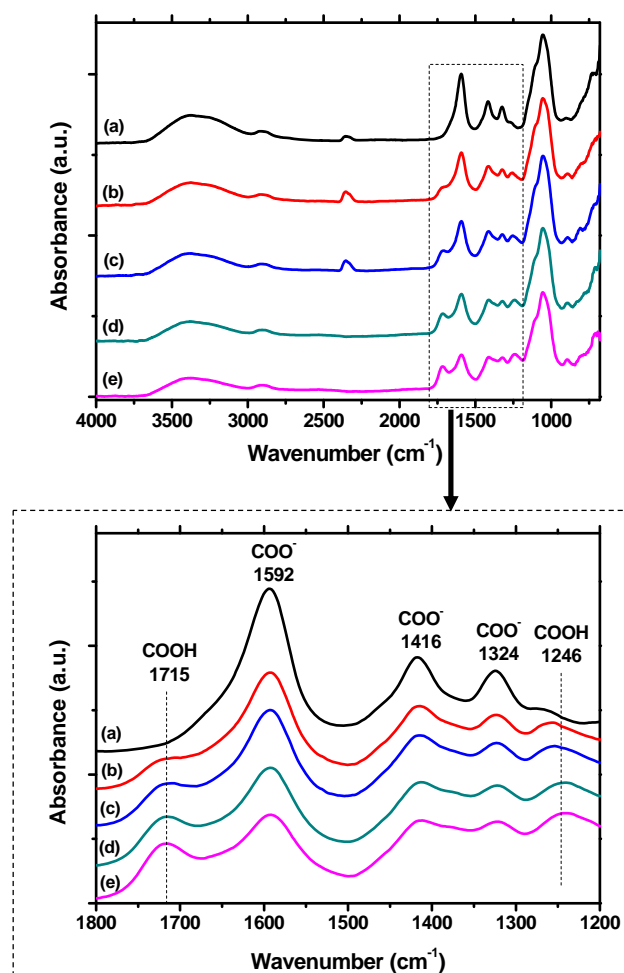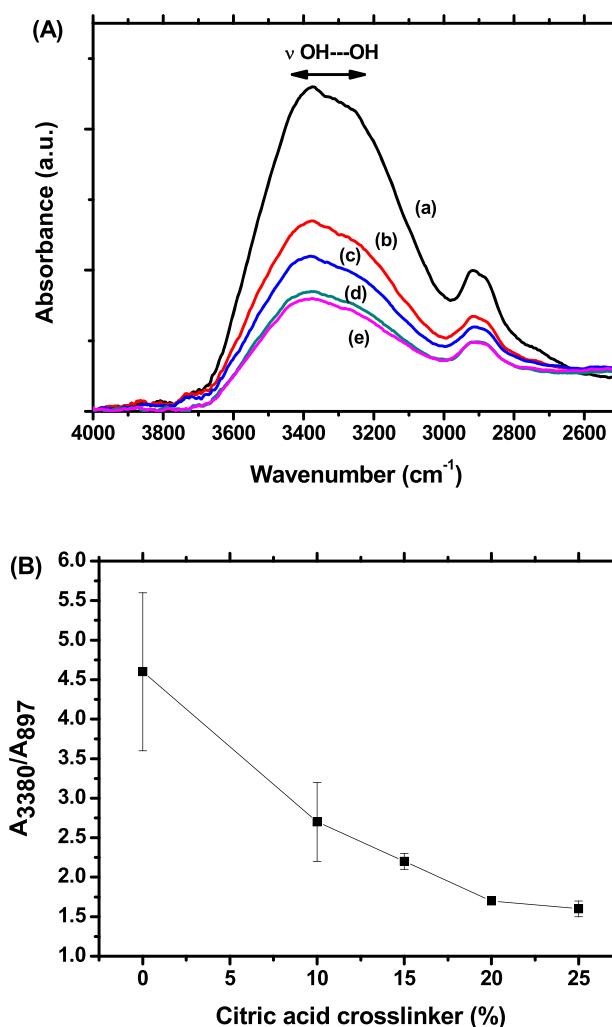
Figure 5. FTIR spectra of CMC hydrogels not cross-linked (a) and cross-linked with 10% (b), 15% (c), 20% (d), and 25% (e) of CA (m/m, CMC/CA). Detail: Expansion of carboxylic/carboxylate region of FTIR spectra (1800–1200 cm^{-1}).

Figure 6. (A) FTIR spectra of CMC hydrogels not cross-linked (a) and cross-linked with 10% (b), 15% (c), 20% (d), and 25% (e) of CA (m/m, CMC/CA) in the range of 4000–2500 cm^{-1}. (B) Evolution of the hydroxyl vibrational band associated with the cross-linking reaction of CMC by CA.

hydrogel samples with reliable response to the formation of the chemical cross-linked network.

3.3. Toxicity characterization of CMC hydrogels

The toxicity of the CMC hydrogel membranes was characterized through the MTT *in vitro* assay according to the international standard (ISO 10993-5:2009/(R)2014, Biological evaluation of medical devices: Tests for *in vitro* cytotoxicity), as a preliminary assessment for potential applications as environmentally friendly adsorbents for wastewater treatment [43]. The immortalized human osteosarcoma-derived (SAOS) cells were used as a model cell line because they have been widely applied in basic and applied researches owing to their ease of access, highly proliferative behavior, and repeatability of results in experiments. However, it is not recommended to directly extrapolate the response of the SAOS cell culture *in vitro* to consider the tested material's

health and environmental safety [44,45]. Figure 10 shows that hydrogels not cross-linked and cross-linked with CA 20% induced no cytotoxic effects, as there were cell viability responses of approximately 90%, similar to the reference control condition (100%, within statistical variation).

Despite differences in the morphological and physicochemical properties of CMC hydrogel membranes before (0% CA) and after cross-linking (e.g. CA 20%) characterized in the previous sections, they demonstrated to be non-toxic toward SAOS cells, which was attributed to the high biocompatibility of naturally derived polymers such as cellulose and its derivatives favoring the cell activity. Moreover, the choice of using CA as the cross-linker for modifying the hydrogel network was based on the fact that it is a natural compound abundantly
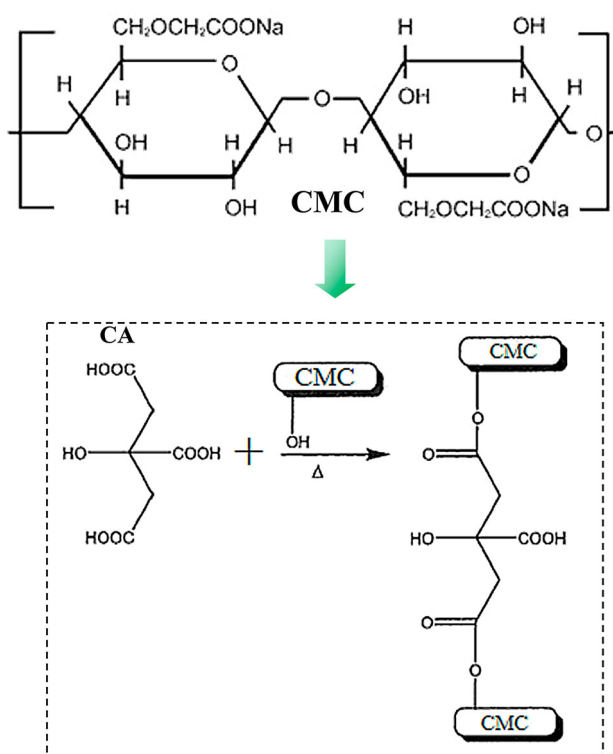
Figure 7. Representation of the chemical cross-linking reaction of CMC with CA.

found in fruits and, therefore, eco-friendly and biocompatible. Therefore, based on the aforementioned results, highly absorbent CMC hydrogels presented

physicochemical properties and biocompatibility to be evaluated as innovative systems for the adsorption of dyes in aqueous medium.

3.4. Dye adsorption by CMC hydrogels

3.4.1. Adsorption analysis of MB – cationic dye

Based on their physicochemical properties combining high water absorption (i.e. SD) and hydrogel stability, CMC hydrogel membranes cross-linked with 10% and 20% of CA were employed for the removal of organic dyes from aqueous solutions. CMC hydrogel not cross-linked was not tested for dye adsorption because it is totally soluble in water. MB was used as the model pollutant molecule due to its cationic properties and similarity with toxic industrial aromatic organic dyes. On the other hand, MO was used as the model anionic dye to validate the hypothesized mechanism of adsorption based on the formation of electrostatic complexes. The CMC hydrogel membrane disks ($d = $ 6.0 cm) were coiled and immersed in the MB solution at an initial concentration of 100 mg L^{-1} (steady pH $= 5.5$ and ionic strength) for 2 h, when the adsorption–desorption equilibrium occurred and the images are showed in Figure 11. Qualitatively, the decolorization of the MB solution was clearly observed after the immersion of hydrogel adsorbents from dark blue (a) to light blue (b).
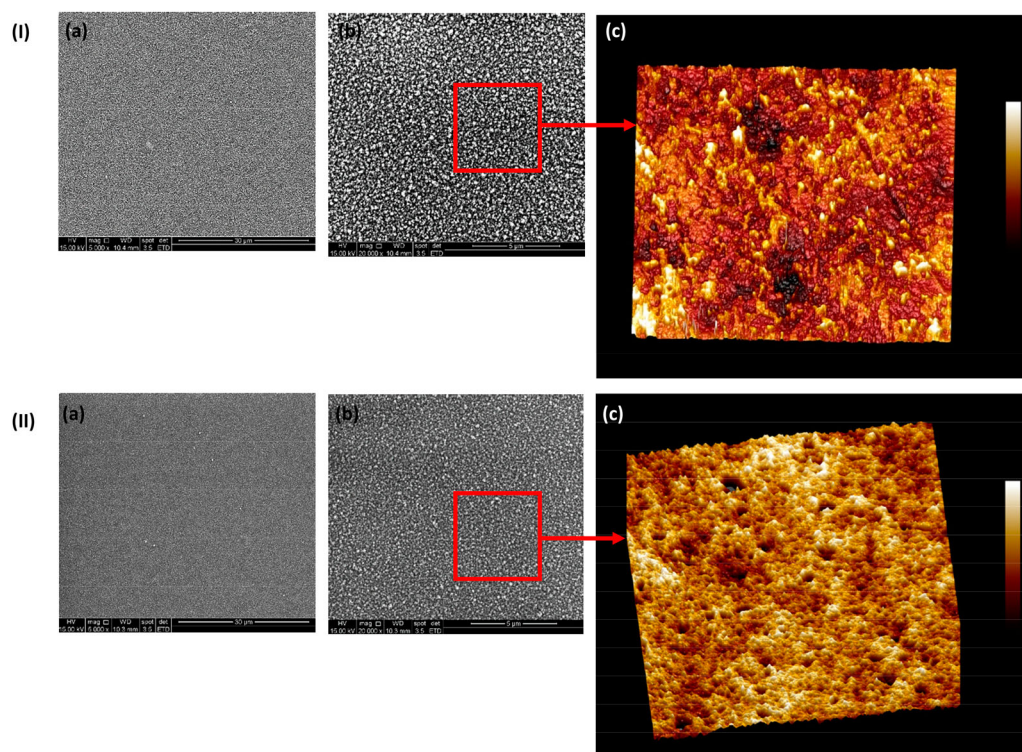
Figure 8. SEM images at magnifications of 5000× (a) and 20,000× (b) and 3D AFM topographical images (5 μm × 5 μm scanning area) (c) of CMC hydrogels before (I) and after cross-linking (II) with 20% CA.
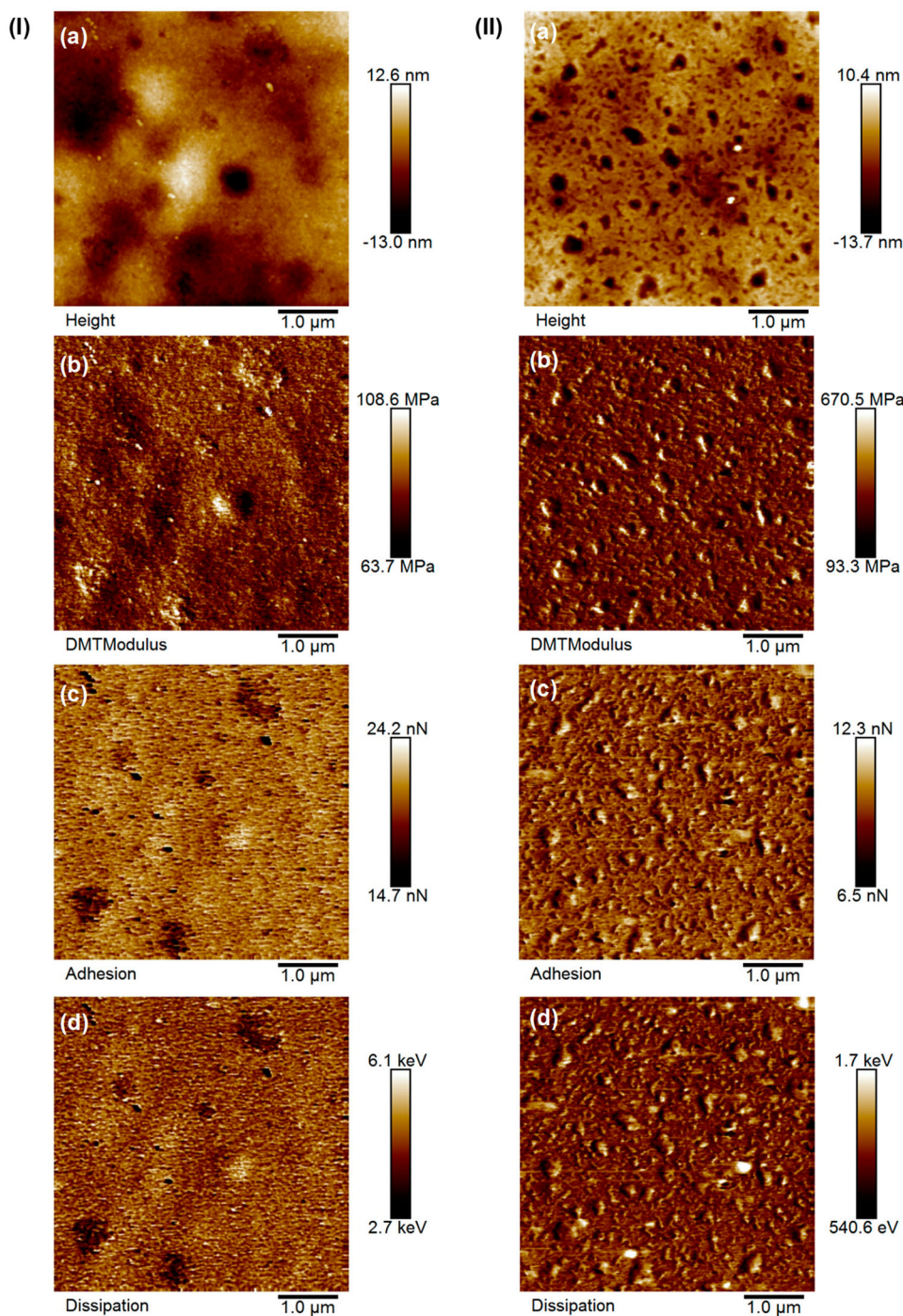
Figure 9. 2D AFM topographical images (a) and the associated mechanical properties: elastic modulus (b), adhesion (c), and dissipation (d) of CMC hydrogels before (I) and after cross-linking (II) with 20% CA (5 μm × 5 μm scanning area).

Quantitatively, the dye concentration was calculated by the Beer–Lambert correlation with absorbance analyzed by UV–VIS spectroscopy at its characteristic maximum absorption wavelength (i.e. $\lambda = 664$ nm for MB) and the spectra are presented in Figure 12(A).

After the immersion of both CMC hydrogel adsorbents (CA 10%, spectrum-b, and CA 20%, spectrum-c), the MB adsorption was verified by the significant decrease of the band related to the MB dye before immersion (reference solution of MB, spectrum-a). In addition, the removal (R) was calculated to be 95% and 92% for CMC hydrogel adsorbents cross-linked with 10% and 20% of CA, respectively. Despite the minor difference, these values demonstrated that both samples behaved as effective adsorbents of MB, which was attributed to the formation of complexes of

90
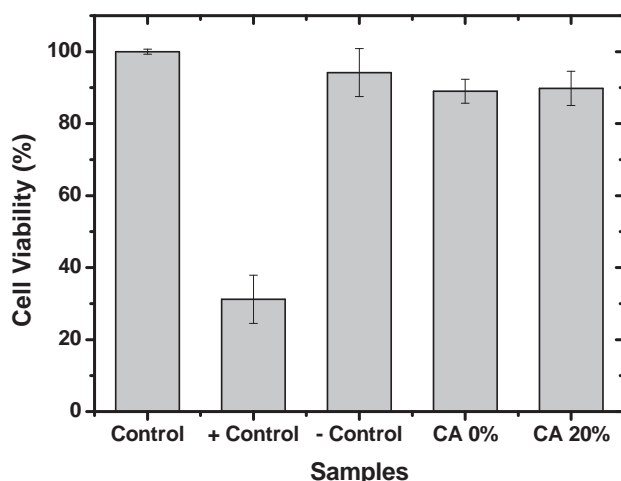
Figure 10. Cell viability response of SAOS culture based on the MTT assay after 24 h of incubation with no cross-linker (CA 0%) and 20% cross-linker (CA 20%).

polyelectrolyte (CMC, anionic) and dye (MB, cationic). The interactions of negatively charged carboxylate groups from CMC with positively charged groups from MB (amine or sulfur) caused the development of strong electrostatic forces favoring the adsorption process by complex formation as depicted in Figure 12(B) [4].

3.4.2. Adsorption kinetics analysis of MB

Figure 13(A) shows a series of UV–VIS absorption spectra of MB dye in the presence of the CMC CA 20% hydrogels. MB has a strong absorption band centered at $\lambda = 664$ nm and an absorption shoulder at approximately $\lambda = 610$ nm

[6,46]. As the time evolved, both absorption bands gradually decreased, indicating the adsorption process of MB by the CMC hydrogel membrane. The adsorption kinetics of the dye was calculated by monitoring the absorbance of the MB solution at the maximum absorption wavelength of $\lambda = 664$ nm. In Figure 13(B), it can be observed that the adsorption capacity of the dye increased rapidly at the initial stages and slowed down as equilibrium was attained at approximately 240 min. In the literature, two types of kinetics are generally used for the study of adsorption process, namely the pseudo-first-order (Figure 13(B), dashed line) and pseudo-second-order (Figure 13(B), solid line) rate laws [6,47]. These reaction kinetics models were analyzed considering the correlation coefficients (R^2) of the models and the chi-square (χ^2) test, which can be used to determine the best-fitted model. Therefore, the adsorption kinetics of MB by the CMC hydrogel was best described by the pseudo-second-order kinetics model ($R^2 = 0.991$, $\chi^2 = 0.482 \ll \chi_c^2 = 16.919$ with a significance level of .05; degree of freedom = 9), which is expressed by Equation (5) [48,49]. Conversely, the adsorption kinetics of MB by CMC was not properly fitted by the pseudo-first-order kinetics model ($R^2 = 0.95$; $\chi^2 = 43.60 \gg \chi_c^2 = 16.919$ with a significance level of .05; degree of freedom = 9).

$$\frac{dq(t)}{dt} = k(q_e - q(t))^2, \tag{5}$$

where k is the pseudo-second-order rate constant (g mg^{-1} min^{-1}) and q_e and q(t) are the amounts of
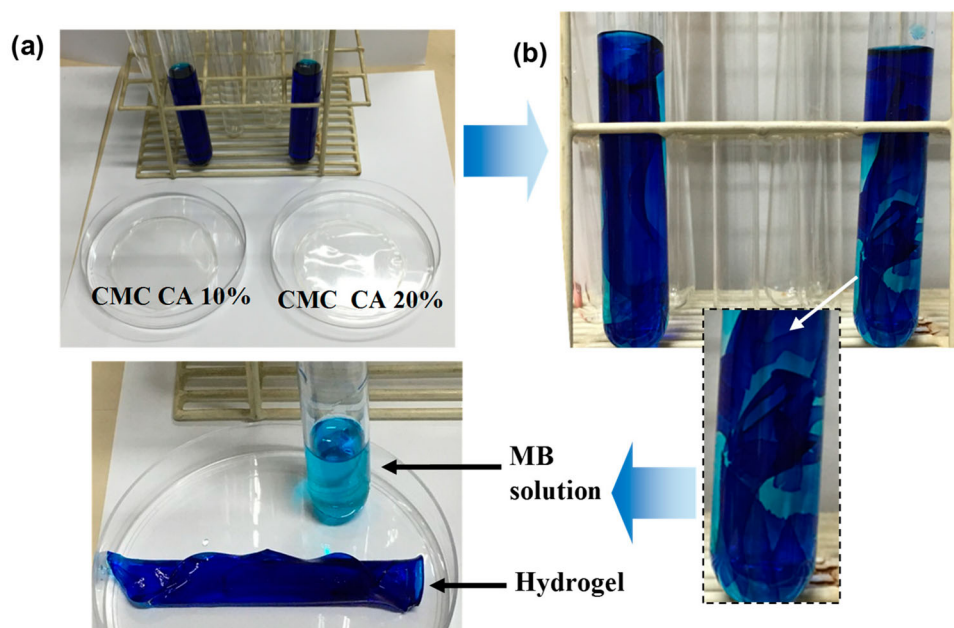
Figure 11. Images of the CMC hydrogel membrane disks ($d = 6.0$ cm) before (a) and after being coiled and immersed in the MB solution (b) for the adsorption–desorption process.
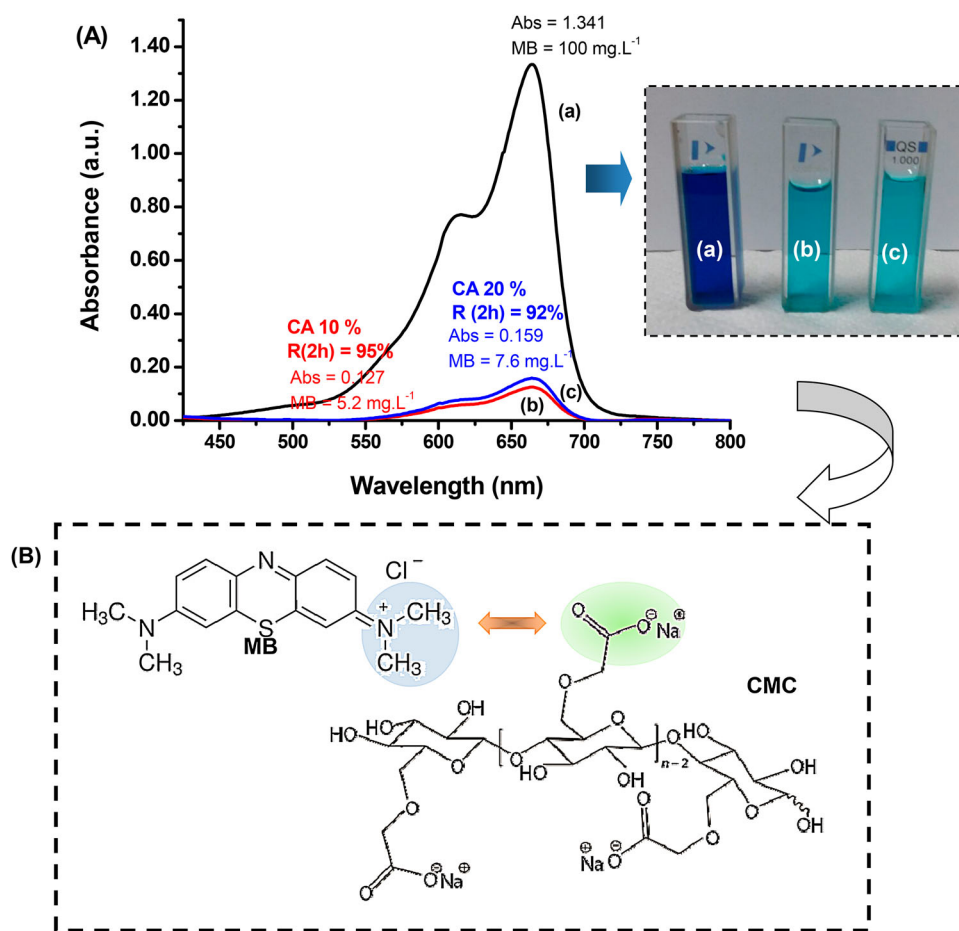
Figure 12. (A) UV–VIS spectra and images of the MB solution before adsorption (a) and after 2 h of the adsorption–desorption process for hydrogels cross-linked with 10% (b) and 20% (c) of CA. (B) Schematic representation of the interactions of negatively charged carboxylate groups from CMC with positively charged protonated amino groups from MB, which caused the development of strong electrostatic forces favoring the adsorption process by a complex formation (not to scale).

adsorbed dye (mg g^{-1}) at equilibrium and at time t (min), respectively. When the initial condition is $q_t = 0$ at $t = 0$, integration leads to Equation (6) [47] and the second-order rate constant for the adsorption of MB was calculated from the intercept and slope of the straight-line plots of t/q versus t (Figure 13(C).

$$\frac{t}{q(t)} = \frac{1}{kq_e^2} + \frac{t}{q_e}. \tag{6}$$

The pseudo-second-order rate constant calculated from Figure 13(C) was 0.0189 g mg^{-1} min^{-1}. The theoretical value of q_e (4.5 mg g^{-1}) also agrees very well with the experimental data. Both facts suggest that the adsorption of MB by CMC fitted properly with the pseudo-second-order kinetic model, which relies on the assumption that the process is controlled by the adsorption reaction at the liquid/solid interface of the adsorbent as reported in the literature [6,47].

Although the pseudo-second-order reaction kinetics model provided the best correlation with the

experimental data, indicating that the adsorption of MB by the CMC hydrogel membrane was governed by a chemisorption process, this is not sufficient to precisely predict the adsorption pathway and mechanism. During a solid/liquid adsorption process, adsorbate transfer may be driven by liquid/phase mass transport (boundary layer diffusion) or intraparticle mass diffusion or both. These phenomena are very complex and subjected to several aspects and properties of the adsorbent–adsorbate systems, which is beyond the scope of this study. Nonetheless, as an exploratory assessment of this subject, the 'intraparticle diffusion model' (IDM) was tested with the mathematical formulation expressed by Equation (7) [49].

$$q(t) = K_{IP}t^{0.5} + C, \tag{7}$$

where K_{IP} is the intraparticle diffusion rate constant and C value is the boundary layer effect, which gives an idea of the thickness of the boundary layer.
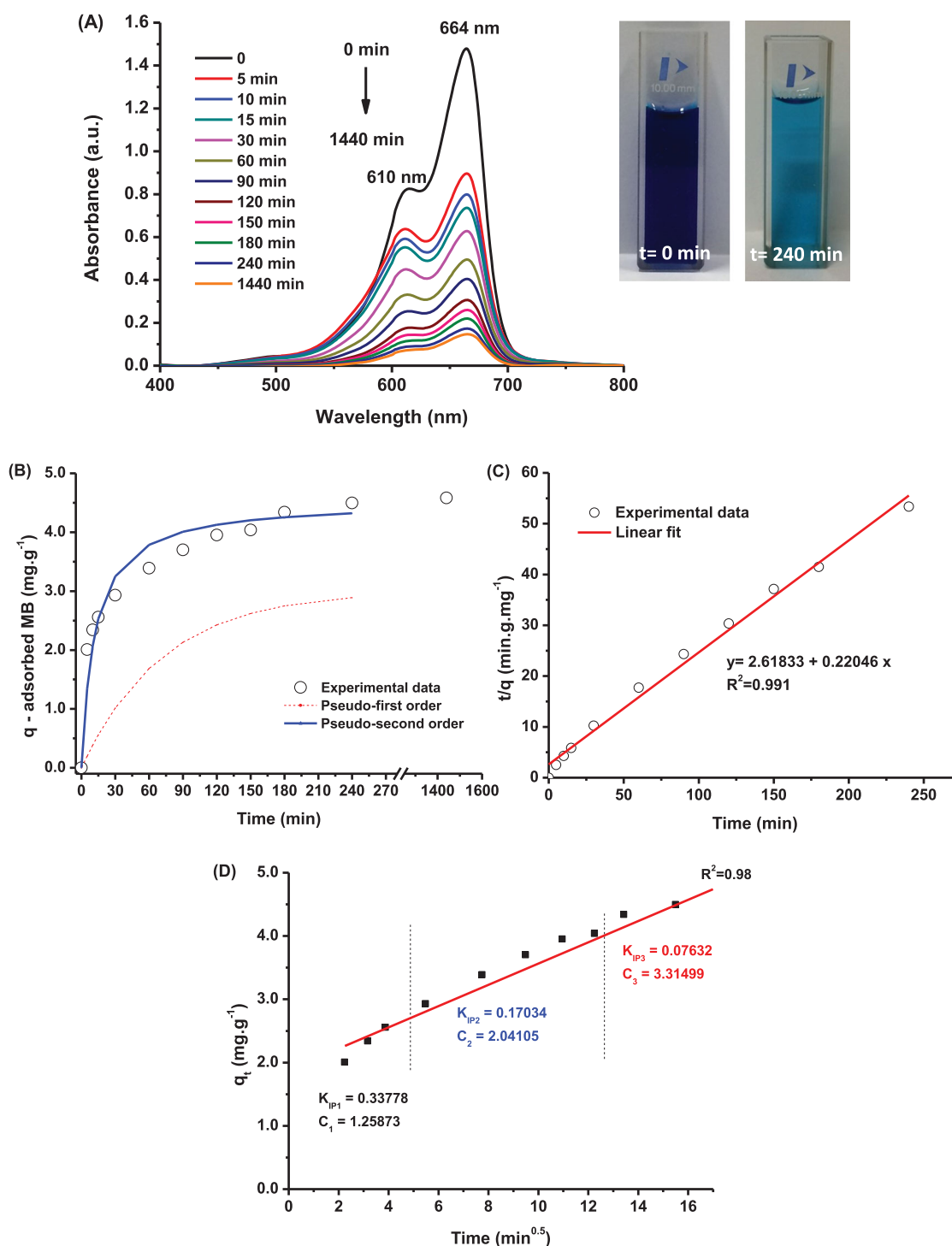
Figure 13. (A) UV–VIS absorption spectroscopy analysis of the MB aqueous solution (at a concentration of 100 mg L^{-1}) in the presence of CMC CA 20% hydrogel with increasing time of immersion; (B) Experimental data (○) of the amount of adsorbed MB (q (t)) in comparison to pseudo-first-order (---, dashed line) and pseudo-second-order (▬, solid line) plots; (C) pseudo-second-order and (D) interparticle diffusion plots for MB adsorption onto the CMC hydrogel.

Figure 13(D) presents the IDM plot for the adsorption of the MB dye (100 mg L^{-1}) by CMC CA 20% hydrogels, where the parameters q(t) versus $t^{0.5}$ were fairly fitted by linear correlation ($R^2 = 0.98$) for the entire adsorption process. However, it can be divided in three regions with distinct K_{IP} and C constants indicating that the adsorption of MB onto CMC hydrogels occurred in stages. Moreover, the plot of q(t) versus $t^{0.5}$ did not pass through the

93
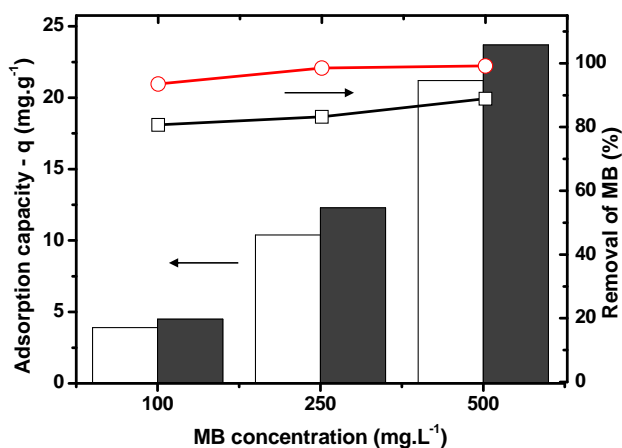
Figure 14. Adsorption capacity (white column: 2 h and gray column: 24 h) and % removal of MB (squares: 2 h and circles: 24 h) by CMC CA 20% at MB concentrations of 100, 250, and 500 mg L^{-1}.
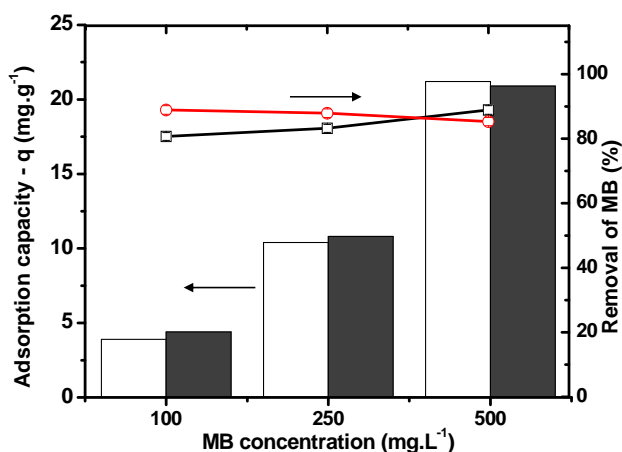

Figure 15. Adsorption capacity (white column: 5.0 ± 0.5 and gray column: 7.5 ± 0.5) and % removal of MB (squares: 5.0 ± 0.5 and circles: 7.5 ± 0.5) by CMC CA 20% at MB concentrations of 100, 250, and 500 mg L^{-1} after 2 h of adsorption.
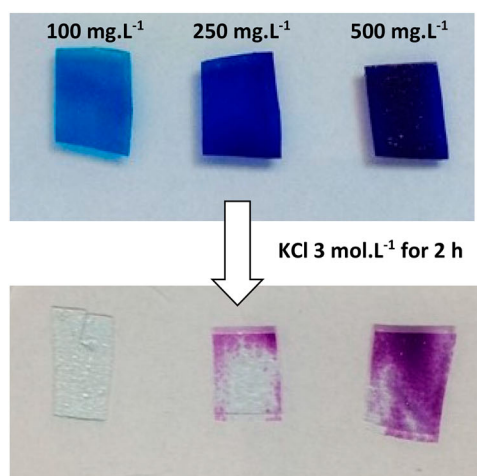
origin ($C \gg 0$) indicating that both intraparticle diffusion and film diffusion played a role in the adsorption process [49].

3.4.3. Adsorption capacity analysis of MB – effect of concentration of MB and pH

The adsorption capacity of the CMC sorbents (CMC CA 20%) was evaluated with three concentrations of MB dye solutions 100, 250, and 500 after 2 and 24 h of immersion time. The results are presented in Figure 14, where a significant effect on the adsorption capacity was observed by increasing the initial concentration of MB in the solution from 100 to 500 mg L^{-1}, causing a proportional increase from approximately 4–5 to 20–25 mg g^{-1} after 24 h of adsorption. In addition, the removal efficiency was less affected by the concentration of MB with values of over 80% after 2 h and 95% after 24 h of adsorption time for all systems. These results indicated that the adsorption capacity was not limited by the saturation of sites of the CMC hydrogels but by the initial concentration of the MB solution. Analogously, the effect of pH of the solution on the adsorption of MB was investigated and the results are presented in Figure 15. No relevant effect was observed on the adsorption capacity using MB solutions under acidic (pH = 5.0 ± 0.5) and moderate alkaline (pH = 7.5 ± 0.5) conditions. These results demonstrated that the formation of charged complexes between MB$^+$ and CMC$^-$ was not significantly altered by either the protonation of carboxyl groups at lower pH (pH = 5.0 ± 0.5, COO$^-$→COOH) or deprotonation under alkaline medium (pH = 7.5 ± 0.5, COOH→COO$^-$), probably because the pH was above the pKa (∼4.7). These systems were not tested at more acidic or alkaline conditions because it would be out of
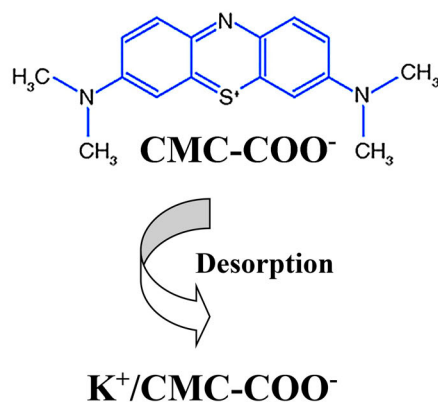
Figure 16. Images of CMC hydrogel samples before (top) and after desorption (bottom) of MB after 2 h of ultrasonication using KCl solution.

94
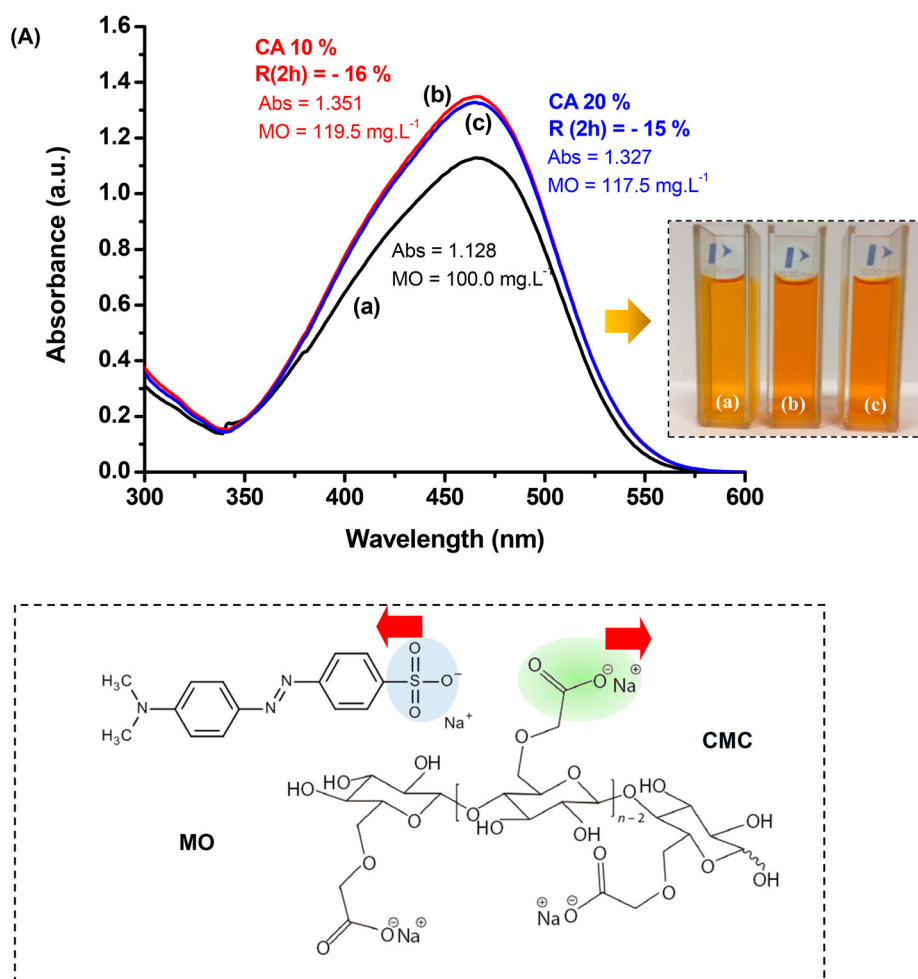
Figure 17. (A) UV–VIS spectra and images of the MO solution before adsorption (a) and after 2 h of the adsorption–desorption process for hydrogels cross-linked with 10% (b) and 20% (c) of CA. (B) Schematic representation of the interactions of negatively charged carboxylate groups from CMC repelling the anionic MO dyes hampering the adsorption process (not to scale).

the scope of this study of designed CMC hydrogels for environmental applications.

3.4.4. Analysis of desorption of MB (dye recovery)

Desorption of MB was performed as a preliminary assessment of possible recovery of the dye and potential reuse of the CMC hydrogels for additional adsorption procedures. Therefore, the desorption procedure was performed using aqueous KCl solution (3 mol L^{-1}) or HCl solution (pH 4.0 ± 0.3), due to the ion exchange (ionic strength = 1.5) and pH effects, respectively, using CMC hydrogel samples previously submitted to adsorption for 24 h by immersion in MB solutions of 100, 250, and 500 mg L^{-1} (Figure 16). The estimated recovery of MB with KCl after just 2 h of ultrasonication was higher than 50% for the evaluated systems, while under mild acidic medium, very low recovery was observed (~1%). These results indicated the predominance of the ion exchange mechanism in the desorption process and the feasibility for the potential use of these new CMC-

based hydrogels as low-cost, biocompatible, and eco-friendly biosorbents for the MB dye removal and recovery for environmental applications.

3.4.5. Adsorption analysis of MO – anionic dye

The immersion of CMC hydrogels in the aqueous solution with MO anionic dye resulted in the opposite behavior compared to MB as presented in Figure 17. The CMC hydrogel matrix went to a swollen state by absorbing water from the solution leading to a significant increase in the concentration of MO from 100 to ~117 mg.L^{-1} (ca. 17%). These results demonstrated unequivocally that, due to the repulsive forces between both anionic species, CMC and MO, the thermodynamics of the system reduced the free energy through the swelling process by the hydrophilic CMC membranes. Thus, these findings proved that the predominant mechanism involved in the adsorption process of MB was based on the formation of charged polyelectrolyte/dye complexes (i.e. CMC$^-$/MB$^+$).

4. Conclusions

In this study, we presented the synthesis and comprehensive characterization of novel eco-friendly and biocompatible hydrogel membranes based on a CM-functionalized cellulose derivative chemically cross-linked by CA using a green aqueous process for the adsorption of cationic dye pollutants. The results evidenced that CMC hydrogels were successfully produced with tailored degree of swelling, ranging from 100% to 5000%, by controlling the concentration of CA for cross-linking. In addition, the results demonstrated that the morphological features, physicochemical and nano-mechanical properties were modified by the extension of cross-linking of the CMC network due to the reaction mechanism involving hydroxyl functional groups of the polymer chains forming the hydrogel matrices. These hydrogels presented no toxicity based on over 90% of the live cell viability responses using the MTT assay. Moreover, they behaved as effective hydrogels for the adsorption of MB used as the model cationic dye pollutant in water. The adsorption efficiency typically of over 90% was attributed to the formation of polyelectrolyte–dye complexes due to the attractive forces of anionic CMC polymer chains (i.e. carboxylates) and cationic groups of MB molecules. The adsorption capacity was significantly increased from 5 to 25 mg g^{-1} by increasing the initial concentration of the MB solution from 100 to 500 mg L^{-1}, but it was not affected by varying the pH from 5.5 to 7.5. Finally, these CMC hydrogels showed MB dye recovery of approximately 60% by desorption using a KCl solution via the ion exchange process, but not by reducing the pH with the HCl solution. To that end, these CMC-based hydrogels are envisioned as promising low-cost biosorbents for wastewater treatment in environmental applications.

Acknowledgments

Disclosure statement

No potential conflict of interest was reported by the authors.

Funding

References

[1] Aksu Z. Application of biosorption for the removal of organic pollutants: a review. Process Biochem. 2005;40:997–1026.

[2] Peng N, Hu D, Zeng J, et al. Superabsorbent cellulose–clay nanocomposite hydrogels for highly efficient removal of dye in water. ACS Sustainable Chem Eng. 2016;4:7217–7224.

[3] Yan H, Zhang W, Kan X, et al. Sorption of methylene blue by carboxymethyl cellulose and reuse process in a secondary sorption. Colloids Surf A. 2011;380:143–151.

[4] Zhang G, Yi L, Deng H, et al. Dyes adsorption using a synthetic carboxymethyl cellulose-acrylic acid adsorbent. J Environ Sci. 2014;26:1203–1211.

[5] Lin Q, Gao M, Chang J, et al. Adsorption properties of crosslinking carboxymethyl cellulose grafting dimethyldiallylammonium chloride for cationic and anionic dyes. Carbohydr Polym. 2016;151:283–294.

[6] Chatterjee S, Chatterjee T, Lim S-R, et al. Adsorption of a cationic dye, methylene blue, on to chitosan hydrogel beads generated by anionic surfactant gelation. Environ Technol. 2011;32:1503–1514.

[7] Mahfoudhi N, Boufi S. Nanocellulose as a novel nanostructured adsorbent for environmental remediation: a review. Cellulose. 2017;24:1171–1197.

[8] Rangabhashiyam S, Anu N, Selvaraju N. Sequestration of dye from textile industry wastewater using agricultural waste products as adsorbents. J Environ Chem Eng. 2013;1:629–641.

[9] Tran TH, Okabe H, Hidaka Y, et al. Removal of metal ions from aqueous solutions using carboxymethyl cellulose/sodium styrene sulfonate gels prepared by radiation grafting. Carbohydr Polym. 2017;157:335–343.

[10] Demitri C, Del Sole R, Scalera F, et al. Novel superabsorbent cellulose-based hydrogels crosslinked with citric acid. J Appl Polym Sci. 2008;110:2453–2460.

[11] Esposito F, Del Nobile MA, Mensitieri G, et al. Water sorption in cellulose-based hydrogels. J Appl Polym Sci. 1996;60:2403–2407.

[12] Passauer L, Liebner F, Fischer K. Synthesis and properties of novel hydrogels from cross-linked starch phosphates. Macromol Symp. 2006;244:180–193.

[13] Raju KM, Raju MP, Mohan YM. Synthesis of superabsorbent copolymers as water manageable materials. Polym Int. 2003;52:768–772.

[14] Barbucci R, Leone G, Vecchiullo A. Novel carboxymethyl-cellulose-based microporous hydrogels suitable for drug delivery. J Biomater Sci Polym. 2004;15:607–619.

[15] Burchard W. Solubility and solution structure of cellulose derivatives. Cellulose. 2003;10:213–225.

[16] Chang C, Zhang L. Cellulose-based hydrogels: present status and application prospects. Carbohydr Polym. 2011;84:40–53.

[17] Ito T, Yeo Y, Highley CB, et al. The prevention of peritoneal adhesions by in situ cross-linking hydrogels of hyaluronic acid and cellulose derivatives. Biomaterials. 2007;28:975–983.

[18] Schulz L, Seger B, Burchard W. Structures of cellulose in solution. Macromol Chem Phys. 2000;201(15):2008–2022.

[19] Clasen C, Kulicke W-M. Determination of viscoelastic and rheo-optical material functions of water-soluble cellulose derivatives. Prog Polym Sci. 2001;26:1839–1919.

[20] Koetz J, Kosmella S. Polyelectrolytes and nanoparticles. Berlin: Springer; 2007.

[21] Lopez CG, Rogers SE, Colby RH, et al. Structure of sodium carboxymethyl cellulose aqueous solutions: a SANS and rheology study. J Polym Sci B Polym Phys. 2015;53:492–501.

[22] Yu L, Liu X, Yuan W, et al. Confined flocculation of ionic pollutants by poly(l-dopa)-based polyelectrolyte complexes in hydrogel beads for three-dimensional, quantitative, efficient water decontamination. Langmuir. 2015;31:6351–6366.

[23] Chang C, He M, Zhou J, et al. Swelling behaviors of pH- and salt-responsive cellulose-based hydrogels. Macromolecules. 2011;44:1642–1648.

[24] Crini G. Non-conventional low-cost adsorbents for dye removal: a review. Bioresour Technol. 2006;97:1061–1085.

[25] Ngah WSW, Teong LC, Hanafiah MAKM. Adsorption of dyes and heavy metal ions by chitosan composites: a review. Carbohydr Polym. 2011;83:1446–1456.

[26] Schanze KS, Shelton AH. Functional polyelectrolytes. Langmuir. 2009;25:13698–13702.

[27] Seow WY, Hauser CAE. Freeze–dried agarose gels: a cheap, simple and recyclable adsorbent for the purification of methylene blue from industrial wastewater. J Environ Chem Eng. 2016;4:1714–1721.

[28] Carvalho, I.C., Mansur, H.S., 2017. Engineered 3D-scaffolds of photocrosslinked chitosan-gelatin hydrogel hybrids for chronic wound dressings and regeneration. Mater Sci Eng C. 2017;78:690–705.

[29] Costa-Júnior ES, Barbosa-Stancioli EF, Mansur AAP, et al. Preparation and characterization of chitosan/poly(vinyl alcohol) chemically crosslinked blends for biomedical applications. Carbohydr Polym. 2009;76:472–481.

[30] Dumont VC, Mansur AAP, Carvalho SM, et al. Chitosan and carboxymethyl-chitosan capping ligands: effects on the nucleation and growth of hydroxyapatite nanoparticles for producing biocomposite membranes. Mater Sci Eng C. 2016;59:265–277.

[31] Ma L, Gao C, Mao Z, et al. Collagen/chitosan porous scaffolds with improved biostability for skin tissue engineering. Biomaterials. 2003;24:4833–4841.

[32] Mansur HS, Costa HS, Mansur AAP, et al. 3D-macroporous hybrid scaffolds for tissue engineering: network design and mathematical modeling of the degradation kinetics. Mater Sci Eng C. 2012;32:404–415.

[33] Cintrón MS, Hinchliffe DJ. FT-IR examination of the development of secondary cell wall in cotton fibers. Fibers. 2015;3:30–40.

[34] Higgins HG, Stewart CM, Harrington KJ. Infrared spectra of cellulose and related polysaccharides. J Polym Sci. 1961;51:59–84.

[35] Luna-Martínez JF, Hernández-Uresti DB, Reyes-Melo ME, et al. Synthesis and optical characterization of ZnS–sodium carboxymethyl cellulose nanocomposite films. Carbohydr Polym. 2011;84:566–570.

[36] Mansur AAP, Carvalho FG, Mansur RL, et al. Carboxymethylcellulose/ZnCdS fluorescent quantum dot nanoconjugates for cancer cell bioimaging. Int J Biol Macromol. 2017;96:675–686.

[37] Zeleňák V, Vargová Z, Györyová K. Correlation of infrared spectra of zinc(II) carboxylates with their structures. Spectrochim Acta Part A. 2007;66:262–272.

[38] Ho FF-L, Klosiewicz DW. Proton nuclear magnetic resonance spectrometry for determination of substituents and their distribution in carboxymethylcellulose. Anal Chem. 1980;52:913–916.

[39] Kono H, Oshima K, Hashimoto H, et al. NMR characterization of sodium carboxymethyl cellulose: substituent distribution and mole fraction of monomers in the polymer chains. Carbohydr Polym. 2016;146:1–9.

[40] Ma J, Li X, Bao Y. Advances in cellulose-based superabsorbent hydrogels. RSC Adv. 2015;5:59745–59757.

[41] Raucci MG, Alvarez-Perez MA, Demitri C, et al. Effect of citric acid crosslinking cellulose-based hydrogels on osteogenic differentiation. J Biomed Mater Res Part A. 2015;103A:2045–2056.

[42] Kaczmarek H, Nowicki M, Vuković-Kwiatkowska I, et al. Crosslinked blends of poly(lactic acid) and polyacrylates: AFM, DSC and XRD studies. J Polym Res. 2013;20:91.

[43] Holden PA, Nisbet RM, Lenihan HS, et al. Ecological nanotoxicology: integrating nanomaterial hazard considerations across the subcellular, population, community, and ecosystems levels. Acc Chem Res. 2013;46:813–822.

[44] Dumont VC, Mansur HS, Mansur AAP, et al. Glycol chitosan/nanohydroxyapatite biocomposites for potential bone tissue engineering and regenerative medicine. Int J Biol Macromol Part B. 2016;93:1465–1478.

[45] Oh E, Liu R, Nel A, et al. Meta-analysis of cellular toxicity for cadmium-containing quantum dots. Nat Nanotechnol. 2016;11:479–486.

[46] Horváth E, Ribič PR, Hashemi F, et al. Dye metachromasy on titanate nanowires: sensing humidity with reversible molecular dimerization. J Mater Chem. 2012;22:8778–8784.

[47] Simonin J-P. On the comparison of pseudo-first order and pseudo-second order rate laws in the modeling of adsorption kinetics. Chem Eng J. 2016;300:254–263.

[48] Ho YS, McKay G. Pseudo-second order model for sorption processes. Process Biochem. 1999;34:451–465.

[49] Erdem A, Ngwabebhoh FA, Yildiz U. Novel macroporous cryogels with enhanced adsorption capability for the removal of Cu(II) ions from aqueous phase: modelling, kinetics and recovery studies. J Environ Chem Eng. 2017;5:1269–1280.